

UNIVERSITY OF OKLAHOMA
GRADUATE COLLEGE

EFFECTS OF SHORT EXPOSURE TO HIGH SHEAR ON NEUTROPHIL STATE
AND FUNCTION

A DISSERTATION
SUBMITTED TO THE GRADUATE FACULTY
in partial fulfillment of the requirements for the
Degree of
DOCTOR OF PHILOSOPHY

By
CHRISTOPHER STEPHEN LEWIS

Norman, Oklahoma

2018

EFFECTS OF SHORT EXPOSURE TO HIGH SHEAR ON NEUTROPHIL STATE
AND FUNCTION

A DISSERTATION APPROVED FOR THE
DEPARTMENT OF CHEMICAL, BIOLOGICAL AND MATERIALS
ENGINEERING

BY

Dr. Edgar A. O'Rear III, Chair

Dr. David W. Schmidtke

Dr. Roger G. Harrison

Dr. Trevor A. Snyder

Dr. Rong Z. Gan

© Copyright by CHRISTOPHER LEWIS 2018

All Rights Reserved.

Acknowledgements

It has been a long and interesting experience to get to this point today, and there have been many people who have supported and assisted me along the way. I would like to take this opportunity to thank everyone involved over the years. To my advisor Dr. Schmidtke, for providing me with the opportunity to work on this fascinating topic area, for his guidance and suggestions throughout the years, and for helping me to grow as both a researcher, as well as a scientific writer. To Dr. O'Rear, for taking over as my committee chair when Dr. Schmidtke transferred universities, as well as for his suggestions and help with the research. To Dr. Snyder, for being both a member of my committee and a collaborator, offering insightful comments and another perspective on my research. To Dr. Harrison and Dr. Gan, for being members of my committee. I would like to thank all my committee members for their time and valuable suggestions on this dissertation.

I would like to thank all the members of the Schmidtke lab that I have had the pleasure of working with all these years. Especially to those of you that have worked with me on the high shear projects investigating neutrophils and platelets: Alexandre Houzelle, Etienne Bendjebbar, Sarah Shapiro, and Dr. Nesreen Alsmadi. A special thanks to Dr. Alsmadi; the work in chapter 4 was a collaborative effort to design and collect all of that experimental data. I would also like to thank all of the undergraduates that have assisted me over the years, with a special thanks to Vinit Sheth for his extra hours and effort. I would also like to thank the other students in the lab for their support, friendship, and entertainment including Kevin Lam, Dr. Jie Chen, and Tarik Shihabeddin. I would also like to thank Dr.

McEver and his lab for their help with protocols and materials early in my graduate career. Finally, a special thanks to all of my friends over the years, both at OU and UTD.

Last and most importantly, I would like to thank my Dad, Mom, and sister for all of their support. For helping to instill in me the dedication and drive to pursue my aspirations to complete a PhD, and for their patience over the years while I did so. I could not have done all of this without you.

Table of Contents

ACKNOWLEDGEMENTS	IV
LIST OF TABLES	X
LIST OF FIGURES.....	XI
ABSTRACT:.....	XIV
CHAPTER 1: BACKGROUND AND SIGNIFICANCE:	1
CONGESTIVE HEART FAILURE AND CARDIOVASCULAR DISEASE:	1
SHEAR RATE IN THE CIRCULATION:	2
PATHOLOGICAL SHEAR RATES:.....	5
<i>Stenosis:</i>	<i>6</i>
<i>Ventricular assist devices (VADs):.....</i>	<i>8</i>
<i>Other blood contacting devices:.....</i>	<i>10</i>
THE ADHESION CASCADE:	11
<i>Selectins:</i>	<i>13</i>
<i>Integrins:</i>	<i>17</i>
NEUTROPHILS AND THE IMMUNE RESPONSE:.....	20
<i>Neutrophil activation:</i>	<i>21</i>
NEUTROPHIL FUNCTIONS:.....	24
<i>Phagocytosis:.....</i>	<i>24</i>
<i>Granules:</i>	<i>27</i>
EFFECTS OF SHEAR ON LEUKOCYTES:.....	32
OVERVIEW AND SIGNIFICANCE:	36

CHAPTER 2: CHANNEL DESIGN AND CHARACTERIZATION	41
INTRODUCTION:	41
METHODS:	50
<i>Materials:</i>	50
<i>Photolithography:</i>	50
<i>PDMS microfluidics:</i>	51
<i>Flow characterization of microfluidic channels:</i>	52
RESULTS AND DISCUSSION:	54
<i>Channel design:</i>	54
<i>Shear rate estimation:</i>	57
<i>PIV analysis: analytical solution</i>	58
<i>PIV experimental analysis: “low” shear rate for rolling studies</i>	59
<i>Exposure time:</i>	64
<i>Reynolds number:</i>	66
<i>PIV characterization: 125-5900s⁻¹ additional constricted channel lengths</i> ...	67
<i>Higher shear rate adhesion studies: 8600 s⁻¹</i>	74
<i>Deformation experiments:</i>	77
<i>Higher shear rates: ~100,000 s⁻¹</i>	87
<i>Corrected flow rates: long exposure constricted channels</i>	92
<i>Double constriction channels:</i>	96
<i>Recirculation zones:</i>	98
CONCLUSIONS:	101

**CHAPTER 3: EFFECTS OF TRANSIENT EXPOSURE TO HIGH SHEAR ON
NEUTROPHIL ROLLING BEHAVIOR 103**

INTRODUCTION: 103

METHODS: 108

Proteins and reagents..... 108

Neutrophil collection and isolation from whole blood 108

Design, fabrication, and assembly of the microfluidic shearing device 109

Neutrophil and bead rolling assays 112

Analysis of PSGL-1 levels..... 114

Statistical analysis..... 115

RESULTS AND DISCUSSION: 116

Effect of transient high shear exposure on neutrophil rolling..... 116

Effect of shear rate magnitude and the critical exposure time..... 123

Effect of transient high shear exposure on PSGL-1 levels..... 127

Effect of transient high shear exposure on GSP-6 coated bead rolling..... 130

CONCLUSIONS: 132

**CHAPTER 4: ALTERED NEUTROPHIL STATE AND FUNCTION FOLLOWING
SHORT EXPOSURES TO HIGH SHEAR 135**

INTRODUCTION: 135

METHODS: 138

Antibodies and reagents: 138

Blood collection:..... 138

Neutrophil isolation: 139

<i>Microfluidic chamber fabrication:</i>	139
<i>Microfluidic device perfusion:</i>	140
<i>Surface receptor staining:</i>	140
<i>Intracellular granule staining:</i>	141
<i>Actin staining:</i>	142
<i>Confocal imaging analysis:</i>	142
<i>Phagocytosis assay:</i>	143
<i>Statistical analysis:</i>	143
RESULTS AND DISCUSSION:.....	145
<i>Surface receptors: selectins and integrins</i>	145
<i>Intracellular granules:</i>	154
<i>Phagocytosis:</i>	166
<i>Actin cytoskeleton:</i>	167
CONCLUSIONS:	172
CHAPTER 5: CONCLUSIONS AND FUTURE DIRECTIONS:	175
CONCLUSIONS:	175
FUTURE DIRECTIONS:	179
CHAPTER 6: LITERATURE CITED:	185
APPENDIX A: VELOCITY AND SHEAR RATE EQUATIONS:	232
APPENDIX B: NEGATIVE PHOTOLITHOGRAPHY PROTOCOL	235
APPENDIX C: NEUTROPHIL ISOLATION PROTOCOL	237
APPENDIX D: ACTIN CONFOCAL IMAGES	239

List of Tables

Table 1.1: Neutrophil shear studies.	33
Table 2.1: Reynolds number	67
Table 2.2: Wall shear rate estimates for channels B-E.	69
Table 2.3: Wider channels for neutrophil rolling with an increased 8600 s^{-1} constricted shear rate.	76
Table 2.4: Channels for high shear studies with calculated shear rates and exposure times.	88
Table 3.1: Protein incubations for channels used for neutrophil rolling.....	111

List of Figures

Figure 1.1: Shear rate schematic.....	4
Figure 1.2: Adhesion cascade.....	12
Figure 1.3: Forces during leukocyte rolling.....	13
Figure 1.4: Schematic of the structure of the three main selectins on leukocytes and their corresponding ligands.....	16
Figure 1.5: Schematic of integrin affinity states.....	19
Figure 1.6: Components of neutrophil activation.....	23
Figure 1.7: Phagocytosis signaling pathways.....	26
Figure 1.8: Granule contents.....	29
Figure 2.1: μ PIV schematic: setup and cross-correlation.....	48
Figure 2.2: Schematic of the constricted microfluidic channels and their dimensions. ...	55
Figure 2.3: Schematic of the channels with the incorporated vacuum design for a temporary seal.....	57
Figure 2.4: Representative velocity vectors and profiles in a constricted microfluidic channel.....	60
Figure 2.5: Velocity profile for a constricted microfluidic channel.....	62
Figure 2.6: Velocity profile for a straight channel microfluidic.....	64
Figure 2.7: Exposure time as a function of z-position.....	66
Figure 2.8: Velocity profiles of constricted channels B-E.....	68
Figure 2.9: Velocity profile across the width of the constriction for a Type D constricted microfluidic device.....	74
Figure 2.10: PDMS deformation.....	78

Figure 2.11: Schematic for the 90-8600 s ⁻¹ channels.....	80
Figure 2.12: Deformation and μ PIV measurements in 8600 s ⁻¹ channels with glass support, sealed to No. 1.5 coverslips.	82
Figure 2.13: Velocity profiles for Constricted channel L, on No. 2 coverslips.....	86
Figure 2.14: μ PIV for high shear conditions for Ch. 4 channels.	90
Figure 2.15: Exposure time as a function of z-position for the 80,000 - 100,000 s ⁻¹ channels.....	92
Figure 2.16: μ PIV velocity profile for Constriction G at 160 μ L/min, with corresponding theoretical profile at 88,000 s ⁻¹	95
Figure 2.17: Double constriction μ PIV.....	98
Figure 2.18: Recirculation zones in buffer solution.....	100
Figure 2.19: Flow profile in whole blood at the post-constriction region for Con. D.	101
Figure 3.1: Overview of the microfluidic device assembly and neutrophil rolling assay.	112
Figure 3.2: Effect of high shear (5900 s ⁻¹) on the instantaneous rolling properties of neutrophils.....	118
Figure 3.3: Neutrophil rolling on glass cover slips.....	120
Figure 3.4: Neutrophil rolling on plastic Petri plates.....	122
Figure 3.5: Effect of increasing shear rate (8,600 s ⁻¹) on critical high shear exposure time for neutrophil rolling on plastic Petri plates.	125
Figure 3.6: Effect of transient high shear exposure on surface levels of PSGL-1.....	129
Figure 3.7: Rolling properties of GSP-6 coated beads upstream and downstream of the constricted region.....	131

Figure 4.1: CD11b and L-selectin surface expression levels.....	147
Figure 4.2: Double constriction channel.	153
Figure 4.3: Specific and tertiary granule components.	158
Figure 4.4: Primary granule component MPO in isolated cells.....	159
Figure 4.5: MPO in whole blood.	162
Figure 4.6: Confocal imaging analysis for MPO content in whole blood.	165
Figure 4.7: Phagocytosis assay.	167
Figure 4.8: Actin content in whole blood.	168
Figure 4.9: Actin content with time of chemical activation.....	171

Abstract:

Cardiovascular disease is an ever expanding global issue. Many pathological conditions have been recently linked to elevated local shear rates ($>3,000 \text{ s}^{-1}$). Such vulnerable regions have also been found in mechanical support devices such as ventricular assist devices (VADs). Patients in these devices have major life threatening issues regularly, including high infection rates and internal bleeding. Extensive studies with other cell types have found a link between shear rate and exposure time on platelet function, as well as on cleavage of blood-based adhesion molecules. However, very little work has focused on leukocytes. The few studies related to elevated shear on leukocytes demonstrate cause for concern with functional damage after exposures of less than 10 minutes to pathological shear. Neutrophils, as the most abundant leukocyte in the bloodstream, have been the most extensively examined. Studies at physiological shear rates show cell-based changes in actin content and receptor levels. It is also known that shear rate modulates several neutrophil behaviors related to rolling and migration. Despite this, very limited work has been done on the effect of sub second exposures to pathological shears. The work in this thesis aims to address that knowledge gap, by examining the effects of short exposures ($<500 \text{ msec}$) to high shear.

In this thesis we present a microfluidic-based study of short exposures to high shear on neutrophil state and function. A microfluidic constricted device was designed and velocity profiles were characterized using a microparticle image velocimetry (μPIV) setup. This setup tracks the positions of small fluorescent particles ($1 \mu\text{m}$) moving with the fluid, and allows us to characterize the fluid

velocity in the channels. Wall shear rates and exposure times were subsequently estimated from these velocity profiles. The majority of the channels used throughout the study have velocity profiles that align well with the expected theoretical values. We also implement a simple glass embeddation technique to reduce channel deformation in the wider channel designs.

We then apply these microfluidic devices to study neutrophil state and function following short exposures to high shear ($> 4,000 \text{ s}^{-1}$). Examining neutrophil adhesion and rolling using a P-selectin based assay, we observed increased rolling velocities following transient ($< 500 \text{ msec}$) shear exposure. This interaction mimics the initial dynamics of the adhesion cascade, the process by which neutrophils and other leukocytes migrate to sites of infection and inflammation. The magnitude of the rolling velocity increase was dependent upon the high shear exposure time, while increasing the shear rate magnitude lowered the critical exposure time required to observe an increase in downstream rolling velocity. We did not detect any evidence that the increase in rolling velocity results from shedding of the neutrophil ligand responsible for the rolling interaction, PSGL-1. The increased rolling velocities suggest an alteration in neutrophil rolling behavior, which could have an impact on the quantity of migrating neutrophils reaching sites of infection, and thus a decreased ability to fight infection at the source.

Expanding the study to higher shear rates ($80,000 - 100,000 \text{ s}^{-1}$), we examined the effect of short exposures ($< 73 \text{ msec}$) on both neutrophil state and function. Neutrophils adopt an activated state in response to stimuli, a process which can be defined by (but not limited to) successive changes in surface

receptors, released proteins from granules, and intracellular calcium levels. These processes correlated with active neutrophil phenotypes typically occur in a step-wise fashion, although the exact response depends on the applied stimulus. Neutrophil state was evaluated by examining a variety of surface receptor and intracellular granule proteins, which provide us with an idea of the current neutrophil phenotype. We observed a significant increase in the activated form of the surface receptor CD11b, an integrin integral to the adhesion cascade and other downstream functions, and a typical (early) neutrophil activation marker, with exposure times greater than 58 msec. No increases were observed in total CD11b levels, only an increase in the activated conformation. Using flow cytometry, we did not detect any indication of degranulation of any granule subtype. However, we did discover increased levels of the primary granule peroxidase myeloperoxidase (MPO) in both isolated cells and whole blood. In an attempt to examine the cause of the MPO increase, we supplemented the flow cytometry data with confocal imaging. Qualitative analysis suggested a potential aggregation and mobilization of primary granules towards the cell membrane. Examining the cell cytoskeleton, we observed an increase in f-actin content for the 67 msec exposure channel at $90,000 \text{ s}^{-1}$. Finally, we observed decreased functionality as measured with a phagocytosis assay. We saw a significant decrease in all sheared samples compared to the unsheared control, with further decreases corresponding with increased exposure times. The results described throughout this thesis suggest an alteration to neutrophil state, as well as neutrophil dysfunction, after short exposures to high shear. The neutrophil state appears to consist of a primed

phenotype, which means that we see partial sign of activation. We suspect the cumulative effect of these shear based changes to reduce the neutrophil's ability to migrate to, and protect against, infections.

Chapter 1: Background and Significance:

Congestive Heart Failure and Cardiovascular Disease:

Cardiovascular disease is the leading cause of death in the United States. There are a variety of conditions that range in severity from small stenosis and arteriosclerosis to total heart failure. Frequently, the individuals suffering from cardiovascular issues have to be placed on mechanical support. While these devices have proven invaluable in improving the quality of life for patients, they introduce a new suite of complications, such as high infection rates^{113,279}. Although many of the infections are believed to be related to device implantation and driveline related events, recent studies have demonstrated a lasting effect on leukocyte activation state and infections not related to the device itself. In addition, for devices such as VADs, sepsis remains one of the leading causes of death^{112,279,291}.

The existence of lasting effects suggests a vulnerability introduced by something in the devices or conditions. A similarity shared amongst the naturally occurring disorders and these devices is the abnormal shear rates. In the case of cardiovascular devices, such issues could arise from a variety of artificial sources, including the blood contacting materials and the shear rates introduced. The latter tend to be higher on average ($>3,000 \text{ s}^{-1}$) or the devices contain very high “hot spots” ($>10,000 \text{ s}^{-1}$) that introduce shear rates well above that encountered in the physiological circulation. These hot spots tend to be small spaces within the devices, such as around the rotors of the pumps, that a small

percentage of the cells encounter on any given pass through the device. Initial concerns related to elevated shear rates focused on the potential for physical cell damage, especially for erythrocytes, and platelets to some extent. Devices are then designed to avoid this range of shear conditions. However, physical cell damage requires extremely high shear rates or prolonged exposure time^{12,18,186,229}. More recently, the focus has shifted towards functional changes, such as in platelet state, with indications that the shear rate and exposure time thresholds required are much lower than for physical damage. Much of the work related to functional damage has revolved around platelets, as well as the blood based proteins involved in thrombosis cascades. Work in this area has uncovered damage to high molecular weight von Willebrand Factor (vWF), leading to decreased binding of platelets under arterial flow conditions, and thus decreased clotting efficiency^{60,309,314}. In addition, functional changes have been observed in platelets, such as shedding of binding receptors, up-regulation of activation markers, and platelet-monocyte aggregation^{57,76,273,334}. However, very little work has investigated an effect on white blood cells, despite the evidence for a recurring vulnerability to infection. This thesis aims to present one of the first examinations into the effect of high shear rates on neutrophil state and function.

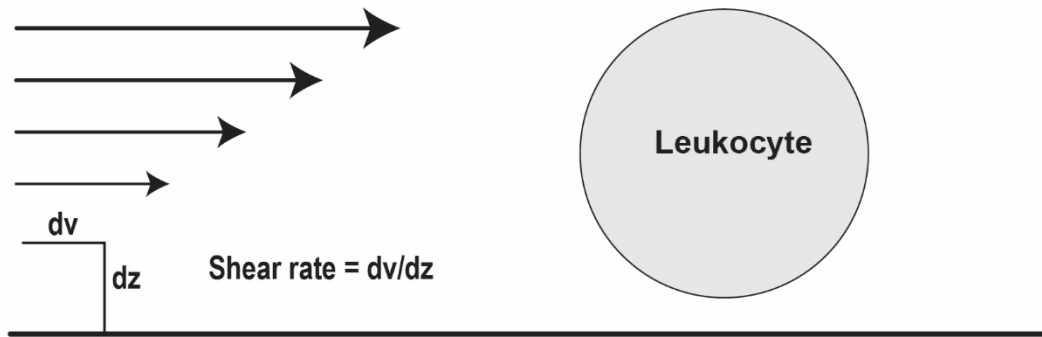
Shear Rate in the Circulation:

Shear rate is defined as the change in velocity over distance (dv/dz), with the distance normal to the channel or vessel wall, and is expressed in units of 1/sec (s^{-1}). Velocity profiles in rectangular channels and cylindrical vessels are generally parabolic in shape, with zero velocity at the wall (no-slip boundary

condition) and the maximum in the center of the channel/vessel. Subsequently, the shear rate will have the highest values at the wall and will approach zero shear rate at the centerline. The typical defining characteristic used for blood cells and conditions in vessels (both physiological and pathological) is the wall shear rate (the shear rate at the boundary of the bottom wall). Cells adhered to the bottom surface will experience a force and torque as a result of the shear stress; shear stress is the product of the shear rate with the viscosity. For blood cells, the shear rate and shear stress are usually inseparable, as the viscosity in medium to large vessels ($>100 \text{ s}^{-1}$) remains relatively constant ($\sim 3.5 \text{ cP}$ for 45% hematocrit)²³⁸. In this thesis we examine the effect of shear rate exposures.

As was just discussed, a new era of artificial blood contacting devices to combat heart failure has brought great success, but at a cost. Current theories to explain many of the lasting complications revolve around shear based effects, as this is the major difference that exists in these devices, as well as certain pathophysiological conditions. However, to understand the differences in the shear rates introduced, we must first examine the normal regime that neutrophils and other leukocytes are exposed to. Typical shear rate values are shown in Figure 1.1.

(A) Shear Rate



(B) Shear Rate in the Circulation

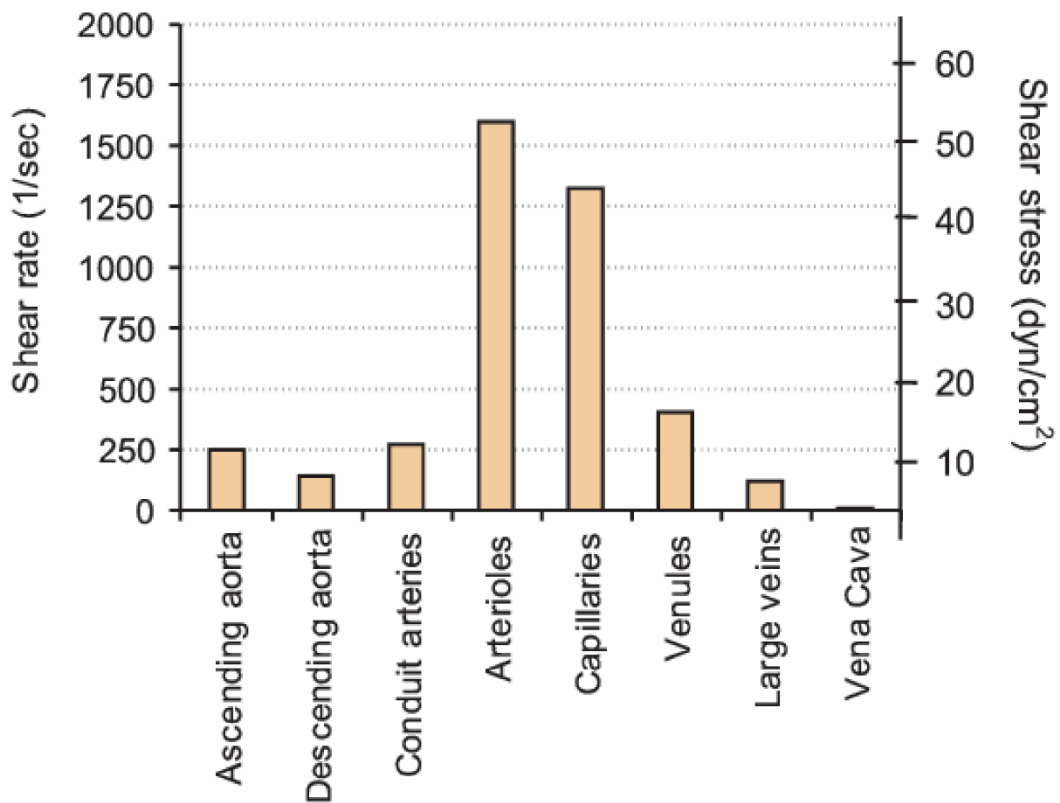


Figure 1.1: Shear Rate Schematic. Representation in (A) shows a neutrophil flowing near the bottom surface. The arrows represent the velocity of the fluid (v) with position moving vertically away from the wall in the z -direction. Typical shear rate values in the circulation shown in (B), from Papaioannou and Stefanadis²³⁸.

Most leukocytes reside within the circulation until their recruitment to sites of inflammation and infection. As such, they routinely experience a range of physiological shear rates found within the venous and arterial system. These values typically lie within $40\text{-}600\text{s}^{-1}$ on the venous side and up to approximately $2,000\text{s}^{-1}$ in the arterioles^{159,238}. Certain processes such as leukocyte migration are controlled in part by the local shear rate. The initial capture and rolling steps of leukocyte migration are modulated by the shear rate found in the venous vessels, which governs the bonding kinetics dominated by the selectin family of adhesion molecules^{8,17,95,171}. Studies have also shown that shear can modulate leukocyte behavior such as cell stiffness^{62,63} or receptor levels^{276,339}; these effects will be discussed later in the introduction.

Pathological Shear Rates:

Pathological shear rates occur in a variety of natural conditions, from points of thrombus that cause disruptions and stenosis, to bifurcations that cause buildups and recirculation zones. Areas of stenosis cause high shear rates ($>3,000\text{ s}^{-1}$), while bifurcations also result in regions of stagnated and negative oscillatory flow⁷⁷. Atherosclerotic lesions have been found to be prone to formation in such low shear stress areas⁴⁹. There has been some work on the effects of abnormal shear profiles on blood flow, with a primary emphasis focusing on platelets and thrombus formation. Both low and high shear regions have been shown to be of interest in causing activation and thrombus growth, as well as disturbances in the flow profiles^{124,191,201,338}. Very little work has focused on leukocytes, and even less on the effect of the higher shear regions. There are

a few different shear regimes to consider, and several conditions that can lead to these elevated shear rates. The two most prominent are stenosis and arteriosclerosis: a partial blockage and a hardening of the arteries respectively, both of which cause a constriction in the vessel and a subsequent increase in the fluid flow and thus the wall shear rate. Both of these conditions can cause pathophysiological shear rates of notable concern, with distinct flow profiles. The low and oscillatory shear regions, while they can occur concomitantly with the higher shear regions at locations such as the carotid bifurcation, are outside the scope of this work and will not be examined in further detail. We instead focus on the high shear aspect.

Stenosis:

Stenosis is one of the most frequent, physiological sources for pathological shear. Stenosis has a range of shear rates as the flow profile is dependent on the thrombus size, location in the body, size of the vessel, degree of occlusion, and more^{25,26,34,258,259,295}. However, in most of these cases the shear rate in medium to severe stenosis are several orders of magnitude higher ($>10,000 \text{ s}^{-1}$) than the typical shear rates ($<2,000 \text{ s}^{-1}$). The elevated wall shear is important for a number of factors. The first is the effect of short exposure to high shear on the blood cells passing through these high shear regions (the focus for the type of work in this thesis). However, high wall shear stress is also a factor in causing the expansion of vessels, and plaque in the high stress areas has been linked to acute coronary syndromes^{259,312}. In addition, it is hypothesized that this high wall shear stress region is a culprit in causing plaque rupture, which is most common in this region

and can lead to obvious health consequences (such as stroke)^{49,77}. A few groups have examined wall shear rates using computational studies. For example, Schirmer et al. found maximum velocities at the throat of the stenosis to be around $40,000 \text{ s}^{-1}$ ²⁶⁴. Another study by Li et al., examined different degrees of stenosis and found wall shear rates to be around $30,000 - 60,000 \text{ s}^{-1}$ for occlusion rates of 50-70%¹⁸¹. In their model they used a stenosis length of 11.6 mm, the same length as one of the shear channels (Con. D) in this thesis (see Fig 2.2). Con. D is the critical length/exposure time found to cause increases in the rolling velocity in chapter 3. Shear rates can increase dramatically with occlusion to values another order of magnitude higher than the ones reported in these studies. For example, Bark et al. estimated shear rates greater than $250,000 \text{ s}^{-1}$ for severe stenosis over 75% occlusion, and up to over $400,000 \text{ s}^{-1}$ for almost complete occlusion. The length of the stenosis also plays a role, and they found that longer stenoses have a lower shear rate, around $100,000 \text{ s}^{-1}$, when increased from 4 to 16 mm²⁵. An *in vivo* animal study examining coronary stenosis observed values of $\sim 10,000 - 90,000 \text{ s}^{-1}$ for a 60% stenosis²⁹⁵. High shear rates for other pathologies, such as at sites of intracranial aneurysms, for example, ranged from $3,000 - 10,000 \text{ s}^{-1}$ ⁷⁷.

The work in this thesis also examines the exposure time to high shear, which is controlled by the length of the stenosis. While typical values are less defined in the literature, values between $\sim 1-20 \text{ mm}$ are observed^{135,327}. A few clinical studies have examined the relationship between stenosis length and fractional flow reserve (FFR), as well as an indicator of pathological conditions.

FFR is a diagnostic test to assess the significance (the extent) of a coronary artery stenosis, and essentially examines the pressure drop⁶¹. One study showed that a length of 16 mm was found to correlate with a measureable drop in FFR¹³⁵. A value of 15 mm was also shown in other studies to define the presence of coronary artery disease, as well as to predict the occurrence of restenosis after balloon angioplasty^{146,299}.

Ventricular assist devices (VADs):

For those with congestive heart failure (CHF), mechanical devices provide a temporary support while waiting to receive a heart transplant. Unfortunately, there are only 2500 heart donors available each year, which cannot provide a practical solution for the 5 million affected individuals^{254,289}. VADs have emerged as a viable option for the treatment of cardiac disease and CHF, created initially as a bridge to transplant, but with the focus shifting to the application of these devices into an end stage therapy of its own²⁵⁶. While VADs have saved many lives since their introduction, their narrow, high flow zones and artificial materials have introduced new complications such as increased infection rates, mucosal and intestinal bleeding, thrombosis, hemolysis, stroke, and several other symptoms^{2,150,289}. Individuals generally have to remain on medication such as blood thinners for the lifetime of the device²²⁴. High infection rates have been reported to be encountered in 30-50% of patients, with sepsis being the leading cause of mortality of VAD patients at 30%²⁷⁹. The increased incidence rate of infection within VAD patients seems to point towards an unnatural disruption of the body's defenses following exposure to the pump's artificial materials and

design. One of the main components of VADs that is altered from a normal heart is the short exposure to very high shear rates as cells pass through the rotors of the pump. It is known that very high shear rate conditions can cause platelet and erythrocyte dysfunction and lysis^{33,98,188,283,293}. The high shear rates encountered can be as high as $100,000\text{s}^{-1}$ ^{98,288}.

However, it is important to note that there are a variety of VAD pump designs, and therefore a range of shear rates. Most of the strategies have been implemented to try and avoid hemolysis and aggregation issues (from platelets or vWF), and haven't focused on conditions that could cause more subtle cell changes, especially in regards to leukocytes^{13,33,97,98,126}. Due to the substantial variety of conditions between devices, as well as the difficulties in accurately measuring shear rates in such devices, most of the current knowledge into shear rates, and especially exposure times, has come from theoretical models. Typical shear rates are high ($10,000\text{-}100,000\text{ s}^{-1}$) for very short exposure times (10 msec or less)^{13,67,269,293}. If the exposure time is an important parameter in determining cell damage (not necessarily physical damage), then the most extreme shear case is not the only condition that needs to be studied. It is therefore important to keep in mind that there is a range of shear rates that persist within any typical VAD, and that cells have a certain probability of going through each region. For any given pass through the device, only a small percentage of cells will actually experience the maximal shear rates. It has been shown that an average cell may more typically encounter a shear rate ($\sim 3,000\text{ s}^{-1}$) that, although high for

physiological conditions ($<2,000 \text{ s}^{-1}$), is typically considered relatively small for VADs ($>10,000 \text{ s}^{-1}$)^{98,101}.

Some studies have attempted to investigate the effects of VADs on leukocytes, focusing on cell counts, and to a limited extent, biochemical alterations. For example, six hour *in vitro* testing of an implantable rotary pump (VentrAssist) and a centrifugal pump (RotaFlow) revealed necrosis, morphological changes via CD45 expression, damage to 20-40% of cells, and a decrease in total cell counts (25 hours). Maximum shear rates were estimated to be $81,000 \text{ s}^{-1}$ and $3,400 \text{ s}^{-1}$, respectively⁵¹. This group, as well as another paper, also reported leukocytes physically fragmented into microparticles (*in vivo*)^{75,260}. Another study using implanted VADs (HeartMate II and Thoratec) in human patients reported temporal changes of leukocyte numbers, with increases at about 14 days postop followed by an eventual decrease below preoperative numbers. Patients on these devices also experienced a corresponding increase in MAC-1 levels, indicating activation that may relate to an increased risk of infection³²⁶. Flow cytometry based studies to evaluate cell state and microparticle formation via various receptors, have become a common and powerful method to examine and compare both *in vitro* and *in vivo* settings²⁴⁸.

Other blood contacting devices:

VADs are an important CHF support device, and one of the more extensively characterized in terms of shear rate responses, due to the high rate of complications observed and known high shear rates, among other reasons. However, there are many other blood contacting devices, and while

complications can result from a variety of sources (such as the material used, etc.), elevated shear rates are again present. This includes, but is certainly not limited to, hemodialysis machines, heart valves, and stents. Many of these devices share similar shear rate regimes to those studied here. For example, heart valves can have similar shear rates to VADs, from 10,000-100,000 s⁻¹, and even upwards of 500,000 s⁻¹ ^{23,108,281}.

The Adhesion Cascade:

Neutrophils, along with other leukocytes such as lymphocytes and monocytes, reside within the bloodstream and thus encounter the high shear environment present within stenoses or VADs many times before cell migration through the endothelium lining the blood vessel into sites of infection. This is the first component of what is referred to as the adhesion cascade, which consists of multiple stages including rolling, activation, and firm adhesion¹⁷⁷. The first step, leukocyte capture and rolling, is essential for the adhesion cascade, and without proper adhesion and rolling, migration cannot occur.

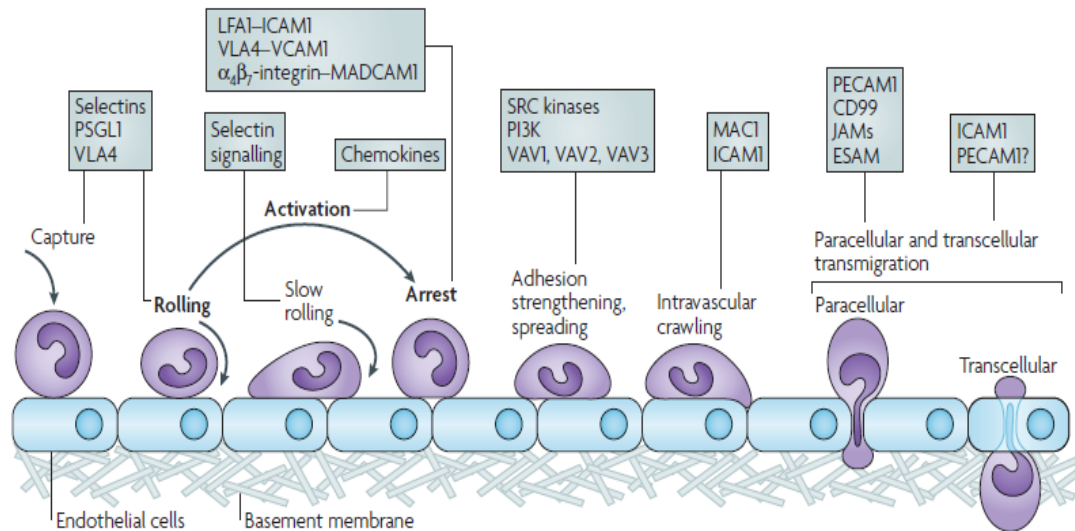


Figure 1.2: Adhesion Cascade. The first steps, capture and rolling, are the relevant selectin mediated events. Selectin signaling contributes to cell activation and arrest. Reprinted by permission from Springer Nature; Ley, K., C. Laudanna, M.I. Cybulsky, and S. Nourshargh. Getting to the site of inflammation: The leukocyte adhesion cascade updated. Nat. Rev. Immunol. pp. 678–689, 2007.

Leukocyte rolling is governed by two important binding interactions, selectins and integrins. The selectins are involved in the initial capture and rolling, as well as during slow rolling, while integrins mediate slow rolling and arrest through intracellular signaling pathways¹⁷⁷. The primary interaction for capture and rolling is between PSGL-1 on the leukocyte surface and P-selectin on the endothelial cells²²⁰. Dysfunction of PSGL-1 based leukocyte rolling from high shear exposure can increase the rolling velocity and potentially decrease the contact time between cells and the inflamed endothelium¹⁷⁶. Decreased rolling time does not allow for proper interaction of cells with the vessel wall (and arrest signals such as integrin ligands and chemokines) and can severely impair leukocyte migration, and therefore the ability to fight infection.

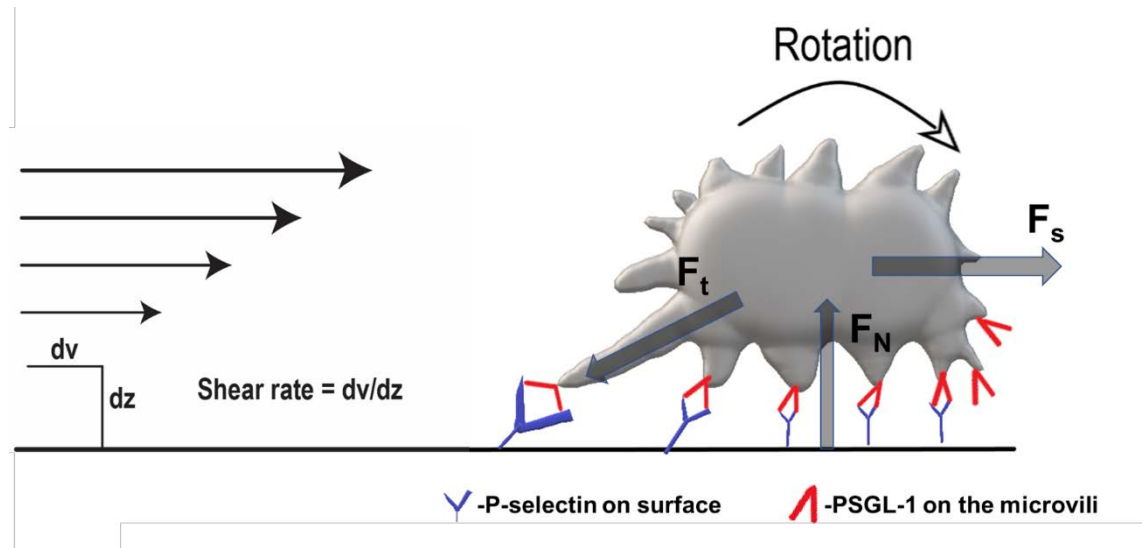


Figure 1.3: Forces during leukocyte rolling. Rolling neutrophils and other leukocytes are first captured from free-flow in the bloodstream by the interaction of PSGL-1 on the microvilli of the leukocyte surface with a selectin, most commonly P-selectin, on the vessel wall. The flowing blood exerts a resultant force (F_s) and a torque on the leukocyte, causing it to rotate. As the leukocyte rotates, new bonds are formed at the leading edge, while bonds at the back end are stretched and released. Tethers and stretched microvilli can apply a force (F_t) through the ligand bond. There is also a contact force (F_N). These forces can slow and even arrest leukocyte movement until the bond is released or new contacts form downstream.

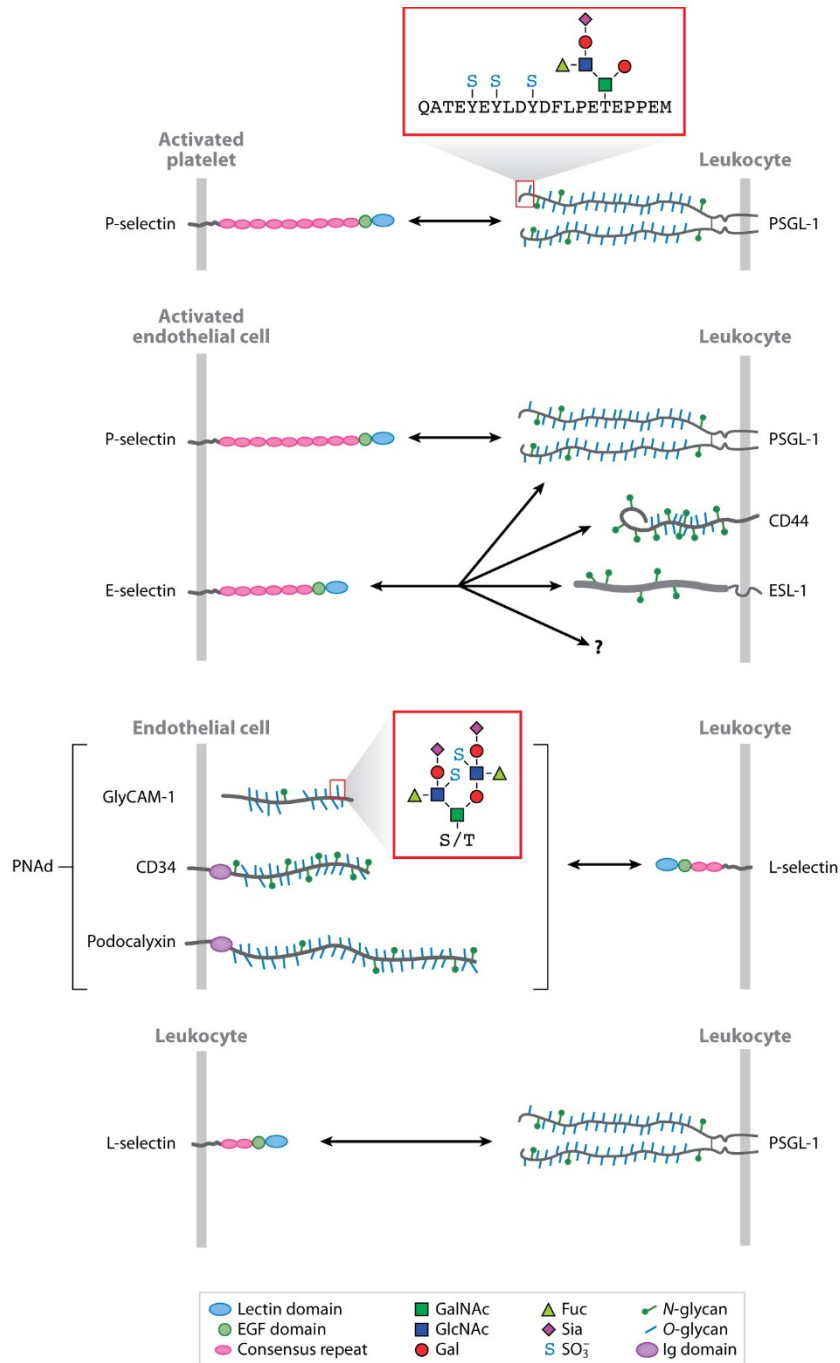
Selectins:

The first adhesion and rolling steps are controlled almost exclusively by the selectin family of ligands. The primary rolling function of the selectins allows leukocytes to survey the vascular endothelium. Interacting with other ligands on the endothelial surface as they roll along provides the necessary signals for activation, arrest, and migration. This occurs primarily from the integrin ligands and chemokines presented on the endothelial cells, although the selectins themselves play a part in altering the cell state. The selectins consist of three molecules which interact rapidly and reversibly with a variety of glycosylated

ligands. Some of the selectin ligands, such as PSGL-1, can interact with all three selectins, while others appear to be much more specific. The three types, P-, L-, and E-selectin all have a similar structure, with a calcium dependent N-terminal carbohydrate-recognition domain, an EGF domain, a transmembrane domain, and a small cytoplasmic tail (Fig. 1.4)²⁰⁵. P- and E-selectin are expressed on activated endothelial cells while L-selectin is constitutively expressed on almost all leukocytes^{205,290,336}.

Each of the selectins can partake in the initial capture of cells, and although there is some redundancy, they appear to have specialized functions. L-selectin provides a secondary capture mechanism resulting from cells binding to already rolling cells, or possibly fragments left behind by previously rolling cells^{85,163,290}. Its dysfunction has been shown to cause a significant decrease in cell migration^{160,290,302,318}. E-selectin can also assist in the capture and rolling of leukocytes, but its primary role appears to be in the transition to slow rolling, and assisting integrins in slow rolling and arrest^{130,284,336}. P-selectin is potentially the most important selectin involved in leukocyte rolling in inflamed venules and provides the primary mode for capturing leukocytes from the flowing blood to the endothelial surface^{55,177,220}. It then contributes to cell rolling as they survey for inflammatory signals. Knockouts of P-selectin in mice have shown up to a 50% decrease in rolling cells²⁰⁴. The location of P-selectin in Weibel-Palade bodies in endothelial cells (while E-selectin is synthesized *de novo*) leads to its expression and importance during the acute phase of inflammation¹⁵⁶. Due to the significance of the PSGL-1 / P-selectin interaction, experiments in this thesis

focused on this interaction. It is also important to note that PSGL-1 interaction with P- and E-selectin can induce the intermediate, extended state of integrins in myeloid cell types^{167,175,292}. It has even been demonstrated that P-selectin from activated platelets can attenuate the NETosis response⁸⁶. NETosis is a process in which neutrophils release condensed chromatin, termed neutrophil extracellular traps³¹⁶. These NETs contain histones and antimicrobial components such as myeloperoxidase (MPO) and elastase, and have been recently demonstrated to be an important neutrophil mechanism of killing microbes^{11,32,210,240}.



McEver RP, Zhu C. 2010. *Annu. Rev. Cell Dev. Biol.* 26:363–96

Figure 1.4: Schematic of the structure of the three main selectins on leukocytes and their corresponding ligands. Republished with permission of Annual Reviews, Inc., from McEver, R.P., and C. Zhu. *Rolling Cell Adhesion. Annu. Rev. Cell Dev. Biol.* Annual Reviews, 26:363–396, 2010; permission conveyed through Copyright Clearance Center, Inc.

Integrins:

Integrins represent the dominating ligand pair in the second phase of the adhesion cascade, generally referred to as slow rolling and arrest¹⁹⁰. These integrins play distinct yet overlapping roles in the adhesion cascade, with the CD18 heterodimers as some of the most influential. LFA-1 (CD11a/CD18) is the dominating ligand in controlling the slow rolling kinetics and firm adhesion and works in tandem with the selectins to control leukocyte rolling at sites of inflammation^{81,128,189,272,319,320}. MAC-1 (CD11b/CD18) plays a cooperative role in slow rolling, but primarily controls the firm adhesion and intravascular crawling, which allows for emigration through the vessel wall^{81,127,177,245}. This arrest and adhesion serves as one of their primary purposes, and is evident from the differences in binding kinetics of these interactions as compared to those of the selectins. The selectins have high association and disassociation rates required for the initial tethering and rolling interactions, whereas those of the integrins are lower²⁰⁸. Upon activation, the dissociation rates decrease significantly for Mac-1 and LFA-1. LFA-1 also has a higher binding rate than Mac-1, which is only involved for adhesion following slowing and arrest mediated by LFA-1^{182,332}. The transition to slow rolling is essential in providing leukocytes with ample time to properly survey the endothelium for inflammatory signals (e.g., chemokines), as well as arresting the cells should these signals be detected. In chapter 3, we will examine changes in selectin based rolling following shear exposures. We would suspect that these shear based changes are likely not only limited to affecting selectin based rolling, but alterations in integrins following shear could also

severely hinder emigration. We will examine integrin states in chapter 4, but we did not explicitly examine the connection to the adhesion cascade.

While integrins play an essential role in neutrophil migration, integrins such as Mac-1 are also heavily involved in cell-cell interactions and even downstream functions such as phagocytosis. Mac-1 has also been linked to cytoskeletal changes, such as through cdc42, a Rho GTPase that partially controls cell polarity³⁰⁰. Integrins also play an important role in a variety of internal signaling processes, including activation based changes within the cell¹³⁴. They have even been linked to interaction with other cell types such as dendritic cells and T-cells²¹⁸.

Integrin binding, or “outside-in” signals are responsible for a variety of downstream functions including degranulation and activation of the NADPH oxidase complex¹. Integrins can increase their binding affinity in two ways upon activating signals, through a conformational shift and receptor clustering, the former of which appears to be the primary way in which binding affinity is modulated⁴⁴. Binding of other ligand/receptor pairs on the neutrophil surface can cause these “inside-out” signaling events that lead to this change in the conformation to an extended, intermediate state¹⁹⁰. Mac-1 receptor avidity can also be increased following degranulation by other chemical activators³⁰. This intermediate extended state typically corresponds with slowed rolling of the cells^{81,175,272}. There is also an additional high affinity extended state for the integrin that is important for cell arrest; the intermediate and high affinity states increase binding affinity by about 500 and 10,000 fold, respectively²⁷⁴. This

results from an opening of the headpiece, exposing the I domain binding site (Fig. 1.5)⁷³. In addition, certain ligands can only be bound following the transition to this high affinity state. Antibodies have been discovered that can detect these different stages, and some of these are used in chapter 4 to examine the state of the leukocytes following short exposure to very high shear rates⁷⁴. The high affinity state usually coincides with and requires further signaling from chemokines or other stimulators (such as n-formylmethionine-leucyl-phenylalanine [fMLP] or platelet activating factor [PAF]), binding to GPCRs on the neutrophil surface.

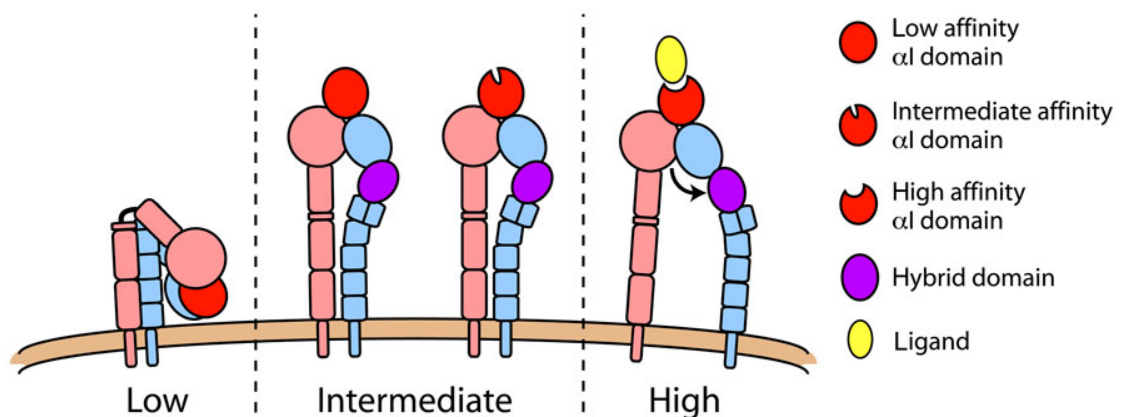


Figure 1.5: Schematic of integrin affinity states. On the left is the low affinity, bent conformation. The intermediate state is extended with closed headpiece and low affinity binding domain, while the high affinity conformation is extended with the available high affinity binding domain exposed¹⁷⁵.

The activated, higher affinity forms of the integrins are often used as a measurable sign for the neutrophil state³²⁶. See “Neutrophil Activation” for more detail. This is an important feature of integrins that is utilized within this thesis.

The conformational changes are some of the first activation events to occur, while total Mac-1 levels are later increased following neutrophil degranulation.

Integrins are important in the context of this work for a second reason. And that is their potential role in neutrophil shear sensing through a mechanosensor(s)⁵. Studies suggest that the neutrophil shear response appears more specific than a global response, and indicates the role of particular receptors rather than an overall membrane response²⁹⁶. While little is known at this point as to how neutrophils sense the fluid environment, some studies have implicated β 2 integrins by demonstrating conformational changes with shear application^{276,339}. Other studies have implicated the potential mechanosensing of G-protein couple receptors (GPCRs) such as FPR, the receptor for fMLP^{125,194}. The mechanosensing through GPCRs has the potential connection to cytoskeletal changes via the Rho GTPases, a set of downstream signaling molecules^{192,193}. If shear induces a response through FPR that leads to inside-out signaling style events, this could present as changes in Mac-1. Mac-1 conformational changes could subsequently cause other downstream effects.

Neutrophils and the Immune Response:

The immune response is very complex and requires a wide array of cells to function properly in defending the body from infection and pathogenic invaders. It consists of two main portions, an innate and an adaptive response, generally differentiated by the specificity of the cells. As well as its role in defending against constant, small infections, the innate immune response provides containment

and support for the adaptive response. Neutrophils are the most prevalent cell of the innate system. The adaptive response consists primarily of lymphocytes, of which T and B cells play distinct roles in responding to pathogens²²¹.

Neutrophils provide an important role as first responders following emigration from the circulation, as well as in assisting effector cells of the adaptive response against bacterial and fungal infections²¹⁸. Upon arrival, neutrophils provide a wide array of functions from the release of cell signaling molecules to the phagocytosis of pathogens³¹⁵. As a result of this diverse function and importance as an early responder, neutrophils play a significant and distinct role in the response to infection. Their functions, location and abundance within the circulation (40-60% of leukocytes in the blood), and high counts (10¹¹ generated each day) make neutrophil dysfunction a likely source for the high infection rates observed within VAD patients^{38,203}.

Neutrophil Activation:

Neutrophil's have a variety of states depending on the stimuli and signals they encounter in the surrounding environment. The process by which neutrophils respond to stimuli is generally referred to as neutrophil activation, which is a highly complicated and regulated process. *In vivo*, these events often correlate with distinct events in the neutrophil cycle, such as during migration (the adhesion cascade) or chemotaxis²¹⁹. As such, neutrophil activation often follows a set process; some of the common components and their approximate timing can be seen in Fig. 1.5. Early stages, such as the up-regulation of surface receptors (e.g., CD11b and NOX2) are generally referred to as a unique state, neutrophil

priming²¹². Traditionally, neutrophil priming has referred to the respiratory burst, which consists of the production of the NOX2 complex in the outer membrane, and the augmented production of radicals after further stimulation⁸⁴. However, while many of the steps and the typical processes are known, much of the intracellular signaling components are still being investigated, and so the neutrophil response to non-typical stimuli (such as pathological shear rates), remains unknown at this time. Neutrophils typically begin in a resting state, which is generally maintained by the low shear levels in the circulation. This helps to prevent entrapment in narrow capillaries and avoid unwanted aggregation or activation. These shear responses are discussed later in the introduction (Effects of Shear on Leukocytes). During the adhesion cascade, rolling interaction of PSGL-1 with P- and E- selectin results in priming signals, which lead to changes in the integrin conformational (extended) states^{167,337}. This often corresponds with the release of secretory vesicles and L-selectin shedding. The release of secretory vesicles increases the concentration of surface receptors such as CD11b. Shedding of receptors such as L-selectin often occur during the migration phase as well, which helps release cells from their interaction with the endothelial cells^{120,213,257}. Some CD18 shedding, for example, also occurs during this time; disruption of this cleavage was shown to reduce emigration²²². Coupled with activating signals from GPCRs (chemokines), the cell slows and moves into the second part of the adhesion cascade, which results in the binding of the high affinity integrin conformation. The cell also polarizes during this process as it adheres and begins to crawl, which results in rearrangements of receptors such

as PSGL-1 and CD11b (to the leading and trailing edge of the cell respectively)^{138,325}. The later stages of activation correspond with the release of the other granule subtypes as well, as the cell begins to migrate through the tissue; the granule subtypes will be discussed in more detail below.

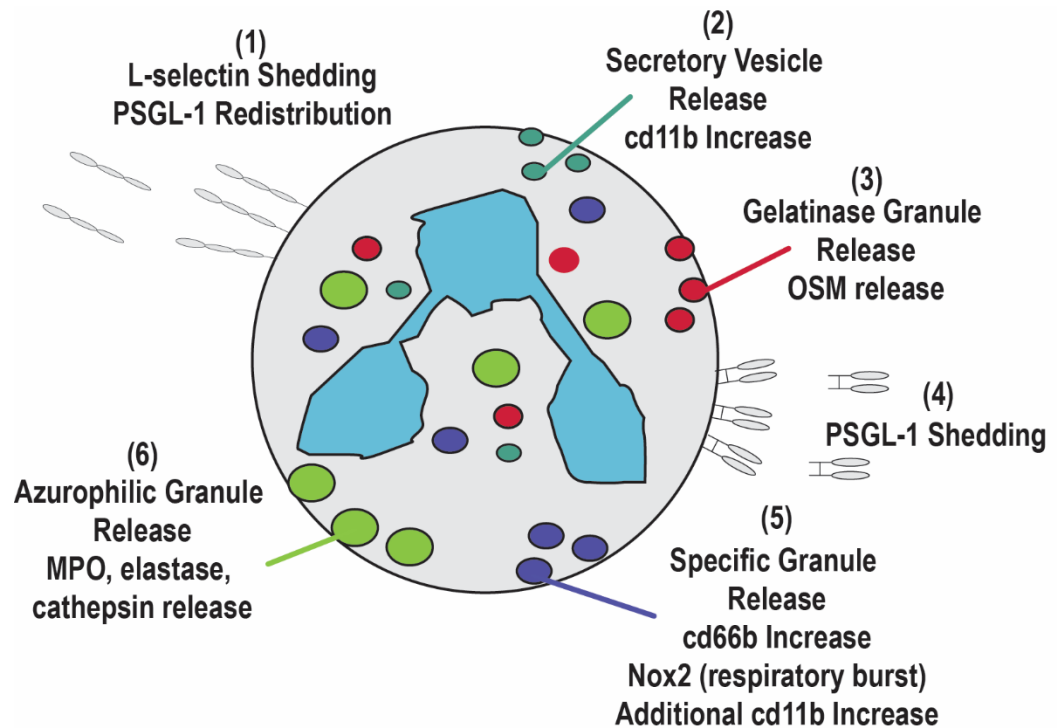


Figure 1.6: Components of Neutrophil Activation. Typical processes that correspond with neutrophil activation are shown, in the approximate order of occurrence. Neutrophil activation does not always follow the same cycle, and differs depending on the types of stimuli applied to the cell. Early stages often consist of cleavage and shedding of L-selectin and redistribution of PSGL-1 to the leading edge of the cell. This often coincides with secretory vesicle release, which results in the upregulation of receptors such as Mac-1 (CD11b/CD18). The gelatinase granules are typically the next released, followed by the specific granules. The specific granules correspond with traditional priming, with formation of the complete NOX2 complex on the cell surface, and an increased respiratory response with further activation. PSGL-1 shedding will occur with later granule release, the exact timing and extent which depends on the stimulus. The azurophilic granules are almost always the last released, and require a strong stimulator. Further activation can eventually lead to NETosis.

Neutrophil Functions:

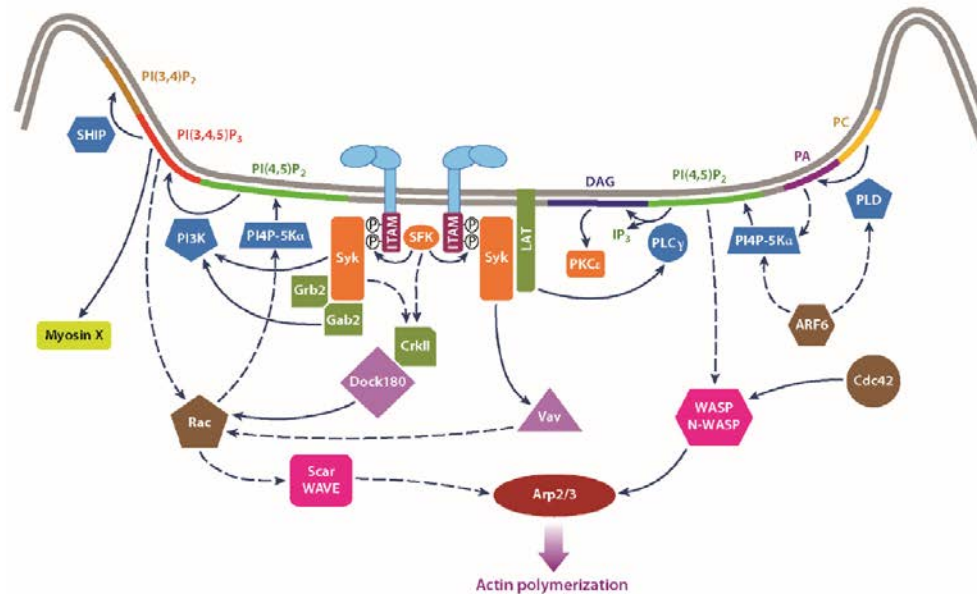
Neutrophils' main purpose within the body is the killing of invading pathogens. This is accomplished directly through ingesting pathogens, the release of toxic molecules, or cytokines/chemokines to indicate inflammation and recruit other cell types^{156,226}. Neutrophils first have to be recruited to the site of infection/inflammation, which was discussed in context of the adhesion cascade and the corresponding molecules that control this behavior. Following emigration, neutrophils then exhibit diverse functions at the sites of inflammation. The two functional aspects discussed in chapter four of this thesis are phagocytosis and intracellular granule release. Neutrophils also produce radical oxygen species (ROS) and under extreme conditions can release their DNA, which can trap pathogens, called neutrophil extracellular traps (NETs)¹⁵⁶. While both of these functions are important, they are outside of the scope of this thesis and will therefore not be elaborated upon in detail. But these would be important factors to be examined for future studies. NETosis is already under investigation in our lab currently.

Phagocytosis:

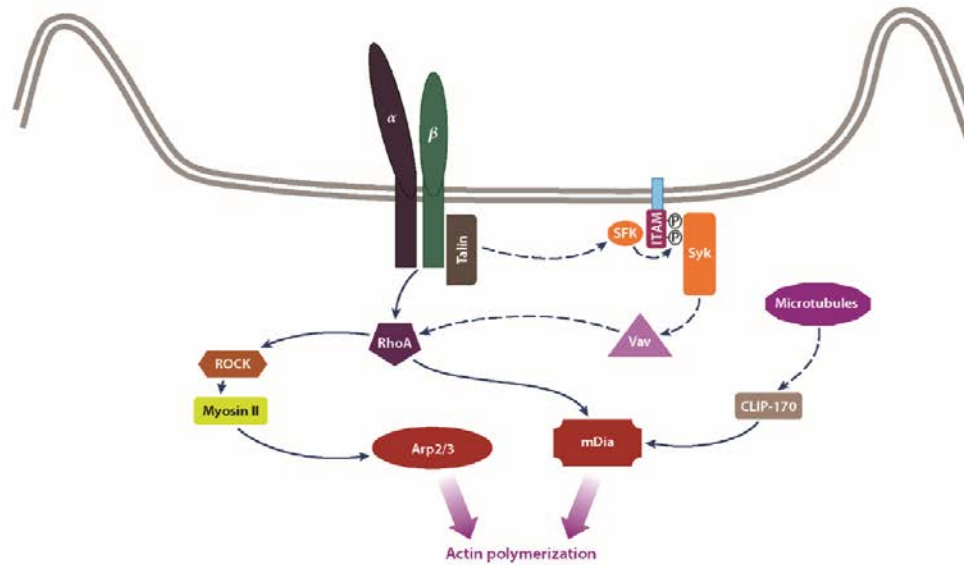
Phagocytosis is one of the most important functional roles of the neutrophil, and along with macrophages they are the primary phagocytic cells. Phagocytosis occurs through different pathways, which can be broken down into two types (Fig. 1.7)⁴⁵. While the downstream events are relatively similar and the end result the same, the mode of engulfment of the pathogen differs. In addition,

the initial binding interactions begin with distinct receptors depending on the opsonization. The first (Type I) is through antibody opsonization, which therefore relies on the various Fc receptors, such as FcγRIIIa. The second (Type II) is through the complement response, which binds through complement receptor 3 (CR3)^{96,99}. We have already encountered this receptor, although by its other name and function: Mac-1. Binding of pathogen to the surface membrane receptor for both types then relies on actin based structural rearrangements, creating a similar actin based “phagocytic cup” created around the pathogen. This phagocytic cup requires actin polymerization creating a branched F-actin structure²⁹⁸. However, the signaling pathways guiding this process differ through the signaling molecules (Rho GTPases) which orchestrate the response. Type I phagocytosis relies on pseudopod extension and membrane ruffling, mediated via cdc42 and Rac1, which control the filopodial and lamellipodial protrusions that surround the pathogen^{66,197,202,321}. Inhibition of RhoA (through Rho kinases) was shown to have no effect²⁶⁹. Type II via CR3 doesn't rely on an extension, but rather an invagination into which the pathogen essentially sinks into, mediated by RhoA and RhoG^{197,236}. This CR3 based phagocytosis is not constitutively active, and first requires inside-out signaling to the high affinity conformation. Binding of CR3 to complement then signals for phagocytosis⁸².

(A) Type I Phagocytosis: FcγR



(B) Type II Phagocytosis: CR3/Mac-1



Flannagan RS, et al. 2012.
Annu. Rev. Pathol. Mech. Dis. 7:61–98

Figure 1.7: Phagocytosis Signaling Pathways. Representation of Type I and Type II phagocytosis pathways. Binding of FcγR or CR3 to IgG or iC3b respectively, lead to intracellular signal transduction, ultimately leading to actin polymerization and engulfment of the pathogen. Republished with permission of Annual Reviews, Inc., from Flannagan et al. *The Cell Biology of Phagocytosis*. Annu. Rev. Pathol. Mech. Dis. Annual Reviews, 7:61-98, 2012; permission conveyed through Copyright Clearance Center, Inc.

Phagocytosis is important in the context of this work for two reasons. The first is as a functional assay, since it is one of the most important effector responses along with the production of reactive oxygen species (ROS). Therefore, it supplements the work on the state of the cell, by showing the potential effects of shear on downstream pathways. In addition, a study by Carter et al. observed a decrease in phagocytosis ability of leukocytes following a short exposure to high shear⁴⁶. Thus, there is a precedent to expect to see changes should the exposure time and shear threshold combination be enough to activate or prime the cells. The second reason of importance relates to the signaling pathways involved. Actin based redistributions are essential for creating the phagocytic cup and the resulting engulfment of pathogens. High shear exposures have been previously demonstrated to cause changes in the proteins related to the control of the actin cytoskeleton, i.e. the Rho GTPases¹⁹³. As such, it is a functional assay that we expect to be directly affected by shear based changes, potentially via the actin cytoskeleton. Altered Rho GTPase activity could lead to decreased actin mobilization or pseudopod projection, which would impair the ability of the phagocytic cup to form (as is shown with knockouts of the various Rho molecules)⁹⁶.

Granules:

Granules provide a very important part of the neutrophil arsenal and due to the wide array of components provide a diverse range of function. Granules are preformed while the neutrophils are still undergoing development, with the

production appearing at the promyelocyte transition and continuing until the segmented stage of maturation. Production ceases after exit from the bone marrow³⁸. The production phase of the granule has been shown to have some level of relation to the selected secretion at later times, the so called “targeting-by-timing” hypothesis^{42,172}. There are several types of neutrophil granules, which are released depending on the stimuli and level of activation of the cell. The granules are divided into several categories: primary, secondary, and tertiary granules. Primarily named from the order during maturation of the cells, and released in the reverse order, with the tertiary granules generally being the first to be released, followed by the secondary, and finally by the primary granules. There are also secretory vesicles that contain a variety of cell surface receptors, and are mobilized quickly and rapidly from neutrophil/endothelial interactions or chemokine signals^{42,65,226,333}. This allows the neutrophil to quickly adapt to a state highly responsive to a wide array of external signals. While granules are categorized by their contents, the distinction between granule subtypes is not exact. Studies examining mRNA content in neutrophils in different stages of development from the bone marrow indicate the time frame for production of various proteins⁶⁴. Packing of granules occurs throughout these stages of development, and therefore leads to the overlap in contents between some granule subtypes^{42,153,252,255}. Azurophilic granules appear to be the most distinct, being formed early and with a somewhat different mechanism^{19,305}; in fact the first studies separated peroxidase containing azurophilic granules from all other, non-peroxidase containing granules. Secretory vesicles also appear to have their own

distinct formation, which is still somewhat unknown, but is hypothesized to be from endocytosis of membrane components⁶⁵. It thus has surface receptor content also present in the secondary and tertiary granules. The largest degree of overlap occurs between these last two types, the specific and gelatinase granules.

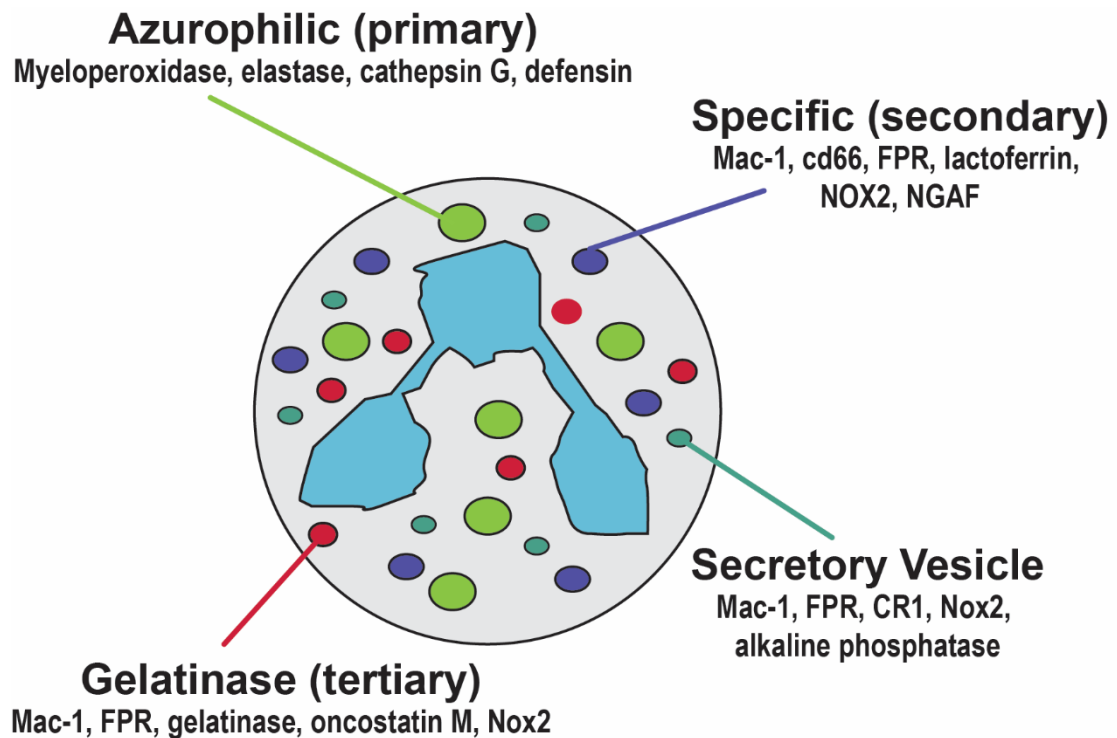


Figure 1.8: Granule Contents. Schematic of neutrophil granules and some examples of important contents found in each subtype, including the various markers to be used in chapter 4.

Primary granules are the first formed during granulopoiesis, and generally the last to be released in the activation cascade. This position in the release cycle makes a lot of sense, as the contents are primarily bactericidal in nature. As such, while they are potent components of neutrophil's pathogen elimination response,

they can also lead to severe tissue damage if activated in an improper manner. Primary granules contain serine proteases such as elastase and cathepsin, as well as myeloperoxidase (MPO). The latter is the defining protein of these peroxidase positive granules (azurophilic)^{20,21}. MPO accounts for almost 5% of all neutrophil protein; it is a peroxidase that feeds off of the respiratory burst to catalyze halogenation reactions. The most common physiological reaction creates hypochlorous acid (HOCl), a potent antimicrobial agent^{14,155,225}. While MPO deficiency is not lethal, patients have reduced antimicrobial function and are prone to infection^{166,250}. MPO may play other protective roles, and has also been implicated in a number of pathologies including plaque rupture, obesity, arthritis, cancer, and even some neurological diseases including Alzheimer's, where MPO is found co-localized with plaque^{170,232,250,304,310,311}. In many of these cases the exact causality remains unknown. Elevated levels of MPO are a biomarker for several acute coronary syndromes and other cases related to oxidative damage^{22,227}.

The other granules play larger roles in the recruitment of other cell types, interaction with signaling molecules, and migration. The secretory vesicles are almost exclusively surface receptor proteins, and are quick to be released, with even low levels of stimulation^{39,41}. These are different in a few ways from the other granule types, and are hypothesized to form in a distinct manner, the exact nature of which is still up for dispute. Current thoughts are from an endocytosis of membrane pieces during the late stages of formation³⁶. But the more recent examination of such content raises the potential that this hypothesis may not be

accurate³⁰⁸. Regardless, secretory vesicles are quickly released, and are the most likely to do so from inside-out signaling, such as during the adhesion cascade²⁷⁰. For example, chemokines such as IL-8 and fMLP can cause complete mobilization of the secretory granules, with only around 20% for the gelatinase granules^{153,154}. Due to the contents of these granules this is unsurprising, as it upregulates the adhesion molecules required, but only after inflammatory chemical signals have been discovered by the cell. In the context of the current study, CD11b/CD18 (Mac-1) is found to some extent in the secretory vesicles. These granules can be thought of as a priming process to increase the diversity of membrane receptors required for the adhesion cascade. Following initial stimulatory signals, a more varied suite of receptors is released to the surface to allow the cell to survey its environment.

The other two granule types, tertiary and secondary, lie somewhere in between. Both contain a subset of surface receptors. Secondary granules have a much larger store, including the most substantial pool of intracellular CD11b, as well as other receptors such as CD66b not found in other granule subtypes^{65,271}. We will use these two surface receptors (CD11b and CD66b) to examine potential granule release. CD11b has a variety of roles, as discussed previously in this introduction. CD66b is another granulocyte activation marker, and one that is specific to granulocytes, and to the secondary granule^{161,294,307}. For example, both of these surface receptors were found in an activated state in rheumatoid arthritis patients³⁰⁷. CD66b binds galectin-3, and plays a role in adhesion and activation in neutrophils and eosinophils, and its activation can

correlate with the upregulation of CD11b^{92,335}. Tertiary granules have a mix of gelatinases that help degrade the extracellular matrix during migration. These granules also contain a mix of cell recruiting molecules, such as oncostatin M (OSM). OSM is a pro-inflammatory cytokine of the IL-6 family³⁰¹. Isolated neutrophils have been shown to contain a preformed stock of OSM, and the ability to synthesize and release additional quantities after stimulation¹¹⁴. It has been recently shown to be a potential marker for leukocyte activation in LVAD patients¹⁸⁴. Secondary granules also contain antimicrobial molecules such as lactoferrin, and thus are again later in the activation response. However, these granule types are also related to the traditional cell “priming”, which generally refers to the radical oxygen species production by neutrophils. Components of the NADPH oxidase reside within the membranes of these granules and are released onto the plasma membrane surface. Later chemical signals are subsequently required and produce a pronounced response⁸⁴. An example of this is LPS based priming, followed by an increased activation upon fMLP stimulation^{83,118}. So these two granule subtypes can be thought of as the traditional priming events. Tertiary granules are released to aid in cell migration through the inflamed tissue³³³. Secondary granules both substantially upregulate the surface receptors for later response to activating signals, and provide critical components for the membrane based oxidative burst complex^{84,333}.

Effects of Shear on Leukocytes:

Most studies involving shear rate have been completed using physiological shear rates and long exposure times, while only a few have

examined heightened shear rates. One of the major limitations of these studies is the increased time scale (min-hours) compared to VAD exposure times (msec). The time scale for almost all of these studies is still at least an order of magnitude higher than that in pathological conditions^{70,278}.

Table 1.1: Neutrophil Shear Studies. Previous studies examining the effects of shear on neutrophils. The various shear responses examined are listed along with the corresponding shear rate, exposure times, and shearing devices.

Shear Response	Shear Rate (s⁻¹)	Exposure Time	Shearing Device	Ref
L-selectin Shedding	150-400	N/A	Flow Chamber	[174]
Pseudopod Retraction	< 500	Seconds-10 min	Micropipette Flow Chamber	[217] [276]
Pseudopod Projection	20-400	1-20 min	Micropipette	[62]
Recoil and Actin Stiffening	100-400	Seconds	Micropipette	[63]
CD18 cleavage	< 1,000	1-10 min	Cone-plate Micropipette Flow Chamber	[339] [276] [102]
FPR Internalization	500	1-10 min	Flow Chamber	[297] [194]
Rho GTPases	100-500	10 min	Flow Chamber Cone-plate	[193]
F-actin content	100-1,200 6-100 / 150-600	60 min 1min / 1min	Rotating Disk Conc. Cylinder / Cone-plate	[278] [54]

Post-Shear Stimulation	10-400	1-120 min	Cone-plate	[214,215]
Cell Viability and Degranulation	10,000-270,000	2-10 min	Conc. Cylinder	[70,71]
Reduced Phagocytosis	3,700-35,000	90, 125 msec	Capillary tube	[46]
	100-1,800	60-180 min	Rotating Disk	[278]
Apoptosis	100-1,400	60 min	Rotating Disk	[278]

The effects of high shear stress on leukocyte function or behavior is not well understood. Some studies have shown that the response of leukocytes to fluid shear involves pseudopod retraction and deactivation of certain pathways, designed to decrease unwanted activation and potential clogging within the microcirculation^{54,62,101,157,214,217,297}. Previous studies have examined essentially two aspects of the neutrophil response to physiological shear rates: cytoskeletal and receptor changes. For the former, changes in stiffness and pseudopods (both projection on surfaces and retraction under flow) have been demonstrated^{54,62,63,278}. An increased stiffness could affect neutrophil rolling and migration, as could changes in pseudopods. In addition, pseudopod spreading can play a role in functions such as phagocytosis. A retraction could result in a decrease in the phagocytic function following shear exposures. Cell receptors, such as those that have been discussed so far in this introduction (e.g., CD11b, L-selectin), play a part in almost every neutrophil functional response. Decreases in surface receptors could affect both neutrophil rolling and migration, as well as downstream functions such as phagocytosis. In the case of decreased leukocyte

recruitment, a deficiency in initial capture and rolling could be explained by the loss of the most important ligands for these interactions: PSGL-1 and L-selectin. Decreases in receptors such as PSGL-1 will also decrease inside-out signaling for integrin state changes. Chemical activation of cells has shown that not only is PSGL-1 redistributed on the cell surface, but it is also shed via protease activity, leading to significant decreases in PSGL-1 expression levels^{43,68,138,139,185,199}. L-selectin has also been demonstrated to be shed during activation, as well as during the rolling process itself^{109,115,152,160,174,303}. Shedding of these receptors generally occurs during the final steps of the adhesion cascade, which aides in releasing the cell from its contact with the endothelium for continued migration into the site of inflammation. Receptor changes following activation also affect integrin levels such as CD11b and CD18, whose up regulation is a hallmark for activation^{6,28,102,175,339}. Previous work has demonstrated a shear sensitivity for several receptors including CD18 and GPCRs such as FPR and PAF^{4,102,193,194,276,297,339}.

Some researchers have examined the effect of shear rate on blood cells and found what appears to be evidence of activation. For example, the work from Mitchell et al used CD11b conformational shifts and L-selectin shedding as markers for neutrophil activation; they found evidence for an increased response to stimulator after shear for the case of PAF²¹⁵. An increased response to activation following shear indicates a potential priming of the cells; a well-known phenomenon for chemical activators such as LPS or TNF α . Chemical activation can also cause changes in receptor localization and mobilization, something not

examined in depth at this point for sheared neutrophils. The few studies with longer exposures have shown evidence of high shear causing activation, and potentially even cell death, under prolonged periods^{70,278}. Interestingly, one of the few studies with pathological shears demonstrated a sensitivity to activation and destruction over time. Shear rates $\geq 20,000 \text{ s}^{-1}$ applied for 10 minutes was sufficient to cause morphological changes, as well as the potential release of secretory vesicles and primary granules⁷¹.

One of the only papers documenting a response to short time exposures of high shear is the work by Carter et al. White blood cells (WBCs) were tested using several analytical methods, including cell count, phagocytosis, and structural viability. This previous study analyzed shear rates ranging from 3,700 to $35,000 \text{ s}^{-1}$ over two exposure times estimated for a rotary blood pump: 90 and 125 msec⁴⁶. This work demonstrated that cell function, rather than cell count, was the primary factor affecting cell behavior following high shear. It also indicated that a short exposure to a high shear environment was sufficient to alter WBC behavior.

Overview and Significance:

Cardiovascular diseases have emerged as one of the most prevalent and costly fields of medicine. In recent years, shear rate has been discovered to be an important factor in complications from a variety of sources, both in natural events such as stenosis, as well as in artificial devices such as ventricular assist devices. Despite the apparent vulnerability, little work has examined the effects

of high shear on leukocytes. The few studies to examine high shear rates show a potential dysfunction and damage at long exposure times. To our knowledge only one study has demonstrated millisecond exposures to pathological shear; this study demonstrated a decrease in phagocytosis ability⁴⁶. In this thesis we use microfluidic constricted devices to examine short exposures to pathological high shear, and the effect on neutrophils. Neutrophils are the most abundant white blood cell and play an essential role in many, if not most immune responses. As such, we suspect neutrophils play an indispensable role in the increased infection rates observed in patients with high shear conditions. We hypothesize that:

1. Transient exposure to high shear causes alterations to the state of the neutrophil, inducing an activated neutrophil phenotype
2. Transient exposure to high shear causes abnormal rolling behavior, leading to less stable neutrophil rolling with increased rolling velocities, resulting in reduced neutrophil infiltration to sites of infection
3. Transient exposure to high shear decreases neutrophil phagocytic function, reducing the neutrophil's ability to fight infection

A microfluidic platform provides many advantages over “traditional” shear assays, including cone and plate viscometers, as well as larger parallel plate flow chambers. Poly-dimethyl siloxane (PDMS) microfluidics are highly customizable, and thus can be adapted easily for different shear rate regimes, as well as the desired effector function to be studied. New molds can be created with well-established photolithography techniques. The efficacy of microfluidics hinges on

well-established flow profiles, especially for shear or adhesion based studies. Techniques in recent years, such as microparticle image velocimetry (μ PIV), have emerged that allow for experimental characterization of the fluid profiles. Chapter 2 discusses the microfluidic device design to be used throughout the rest of the chapter. We describe the μ PIV characterization of the channels' velocity profiles and corresponding shear rate estimations. We present a simple and easy to use method of glass embeddation to support high aspect (W:H) ratio PDMS channels. We examine elevated flow rates to compensate for the high pressure drops in the longest constricted length channels, and evaluate the potential presence of recirculation zones in the exit of the constriction.

One of the first steps for neutrophils in the bloodstream is the emigration at sites of inflammation. The initial capture of neutrophils and other leukocytes is governed by the interaction of selectins and their ligands. The PSGL-1 / P-selectin combination is responsible for the initial capture and rolling. We examine potential defects in this step, using the microfluidic devices, in chapter 3. The rolling study presented provides one of the first glimpses into functional changes following short exposure to high shear. Shear rates in this section were under $10,000 \text{ s}^{-1}$. Based on the results observed, it is suspected that with increasing shear rates the critical exposure time causing the alterations in the rolling behavior will decrease.

Following migration from the bloodstream, neutrophils have a variety of functions in clearing pathogens and in signaling the recruitment and activation of other cell types. We expand the study in chapter 4 to examine the neutrophil state

with a broad variety of markers throughout the cell and on the cell surface. We simultaneously move into a higher shear rate, lower exposure time regime; these conditions are reminiscent of very severe stenoses and conditions in devices such as VADs. We utilize a high throughput analysis method, flow cytometry, to quickly analyze multiple shear conditions in parallel. We adapt these methods for intracellular staining of granule components. We include surface receptors for each granule type as well, except for the primary granules, which contain content that is generally released either into the phagosome or into the extracellular space. However, to supplement that granule, we also use confocal imaging to visualize the state of the granules. By incorporating an examination of actin content, we further examine potential cytoskeleton changes hypothesized to occur in chapter 3 as the cause of the increased rolling velocities. We also examine a second functional assay, using a flow cytometry based phagocytosis assay.

Throughout this thesis we introduce evidence that indicates an alteration in the neutrophil state with short exposures to high shear, for flow rate regimes not previously examined. The objectives are as follow:

1. Design constricted microfluidic devices to expose cells to pathological ($> 3,000 \text{ s}^{-1}$) shear rates
2. Characterize and compare experimental velocity profiles with the theoretical profiles
3. Examine the effect of high shear ($\sim 5,000 - 10,000 \text{ s}^{-1}$) on neutrophil rolling behavior

4. Investigate neutrophil activation state after extremely high shear rates
(80,000 – 100,000 s⁻¹)
5. Evaluate phagocytic function after short exposures to high shear rates
(80,000 – 100,000 s⁻¹)

Chapter 2: Channel Design and Characterization

Portions of this chapter were reproduced in part with permission from:

Springer Nature: *Cellular and Molecular Bioengineering*, Lewis, C.S., N.Z. Alsmadi, T.A. Snyder, and D.W. Schmidtke. Effects of Transient Exposure to High Shear on Neutrophil Rolling Behavior. Copyright 2018.

Alsmadi, N.Z., S.J. Shapiro, C.S. Lewis, V.M. Sheth, T.A. Snyder, and D.W. Schmidtke. Constricted microfluidic devices to study the effects of transient high shear exposure on platelets. *Biomicrofluidics* 11:64105, 2017, with the permission of AIP Publishing

Introduction:

Microfluidic devices have emerged as a powerful and simple benchtop tool for studies in a wide range of areas, and with flow conditions that were previously unattainable. In the context of blood related biological studies, microfluidics vastly reduce the amount of blood required (<200 μL), which even allows studies to use blood from small animals (e.g., mice, rats). Current commercial microfluidic technologies often operate using less than 100 μL of fluid¹⁹⁸. It also allows for many conditions to be run simultaneously with the same donor in parallel. Previous techniques generally required larger volumes (few mLs) that would thus be unattainable, and often require studies such as those with bovine blood or cultured cells²⁴⁹. Furthermore, the extremely high shear rates now of interest for VADs and stenosis increase the flow rates significantly. In addition to reducing the material amount/costs, microfluidics offer a simple way for a high level of control over fluid dynamics in the laminar flow regime relevant to the human

cardiovascular system, such as the applied shear rate or, for the example of this thesis, the exposure time to various shear rates.

PDMS has become one of the most prominently used materials for microfluidic chambers since its development⁸⁰. This comes from a variety of factors such as low costs and rapid, reusable casting. Fabrication for PDMS devices is very simple and does not require an extensive amount of specialized equipment or training²⁸⁶. Designs are almost as endless as the imagination, and thus can allow for complicated combinations of fluid conditions. In addition, PDMS is air permeable and is compatible for long term cell culture, and can be combined with other various materials quite readily. It also has good optical clarity to allow for direct imaging into the device. As such, it has become the standard material throughout the microfluidic research field²⁸⁰. Finally, should more rigid structures or chemical compatibility be necessary, there are a few other material options that can replace PDMS for microfluidic applications. Materials such as polyurethane methacrylate and thermoset polyester, can be fabricated with similar replica molding techniques^{165,286}. Another recent technique developed a liquid polystyrene that can be cast using PDMS based molds, and thus shares many similarities with existing fabrication²²³.

There are other, more “conventional”, or at least traditional, assays for exposures to shear, which have allowed for the study of various types of blood cells under high shear conditions. Much work has been done, especially in the relevance of platelets and erythrocytes but also for neutrophils, primarily using cone and plate viscometers^{7,52,91,104,110,111,136,235,265,282}. Cone and plate

viscometers consist of a flat plate and a rotating cone with a very large obtuse angle. They are typically used because they create a uniform shear profile across the device, unlike the varying shear rate present in a couette viscometer²⁰⁶. While simple to use and with well-defined shear profiles, cone and plate viscometers are lacking for some of the most relevant, and perhaps least well understood, cardiovascular conditions: specifically the types of events discussed in this thesis in terms of stenosis, current blood contacting devices (e.g., VADs), and arteriosclerosis. While cone and plate viscometers can achieve virtually any of the shear rates relevant to such conditions, and while the current versions have improved upon the issue of blood quantity required, the exposure time remains virtually impossible to recreate at the scale relevant for such studies. Cone and plate viscometers have been used to study conditions down to as low as 1 minute in recent studies of neutrophils and to a few seconds for platelets¹¹⁰. For example, the work by Mitchell et al. used such conditions to examine important neutrophil receptors sensitive to shear^{214,215}. Despite the recent advances, the exposure time for most of these types of devices is still several orders of magnitude higher than pathological cardiovascular conditions, especially for a single pass exposure. However, there have been other devices created; one recent study created a custom syringe capillary viscometer to study repeated exposures to high shear with exposure times as low as 25 msec. Although, this device still used up to 5 mL of isolated platelets²⁷³. The studies with longer exposure times might demonstrate the type of effect that could occur from compound (multiple, sequential) exposures to high shear. However, additional devices and studies are

needed that will allow for each individual pass to experience low exposure times, and the study of how such repeated exposures compound the shear effect. Microfluidics are posed to answer these questions, yet to the author's knowledge there has been only one study to date using such a type of system to study high shear ($>3,000 \text{ s}^{-1}$) effects (on neutrophils), and this still used a larger glass capillary tube⁴⁶. Some studies have used parallel plate flow chambers, primarily to study neutrophil adhesion^{31,211,242,251,263,329,330}. While these are simple and commercially available, flow rates are too high and require too much blood to be usable for high shear applications. Some recent work in the microfluidic field has focused on the creation of microfluidic rheometers, but so far these devices have been applied for measurements (e.g., viscosity) rather than for shear application^{117,237,249}.

Microfluidic devices with constrictions and stenoses have been previously created and utilized, and allow for the study of atherosclerotic shear rates. However, these studies have almost exclusively focused on platelets. For example, a study by Colace et al. used a constricted channel to study the effect of high shear rates on von Willebrand Factor (vWF) unfolding⁶⁰. The unfolding of vWF, and subsequent cleavage by ADAMTS13, is believed to play an integral part in the bleeding deficiencies observed in VAD patients. The Ku group has used stenotic devices to examine several factors related to thrombosis in pathological conditions ($> 2,000 - 6,000 \text{ s}^{-1}$) mimicking arterial stenosis. These devices consisted of both glass capillary tubes and PDMS microfluidic stenotic devices. Using these stenotic devices they were able to predict high shear

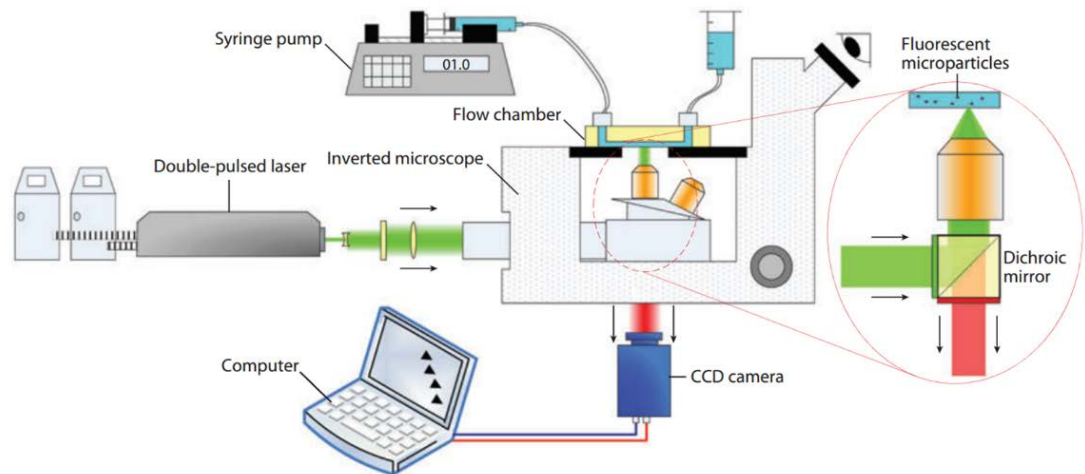
thrombus growth²⁰⁷, correlate thrombosis growth rates with wall shear rates²⁶, examine platelet deposition with high shear rate, pulsatile flow⁴⁸, and examine the role of vWF in high shear thrombosis⁴⁷. They even used these devices to examine anti-platelet therapies, to examine the effect on thrombus formation and occlusion within the device^{116,180}. A study by Ha et al. performed velocity measurements in a similar style of constricted channel and examined flow velocities and circulation zones at different Reynold's numbers, as well as the effect of these regions on platelet adhesion¹¹⁹. In addition, other groups have studied atherosclerotic conditions with adaptations of the constricted design, by having a short, circular stenosis style constriction. For example, Westein et al., created a microfluidic stenotic device to mimic stenosis in the carotid artery, with shear rates up to $8,000 \text{ s}^{-1}$. They examined the effect of such a stenotic region on thrombus formation, by patterning vWF and fibrinogen strips. This design allowed them to examine platelet aggregation and the tendency for thrombus formation in the post-stenosis region³²³. A unique microfluidic system was implemented by Mannino et al., who used PMMA fibers to create cylindrical channels embedded in a slab of PDMS. The geometry could be manipulated by the removal of a section to create a stenosis, or adding/fusing fibers to create bifurcations. They demonstrated the functionality of such devices with seeded endothelial cells and the adhesion of platelets and erythrocytes in different regions of the devices¹⁹⁶. The microfluidic field has been expanding rapidly in recent years, and as seen here, a variety of techniques can be used to examine cardiovascular conditions.

Due to the importance of shear rate and exposure time for the work described in this thesis, it is important to verify the shear rate at each of the regions of interest in the channel. Estimates for wall shear rates in rectangular channels can be made from analytical solution of the Navier Stokes equation and related approximations, but there are a variety of variables that can affect the shear rate along the channel length. Many of these factors are very difficult to account for, and things such as the pressure drop are more prevalent for the small dimensions present in microfluidics, especially with high flow rates. Combined with long constriction lengths, high pressure drops can alter the velocity in the channel, and therefore the shear rate deviates from that expected from theoretical calculations. The longest channels in this study, designed for exposure times greater than 50 msec at shear rates in excess of $80,000 \text{ s}^{-1}$, are prone to this high resistance to fluid flow (Cons. F and G in Fig. 2.2). As such, for high velocity conditions such as those presented throughout this thesis, velocity and shear rate estimations can be quite difficult. However, recent advances in digital cameras and electronics has allowed for great steps in systems designed to measure velocities. Particle image velocimetry (PIV), a technique established more than 30 years ago for macroscopic flows³, has emerged in recent years for applications on a much smaller scale with studies investigating flow profiles in microfluidic devices, and even in some in vivo systems^{209,247,261,277}.

Micro-PIV tracks the locations of small particles, of sufficiently small size to move with the fluid flow. A fast firing double pulsed Nd:YAG laser (pulse duration of $\sim 10 \text{ ns}$) illuminates the beads twice successively with a defined

exposure time between images. Automated programs track the location of the particles between paired frames, with images divided up into a grid of interrogation windows. The exposure time is chosen such that the particles ideally move about a quarter of the grid window size, so that the majority of particles remain within each grid. A cross correlation method is used to determine the displacement for particles in the pair of images in each interrogation window, with the displacement (pixel shift between images) corresponding to the highest peak in the correlation plane (Figure 2.1B). Essentially, the product of the intensities between shifted images are summed over the total particles in the interrogation window, with the highest peak corresponding to the shift where all (or the majority) of the particles are aligned. The presence of multiple particles in each interrogation window helps increase the accuracy of this technique. This determined displacement is then averaged over the series of image pairs. The individual vectors for each grid comprise the velocity field, examples for the constricted channel are shown in Figure 2.4. The accuracy of such techniques requires an illumination and capture source that can operate on the nanosecond scale^{183,322}.

(A) PIV Setup



(B) Cross-Correlation

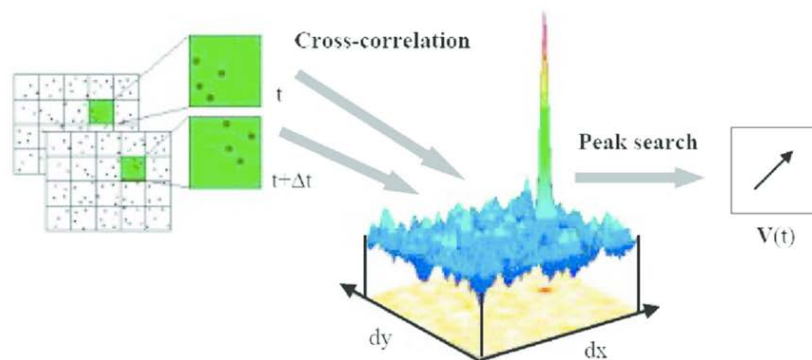


Figure 2.1: μ PIV Schematic: setup and cross-correlation. The top panel (A) shows a typical μ PIV setup with a double pulsed laser system and inverted microscope; a similar system is used in this thesis. (B) Shows the cross-correlation method for an example pair of images at time t and $t + \Delta t$, in which particle displacement is examined for each interrogation window. The displacement is determined from the highest peak in the cross correlation plane. Dividing this displacement by the time provides the velocity vector for the interrogation window. (A) Republished with permission of Annual Reviews, from *Recent Advances in Micro-Particle Image Velocimetry*, Wereley and Meinhart, Volume 42, 2010; permission conveyed through Copyright Clearance Center, Inc. (B) from Deng et al.⁶⁹

In this chapter, the microfluidic system to be used throughout the thesis to examine neutrophil state and function following short exposures to high shear is described. As can be seen in Figure 2.2, the PDMS based device consists of low shear regions flanking a high shear constriction, to allow for the simultaneous study of cell adhesion, with a controlled exposure to high shear. The shear rates were chosen to represent physiological levels in the upstream and downstream regions for adhesion studies, and higher pathological shear in the constrictions. A μ PIV system is used to characterize the velocity profiles throughout the various regions of the device. This profile is then used to calculate fluid dynamic variables, such as the wall shear rate and exposure time. There are three main sets of channels / conditions to be introduced: the 125-5900-125 s^{-1} channels, the 90-8600-90 s^{-1} channels, and the 2400-100,000-2400 s^{-1} channels. The shear rates for each set of channels represent the values in the upstream, constricted, and downstream regions (Up-Con-Down). The first two sets of channels are used in chapter 3 to examine neutrophil rolling, while the last will be used for a variety of tests designed to examine neutrophil state and function in chapter 4. The last set of channels was also used to study both platelet activation and aggregation following short exposures to high shear^{10,133}; these reports and the follow up studies (in progress) are outside of the scope examined in this thesis. In the current chapter we will also further discuss the general design components of the device, and a simple adaptation to reduce collapsibility in the highest aspect ratio channels.

Methods:**Materials:**

PDMS (Sylgard 184, Dow Corning) was purchased from Krayden. Elbow and connecting pieces were purchased from Value Plastics Inc. (Fort Collins, CO). Glass coverslips No. 1.5 (50 x 45 x 0.16-0.19 mm L x W x H) and No. 2 (50 x 45 x 0.17-0.25 mm) were purchased from Fisher Scientific, while glass slides (3 inch x 1 inch x 1 mm) were purchased from VWR. 0.5 and 1 μm fluorescent particles (Fluospheres, polystyrene, red 580/605) for μPIV experiments were purchased from ThermoScientific. The PIV laser system was acquired from TSI (Shoreview, MN).

Photolithography:

PDMS based microfluidics were created from master molds fabricated through standard negative photolithography techniques. KMPR 1050 photoresist (MicroChem, Westborough, MA) was first poured onto silicon wafers and a 60 μm layer was created via spin coating. The wafer was baked at 100 $^{\circ}\text{C}$ for 20 min and then exposed using UV light for 12 $\text{mJ}/\text{cm}^2\text{s}$. The wafer was post-baked for 4 min at 100 $^{\circ}\text{C}$ and then developed for 5 min in SU-8 developer (MicroChem). Prior to PDMS pouring the wafer was coated with (Tridecafluoro-1,1,2,2-Tetrahydrooctyl) Methyl dichlorosilane for 6 hours, for easy release of the PDMS. A more detailed method can be found in Appendix B.

PDMS microfluidics:

PDMS devices were made from a 1:10 (w:w) ratio of curing agent to base. PDMS was mixed and poured over the photolithography molds. PDMS was allowed to degass for one hour in a desiccator at room temperature. Elbow pieces were placed at one end to form the inlet or outlet of the device, depending on the experiment to follow. For higher shear applications, metal rods were put in place of the elbows. Molds were placed in an oven at 80°C for an hour to cure. For high shear devices, the metal rod was then removed and tubing was inserted. Additional PDMS was poured on top of the device around the tubing, and then desiccated and cured as before. An example of this process from our lab can be found in Lam et al.¹⁶⁹. Devices were then cut out and kept in a desiccating box until use.

Prior to sealing, devices were cleaned with tape to remove any residual dust. Channels for rolling experiments were placed on coverslips and sealed with a vacuum line. For high shear conditions (80,000 s⁻¹ and above), devices were first cleaned in acid. This consisted of a series of washes with 10% HCl, 100% acetone, and 100% ethanol for five minutes each. Stamps were thoroughly rinsed with water and allowed to dry for 30 minutes at 80°C. PDMS stamps and glass coverslips (No. 1.5) were placed in a PDC-32G plasma cleaner (Harrick) for 1 minute on high RF power (18 W). Stamps were sealed immediately to the glass coverslips and allowed to sit for 2 days before use. For channels with elbow piece connections, silastic tubing was attached to the elbow piece, and a layer of epoxy was poured on top of the device, around the elbow piece. The epoxy surrounds

the elbow piece, to help strengthen this potential vulnerability from leaks. The epoxy support is almost identical to the extra PDMS poured around the embedded tubing for the long exposure time devices, as was described above.

Flow characterization of microfluidic channels:

The shear rate and exposure time in the constricted region were controlled by both the channel dimensions and the perfusion flow rate. Theoretical velocity profiles and wall shear rates were calculated based on the channel dimensions using an approximation for rectangular die with low aspect (width: height) ratios²⁸⁷. More detail about this approximation can be found in Appendix A. Experimental velocity profiles in the channels were measured using a microparticle image velocimetry (μ PIV) system. A double pulsed Nd:YAG laser was used to illuminate 1 μ m fluorescent beads (Molecular Probes, Eugene, OR). The velocity of the fluorescent beads was measured at three regions: 3.5 mm upstream of the constriction, 3.5 mm downstream of the constriction, and within the center of the high shear constriction. In the upstream and downstream regions of the microfluidic channels, z planes at 5 μ m intervals were taken to characterize the velocity profile from the channel floor to the center region of the channel, while in the constricted region z planes were taken throughout the entire height. To ensure accuracy of the z position, a low density of 0.5 μ m beads (1:100) was first introduced into the channel and allowed to adhere to the top and bottom walls for 5-10 minutes prior to start. For each z position, the bottom wall was determined by focusing on this bottom layer of beads, and then moved to the corresponding position with the automated z control of the microscope.

Fluorescent images of the beads were taken using a Zeiss AxioObserver microscope equipped with a 40x oil objective (1.4 NA), a 16MP PowerView camera, and a synchronization controller. A high aperture objective is essential for accurate measurements to reduce out of focus effects. The delay between laser pulses was set from 0.4-2,000 μs depending on the location within the channel and the flow rate. A pixel binning spot size of 64 was used. Velocities were determined using Insight 4G software. Velocity profiles and wall shear rates were then subsequently created and calculated in Matlab.

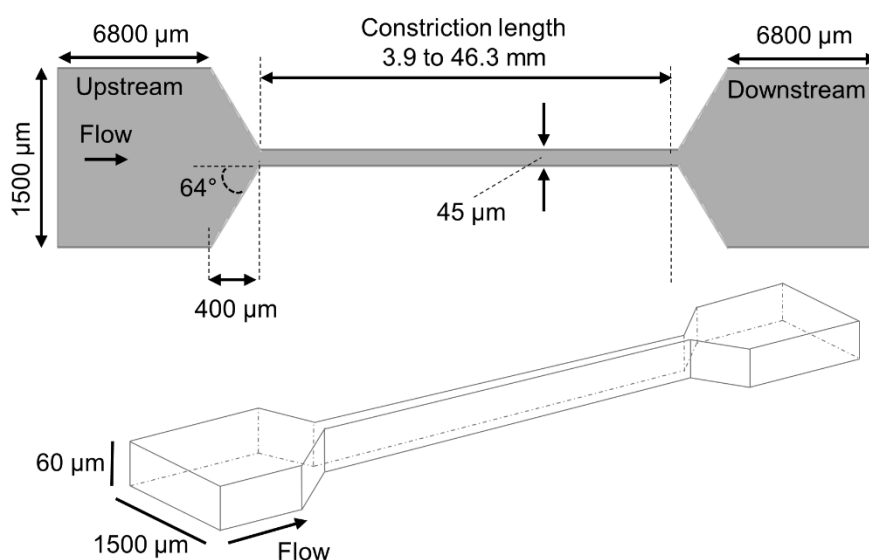
Results and Discussion:

Channel design:

Channels were created to allow for the analysis of high shear rates utilizing small sample sizes, a prerequisite for studying human samples. The design centers on a constricted region for introducing these shear rates with a well-defined exposure time. In addition, the devices contain two low shear regions flanking the constriction. A schematic of the channel design is shown in Figure 2.2. This design allows for adhesion and rolling based studies to occur in the same devices as the shear exposure, something not possible with many other shear exposure methods. The cells remaining in the same device also greatly decreases the potential for artifacts from handling and time delays.

This shear inducing constricted channel is a simple and relatively easy to fabricate design. In the current study, we implement shear rates to mimic pathological shear conditions ($>3,000 \text{ s}^{-1}$) and extremely high shear rates ($>10,000 \text{ s}^{-1}$)⁷⁷. We first had to choose a set of dimensions. A 33:1 (upstream width: constricted width) ratio allows for adhesion under venous/arterial conditions, and high shear exposure to pathological shear. While the ratio was maintained constant between the upstream/downstream regions and the constriction, the widths were adjusted. Constriction sizes tested were 15, 30, 45, and 60 μm , with a height of 60 μm . These provide dimensions comparable to smaller venules and arterioles, which range from approximately 10-100 μm ^{195,241}. Based on several factors the 45 x 60 μm (constriction width x height), 1500 x 60

μm (up/downstream width x height) channel was chosen; this provided a balance between the volume of blood required, potential clogging issues, and expected rolling velocity, among other variables. The angle was chosen in an attempt to reduce the formation of recirculation zones in a fast expansion area, and based on some of the previous constricted channel devices in the literature that were used for platelet studies^{60,119}.



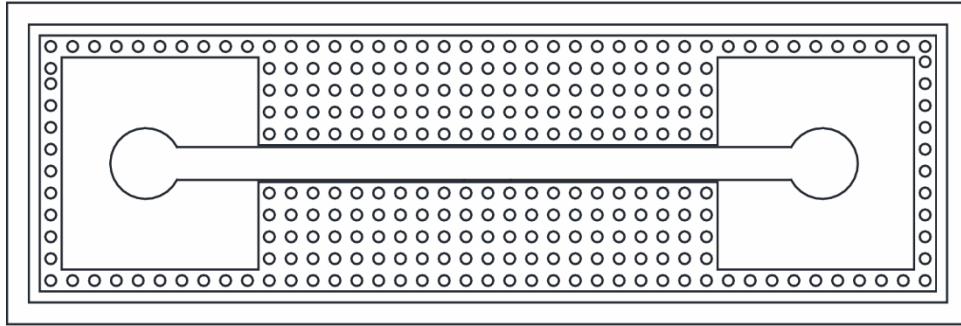
Channel Type	Upstream Width	Constricted Region Length	Constricted Region Width	Downstream Width
Straight A	1500 μm	NA	NA	1500 μm
Constriction B	1500 μm	3.9 mm	45 μm	1500 μm
Constriction C	1500 μm	7.7 mm	45 μm	1500 μm
Constriction D	1500 μm	11.6 mm	45 μm	1500 μm
Constriction E	1500 μm	15.0 mm	45 μm	1500 μm
Constriction F	1500 μm	38.6 mm	45 μm	3000 μm
Constriction G	1500 μm	46.3 mm	45 μm	3000 μm

* Channel height: 60 μm

Figure 2.2: Schematic of the constricted microfluidic channels and their dimensions.

Initial adhesion experiments used a one sided plasma cleaning method which could provide a seal for a short time. However, this method was not reliable consistently and led to leaking issues. To fix sealing concerns, a vacuum design was implemented, based on previous work²²⁸. Surrounding the channel is around 5 mm of empty space to create a vacuum seal around the channel. Posts embedded within this region support the PDMS and prevent collapse from the vacuum, which is introduced via tubing and supported by an external vacuum pump. Posts are 500 μm wide with 500 μm spacing. The vacuum design allows for a reversible seal, essential for the combination with adhesion based experiments such as that presented in chapter 3, as the deposited protein cannot survive the plasma cleaning process (will be etched away). There are ways in which proteins can be protected during the plasma cleaning process²⁶², although the protein is still vulnerable to changes in concentration, leaving these methods as a potential source of added variability. Similar vacuum incorporating designs have been demonstrated for such adhesion applications, although without the high shear regions^{24,263}. A schematic of the device is shown below in Figure 2.3. For higher shear applications in which the devices are permanently bonded, the vacuum design does not interfere, allowing for the same masks to be used for all applications presented in this thesis.

(A) Straight Channel A



(B) Constricted Channel D

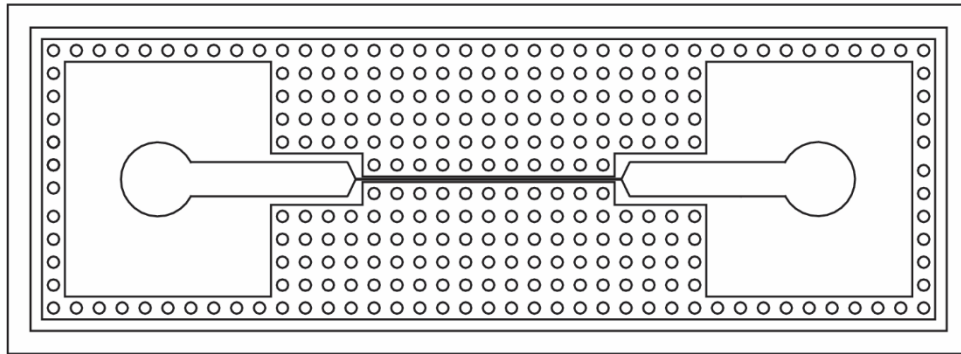


Figure 2.3: Schematic of the channels with the incorporated vacuum design for a temporary seal. Circles become posts in the PDMS stamp and support the vacuum in the surrounding empty space. Posts are 500 μm wide with 500 μm spacing.

Shear rate estimation:

The shear rate depends on both the physical dimensions, as well as the velocity of the fluid in the channel. We have chosen a range of shear rates for our study, as well as the channel dimensions, to mimic the pathological shear rates in conditions of interest (e.g., stenosis, VADs). We thus need an equation to correlate these variables with the flow rate. Commercial flow chambers and other commonly used devices in the microfluidic field often have aspect ratios equal to or greater than 10:1 width: height, and it is assumed that the solution to the Navier

Stokes equation reduces to a so called rectangular approximation when the width is sufficiently large compared to the height⁵⁸. However, the low aspect ratio design for the constricted region in these experiments does not fit within this approximation, and therefore we cannot use the reduced form of the solution to estimate the flow rate. Other groups have examined the shear rate in rectangular die, with aspect ratios close to one. We use the solution from one such study, to be able to approximate the wall shear rate in the channels, in which the equation is given by²⁸⁷:

$$\gamma_w = \left(\frac{6Q}{WH^2}\right) \left(1 + \frac{H}{W}\right) f^*\left(\frac{W}{H}\right) \quad \text{Eq. (1)}$$

Where the function $f^*(H/W)$ is given as:

$$f^*\left(\frac{H}{W}\right) = \left[\left(1 + \frac{1}{x}\right)^2 \left(1 - \frac{192}{\pi^5 x} \sum_{i=1,3,5,\dots}^{\infty} \frac{\tanh\frac{\pi}{2}ix}{i^5}\right) \right]^{-1} \quad \text{Eq. (2)}$$

H, W, and Q are the height, width, and flow rate respectively. This equation is used for almost all the channels throughout the study for calculations of the necessary flow rate. We will later also estimate the shear rates based on the velocity profiles with parabolic fits for the theoretical and experimental curves and compare the results in Table 2.2.

PIV analysis: analytical solution

In order to determine the fluid velocity and shear rate profiles in the microfluidic channels, both theoretical and experimental analyses were performed. The theoretical velocity profiles in the microfluidic channels were calculated using the Navier Stokes (NS) equation for a rectangular channel. This

equation can be simplified to and solved for the velocity at a position y and z from the center of the channel²³¹:

$$v_x = \frac{16a^2}{\mu\pi^3} \left(-\frac{dp}{dx} \right) \sum_{i=1,3,5,\dots}^{\infty} (-1)^{(i-1)/2} \left[1 - \frac{\cosh(i\pi y_c/2a)}{\cosh(i\pi b/2a)} \right] \frac{\cos(i\pi z_c/2a)}{i^3} \quad \text{Eq. (3)}$$

Here, y_c is the position from the center of the channel moving towards the side walls, z_c is the height position from the center of the channel, a and b are half of the height and width of the channel respectively, μ is the viscosity, and p is the pressure. Integration of Eq. (3) results in a solution for the volumetric flow rate:

$$\dot{Q} = \frac{4ba^3}{3\mu} \left(-\frac{dp}{dx} \right) \left[1 - \frac{192a}{\pi^5 b} \sum_{i=1,3,5,\dots}^{\infty} \frac{\tanh(i\pi b/2a)}{i^5} \right] \quad \text{Eq. (4)}$$

Rearranging Eq. (4) for the pressure drop (dp/dx) and substituting into Eq. (3) allows for the determination of theoretical velocity profiles over the width and height of the channel. The viscosity of the system (beads or isolated neutrophils) was assumed to be 1 cP.

PIV experimental analysis: “low” shear rate for rolling studies

We begin our experimental μ PIV analysis with the “low” shear, 5900 s^{-1} condition, with channels A and D (straight channel and long exposure shear channel). In chapter 3, we use these shear conditions to investigate the effect of short exposures to high shear on neutrophil rolling. This condition corresponds to a flow rate of $5 \mu\text{L}/\text{min}$. Figure 2.4 shows the theoretical and experimental fluid velocities determined for three regions of the microfluidic channel D: the low shear upstream region, the high shear constriction region, and the low shear downstream region. As shown by the theoretical curves (Fig. 2.4), in the low shear regions of the channel, the rectangular design produced a constant velocity

profile over approximately 90% of the channel, creating a uniform wall shear rate. In contrast, the constricted region exhibited a parabolic velocity profile in both the y and z directions, creating a range of velocities depending on the cell position. The experimental velocity profiles were determined by performing microparticle image velocimetry (μ PIV), using a synchronized, double pulsed PIV system to track the positions of fluorescent particles. Figure 2.4 shows representative velocity profiles in the xy plane that were acquired by μ PIV for the upstream region (Fig. 2.4A), constricted region (Fig. 2.4B), and downstream region (Fig. 2.4C) of a microchannel.

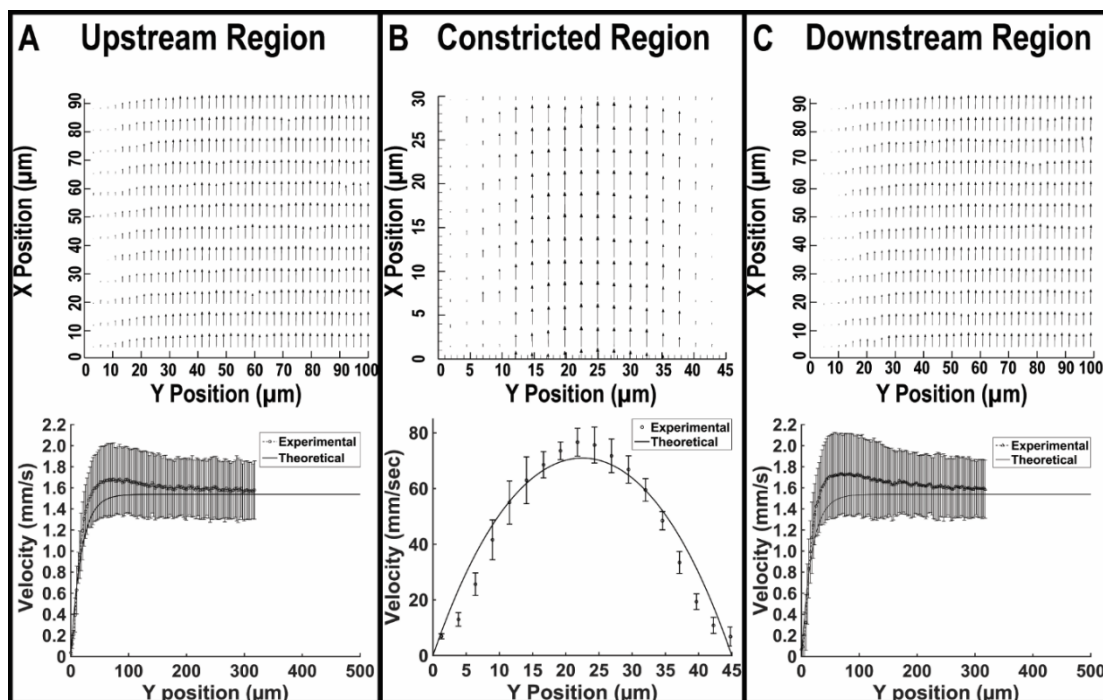
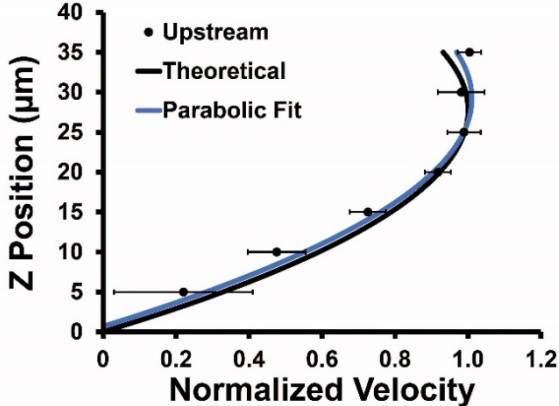


Figure 2.4: Representative velocity vectors and profiles in a constricted microfluidic channel. The velocity vector maps (top panel) are shown for a Type D constricted microfluidic device at (A) a position upstream of the constriction, (B) in the middle of the constricted region, and (C) downstream of the constriction for $z = 30 \mu\text{m}$. The bottom panel compares the theoretical values for the velocity profiles to the experimentally measured velocity profiles near the wall for the upstream and downstream locations and throughout the constricted region.

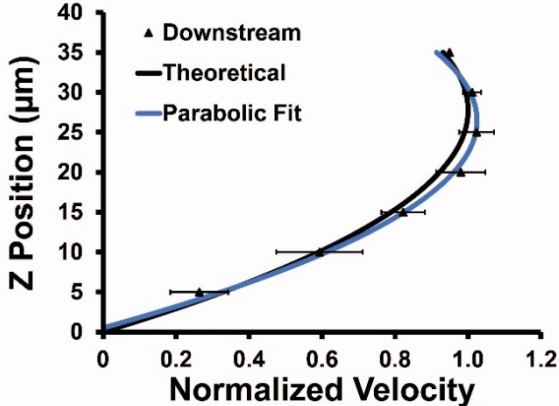
In order to measure the 3-D velocity profile, the focal plane of the microscope was moved vertically from near the bottom wall to the center of the channel, and velocity measurements in the xy plane were taken at several different heights. Measurements near the wall, while theoretically ideal for wall shear rate calculations, are known to be difficult to measure accurately and tend to be more prone to error²³⁰. Thus, velocities were measured at several z positions away from the wall, with the z position defined as the distance from the bottom wall. Because of the symmetry present in the flow profile, approximately half of the channel height was measured in the upstream/downstream regions, past the maximum velocities at the center. Figure 2.5 shows the results of the μ PIV measurements in the upstream, downstream, and constricted regions of a type D microfluidic device and compares them to the theoretical predictions. Velocities were normalized to the maximum velocity of the theoretical curve, so that the centerline velocity of the theoretical curve equals one. As can be seen, we observed good agreement between the upstream (Fig. 2.5A) and downstream (Fig. 2.5B) velocity profiles with the theoretical profiles, and between the μ PIV measured and theoretical velocity profile in the constricted region (Fig. 2.5C). The similarities between the upstream and downstream velocity profiles in the constricted channels suggest that any pressure drop due to the constricted regions had a minimal effect on the downstream velocity profile. We also observed good agreement between the theoretical and experimental curves for

straight channel microfluidic devices (Fig. 2.6), and no significant difference was observed in the velocity profiles of the upstream and downstream regions.

A) Constricted Channel: Upstream



B) Constricted Channel: Downstream



C) Constricted Region

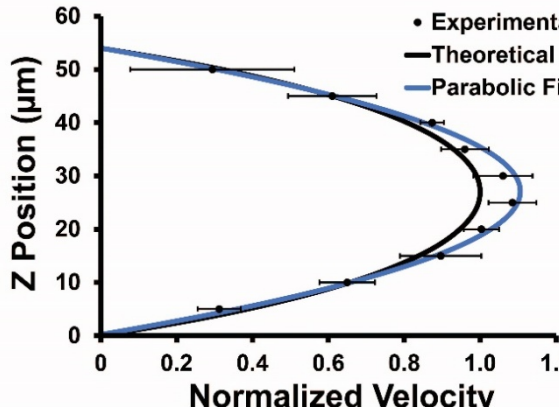
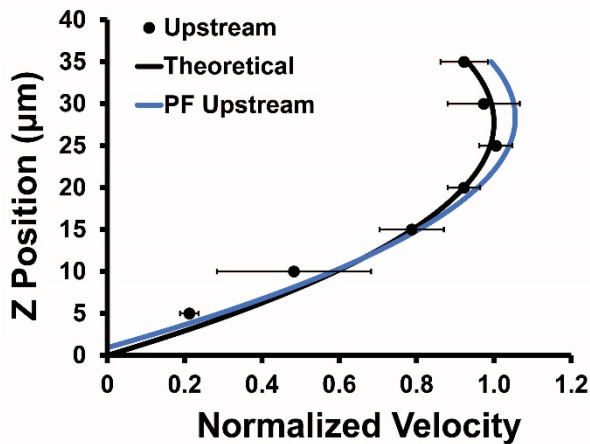


Figure 2.5: Velocity profile for a constricted microfluidic channel. Experimental velocity profiles measured by μ PIV in a constricted microfluidic channel (Type

D) at an (A) upstream, (B) constricted region, and (C) downstream location are compared to the analytical solution for flow through a rectangular channel and a second-order polynomial fit to the experimental velocity measurements. Velocity profiles are normalized to the maximum centerline value of the theoretical curve.

Wall shear rates were calculated by fitting a parabolic regression to the measured velocities to estimate the curvature^{141,209,230}. The derivative of this second order fit, plugging in the z position at the wall (0 μm), provides the wall shear rate. Parabolic fits of the upstream and downstream regions of the straight microfluidic channels (Str. A, Fig. 2.6) provided an estimated shear rate for the upstream region of $122 \pm 30 \text{ s}^{-1}$ and a shear rate of $123 \pm 14 \text{ s}^{-1}$ for the downstream region. These values were similar to the theoretical value of 125 s^{-1} . For the constricted microfluidic channels, the parabolic fits of the upstream and downstream regions of constricted microfluidic channel D (Fig. 2.5) provided estimated shear rates of $111 \pm 21 \text{ s}^{-1}$ (upstream) and $124 \pm 16 \text{ s}^{-1}$ (downstream), which were similar to the theoretical value of 125 s^{-1} . Parabolic fitting of the μPIV measurements in the constricted region estimated the wall shear rate to be $5900 \pm 300 \text{ s}^{-1}$.

A) Straight Channel: Upstream



B) Straight Channel: Downstream

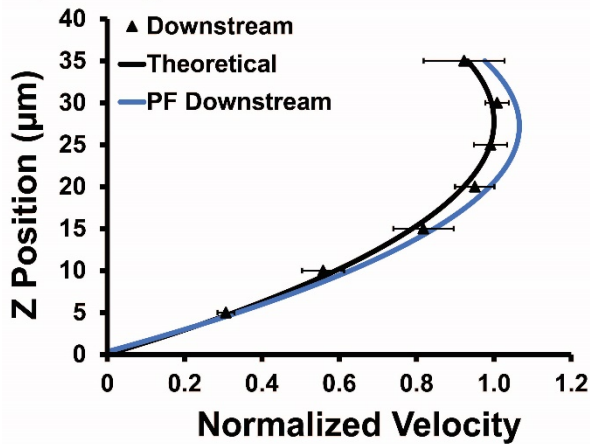


Figure 2.6: Velocity profile for a straight channel microfluidic. Experimental velocity profiles measured by μPIV for a type Str. A channel at (A) the upstream region and (B) the downstream region are compared to second order polynomial fits of the experimental data and the analytical solution

Exposure time:

The exposure time is a critical component used throughout this thesis and corresponding papers. The microfluidic device allows for the simple modification of this shear exposure time as a direct function of the constriction length (L). The average exposure time is calculated based on the ratio of the constriction volume

to the volumetric flow rate (Q), or equivalently of the length to the mean fluid velocity (v):

$$\tau_{exp} = \frac{L*W*H}{Q} = \frac{L}{v} \quad \text{Eq. (5)}$$

While this is a relatively simple value to calculate, it can be affected by changes in velocity from pressure drops across the channel. We can adjust the estimate for this value from the collected μ PIV data. We can use the change in velocity from the theoretical profile to the experimental μ PIV velocity, and assume a linear relation for the centerline velocity and the average velocity (and therefore the flow rate). Increasing/decreasing the flow rate by this percentage provides the approximate flow rate, and therefore a new calculated exposure time. Using the μ PIV data collected from Con. D, we estimate the exposure times for channels B-E to be 100, 210, 310, and 390 msec. It is important to note that this is a calculated value that is based on the average flow rate and is therefore an average transit time for the cells passing through the constriction. The exposure time for individual cells will vary due to their velocity, which depends on their position from the walls. Since the flow is laminar, cells will maintain this distance and velocity throughout the constricted region. Estimates for the exposure time as a function of the distance from the bottom wall can be created from the μ PIV data, by using the velocity at each of these points. Dividing the constriction length by this velocity provides an exposure time for each streamline position at intervals of 5 μ m moving up away from the bottom wall. The results of these exposure times can be seen in Figure 2.7.

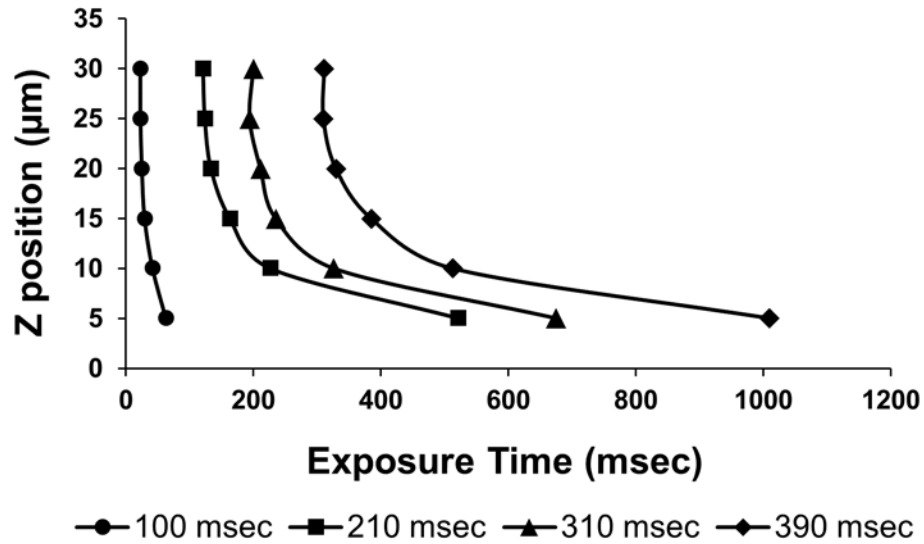


Figure 2.7: Exposure time as a function of z-position. Velocities at 5 μm z-intervals (height from the bottom wall) can be used to estimate the exposure time for a cell at that position, shown here for the wall shear rate condition of 5900 s⁻¹. Velocities are taken in the center of the channel along the width (y-direction) of the channel. Since the flow is laminar and the exposure time is short, we assume the z-position of the cells remains constant over the length of the constriction. Each curve represents a given channel length, for Cons. B-E, from left to right, labeled by the average exposure times.

Reynolds number:

The Reynolds number is a very typical and useful dimensional number to engineers in fluid mechanics applications. It is the ratio of inertial to viscous forces, and can be used to estimate the type of flow (i.e., laminar or turbulent).

The Reynolds number is given by the formula:

$$Re = \frac{\rho Q D_h}{\mu A} \quad \text{Eq. (6)}$$

Where Q is the flow rate, D_h is the hydraulic diameter, ρ is the density, μ is the viscosity, and A is the cross-sectional area. For the case of a rectangular channel

the hydraulic diameter is $4A/P$, with P being the wetted perimeter. The Reynolds numbers for the high shear conditions can be seen in Table 2.1. The Re numbers for the channels used in this study are well below the beginning of turbulent flows at around 2300. Only the highest shear conditions are shown since these will have the largest Re .

Table 2.1: Reynolds number for the high shear conditions (80,000-100,000 s^{-1}) in isolated cells and whole blood

Condition	Re	Re (Constriction)
	(Up/Downstream)	
Isolated Buffer	3.0	44
Whole Blood	0.81	12

PIV characterization: 125-5900 s^{-1} additional constricted channel lengths

Fluid flow in the microfluidic devices is driven by a pressure difference. For this shear rate set (125-5,900 s^{-1}), we use the withdraw feature; the plunger on the syringe is pulled to create a vacuum, and therefore a pressure driving force, which causes the fluid flow. There is a possibility that, with increasing constriction lengths, a significant pressure drop over the channel can cause a decrease in the velocity. For these flow rate conditions, we do not expect this effect to be significant. The similar velocities in the up/downstream regions of the constricted and straight channels (D and A) suggested that this was indeed the case, and that the constriction length did not cause any differences for the shear rates in this portion of the study. There is also a second possibility: that the pressure

causes deformation in the PDMS. We detected no evidence of deformation, which would have been most prevalent in the downstream region under these conditions (withdraw). We also did not see much variation from the theoretical velocity profile. We used the μ PIV system to examine the other constricted lengths, constrictions B, C, and E. Similar to Con. D, the velocity profiles for the other constrictions match up well with the theoretical velocity.

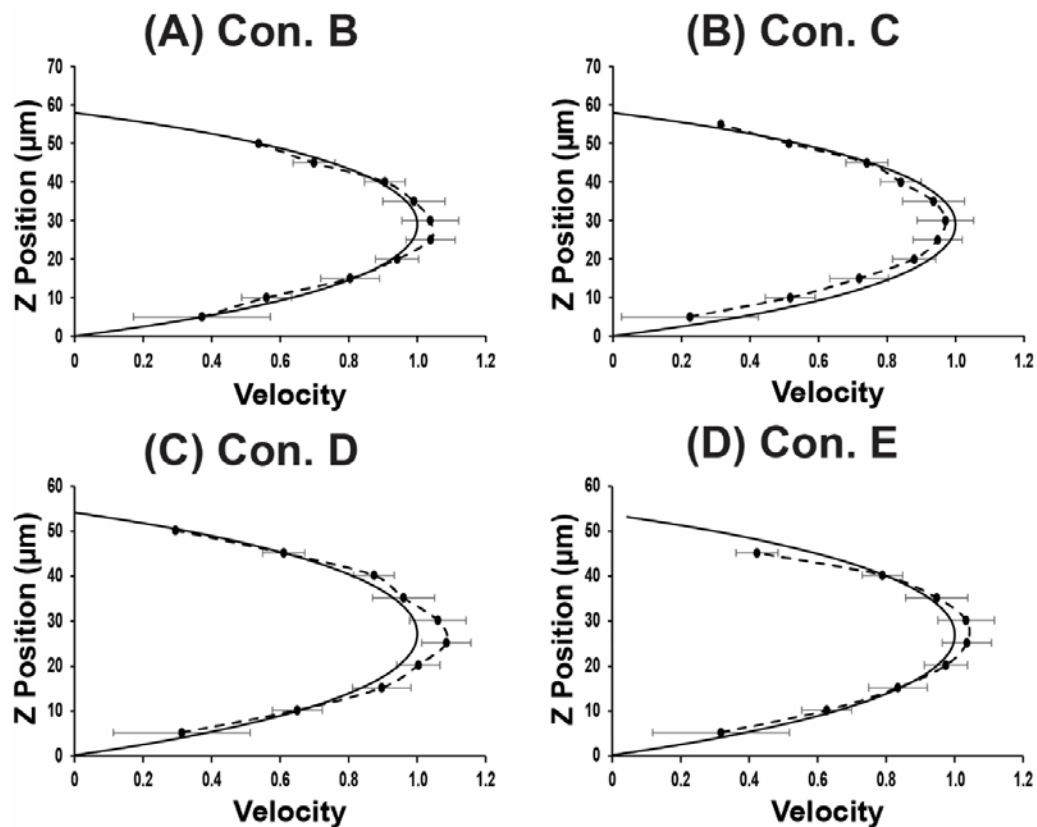


Figure 2.8: Velocity profiles of constricted channels B-E. Experimental and theoretical velocities are normalized to the theoretical profile for each channel. Constricted lengths for B-E are 3.9, 7.7, 11.6, and 15.0 mm, respectively. Exposure times for B-E are 100, 210, 310, and 390 msec.

Surprisingly, we saw a slight difference in the shear rate between channels B/C and D/E (Table 2.2). The shear rate magnitude from the μ PIV experiments

for channel D were around 5900 s⁻¹, as mentioned previously. We observed a similar estimation for the 390 msec channel (E), with a shear rate of around 5600 s⁻¹. However, constricted channels B and C were both lower, at 4700 and 4500 s⁻¹. In each case, the shear rate estimates from the parabolic fit from the μ PIV data (Exper. SR, Table 2.2 below) is similar to the calculated shear rate (Equation 1, from Son²⁸⁷, Calc. SR Theor.), as well as an estimate fitting a parabolic curve to the theoretical velocity profile (SR Theor. Parabolic Fit). The calculated and theoretical fits match for channels B and C, and are different by 200 s⁻¹ for D and E.

Table 2.2: Wall shear rate estimates for channels B-E. Columns from left to right show the channel name, constriction length, constriction height, exposure time, calculated theoretical shear rate (SR), parabolic fitted theoretical shear rate, the experimental shear rate estimate from the parabolic fit, and the experimental average of the parabolic fits for each individual channel run for each condition. All constricted regions are 45 μ m wide.

Channel	Con. Length (mm)	Con. Height (μm)	Exp. Time (msec)	Calc. SR Theor. (s⁻¹)	SR Theor. Parabolic Fit (s⁻¹)	Exper. SR (s⁻¹)	Exper.SR Ch Avg (s⁻¹)
Con. B	3.9	58	100	4500	4500	4700	5000
Con. C	7.7	58	210	4500	4500	4500	4600
Con. D	11.6	53	310	5400	5200	5900	5500
Con. E	15.0	53	390	5400	5200	5600	5800

The differences in the shear rates between channels appears to stem directly from the height, which was found to be 5 μm shorter in channels D/E, at 53 μm as opposed to 58 μm . Channel heights were measured in a similar fashion as the z positions, using beads attached to the top and bottom walls. A variation in the velocity from an increased pressure drop with increasing length would most likely cause a decrease in the velocity in the longer channels, rather than an increase. In fact, we will see such an effect in the higher shear rate conditions ($>80,000 \text{ s}^{-1}$) with the longer Cons. F and G. Since the height correlates with the shear rate by a factor of two, any differences in the height amplify variations in the shear rate. Thus, the main source of error results directly from the photolithography, which has an inherent height variability, even across a single wafer. Unfortunately, this can also cause differences between wafers and constriction types, as well as in a single channel across the length. The extremely long channels are vulnerable to increased height on the edges of the wafer. The symmetry of the mask design and placement over the wafer during the photolithography process means that upstream and downstream locations are similar for a given channel, as the design and spin coating of the photoresist are symmetrical. The photolithography process with the current equipment available to us allows for construction of master molds with an accuracy in the height of around 2-3 μm for a given wafer. Any wafers that vary outside of this range are excluded. Wafers also have a limited lifetime and may lose some height over time. The μPIV characterization on these constricted channels was done at different times with molds from separate silicon wafer master molds. The taller

constricted channels from molds B and C were from newer wafers; by the time of the μ PIV the previous molds for these channels were unusable. Another very important note is that for all of the rolling experiments in chapter 3, the channels for a given experiment were taken from the same master mold (wafer). Comparing the upstream and downstream velocities for each channel also helps to account for this type of error. The accepted range for the height between master (photoresist) molds varied from 57 to 63 μm . But any single wafer with such an inherent height variation across the wafer would not be used; wafers were all measured after production and before use. Additionally, it appears that the vacuum seal causes a small deformation, as application of the vacuum decreased the height of the channel by up to about 4 μm . The channels for the μ PIV were at 53 and 58 μm . The same mold (Con. D, 53 μm here) used for the high shear applications later in the chapter were in the expected >57 μm .

The shear rate calculations completed and used throughout this work were based on compiling an average velocity profile from multiple channels, and then using this profile to create the second order polynomial fit and the corresponding wall shear rate. Individual velocity points can be influenced by the accuracy of the height (z position) from the bottom wall. Ideally, all measurements in the z direction are accurate to within 1-2 μm . A portion of this comes from the accuracy in measuring the wall position. In this case we used small, 0.5 μm beads for this estimation, which should give accuracy to within a micron or so. Using fluorescent signal reduces the depth of focus in order to increase this accuracy in the z measurement, but even with a high numerical aperture, the depth of focus

remains a few microns. Due to the small size of these channels, even small differences in the z position greatly affect the velocity, especially around the center of the channels. Averaging the velocity profiles between channels at each point helps to account for any error in the individual measurements, optimally thus approaching the velocity profile with an increasing number of channels run. The alternative method is to use each individual channel velocity profile for the parabolic fit to calculate a shear rate for each channel, and then take the average of these values to find the measured shear rate for a given channel/condition. This method can reduce error from the normal variation between points, but seems more vulnerable to especially aberrant points. We can counter this issue by taking the profile along a sufficient number of points across the channel height, and we thus use approximately ten points in the constriction. Additionally, we can remove outlier points that don't fit with the rest of the curve. Table 2.2 shows the comparison between these two methods of calculating the shear rate. The shear rate estimate from the parabolic fit on the average velocity profile, and the calculated shear rate values referenced throughout this text, is referred to as the experimental shear rate (Exper. SR). The shear rate estimate by taking the shear rate from a parabolic fit for each individual channel, and then averaging these shear rates, is referred to in the last column of the table as the experimental shear rate, channel average (Exper. SR Ch Avg.). The difference between these two values is within a few hundred s^{-1} , with the most pronounced difference for Con. D, which decreases from the calculated $5900 s^{-1}$ to $5500 s^{-1}$.

Based upon the results observed here, it is recommended for future studies to have a more stringent height requirement, if possible. Decreasing the accepted range may require a few additional wafers to be created, but a range of 2-3 μm overall would reduce errors in the shear rate and velocity by half. It would also be recommended to measure wafers before critical experiments to make sure heights are maintained within the strict standards. Most of the experiments throughout this thesis used relatively new wafers and thus should not have this issue.

The wall shear rates mentioned throughout this thesis were calculated using the velocity profile in the z direction; this was due for a few reasons, such as inaccuracies in near wall velocities. Furthermore, determining the position of particles from the side wall accurately is much more difficult compared to the z-direction, as the bottom wall location could be determined with adhered beads, and the microscope stage subsequently moved to the desired z-position. An approximate location along the channel width (and step size across the width) can be determined based on the velocities of the beads, accurate to within $\sim 2.5 \mu\text{m}$ (based on the size of the interrogation windows). As the channel is rectangular and not square in cross-sectional shape, using the larger side (z-direction or height) may underestimate the shear rates in the channels. Although, similar to the exposure times, there is a range of shear rates that the cells actually experience depending on their position within the channel. This was not an issue for the wider regions, where the wall shear rate in the z-direction is the desired wall shear rate affecting the rolling cells. We can create horizontal velocity

profiles, and use these to get an approximate wall shear rate in the y-direction (across the width). This helps provide a better idea of the possible shear rates present within the channel. When we do this for the 5900 s^{-1} (wall shear rate z-direction), 310 msec (Con. D) channel, the wall shear rate from the parabolic fit of the velocity across the width of the constriction is indeed somewhat higher, at 6700 s^{-1} .

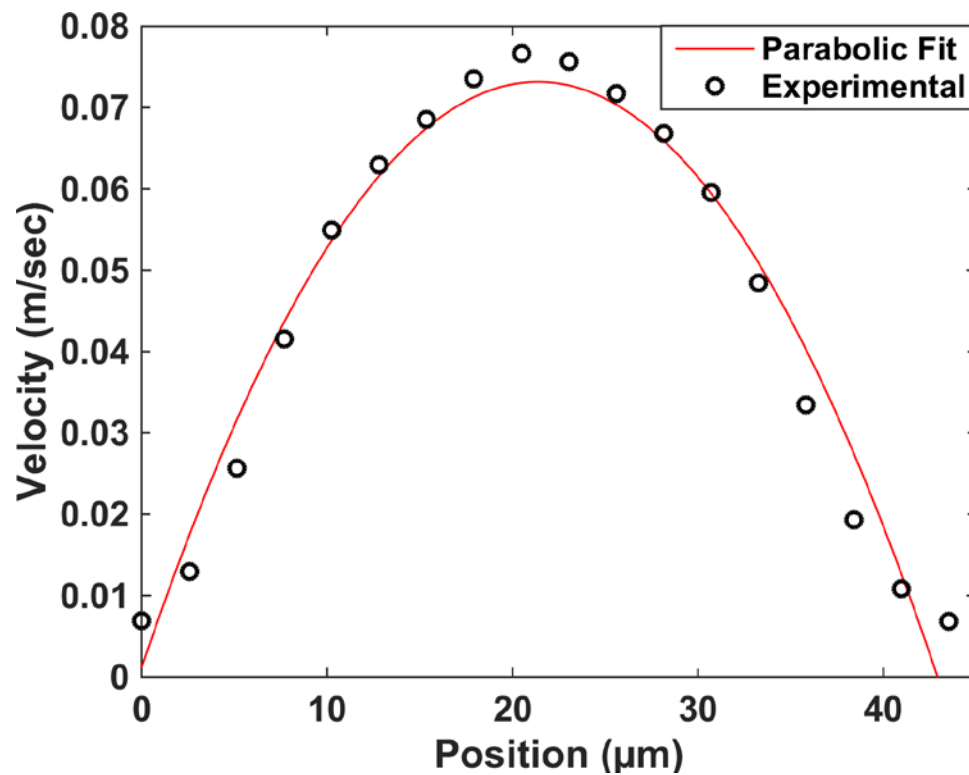


Figure 2.9: Velocity profile across the width of the constriction for a Type D constricted microfluidic device. A parabolic fit of this velocity profile estimates the wall shear rate in the y-direction to be 6700 s^{-1} , in contrast to the 5900 s^{-1} wall shear rate estimate in the z-direction.

Higher shear rate adhesion studies: 8600 s^{-1}

The rolling/adhesion assays add some complications that aren't present in other studies utilizing such high flow rates. In order to expose the cells to high

shear rates and directly study their adhesion in the same devices, there will be a large difference between the shear rates in each region of the device. For the second set of channels we wanted to increase this shear rate in the constricted region, while maintaining the same shear rate in the up/downstream regions, as these channels were also to be used for the study of neutrophil rolling. These constraints in the shear rates to be used in each section will therefore force the change in velocity to result from altering either the height or width of portions of the channel. While changing the height has a larger effect on the shear rate, it is much more difficult production wise to create different heights across a single wafer, as differences in the height come through the photolithography process. While changing the ratio in the width from the wide to constricted regions is a simple process, varying the height along the channel is not. In addition, focusing and lift effects in the channels cause an additional problem for the rolling experiments. We had to pattern the downstream protein drops further back than originally expected, which we later determined was a result of cells being lifted away from the bottom surface within the constriction⁷². It then took additional time for the cells to settle and interact with protein on the surface.

A set of channels was designed to add a second shear rate with a similar exposure time range. The dimensions for these channels are shown in Table 2.3. In order to try and maintain the shear exposure flow profile between the two conditions as closely as possible, we use the same constricted region dimensions. Therefore, to achieve approximately twice the shear rate, we correspondingly double the flow rate in the channel. We thus have to adjust the

wider regions by about the same amount. This will lead to a 50:1 aspect ratio. And in conjunction with the long constricted lengths, these two factors make collapse a very serious issue. The strength (stiffness) of the PDMS leads to a lower barrier to relieving the pressure through collapse, as opposed to fluid being pulled through the device. So we end up with a large collapse in the PDMS in the downstream region, which then alters the flow rate throughout the channel. As shown in Figure 2.10, this leads to an increased velocity in this region of the channel, which renders these channels unusable for adhesion studies due to the large difference between the upstream and downstream regions. Or at least unusable without any modifications to the device.

Table 2.3: Wider channels for neutrophil rolling with an increased 8600 s^{-1} constricted shear rate.

Channel Type	Up/Downstream Width	Constricted Region Width	Constricted Region Length	Exposure Time
Straight H	3000 μm	N/A	N/A	N/A
Constriction I	3000 μm	45 μm	1.5 mm	30 msec
Constriction J	3000 μm	45 μm	7.7 mm	120 msec
Constriction K	3000 μm	45 μm	15.4 mm	240 msec
Constriction L	3000 μm	45 μm	23.1 mm	350 msec

Deformation experiments:

One serious issue for these studies is the potential collapse of the downstream region resulting from the high pressure drop across the channel. In fact, the very high aspect ratio even makes these channels prone to collapse in the upstream region. The application of the vacuum seal further exacerbates this issue. There are a few ways to measure height in a fluid filled channel. Certain fluorescent molecules such as fluorescein or rhodamine demonstrate variation in signal with height; at certain concentrations this effect can be linear^{122,148}. However, we were able to directly measure the height in a simple manner, by using the μ PIV setup in conjunction with small beads that were pulled through the channel. 0.5 μm beads would attach to both the top and bottom surfaces, and remained even after the application of high flow rates. When the 8600 s^{-1} channels were run under flow, we saw significant collapse over time, up to 20 μm or more (about a third of the channel). μ PIV measurements in a Con. L channel demonstrated that this led to a significant increase in the velocity, with estimated shear rates of 150 and 250 s^{-1} in the upstream and downstream areas, respectively.

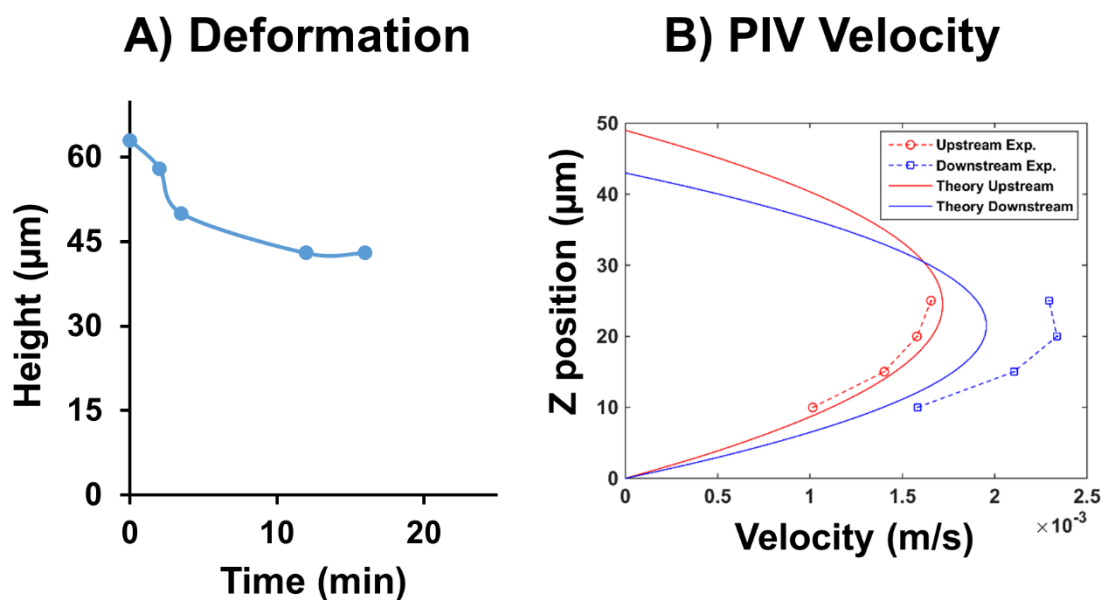


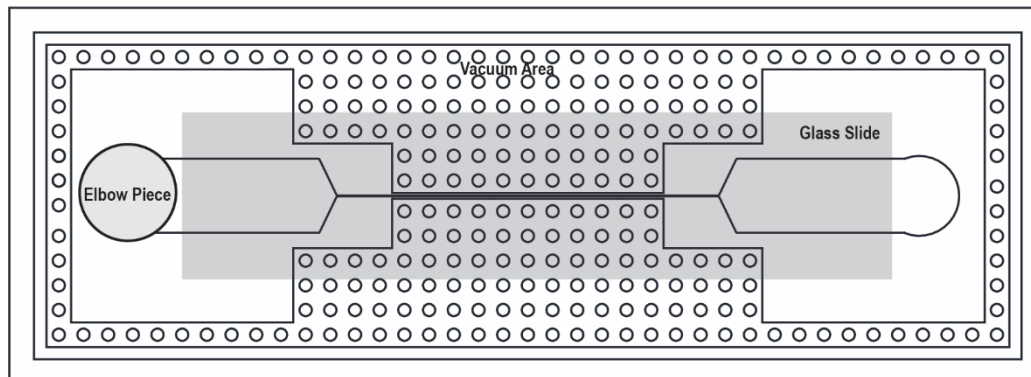
Figure 2.10: PDMS Deformation. (A) Shows the deformation in the downstream region of Con. L (8600 s^{-1} , 350 msec) for time of fluid flow (withdraw on syringe pump), while (B) shows the effect of deformation on the velocity as measured by μPIV

To address the deformation, we decided to add support to the top wall of the device (the PDMS side). A sandwich of glass slides around the device was first tested. An additional support was plasma cleaned and sealed to the top of the device. This did not prevent collapse, so the glass was then embedded directly into the device, with a thin layer of PDMS underneath. Therefore the glass would be much closer to the top wall of the channel and ideally prevent deformation. A few other groups have placed a very thin layer of PDMS with a piece of glass on top; this layer is often difficult to remove, and the brittle silicon wafer mold can easily be broken¹³⁷. These wafers are time consuming and

expensive to make, and a few recent studies have employed methods to try and circumvent this issue^{56,179}. Several iterations of the method for embedding the device led to a positive result, with a drastic decrease in the deformation in the channels (Figure 2.12 A and B). A schematic of the device with embedded glass is shown in Figure 2.11. Briefly, a small layer of PDMS is first poured on the mold and degassed. Bubbles can form in this very short layer around the vacuum posts, so these are checked and removed as needed after ~10-20 min. The molds are then allowed to cure with the elbow piece in the oven for 30 min. The glass piece is then placed and poured with the second layer, so that it is directly embedded within the device, at the surface of the bottom cured layer. Glass coverslips (~0.17 mm) were insufficient in preventing collapse, but the thicker glass slides (1 mm) provided enough support to prevent deformation. By allowing this first layer to cure before adding the glass, we were able to have reproducible success in removing the stamps without breakage. This may be a result of a slightly thicker layer of PDMS in this region. A method such as spin coating of PDMS could be implemented to create a uniform, consistent height for future studies if desired. By barely filling this area we maintained a similar height between pours.

Constricted Channel 90-8600s⁻¹

Top View



Side View

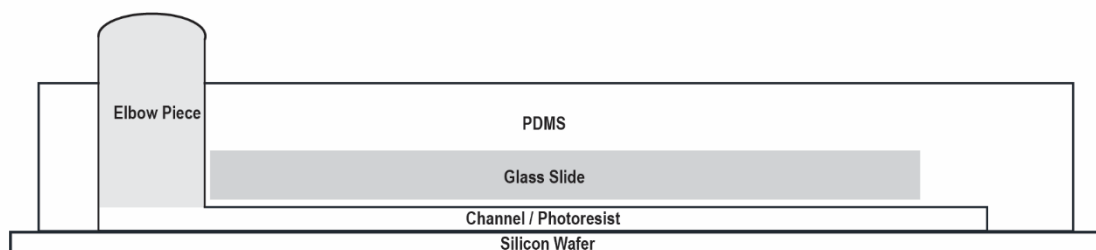


Figure 2.11: Schematic for the 90-8600 s⁻¹ channels. Top panel shows a top down view of the design with the incorporated glass and elbow outlet piece. Bottom panel shows a side view. A biopsy punch is then used after this fabrication to create an inlet reservoir hole in the right side of the channel, and the channel is sealed to coverslips or Petri plates with the vacuum seal.

As was mentioned above, these channels had significant deformation in the wide regions without any support. The incorporation of this glass greatly reduced the deformation occurring, by almost 50%. In shorter exposure time channels it was virtually eliminated, although there was still some deformation measured with the μ PIV system for the longer constricted lengths, channels K and L (240 and 350 msec, respectively). Figure 2.12 shows the deformation and corresponding μ PIV for these two channels. For the μ PIV, channels were sealed

to a No. 1.5 coverslip, which is required for the low working distance of the 40x oil objective (0.3 mm). With glass slide support on top and the thin coverslip as the bottom substrate, deformations of about 5 and 7.5 μm were observed for constricted channels K and L, respectively. Deformations for some Con. L channels were just over 10 μm , even with glass support.

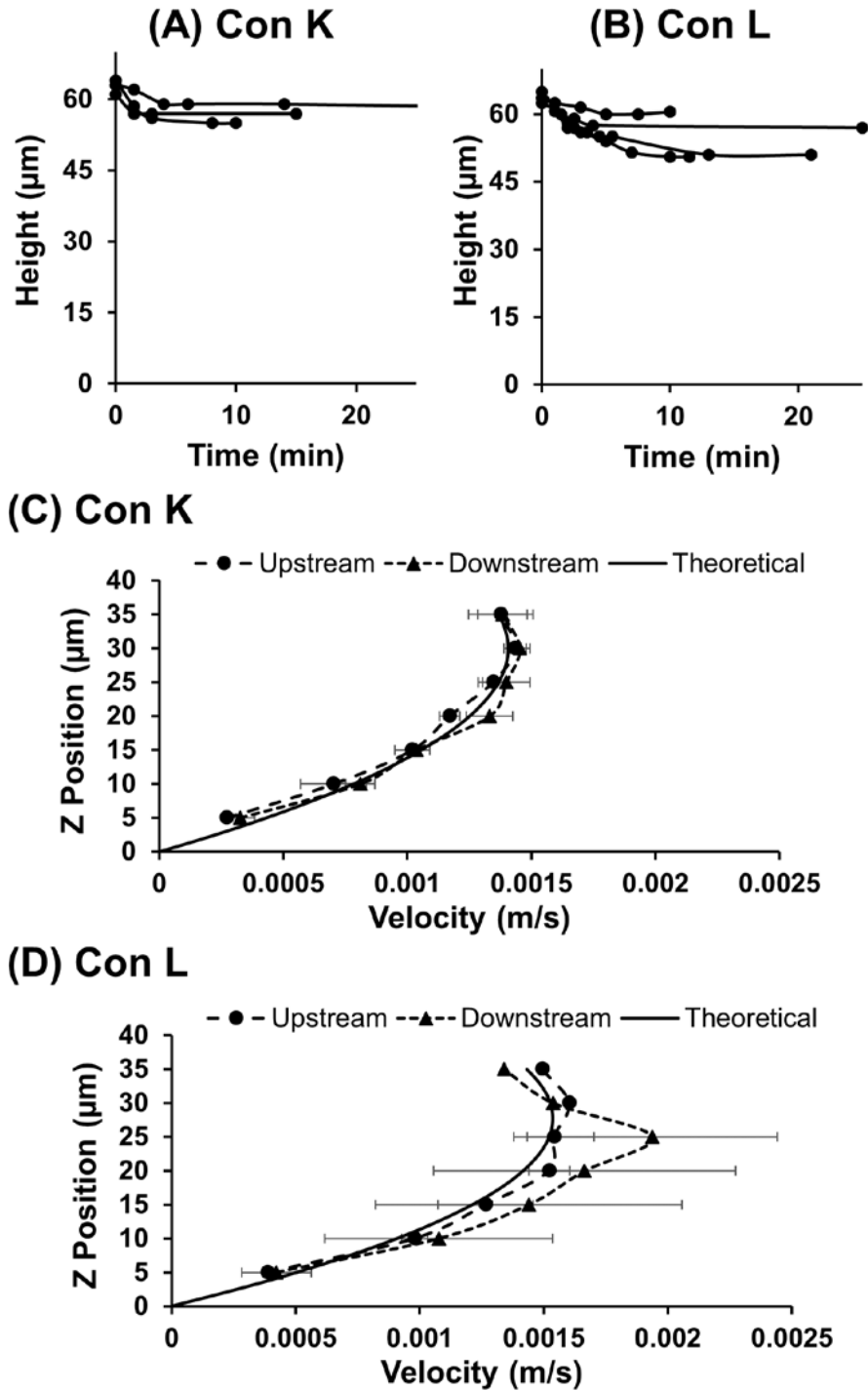


Figure 2.12: Deformation and μ PIV measurements in 8600 s^{-1} channels with glass support, sealed to No. 1.5 coverslips. Panels A and B show deformation in the downstream regions for the time under flow (withdraw on syringe pump) for Con. K (240 msec) and L (350 msec), while panels C and D show the μ PIV measurements for these two channels in the upstream and downstream regions.

At this point, we suspected that the remaining deformation with these longer channels could be flexion of the thin glass coverslip creating the bottom surface, since the top should be heavily reinforced. Unfortunately, the most accurate method we currently had validated at our disposal was the μ PIV, which requires these thin coverslips for use with the 40x oil objective. Measuring velocities with a long working distance air objective proved sufficient for imaging throughout the channel, but the z position was not accurate, and with refraction the distance covered with each increment was about double that with the oil objective. To overcome this, we purchased slightly thicker coverslips to see if this would have any effect. Instead of the original No. 1.5 (0.16-0.19 mm), we used No. 2 coverslips (0.17-0.25 mm). These coverslips were slightly thicker (possible increases of 10-90 μ m) than the No 1.5, so it made it difficult to measure the height all the way to the top of the channel. However, we could get close and make estimates in some. More importantly, we could measure the velocities through the majority of the channel, up through and past the center point. This allowed us to analyze the velocity profiles in all regions of the channels. Regardless of the height measurements, we can thus calculate shear rate estimates from our velocity fitting method. As was seen in Figure 2.10 and Figure 2.12, for the No. 1.5 coverslips we were able to observe velocity differences between the upstream and downstream regions in channels with deformation. In Figure 2.12 (glass embedded, No 1.5 coverslips) we see a small but insignificant difference between up/downstream velocities in Con. K (240 msec, 15.4mm constriction length) with small amounts of collapse, and a noticeable difference

(especially at the center) for Con. L (350 msec, 23.1 mm constriction). In addition, deformation is indicated by a shift in the maximum velocity to the $z=25\ \mu\text{m}$ point, something we saw previously in the $5900\ \text{s}^{-1}$ channels for the shorter ($53\ \mu\text{m}$) channels. With the glass embedded and the No. 2 coverslips used for the bottom wall, we see no indication of deformation, and equivalent velocities in the upstream and downstream regions (Figure 2.13A). The difference in thickness between the No. 1.5 and No. 2 coverslips is small at approximately $30\ \mu\text{m}$, and even this small difference in thickness virtually eliminated the deformation occurring. The petri plates used for the rolling experiments are much thicker than either of the glass coverslips, at over 4-fold thicker than the No.2 coverslips. The deflection of the bottom surface depends on both the stiffness and thickness of the material. The deflection of the wall (change in height Δh) for a rectangular microchannel can be provided by the following relation²³⁹:

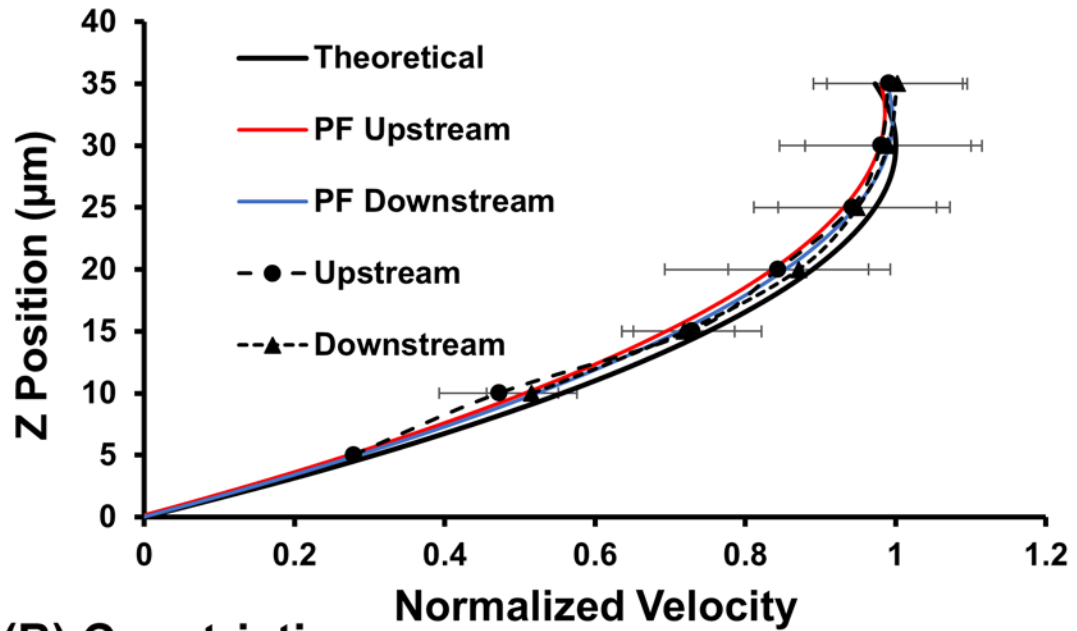
$$\Delta h = \frac{\alpha|P|w^4}{Et^3} \quad \text{Eq. (7)}$$

Where α is a constant related to the geometry, P is the applied pressure difference, w is the channel width, E is the Young's modulus, and t is the wall thickness. The pressure driving force (vacuum, withdraw on the pump) and the geometry are assumed to be constant, as the PDMS stamp used does not change. Only the latter two variables will change when the bottom material of our channel is substituted. Glass has a higher Young's modulus at around $63\ \text{GPa}$ ^{16,286} compared to around $3.2\ \text{GPa}$ ¹⁶² for a polystyrene plastic plate. However, as mentioned, the plastic plate is around 4 times thicker than the No. 2 coverslips used. Since the deflection of the wall is inversely proportional to t^3 , we

expect significantly less deflection/deformation in the plastic Petri plates used as compared to either of the glass coverslips. As we observed no evidence for deformation or increased velocities in the μ PIV setup for the No. 2 coverslip, we thus do not expect any deformation when using the Petri plates.

The shear rate was calculated to be 85 ± 11 and $87 \pm 4 \text{ s}^{-1}$ for the upstream and downstream respectively, while the parabolic fit on the theoretical velocity profile comes to 94 s^{-1} . The shear rate in the upstream and downstream regions is thus similar to the expected value, all around 90 s^{-1} , and a little lower than the 125 s^{-1} found for the $1500 \text{ }\mu\text{m}$ wide channels (A-E). Although as noted, the previous channels were shorter than expected. To fully characterize the channel, μ PIV was also run for the constriction of this channel (Fig 2.13B); the shear rate was found to be 8600 s^{-1} . Similar to the previous channels, the shear rate is comparable to, and slightly faster than, the expected shear rate at 8200 s^{-1} . Adjusting the exposure times using the experimental μ PIV velocities provides the values shown in Table 2.3. These values end up being 30, 120, 240, and 350 msec for the channels used in this section, Con. I-L, respectively. Con. I (1.5 mm) is shorter than the previous constricted lengths ($> 3.9 \text{ mm}$), while channels J-L (120-350 msec) are designed to maintain similar exposure times to channels B-D (100-310 msec). Due to the decreased height and increased shear rate in Cons. B-D, the exposure times for Cons. I-L are slightly higher than their counterparts.

(A) Up/Downstream



(B) Constriction

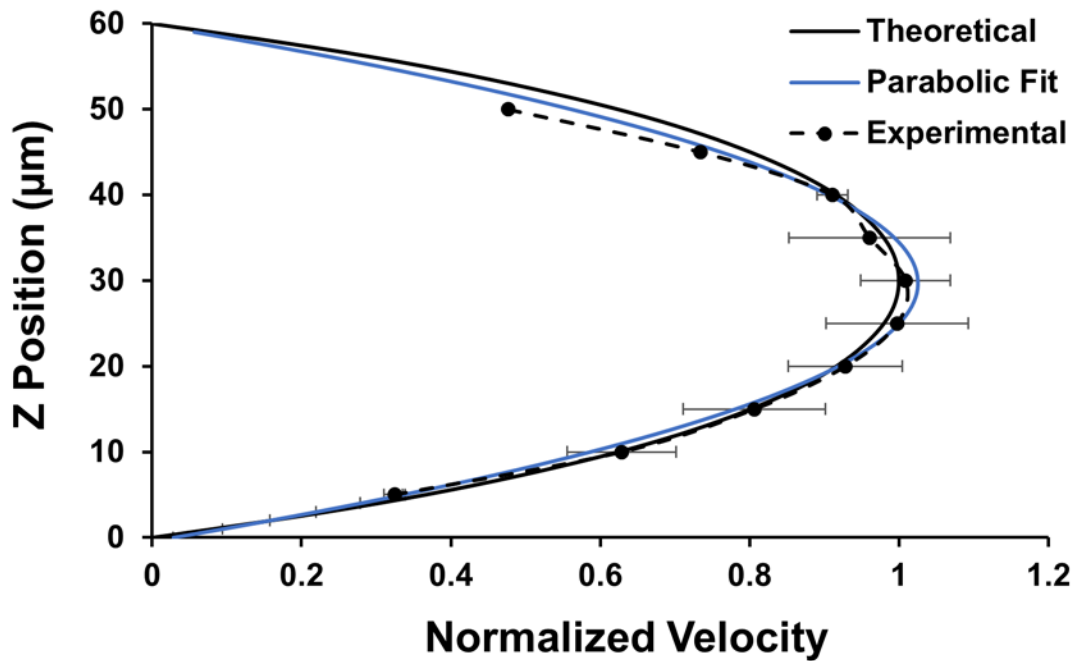


Figure 2.13: Velocity profiles for Constricted channel L, on No. 2 coverslips. Con. L has a constricted region (23.1 mm in length) that corresponds to an exposure time of 350 msec. (A) Shows velocities, parabolic fits (PF), and theoretical velocity for the upstream and downstream regions, while (B) shows the profiles for the constricted region.

Higher shear rates: ~100,000 s⁻¹

Up to this point in the chapter we have discussed the channels used for neutrophil rolling studies. The other aspect investigated in this thesis involves conditions for higher shear rates utilized to examine both platelet and neutrophil states and function. The neutrophil work will be examined in chapter 4, while the platelet studies can be found in the corresponding paper by Alsmadi et al¹⁰. While all of the shear rates throughout this study are greater than physiological levels, the second half of this thesis are an order of magnitude higher than the rolling studies, focusing on extremely high shear rates (>80,000 s⁻¹). These shear rates are more reminiscent of the hot spots (small areas of significantly increased shear rates) around the rotors of VADs, and very severe stenosis. This section provides a more difficult case to achieve the desired shear rates due to the very high pressure drops encountered at these highly elevated flow rates.

Based on preliminary results for these higher velocity channels, we added two additional constricted lengths that were significantly longer than those for the rolling assay (Cons. F and G, 38.6 and 46.3 mm, respectively). These were over three times longer than the channels previously discussed. Taking constriction D from the rolling section, at a flow rate corresponding to 2500-100,000 s⁻¹, provides an exposure time of 15 msec. The new longer lengths, constrictions F and G, are 50 and 60 msec for the same shear rate condition. The constriction, due to its low size and aspect ratio, is not expected to have significant deformations. However, pressure drops due to the long length and the high flow rates of these channels could cause a decrease in the velocity in the constriction, leading to decreased

wall shear rates. The much higher flow rates (25 times higher than for the rolling experiments) also make the wider regions prone to collapse or deformation. Initial experiments with these elevated conditions used the same “withdraw” on the syringe pump to create the pressure driving force. Under flow, we noticed that the volumes collected from the channels for downstream assays were lower than those of the corresponding straight channels. We thus switch the method of driving force for this section to “infuse” on the syringe pump, forcing the liquid through the channels. This maintains the flow rate through the channels, but there may now be the opposite effect, with bulging in the upstream region. We do in fact see this effect in the longer constricted channels, but without the high reduction in the flow rate observed in the withdraw case. Thus we see an appropriate flow rate for constriction D.

Table 2.4: Channels for high shear studies with calculated shear rates and exposure times. Wall shear rates using the velocity profile in the z-direction (dv/dz) and corresponding average exposure time, as well as the wall shear rate from the velocity profile in the y-direction (dv/dy) are shown.

Channel	Wall Shear Rate	Exposure Time	Wall Shear Rate
Type	(s^{-1})	(msec)	(s^{-1})
	dv/dz		dv/dy
Straight A	2,400	N/A	N/A
Constriction D	98,000	16	120,000
Constriction F	86,000	58	95,000
Constriction G	80,000	73	90,000

μ PIV was performed on the constricted regions of these channels following the same general method described in the previous sections. As these conditions were not used for adhesion based studies, only the constriction was examined in detail. In terms of the μ PIV setup, the time delay between pulses for the laser, in the constricted region, is decreased from 6-10 to 0.4 μ s. This is on the verge of the exposure time limit for the current PIV system. Velocities using these channels saw no virtually no decrease in velocity in Constriction D (Fig. 2.14 B and D) as compared to the theoretical. The amount of deformation that may be present in the upstream region is unknown, but the calculated shear rate value of 98,000 s^{-1} is very close to the expected 100,000 s^{-1} . The straight channel at 2400 s^{-1} was also very similar to the expected 2500 s^{-1} (Fig. 2.14C). We thus do not expect a large deformation to be occurring. Shear rates were calculated with the same parabolic fit profile as described previously. Constricted channels F and G though, have large deformations and corresponding drops in the fluid velocity. Shear rate estimates were found to be around 86,000 s^{-1} and 80,000 s^{-1} , respectively. Correcting for the flow rates in this section we get average exposure time values of 16, 58, and 73 msec for Cons. D, F, and G, respectively. We can once again use the μ PIV data to determine the exposure time as a function of the z-position, to evaluate the range of exposure times present, in comparison with the average exposure time. These values are shown in Figure 2.15 below.

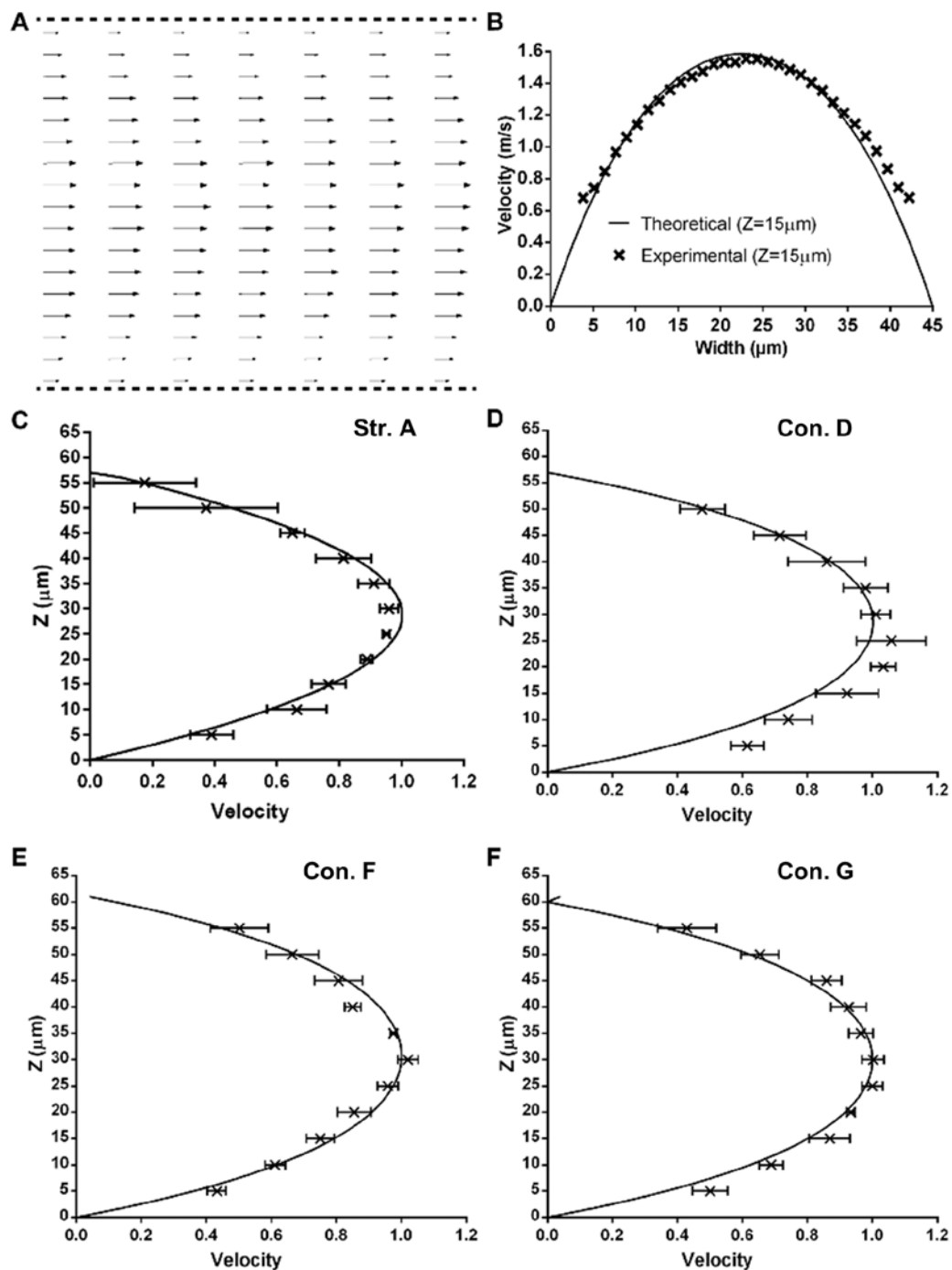


Figure 2.14: μ PIV for high shear conditions for Ch. 4 channels. Panels (A) and (B) show representative images of the velocity vectors from the μ PIV and a velocity profile across the width of the constricted region for Con. D. Panels (C)-(F) show the velocity profiles for the channels at the 125 μ L/min flow condition. X symbols represent the experimental data. Solid curves show the theoretical profiles for the matching shear rates, i.e., 2400; 98,000; 86,000; and 80,000 s^{-1} respectively. Figure adapted with permission¹⁰.

The wall shear rate can also be examined across the width of the channel, using the velocity profiles in the y-direction. The values for this wall shear rate estimate are shown in the last column of Table 2.4. This shear rate estimate was described in the earlier section for the lower shear (5900 s^{-1}) channels, which showed an increase in the estimated shear rate to 6700 s^{-1} (Figure 2.9). For these higher shear rate channels ($> 80,000 \text{ s}^{-1}$), the wall shear rate estimate across the width is again higher than that calculated using the velocity profile in the z-direction. Some caution is needed in interpreting these results however, as there is the potential for additional artifacts in the creation of the velocity profiles. One of the largest issues, as discussed previously, is the location of the side walls. This wall position is much more difficult to estimate across the width, and even small variations in the position across the channel affect the parabolic fit estimate dramatically. As the velocity profile has a sharper, steeper curve with increased flow rates, deviations in position have a more pronounced effect on the velocity for a given position.

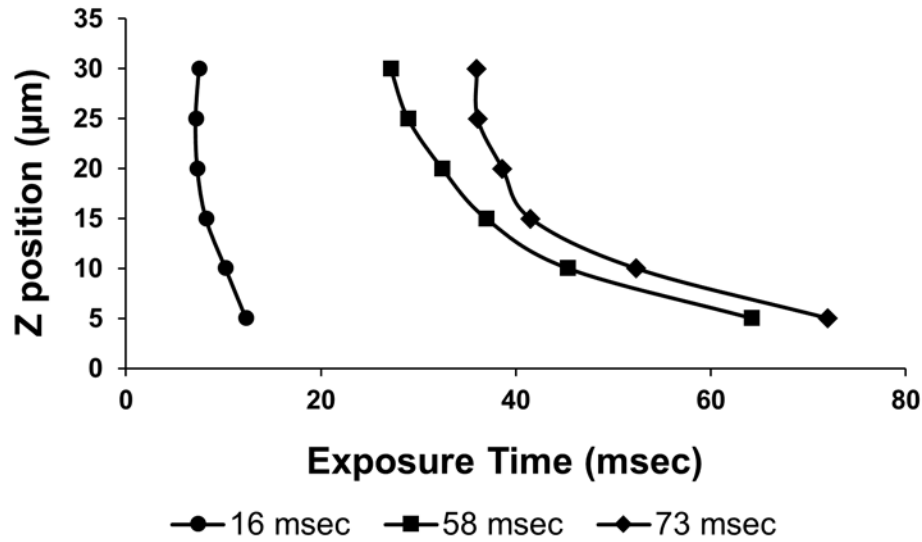


Figure 2.15: Exposure time as a function of z-position for the 80,000 - 100,000 s^{-1} channels. Exposure times are presented as a function of the z-position, determined by the velocity at each position from the μ PIV data, with y-position at the center of the channel. 16, 58, and 73 msec refer to Cons. D, F, and G.

Corrected flow rates: long exposure constricted channels

It is not too surprising that these extremely long channels contain high pressure drops and reduced velocities. Pressure drop is a significant concern in a variety of chemical engineering applications, and can occur through frictional losses along the length of a pipe or channel, among other factors (e.g., various fittings/connections). For microfluidic channels frictional losses are going to be one of the primary concerns, along with losses from sudden contractions and expansions. These frictional losses depend on a few factors, including but not limited to the cross sectional area, the length, and the viscosity, while the pressure drop is furthermore dependent upon the flow rate^{142,244}. These losses can be thought of as the channel's resistance to flow (R), such that the flow rate $Q = \Delta P / R^{29}$. We observed a decrease in velocity in the longest constricted

channels (> 58 msec), and since the cross-sectional area is kept consistent throughout the high shear studies ($> 80,000 \text{ s}^{-1}$), the main difference stems from the length of the constricted region. The pressure drop and channel resistance are both related to the length of this constricted region. An often used term in calculating pressure drop is the friction factor; the multiplication of this factor and the Reynold's number ($f \cdot \text{Re}$) is equal to some constant (C), for channels of non-circular cross sections. This constant depends on the geometry of the channel¹⁴². The exact nature of the frictional pressure drop and values for the friction factor for microfluidic channels has endured some debate, as groups have observed inconsistencies and deviations from the classical theory (values at larger physical dimensions)¹⁵⁸. Unfortunately, at this time models of the pressure drop for microfluidic systems such as those described in this thesis are limited, complicated by the interconnection of many of the factors such as the flow rate, velocity, and pressure drop, as well as variables such as PDMS deformation and varying geometries along the length of the channel²⁸⁶.

The high pressure drops in these channels led to several design issues. In fact, these channels had to be moved to glass slides instead of coverslips to accommodate the extra length (and still barely fit). In addition, the pressure in the device was so large as to compromise the integrity of the seal around the plastic elbow pieces typically used in our lab. These elbow pieces are able to be placed directly into the PDMS and are a convenient way to have consistent outlet/inlet ports for the microfluidics. For the previous channels, these posed relatively little concern, and as we saw, the μPIV data was similar to the expected values. When

using constricted channel D (16 msec) for the high shear applications, epoxy was added around the elbow to protect the seal around this potential vulnerability. With shear channels F and G, failure of the channel was much more frequently occurring, with the most common location of vulnerability being this elbow piece. We had previously worked on a method to directly embed the silastic tubing into the devices, and thus incorporated that design element here. While fabrication subsequently takes longer, it allows for the inlet/outlet port (tubing) to be surrounded by the PDMS. The plastic elbow and PDMS is not as securely bound as PDMS around the tubing. We then reinforce this area with additional PDMS to form a thick layer around the tubing. This significantly increased the success rate of the channels.

The simplest fix to adjust for the decrease in shear rate is to use existing channel designs with an increased flow rate. Based on estimates of the wall shear rates with the 125 $\mu\text{L}/\text{min}$ conditions, we can estimate the necessary increase in flow rate to achieve the desired 100,000 s^{-1} . Utilizing the decrease observed in the original channels, we examined the flow velocity with elevated flow rates in the range of 150-165 $\mu\text{L}/\text{min}$, with the possibility that even higher flow rates would be needed to compensate for the pressure loss. We first ran constricted channel G with an increased flow rate of 160 $\mu\text{L}/\text{min}$. Increasing the flow rate increased the shear rate, but not as much as expected, from 80,000 s^{-1} to 88,000 s^{-1} (Figure 2.16). This was now similar to the value for Con. F at 125 $\mu\text{L}/\text{min}$. As we increased the flow rate we noticed that we had diminishing returns on the velocity increase. This is most likely a result of channel deformation, which results in an increased

pressure drop resulting from the elevated flow rate. Previous studies have demonstrated that deformation of the microfluidic channels results in a non-linear relationship between the deformation, the flow rate, and the pressure drop^{27,107,131}. Incrementally increasing the flow rate we do not see the centerline velocity approach the theoretical $100,000 \text{ s}^{-1}$ value until around 180-185 $\mu\text{L}/\text{min}$ (data not shown). Unfortunately, at this flow rate we also very quickly run into failure within the channel. The high pressure compromised the integrity of the seal between the PDMS stamp and the glass slide, and led to leaks from the channel. With the 160 $\mu\text{L}/\text{min}$ providing a second set of channels at an equivalent shear rate ($\sim 90,000 \text{ s}^{-1}$); this condition was used as a supplement for some of the work to be seen in chapter 4. This can be useful in comparing the effect of exposure time.

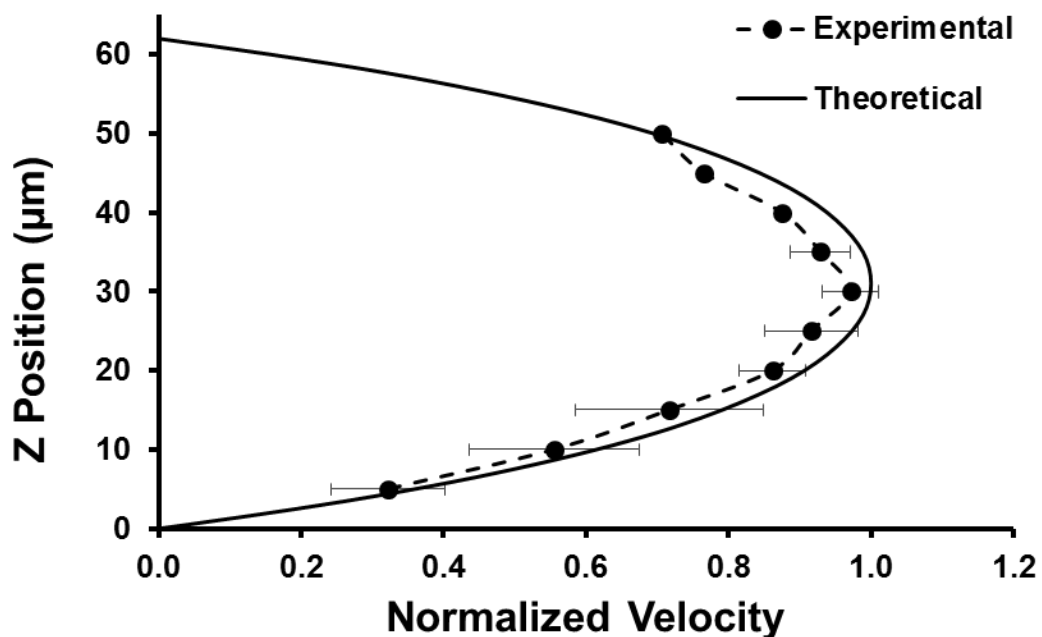


Figure 2.16: μPIV velocity profile for Constriction G at 160 $\mu\text{L}/\text{min}$, with corresponding theoretical profile at $88,000 \text{ s}^{-1}$

Since Con. F has a shorter constriction (38.6 vs 46.3 mm) and higher starting shear rate (86,000 vs 80,000 s^{-1}) than Con. G, it will have a lower pressure drop and resistance to flow, and it could be possible to achieve the desired 100,000 s^{-1} condition for future experiments. We tested several flow rates for the maximum velocity and found that a flow rate of around 165 $\mu\text{L}/\text{min}$ seemed sufficient. Moving forward with this flow rate we set out to create the shear profile needed for the fitting used throughout this chapter. However, these channels run into similar issues as Con. G, and almost all failed around the 10 minute mark. While this prevents measuring points throughout the height of the channel to create the parabolic velocity profile, it does allow for measurement of the centerline velocity, and it is sufficient for actual blood/cell experiments. The shear rate will thus have to be approximated from the centerline velocity. And as has been shown by this point in the chapter, such as in Figure 2.14, the velocity curve from the analytical solution for a given shear rate matches up closely with the experimental velocity profile. We can thus do the reverse calculation, and utilize the centerline velocity to provide an approximation for the shear rate, without having the full velocity profile. So with that, normalizing the experimental velocity to that of the theoretical velocity, provides a shear rate estimate of 103,000 s^{-1} for the 60 μm tall channels. The exposure time with this shear rate will be very close to the originally calculated 50 msec, at about 49 msec.

Double constriction channels:

In chapters 3 and 4 we will observe a few significant effects on neutrophil state and function with a single (low exposure time) pass to high shear. The

clinical condition consists of repeated exposures, and thus one of the major follow-up areas to this study is the effect of cumulative exposures. This phenomena has been previously described for platelets, and repeated exposures were shown to have an effect on platelet activation state^{273,285}. We examined this next step, of repeated exposures, with a preliminary double constriction channel based on the single pass exposure design. Con. D, at 16 msec, was chosen for the device to double. Design constraints limited the potential length so that a double 30 msec channel was difficult without other modifications, and we have not tested any results with exposure times in between 16 and 58 msec at this time.

This double constriction channel was first characterized using the μ PIV system at the starting 125 μ L/min that provided the 98,000 s^{-1} shear rate for the single pass channel. With the second constriction we observed a drop in the velocity, with corresponding shear rates of 85,000 and 90,000 s^{-1} for the first and second constriction respectively. We then increased the flow rate, and found a centerline velocity approximately matching the expected theoretical value at 150 μ L/min. Over half of each constriction was analyzed to create the z-velocity profile for both constrictions, as seen in Figure 2.17. At this flow rate, the observed velocity profiles match up closely to the theoretical velocity; surprisingly we again see a higher velocity in the second, downstream constriction. Constriction 1 matches up almost identically with the theoretical shear profile at 100,000 s^{-1} , while the second constriction was around 110,000 s^{-1} . It is currently unknown what causes this slight, potential discrepancy between the two

constricted regions. It could be a result of a slight deformation around and even in the first constriction, although no height difference was observed during the μ PIV between the two constrictions. Previous studies have shown the decreasing pressure along the channel length leads to non-linear deformation along the length¹³¹. It will be interesting to observe this potential effect in the future with longer exposure times, or a third constriction.

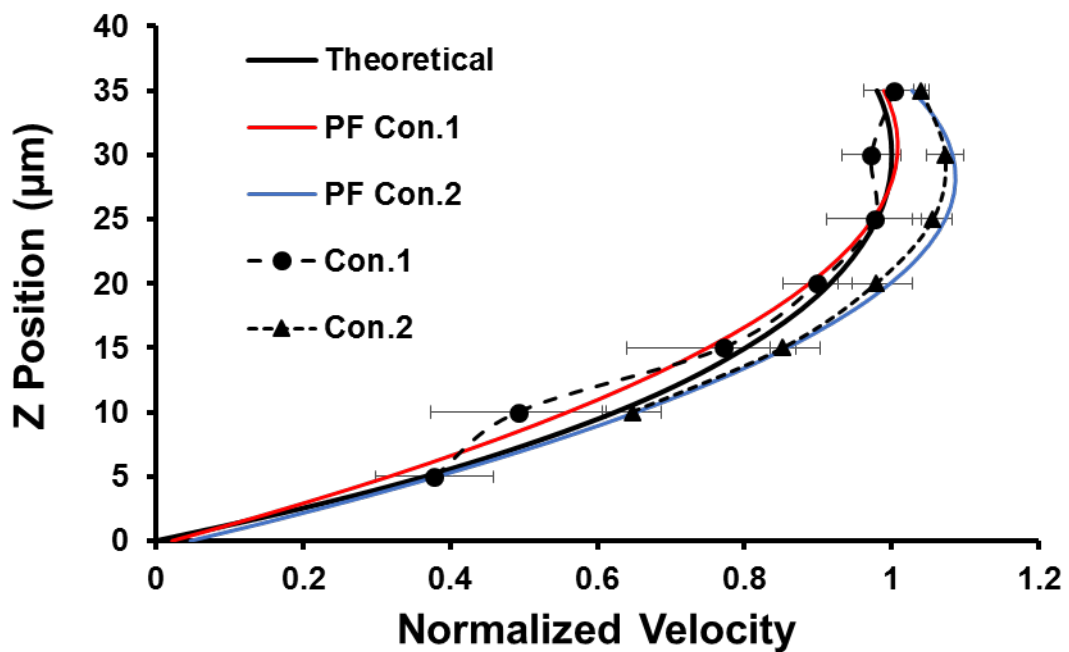


Figure 2.17: Double constriction μ PIV for the 150 μ L/min condition with experimental data (dotted lines), corresponding parabolic fits on these profiles (red and blue lines), and the theoretical velocity profile (solid black line).

Recirculation zones:

With high flow rates a potential concern, which has been demonstrated in other studies, is the existence of recirculation zones. While the Reynolds number remains low for all of the conditions used within this study (<100), the potential

for these zones occurs with a large sudden expansion. With the lower flow rates used for the rolling components of this study ($<10,000 \text{ s}^{-1}$ conditions), no such zones are observed. However, with the $80,000\text{-}100,000 \text{ s}^{-1}$ conditions we noticed the presence of a recirculation zone with the μPIV (Fig. 2.18B). A previous study by Ha et al. studied the effect of increasing flow rates on the creation of recirculation zones, and the resulting platelet aggregation in the low shear regions created. They used a similar microfluidic design, although with different channel dimensions. In that study, using whole blood, they observed recirculation zones starting between a Reynold's number (Re) of 5.4 and 6.7^{119} . We saw evidence of a recirculation zone at a Re number of ~ 3 when flowing beads in buffer solution. The increased shear stress for the whole blood case decreases the Re to 0.8, and correspondingly the recirculation zone disappears. Figure 2.19 shows a time lapse of whole blood being introduced to a channel filled with buffer solution, and the zone disappears within about 10 seconds. The difference in the Reynold's number corresponding to the formation of a recirculation zone between our study and that of Ha most likely depends on the differences in the channel design. The expansion angle in our study is larger by 4° , and the ratio between the downstream width and the constricted region width is five times higher in our study (wider downstream region and a narrower constriction). We thus have a larger relative expansion (or a more severe degree of stenosis). They also use red blood cells as the tracer particle, while we use small $1 \mu\text{m}$ beads. The smaller particles may provide a more sensitive indication of the presence of a recirculation zone. For example, when we introduce $10 \mu\text{m}$ beads or isolated

neutrophils we do not notice the presence of a zone, as the particles exiting the constriction do not pass in that region close to the wall (Fig. 2.18D). The double constriction channel has the same recirculation zone effects as the single pass channel. Based on the profiles observed we thus do not suspect the cells to pass through such a recirculation zone in our later studies.

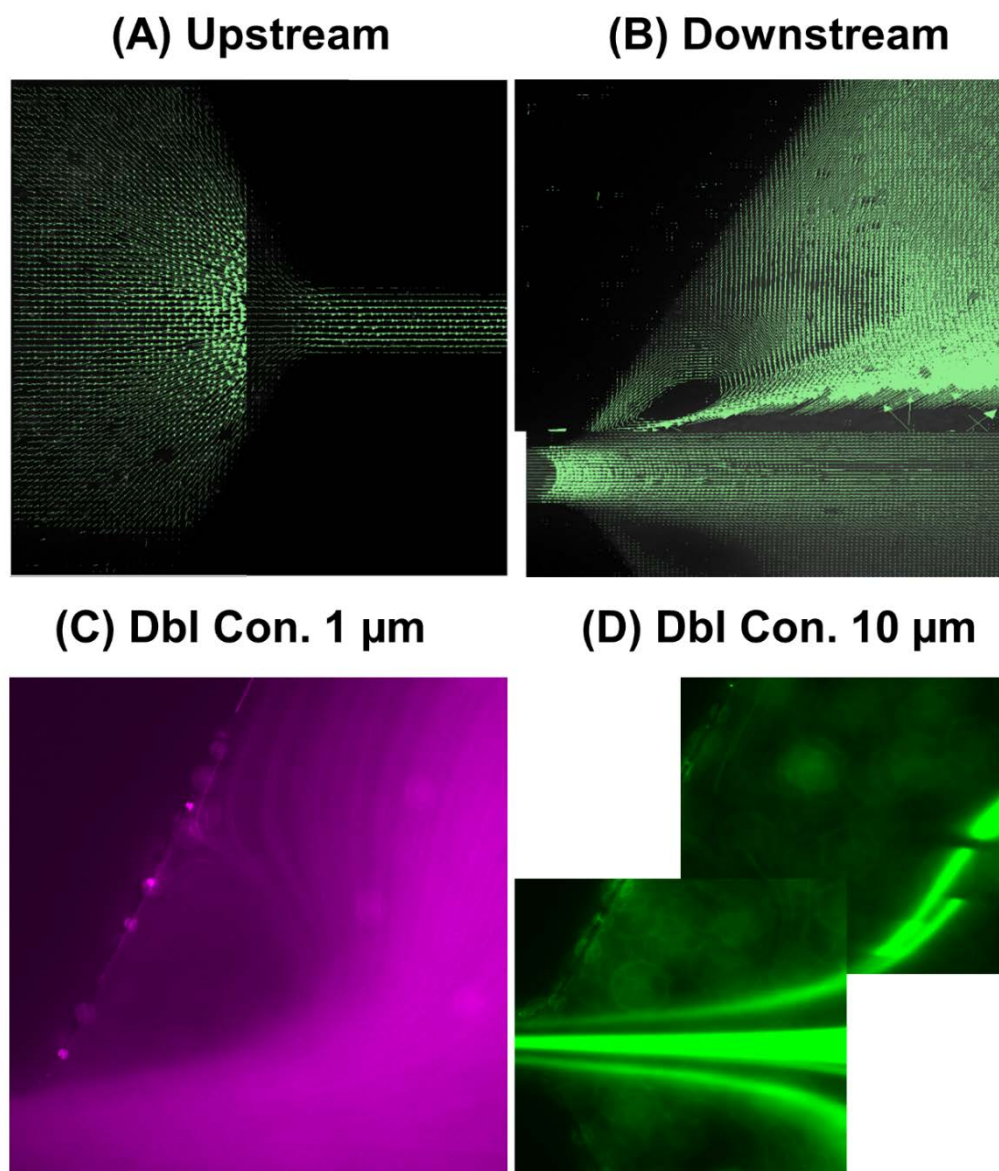


Figure 2.18: Recirculation Zones in Buffer Solution. Panels (A) and (B) show μ PIV data for a type D constricted channel. The constriction and wider region

velocities have to be measured with separate exposure time delays, and have been positioned overlapping. In each section arrow length corresponds to velocity magnitude, but cannot be compared between the two images for each section, as the constricted velocities are much higher. The bottom panels show bead flow paths for beads exiting the double constriction channel with (C) consisting of the $1\ \mu\text{m}$ beads, while the large streaks in (D) show the $10\ \mu\text{m}$ beads. Beads are traveling faster than the camera capture, and thus appear as streaks.

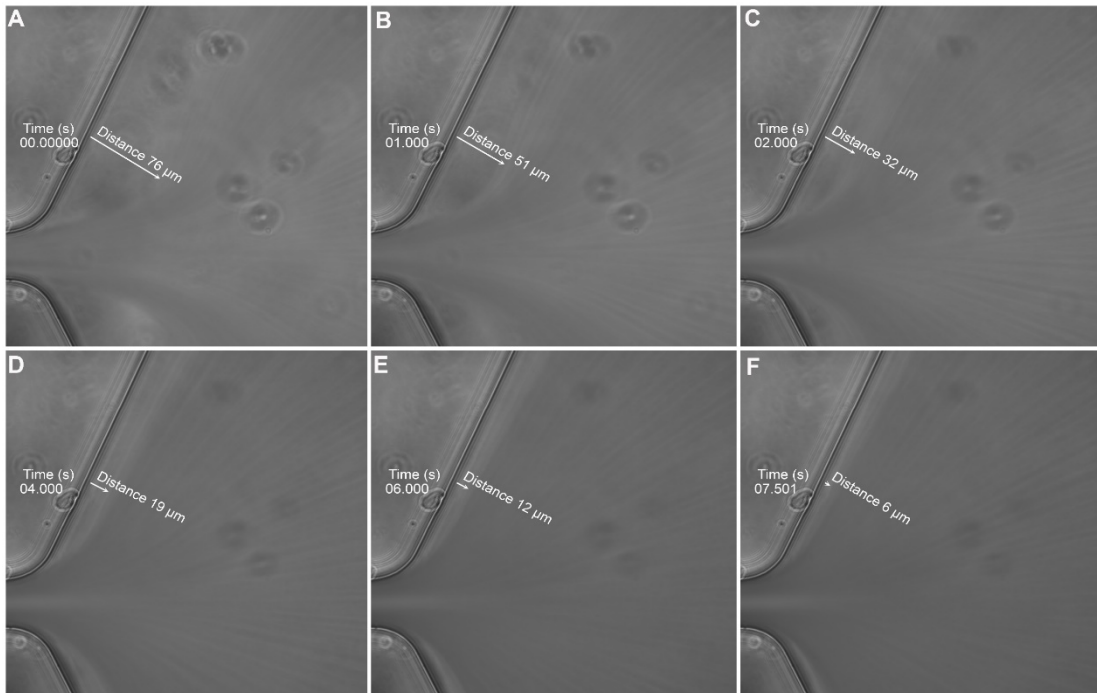


Figure 2.19: Flow profile in whole blood at the post-constriction region for Con. D. Conditions correspond to an exposure of $98,000\ \text{s}^{-1}$ for 16 msec. The recirculation zone disappears quickly with the introduction of whole blood. Images are taken from a video sequence and the white arrow represents the approximate thickness of the cell free layer. Image reprinted with permission¹⁰.

Conclusions:

In this chapter we outlined the design and characterization of a versatile set of microfluidic devices to study the effects of short exposures to high shear

on blood cells. The channel design is highly adaptable and can be easily altered to create different shear rate and exposure time regimes. It can also be used with a variety of cell types and downstream assays, and the incorporation of the vacuum design allows for use with protein patterning and adhesion assays^{10,176}. Additional constrictions can expand the study to examine the compound effect of sequential exposures.

We used a μ PIV system to characterize the fluid velocity profiles in all of the designs to be used throughout this study. The shear rate was subsequently estimated from a second order polynomial fit on these profiles. For the majority of the conditions tested, the experimental velocity profiles aligned closely with the expected theoretical velocities from the analytical solution. For the lower shear conditions ($<10,000 \text{ s}^{-1}$) the shear rate was a little higher than originally predicted. Significant deviations due to an increased pressure drop were observed with the highest flow rates and longest constricted lengths, leading to significant decreases in the velocity and shear rates for these channels. Using the μ PIV system we were able to determine the increase in flow rate needed to adjust the shear rates to be used for later studies.

In addition to the μ PIV characterization, we also introduced a simple method to support and reinforce the PDMS for higher shear applications. We demonstrated that the incorporation of glass near the top wall of the device prevented collapse, and maintained a constant shear rate upstream and downstream of the constriction. This allows for the study of higher pathological shear rates for adhesion studies with leukocytes.

Chapter 3: Effects of Transient Exposure to High Shear on Neutrophil Rolling Behavior

Major portions of this chapter were reproduced in part with permission from:

Lewis, C.S., N.Z. Alsmadi, T.A. Snyder, and D.W. Schmidtke. Effects of Transient Exposure to High Shear on Neutrophil Rolling Behavior. *Cell. Mol. Bioeng.* Springer US, 11:279–290, 2018. Springer Nature, copyright 2018

Introduction:

Neutrophils are one of the most important cell contributors to the immune response, due to their role as first responders of the innate immune system. This role requires a diverse range of function and behavior including rolling, migration, phagocytosis, secretion of activating molecules for the recruitment of other leukocytes and platelets, apoptosis, and extracellular trap formation^{38,203}. In addition, neutrophils have been implicated to play a role in a number of health complications such as cancer^{100,246} and thrombosis^{145,317}. Since neutrophils reside within the bloodstream, they are naturally exposed to a wide array of shear conditions, at both arterial and venous levels. On the venous side, it is well known that wall shear rates, which normally range from approximately 10-1,000 s⁻¹, modulate neutrophil rolling via selectins^{9,17,95,149,163,171}. Furthermore, there have been reports that fluid shear can affect other neutrophil behavior such as the activation state or receptor levels^{102,104,214,215,278}.

Most studies of neutrophil behavior in response to shear have focused on physiological shear stresses in the range of 50-2,000 s⁻¹. However, neutrophils and other blood cells can be introduced to a wide variety of higher shear rates

stemming from both physiological and non-physiological origins. Shear rates can range up to approximately $2,000 \text{ s}^{-1}$ in the arterial system, with pathophysiological shear rates starting around $3,000\text{-}10,000 \text{ s}^{-1}$ in atherosclerotic vessels and stenosis, with severe stenosis (above 90% blockage) potentially increasing beyond this point^{159,238,295}. In addition to these pathophysiologic sources, a variety of devices can introduce blood cells to increased shear rates. Ventricular assist devices are one such example, with high shear rates present primarily around the rotors of the pumps. Maximum shear rates in these devices vary depending on the type of device and flow path of the cell, but can reach as high as $100,000 \text{ s}^{-1}$. The exposure time for such shear rates ranges from approximately 1-15 milliseconds²⁸⁸. Average shear exposures in certain types of VADs can be encountered over several hundred milliseconds at relatively lower shear rates around $3,000 \text{ s}^{-1}$ ⁹⁸. Other devices, such as hemodialysis machines designed to filter blood, also create new points of high shear in the approximately $2,000 \text{ s}^{-1}$ range, as well as possible atherosclerotic vulnerable regions²⁹¹. Many of these devices, despite their clinical utility, have seen a variety of complications encountered throughout the device lifetime, including high infection rates, bleeding rates, thrombosis, hemolysis, and several other symptoms^{112,279,291}. Infection has been reported in 20-60% of VAD patients, with sepsis as the leading cause of death. While this is generally attributed to biomaterial interaction with tissue, the persistence of infections throughout the device lifetime suggests that this viewpoint may be incomplete. In addition, some studies have indicated that

approximately 40% of these infections are not directly related to the device itself¹¹².

Recent studies have revealed that shear not only affects rolling but other neutrophil functions and receptor levels as well. Fluid shear can affect cell shape and pseudopod retraction^{62,103,104,193,217,278}, cell stiffness^{63,217}, receptor integrin levels^{4,102,339}, and cell activation^{276,278}. More recent studies have elucidated the ability of neutrophils to sense and react to shear through various surface receptors. Notably, Mitchell et al.^{214,215} have examined the effect of venous shear rates (10-400 s⁻¹ for 1-120 min) on various receptors related to neutrophil activation and sensing. Surprisingly, the n-formylmethionine-leucyl-phenylalanine (fMLP) receptor decreased in expression level following shear exposure²¹⁴, while shear exposure caused the platelet activating factor (PAF) receptor level to increase²¹⁵. Similarly, other studies have reported a change in receptor expression levels, such as a decrease in CD18 levels due to cleavage following prolonged exposure to shear¹⁰².

Few studies have examined the effect on leukocyte behavior of high shear rates above 3,000 s⁻¹ present in pathological conditions and in some blood-contacting biomedical devices such as VADs and hemodialysis. Almost all of the leukocyte studies that have examined the exposure time have been on the scale of minutes to hours, rather than a clinically relevant, millisecond exposure time encountered in vivo^{62,102,104,214}. Since 2003, there has been only one study examining the effects of millisecond exposure to high shear rates on leukocyte function. In the study by Carter et al.⁴⁶, whole blood was perfused through

capillary flow chambers of various lengths and diameters to produce shear rates of $3,700 - 34,000 \text{ s}^{-1}$ and exposure times of 90 and 125 msec. They observed that exposure of whole blood to a shear rate of $\sim 3700 \text{ s}^{-1}$ for 90 or 125 msec was sufficient to reduce the phagocytic ability of leukocytes.

The traditional method to expose leukocytes to high shear is with the cone and plate viscometer, due to the fact that it applies a uniform shear magnitude to all of the cells in a sample. Although studies employing the cone and plate viscometer have led to an abundance of information on the effects of shear on neutrophil biology, the startup times for these devices limit their use in studies that involve transient ($< 1 \text{ sec}$) high shear exposure. In addition, they do not mimic the flow geometry that neutrophils experience during interactions with the vessel wall or allow for rolling behavior to be studied.

The aim of this study was to develop a microfluidic assay that could mimic the transient, high shear exposure environments that are relevant to pathological conditions present in stenosis and blood-contacting medical devices. We describe the fabrication of a series of microfluidic channels that have constricted regions of varying length. The microfluidic devices were designed to (i) utilize small sample amounts ($< 200 \mu\text{l}$), (ii) allow for precise control over fluid shear rates and high shear exposure times, and (iii) allow for real-time optical microscopy imaging. By perfusing suspensions of isolated neutrophils over P-selectin coated Petri dishes through constricted microfluidic devices, we were able to detect changes in neutrophil rolling velocities over P-selectin coated regions following transient exposure to high shear conditions. We demonstrated

that the changes in rolling velocity were related to the duration of the high shear exposure.

Methods:

Proteins and reagents.

FITC tagged mouse-anti-PSGL-1 mAb PL1 was purchased from MBL (Woburn, MA), while unlabeled PL1 was purchased from Ancell (Bayport, MN). P-selectin purified from human platelet membranes and 2-glycosulfopeptide (GSP-6) were kindly provided by Dr. Rodger McEver (Oklahoma Medical Research Foundation). Recombinant P-selectin was purchased from R&D systems (Minneapolis, MN). Phorbol 12-myristate acetate (PMA) was purchased from Sigma Aldrich (St Louis, MO).

Neutrophil collection and isolation from whole blood

Blood was collected via venipuncture into heparin coated vacutainers from healthy adult volunteers after informed consent was acquired, according to a process approved by the Institutional Review Board (IRB). Neutrophils were isolated from whole blood using Poly-lympholyte solution (Cedarlane, Burlington, NC) according to the manufacturer's instructions. Five milliliters of whole blood was slowly layered upon an equal volume of the lympholyte solution and spun for 35 minutes at 500xg. The granulocyte layer was carefully removed and washed in an equal volume of 0.4% (w/w) sodium chloride (NaCl), followed by Hanks balanced salt solution (HBSS, Lonza BioWhittaker, Allendale, NJ) without calcium and magnesium. Cells were centrifuged at room temperature at 450xg for 15 minutes. Residual erythrocytes were then lysed with a hypotonic salt solution: 0.2% NaCl followed by an equal volume of 1.6% NaCl. After

centrifugation for 10 minutes, the isolated neutrophils were washed three times with 0.5% human serum albumin (HSA; Octapharma, Hoboken, NJ) in HBSS without calcium and magnesium. Washes were done for 5 minutes each. All spin steps were done at room temperature at 450xg unless otherwise noted. Cells were then resuspended at 4×10^5 cells/mL in 0.5% HSA in HBSS with calcium and magnesium.

Design, fabrication, and assembly of the microfluidic shearing device

To assess the effect of short exposure to high shear on neutrophil behavior, microfluidic chambers were designed to create two low shear regions flanking a high shear constriction, as described in chapter 2 (Figure 2.2). The two wider regions flanking the high shear constriction provide low shear regions that allow one to measure the effects of shear exposure on cell rolling velocity. Straight microfluidic channels with a constant width were also fabricated and served as a control by providing a baseline rolling velocity. Microfluidic devices were prepared from poly-dimethyl siloxane (PDMS; Dow Corning, Midland, MI) in a 10:1 ratio as previously described^{59,275}. Briefly, the master mold was fabricated through a standard negative photolithography technique using KMPR 1050 photoresist (MicroChem, Westborough, MA). PDMS was poured over the photoresist mold and degassed for one hour. Elbow outlet ports (Value Plastics, Fort Collins, CO) were then placed at one end, and wafers placed in an oven at 80°C for at least 1 hour to cure.

In order to fabricate the wider channels designed for higher shear rates ($100\text{-}8,600\text{ s}^{-1}$), while avoiding deflection issues, glass was embedded in the top

PDMS layer. Thick plastic Petri plates were used for the bottom surface of the assembled device. These devices were therefore created in a similar fashion to the lower shear channels, but required a two-step PDMS pouring process. First, a thin layer of PDMS was poured over the photoresist mold; this layer was just enough to cover the entire surface. The PDMS was degassed and then placed in an oven with the elbow outlet port for 30 minutes. Glass strips cut from microscope slides (VWR, Radnor, PA), wider than the channel, were placed to span across the width of the device. The glass pieces went from the elbow to the front reservoir, leaving a small amount of room on either end. Additional PDMS was then poured on top of the solidified layer, to the final PDMS device height. See Figure 2.11 for a schematic of the device with embedded glass.

Glass coverslips (No. 1.5), when used as a bottom substrate, were first acid cleaned. Slides were rinsed three times with water and then placed in a 28% nitric acid solution for one hour. Slides were then rinsed an additional three times in water, followed by a 5 minute incubation in water before being placed in a vacuum oven to dry for 2-3 hours. Nitric acid cleaned slides were then coated with an Aquasil solution (ThermoFisher Scientific, Waltham, MA). Slides were dipped in a 1% Aquasil solution for 15 seconds, and then removed and rinsed three times in water. Slides were then dried for 30 minutes in a vacuum oven.

To assemble the device, 15 μ l drops of P-selectin (Ps) were deposited on plastic Petri dishes or glass coverslips and incubated in a humidified environment. Incubation conditions are listed in Table 3.1 below. Two types of P-selectin were used: membrane and recombinant (mPs and rPs respectively).

Previous experiments in our lab (unpublished) suggested that 3 hours at room temperature (RT) and overnight (O/N) at 4°C provide relatively similar site densities of P-selectin adsorption. P-selectin drop concentrations were optimized to ensure that rolling velocities for all three conditions were similar. In this study, we observed that less protein was required when the concentration was saturated overnight on Petri dishes, while a much higher concentration was needed for the recombinant P-selectin. After incubation, the P-selectin was rinsed with HBSS, and the Petri dishes were incubated with a 0.5% HSA solution to prevent non-specific binding.

Table 3.1: Protein incubations for channels used for neutrophil rolling. Two different surfaces were used to create the bottom surface of the microfluidic devices. In addition, two types of P-selectin and incubation conditions were used. Membrane P-selectin (mPs) and recombinant P-selectin (rPs) were used.

Bottom Substrate	Channels	Con. Shear Rate (s⁻¹)	Protein Conc.	Incubation
Glass coverslip	A-E	4700	mPs 1 µg/mL	3 hours RT
Plastic Petri dish	A-E	5900	mPs 0.75 µg/mL	O/N 4°C
Plastic Petri dish	H-L	8600	rPs 4 µg/mL	O/N 4°C

After 30 minutes of blocking, the HSA solution was carefully removed and replaced with HBSS until use in the rolling assay. Next, the HBSS solution was removed from the Petri dish, and the PDMS microfluidic channel was carefully positioned on the Petri dish (via alignment marks built into the PDMS structure) so that the wide upstream and downstream regions on the channel were placed

over the P-selectin coated regions. The PDMS stamps were sealed to the plastic Petri dishes using a vacuum seal (Figure 3.1). Channels were charged and blocked with the 0.5% HSA solution for 10 minutes prior to cell rolling experiments. Channels sealed to glass coverslips were prepared in an almost identical manner. However, to seal the PDMS channels to the glass coverslips, stamps were placed in a plasma cleaner at high RF for 1 minute and then placed over the protein drops. Channels were charged with HSA and allowed to incubate for 30 minutes, and were then charged with HBSS until use.

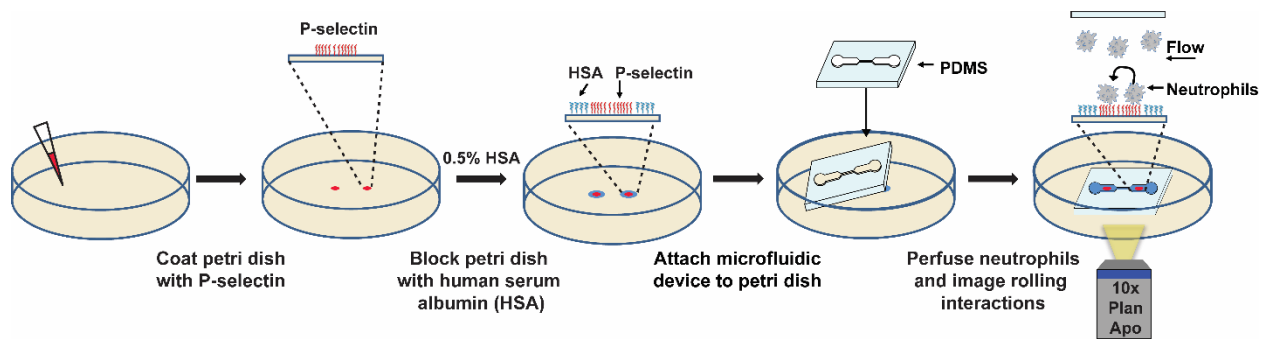


Figure 3.1: Overview of the microfluidic device assembly and neutrophil rolling assay. Drops of P-selectin are deposited on a plastic Petri dish and incubated at the conditions listed in Table 3.1. The Petri dish is then washed with buffer (HBSS) and blocked with human serum albumin (HSA). The constricted microfluidic device is carefully placed on the Petri dish so that the low shear upstream and downstream regions are positioned over the P-selectin coated regions. The microfluidic device is reversibly bonded to the Petri dish by applying a vacuum, placed on an inverted microscope stage, and filled with buffer containing HSA to prevent nonspecific adhesion to the channel ceiling and walls. A suspension of isolated neutrophils is then perfused through the device and images of rolling neutrophils are recorded.

Neutrophil and bead rolling assays

Isolated neutrophils were perfused through the microfluidic devices at 4×10^5 cells/mL. The channels were perfused with buffer for two minutes to

stabilize the flow prior to the introduction of the cells. Cells were imaged using a Zeiss AxioObserver equipped with a 10X phase contrast objective (0.25NA) and a digital camera (Orcaflash 4.0; Hamamatsu, Bridgewater, NJ) set at 30 frames per second. At least 30 cells were tracked in both the upstream and downstream region for each channel and shear condition, and instantaneous velocities were measured over a five second interval. Instantaneous velocities were determined using the particle tracking function in ImagePro Premier. The average of the instantaneous velocities was then determined and the average taken over the 30 cells. The instantaneous velocities were also used to determine the variance. To calculate the variance, the square of the difference between the instantaneous velocity and the average instantaneous velocity was averaged over the five second interval for each cell. Averages over the 30 cells were then taken for each channel. Channels using neutrophils from at least five different donors were collected for each condition.

Microspheres bearing 2-glycosulfopeptide (GSP-6), which is a glycosulfopeptide modeled after the P-selectin binding region of PSGL-1, were prepared as described previously³²⁹. Briefly, 10 μm polystyrene beads (Polysciences, Warrington, PA) were washed three times with HBSS to remove the surfactant in the storage buffer. The beads were then coated overnight with end-over-end rotation in 1% neutravidin in HBSS. Beads were blocked for 30 minutes with rotation in a 1% HSA solution in HBSS before being incubated with biotinylated GSP-6 for 3.5 hours on ice, with vortexing every 30 minutes. The beads were then washed 3 times with HBSS. GSP-6 concentration on the bead

surface was measured via flow cytometry using a FITC conjugated mAb PL-1. Samples were analyzed on a BD Accuri™ C6 flow cytometer (Franklin Lakes, NJ).

Analysis of PSGL-1 levels

In order to collect sufficient sample volume for flow cytometric analysis, a second set of channels was designed and fabricated with cross-sectional dimensions (height = 120 μm , width = 90 μm) that were two times larger than the original channels. These larger channels exposed the cells to the same wall shear rate, but at a flow rate (40 μl /min) that was 8 times larger, which provided enough neutrophil sample volume (200 μl) for flow cytometric analysis. These experiments were performed in a similar manner to the rolling experiments. First, buffer was perfused through the channels for two minutes to stabilize the flow before the addition of cells. Cells were then perfused through the channels and collected for five minutes. In control experiments, suspensions of unsheared, isolated neutrophils were incubated for 10 minutes at 37°C in buffer (unstimulated) or with 10 nM phorbol 12-myristate acetate (PMA) (stimulated). It has been reported that exposure to PMA reduces surface expression of PSGL-1 on neutrophils^{68,106}. Cells were then spun down at 500xg for 5 min and labeled with PL-1 on ice for 30 minutes. Cells were washed with 1 mL of 0.5% HSA in HBSS, then resuspended in anti-mouse 488 secondary antibody for 30 minutes on ice. Cells were washed again with 1 mL of 0.5% HSA in HBSS, then resuspended in this same solution for flow cytometric analysis.

Statistical analysis

All velocity values are reported as the mean \pm standard error of the mean. Statistical significance of rolling velocities and variances were assessed using paired student t-tests with $P < 0.05$ considered significant. PSGL-1 levels were analyzed via ANOVA with a Sidak post hoc test and compared to the unsheared sample, with $P < 0.05$ considered significant.

Results and Discussion:

Effect of transient high shear exposure on neutrophil rolling

To investigate the effect of transient high shear exposure on neutrophil rolling behavior, isolated neutrophils were perfused through the microfluidic devices and allowed to roll on P-selectin coated regions upstream and downstream of the constriction at a wall shear rate of 125 s^{-1} . Cells were exposed to high shear rates, in the constricted regions, of $4,700$ and $5,900 \text{ s}^{-1}$. These shear rates correspond to the values for constricted channels B-E sealed to the glass coverslip and the plastic Petri plate, respectively. Differences in the estimated shear rate in the constriction is due to the height of the channels. In chapter 2 we showed that the height was a significant factor in determining the shear rate in the constricted region.

Isolated neutrophils rolling on P-selectin coated regions were tracked for five seconds, and the instantaneous rolling velocities were measured for each cell. Figure 3.2 shows representative plots of a frame-by-frame analysis of the fluctuations in the rolling velocities of neutrophils rolling on P-selectin upstream (Fig. 3.2A) and downstream (Fig. 3.2B) of a constricted region having a high shear exposure time of 310 msec at $5,900 \text{ s}^{-1}$. Neutrophil rolling on the P-selectin coated region upstream of the constriction displayed a relatively constant rolling velocity with a limited number of large velocity spikes ($> 15 \text{ } \mu\text{m}/\text{sec}$) and a substantial number of pauses. In contrast, at the P-selectin coated region downstream of the constriction, neutrophil rolling was faster and characterized by a more variable rolling behavior, which consisted of a large number of velocity

spikes and only a handful of pauses. Figure 3.2C shows a cumulative histogram of the rolling velocities measured at the upstream and downstream P-selectin coated regions. As indicated by a shift to the right, the mean rolling velocity of neutrophils rolling after high shear exposure (i.e., downstream region) was faster than neutrophil rolling prior to high shear exposure (i.e., upstream region). Instantaneous velocities had a similar behavior between plastic and glass substrates (data not shown).

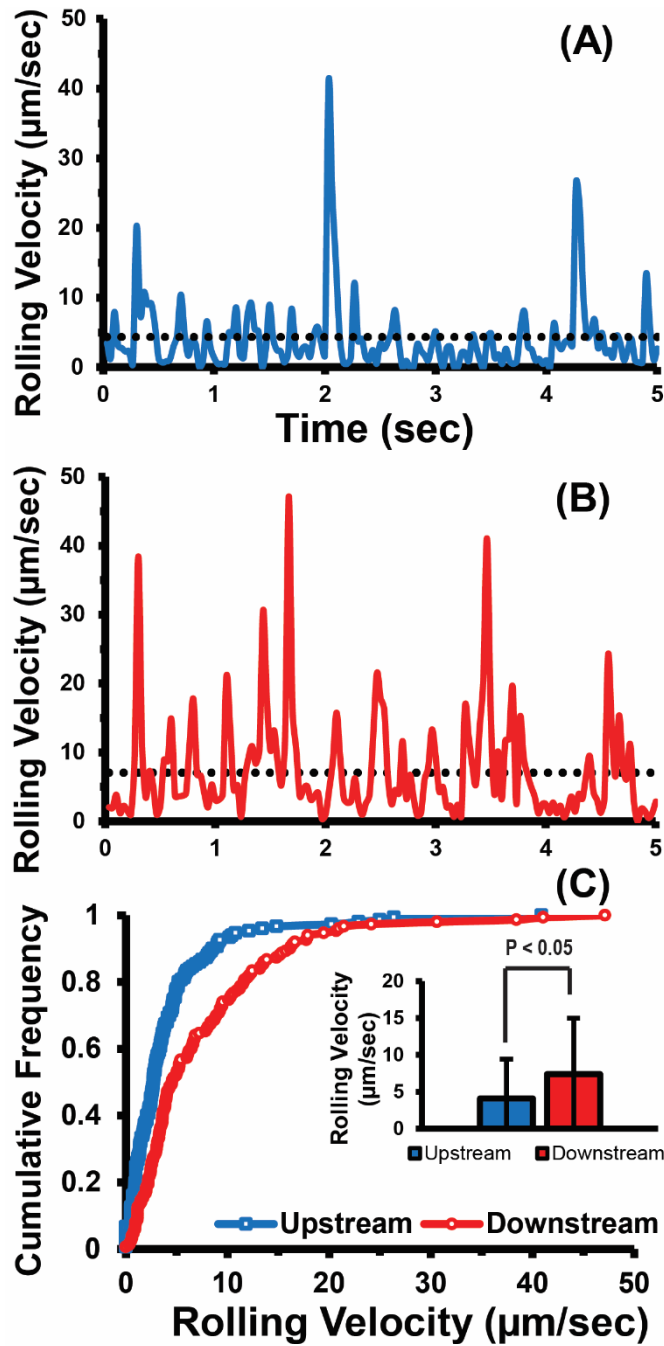


Figure 3.2: Effect of high shear (5900 s^{-1}) on the instantaneous rolling properties of neutrophils. Instantaneous velocities of representative neutrophils rolling on P-selectin in the (A) upstream and (B) downstream regions of a Type D constricted microfluidic channel. The dotted line in each plot represents the average rolling velocity. Upstream and downstream shear rate = 125 s^{-1} , high shear exposure time = 310 msec. (C) Cumulative histogram and average rolling velocities for the individual cells shown in (A) and (B).

To probe whether this observation, that transient high shear exposure caused neutrophils to roll faster, was dependent upon the exposure time, we perfused neutrophils through a complementary set of microfluidic channels with varying lengths (3.9 – 15.0 mm) of the constricted region, and we measured neutrophil rolling velocities upstream and downstream of the constriction. The lengths of these constricted regions are comparable to the lengths reported for coronary lesions (12.49 ± 7.52 mm)¹³⁵ and to the stenosis lengths (> 15 mm) used as a criteria for defining diffuse coronary artery disease (CAD)²⁹⁹.

We began our investigation into the effect of exposure time on neutrophil rolling velocity with a constricted region exposure of $4,700$ s⁻¹. Upstream and downstream regions were coated with mPs. Since these channels were the first set to be run, a one sided plasma cleaning method was used to seal the channels to glass coverslips, which creates a temporary seal. These channels were measured to be 58 μ m tall. Based on our observations during the μ PIV experiments in chapter 2, this height corresponded with a shear rate of $4,700$ s⁻¹. The estimated exposure times were then adjusted accordingly for these channels. Figure 3.3 shows the mean rolling velocities of neutrophils rolling on mPs coated regions upstream and downstream of the constricted region. The resultant high shear exposure times in our microfluidic devices ranged from 5 to 440 msec. As a control, we also perfused neutrophils through straight channel microfluidics. When neutrophils were exposed to a constant low shear rate (125 s⁻¹) in microfluidics with a straight channel geometry, we observed no statistical difference between the upstream and downstream rolling velocities. Exposure of

neutrophils to $4,700 \text{ s}^{-1}$ for 340 and 440 msec led to rolling velocity increases of 1.6 and 1.8 fold, respectively. A minimal 1.1 fold increase was observed in the 230 msec channel, with no differences observed in the 5, 10, and 110 msec channels.

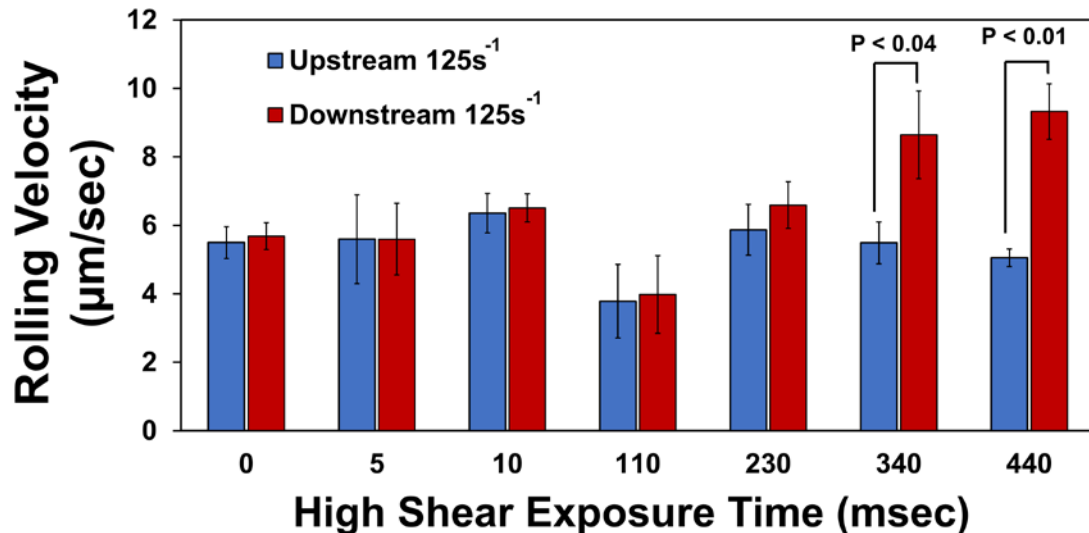


Figure 3.3: Neutrophil rolling on glass cover slips. Average rolling velocities of neutrophils rolling on mP-selectin at upstream and downstream locations in a straight channel (0 msec high shear exposure) and six constricted microfluidic channels are shown. Channels 110-440 represent Con. B-E as described in chapter 2. Two other constricted channels with short exposure times were included at 5 and 10 msec for this portion of the study. High shear rate exposure = $4,700 \text{ s}^{-1}$. Bars represent the standard error of the mean. N = 4-9 donors per condition.

To further examine the effect of high shear on neutrophil rolling velocity, the equivalent study was next completed on a second bottom substrate surface: plastic Petri plates. We wanted to examine the effect of high shear on neutrophil rolling on both glass and plastic surfaces, two commonly used substrates for neutrophil rolling studies. The channels on the plastic substrate were sealed with

a built in vacuum feature, to provide a more consistent seal (schematic Fig. 2.3). As was described in the corresponding μ PIV section in chapter 2, the heights of these channels was found to be lower, at approximately 53 μm . Consequently, the shear rate was increased in these channels, with a constricted region value of $5,900 \text{ s}^{-1}$. While there were a few differences between the two substrates, the overall results remained the same between those on plastic with those shown in Figure 3.3 on glass. Figure 3.4A shows the mean rolling velocities of neutrophils rolling on mP-selectin coated regions upstream and downstream of the constriction. In this section we added another analysis component; the variance in velocity is shown in Fig 3.4B. Exposure of neutrophils to high shear (5900 s^{-1}) for 100 or 210 msec showed small increases (1.2 fold and 1.3 fold) in their downstream rolling velocity; however, these increases were not statistically significant ($P > 0.05$). Increasing the high shear exposure time to 310 msec led to a 1.5 fold increase in the rolling velocity while an exposure time of 390 msec resulted in a 1.4 fold increase. Analysis of the variances of the upstream and downstream rolling velocities (Fig. 3.4B) showed a similar, significant increase in the downstream region compared to the upstream region for exposure times of 310 and 390 msec. The variance results suggest that the degree of rolling irregularity increased with exposure time. In other words, that the increases in rolling velocity observed are heavily influenced by the high instantaneous velocity spikes, rather than the velocity uniformly increasing. Taken together the velocity and variance results suggest that transient exposure to high shear causes neutrophils to roll faster and less uniformly.

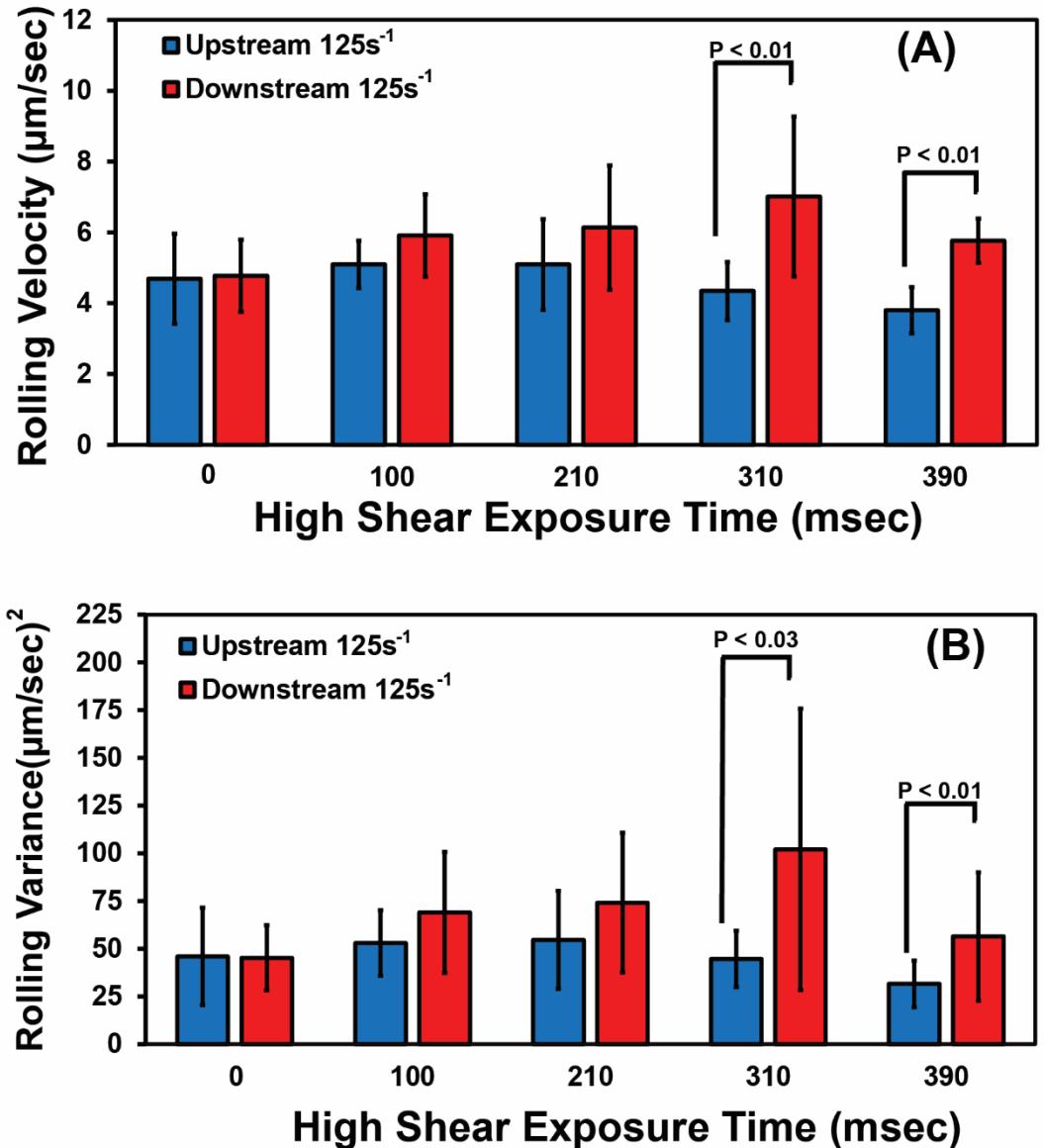


Figure 3.4: Neutrophil rolling on plastic Petri plates. (A) Average rolling velocities and (B) average velocity variances of neutrophils rolling on mP-selectin at upstream and downstream locations in a straight channel and four constricted microfluidic channels (Con. B-E). High shear rate = $5,900 \text{ s}^{-1}$. Bars represent standard error of the mean. $N = 6-12$ donors per condition.

The critical exposure time required to observe a statistically significant increase in the rolling velocity in the downstream region was similar for rolling on

plastic and glass, at exposure times of 310 and 340 msec (constricted channel D in both cases). Rolling behavior was likewise comparable between the two substrates, with increases in the magnitude and frequency of elevated velocity spikes in the downstream regions of Con. D and E. Although the general results are the same, there are a couple of differences between these two parts of the rolling study. By examining Figures 3.3 and 3.4, we notice that there is less variation in the upstream velocities on the plastic substrate, suggesting that the plastic Petri plate provides more consistent rolling than that on the glass. We see the starkest contrast in the velocities of Con. B (100-100 msec) between the two substrates. This variation has a couple potential sources and was a factor in transitioning to the plastic Petri plates with an overnight incubation. For example, the glass coverslips are coated with a silicanized surface to assist with the uniformity of the protein coating; coating conditions are kept constant between batches of slides, but this remains a potential source of variation. The plastic dishes from the manufacturer require no additional treatment for uniform protein binding. For the channels on both substrates, there is no significant difference in the upstream velocities for the constricted channels with the upstream and downstream velocities of the straight channel (Str. A). We can thus conclude that the rolling velocities between the two substrates are similar.

Effect of shear rate magnitude and the critical exposure time

To expand the study, a second set of channels were designed in order to approximately double the shear rate magnitude. This allowed us to investigate the combined effect of shear rate and exposure time, as well as introduce a higher

pathological shear. In order to preserve the shear rate profile as accurately as possible between the sets of channels, the same constriction dimensions were used (45 x 60 μm). Doubling the flow rate from 5 to 10 $\mu\text{L}/\text{min}$ therefore allowed us to increase the shear rate in the constriction, up to 8600 s^{-1} . Since neutrophil rolling, especially *in vitro*, resides in a limited range, we needed to preserve the shear rate used. The wider regions were correspondingly increased by a factor of two in width, to 3000 μm wide. The resulting shear rate in the upstream and downstream regions was a little lower for this set of channels, at 90 s^{-1} . A detailed description of the design for these channels, H-L, and μPIV characterization was examined and found in chapter 2, and dimensions can be found in Table 2.3. A previous study from our lab displayed a difference in neutrophil rolling behavior and velocity with channel height⁵⁹, thus we wanted to maintain height consistently throughout the channels used (at $h = 60 \mu\text{m}$). Taken together, this channel design allowed us to examine neutrophil rolling while maintaining similar exposure times, but with a higher shear rate exposure.

Previous studies, although with platelets primarily, have examined a cumulative effect of shear rate magnitude and exposure time²⁷³. They showed that it was a combination of these two factors that could affect the degree of activation. We expected to find a similar trend for neutrophils after shear exposure. The expectation was that doubling the shear rate magnitude would lower the critical exposure time required to see an alteration in the neutrophil rolling velocity, and thus the exposure time required for dysfunction in a portion of the adhesion cascade.

Isolated neutrophils were perfused through the 100-8,600 s^{-1} set of channels (Str. H – Con. L) and, similar to the lower shear conditions (4,700 and 5,900 s^{-1} using channels Str. A – Con. E), an increase in rolling velocity was observed in a subset of the channels. We observed a significant increase in the downstream velocities following exposures of 240 and 350 msec, in constrictions K and L respectively. These exposure time values are nearly identical to the exposure times for Cons. C (230 msec) and D (340 msec) on the glass substrate at $\sim 4700 s^{-1}$. The increase in the downstream to upstream rolling velocity ratios were around 1.5 and 1.6 respectively. The 120 msec channel (Con. J) again had a 1.2 fold increase.

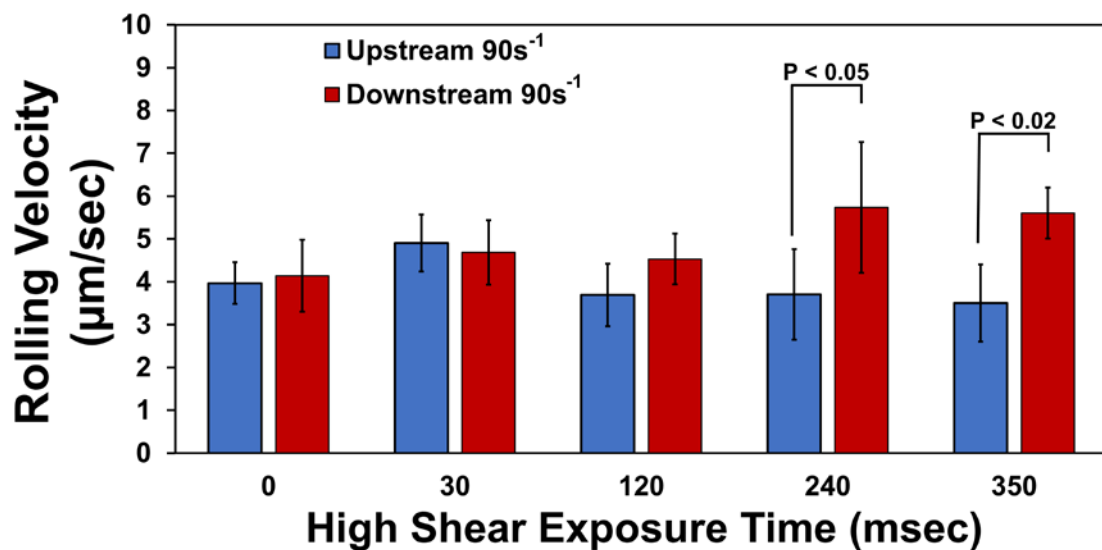


Figure 3.5: Effect of increasing shear rate ($8,600 s^{-1}$) on critical high shear exposure time for neutrophil rolling on plastic Petri plates. Average rolling velocities of neutrophils rolling on rP-selectin at upstream and downstream locations in a straight channel (0 msec high shear exposure) and four constricted microfluidic channels are shown. Channels (H-L). Bars represent the standard error of the mean. $N = 4-5$ donors per condition.

These results give us some indication that the physiologically relevant lengths found in severe stenoses could cause an impact in neutrophil adhesion behavior. Increasing the shear rate leads to a decrease in the critical exposure time, as the increased rolling velocity occurred after a shorter exposure time, as low as 240 msec at 8600 s^{-1} , rather than the 340 msec exposure needed at lower shear (4700 s^{-1}). This suggests (as expected) that both factors play a role in affecting the neutrophil's state and function. Increasing the shear rate by less than double decreased this critical exposure time by 100 msec, almost half. However, some caution in extrapolating these results is required. At this time we only have two shear rates to compare and we do not know the shape of the curve for the relation between shear rate and the critical exposure time. In addition, our shear rate exposure time range is broken into segments, and so we do not know the exact threshold time for each case more accurately than the approximately 100 msec intervals. However, based on these results we can expect increasing shear rates to decrease the critical exposure time, even if the slope of this relationship decreases or plateaus with higher shear rates. As mentioned, these lengths are representative of *in vivo* arterial stenoses, and the shear rates represent typical stenosis values. As discussed in the introduction chapter, severe stenoses could have significantly elevated shear rates an order of magnitude higher. If the critical exposure time continues to scale inversely with the shear rate, the results could be concerning for patients with cardiovascular disorders. On top of this fact, these results show an alteration with just a single pass to high shear, let alone the repetitive effect that could occur with additional

exposures. Both of these effects are extremely important and relevant to patients, and warrant further examination.

Effect of transient high shear exposure on PSGL-1 levels

One potential explanation for the increased neutrophil rolling velocities observed is that exposure to high shear may induce shedding or redistribution of PSGL-1, the native ligand on neutrophils for P-selectin. In support of this suggestion are the reports that fluid shear can activate and induce the cleavage of other neutrophil receptors such as CD18^{4,52,102,276,339} and the formyl peptide receptor (FPR)²¹⁴. Likewise, activation of neutrophils can lead to shedding and/or redistribution of PSGL-1^{43,68}, as well as L-selectin¹⁴⁴. It should be noted, however, that there are no reports that PSGL-1 is shed due to high shear exposure.

To examine the possible role of PSGL-1 shedding as the mechanism inducing faster rolling velocities in the downstream region of the devices, PSGL-1 levels were examined via flow cytometry. The antibody used, PL-1, recognizes an epitope in the binding region of PSGL-1 and is function blocking for PSGL-1 interaction with P-selectin. The channels used for the rolling experiments were designed to utilize very small sample volumes, < 50 μ L. As such, the flow rate on these channels was insufficient to collect enough cells for flow cytometric analysis. To circumvent this issue, a second set of channels was designed in which the cross-sectional dimensions of the channels were doubled (i.e., constricted region height x width dimensions = 120 μ m x 90 μ m). By keeping the channel height to width ratio constant, we were able to generate a similar shear rate profile but with an eight-fold increase in the flow rate, which allowed for

enough cells to be collected for flow cytometry within a few minutes. Figure 3.6 shows that there was no difference in the PSGL-1 levels for unsheared neutrophils, neutrophils perfused through a straight channel at a constant low shear rate (125 s^{-1}), and through a high shear (5900 s^{-1}) constricted microfluidic channel with a 310 msec exposure time. As a positive control, we also performed flow cytometric analysis of PSGL-1 levels on neutrophils exposed to PMA, which has been shown to reduce PSGL-1 levels^{68,106}. Similar to these previous studies, we also detected a significant drop ($\sim 50\%$) in PSGL-1 levels upon exposure to PMA. These results suggest that PSGL-1 shedding was not the cause for the increased rolling velocities following shear.

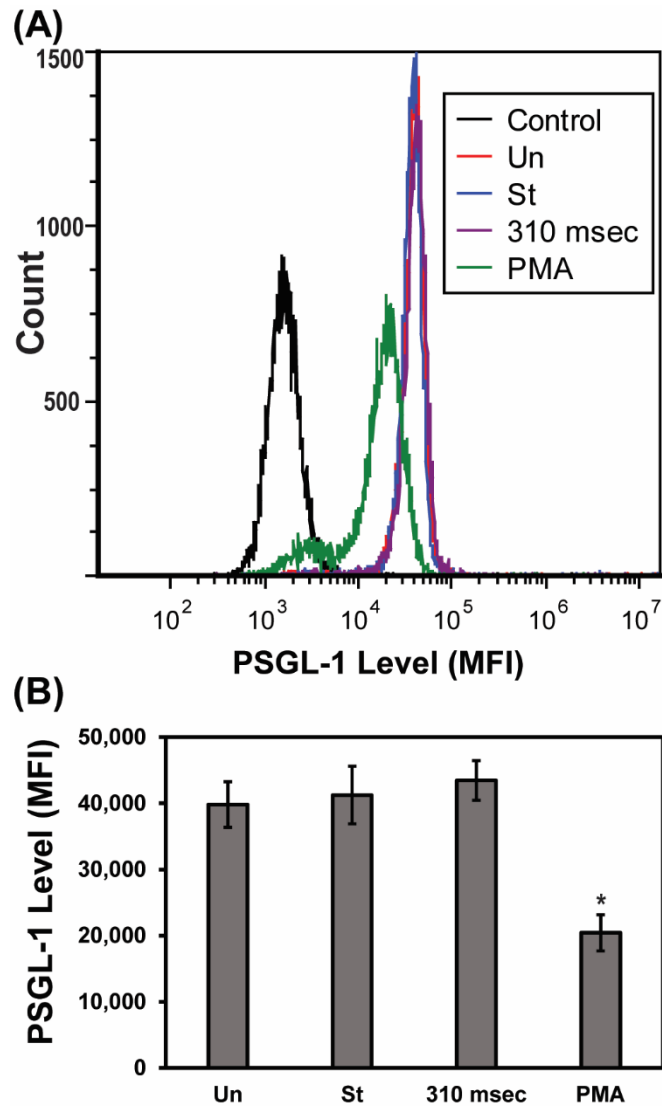


Figure 3.6: Effect of transient high shear exposure on surface levels of PSGL-1. Flow cytometry on isolated neutrophils from effluents from microfluidic channels. (A) Shows a representative histogram for the PSGL-1 signal for each sample. Control listed is a negative, secondary antibody only control. No difference is observed between the distributions in PSGL-1 for the unsheared (Un), straight (St), and 310 msec channels. (B) Shows averages of the mean fluorescent intensity \pm standard error of the mean and is representative of five independent experiments with different donors. Statistical significance of the differences between the samples and the unsheared sample was measured using ANOVA with a Sidak post hoc test (* $P < 0.05$). $N = 6$.

Effect of transient high shear exposure on GSP-6 coated bead rolling

A second possible explanation for the increase in rolling velocities downstream of the constriction is that, despite the agreement between the upstream and downstream μ PIV measurements, there may be small differences in the upstream and downstream shear rates. To test this possibility, we performed a complementary set of experiments in which we perfused GSP-6 coated polystyrene microspheres through the 310 msec constricted channels (Con. D) at $5,900 \text{ s}^{-1}$ and examined their rolling behavior. Frame-by-frame analysis of the rolling microspheres showed that they exhibited an irregular velocity profile at both the upstream (Fig. 3.7A) and downstream (Fig. 3.7B) P-selectin coated regions. Analysis of the upstream and downstream cumulative velocity profiles (Fig. 3.7C) showed no shift, suggesting no difference in the rolling velocities following high shear exposure. These observations were statistically confirmed by comparing the mean rolling velocities (Fig. 3.7D) and velocity variances (Fig. 3.7E) for a total of 60 beads rolling on the upstream and downstream P-selectin coated regions. Since the rolling velocity of GSP-6 coated beads are more sensitive to changes in shear rate^{253,329}, these results provide strong evidence that the rolling velocity changes observed with neutrophils were not due to differences in the upstream and downstream shear rates.

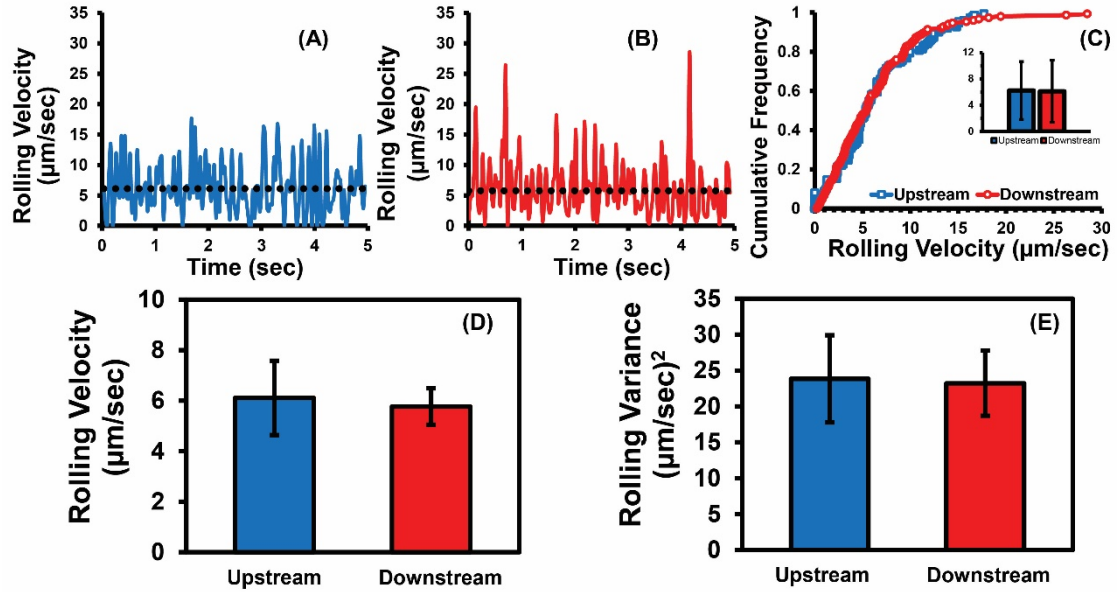


Figure 3.7: Rolling properties of GSP-6 coated beads upstream and downstream of the constricted region. Instantaneous velocities of GSP-6 coated polystyrene beads ($D = 10 \mu\text{m}$) rolling on P-selectin in the (A) upstream and (B) downstream regions of a Type C constricted microfluidic channel. The dotted line in each plot represents the average rolling velocity. Upstream and downstream shear rate = 125 s^{-1} , high shear exposure time = 310 msec, high shear rate = $5,900 \text{ s}^{-1}$. (C) Cumulative histogram and average rolling velocities for the individual cells shown in (A) and (B). (D) Average rolling velocities or (E) average velocity variances of GSP-6 beads rolling on P-selectin at upstream and downstream locations. The velocities in panel (D) and variance in panel (E) are average rolling velocities for at least 60 beads. Bars represent the standard error of the mean.

Conclusions:

In this section, we demonstrate an increase in the rolling velocity after short exposures to high shear. We hypothesized that this increase would be a factor of both the shear rate, as well as the exposure time. Two sets of data were examined for the first set of rolling conditions investigated. Membrane P-selectin used in both cases was adsorbed with static drops over time, while the exact time and concentration varied between and along with the bottom substrate (glass or plastic) used. The overall result was similar between the two sets of channels. In both cases the rolling velocity increases began at an exposure time greater than 310 msec (Con. D), with significant increases in the downstream velocity in this as well as the higher exposure time channel (Con. E). No significant difference in downstream velocities was observed for the two channels above the critical exposure time in either case. Any velocity differences observed between these two exposure times and channels (D and E) for the two cases is likely just from the natural variation in rolling velocities, which can have a large range even for normal cells in a straight channel. It is also possible that the rolling velocity appears to plateau because the *in vitro* P-selectin concentration is insufficient to support adhesion and rolling from what would be faster rolling cells that had more activation as a result of the shear exposure. Higher ligand densities of P-selectin would be required to examine if longer exposure times would continue to increase neutrophil rolling velocities in the downstream regions. The second set of data demonstrated the effect of shear rate on this critical exposure time. The critical

exposure time decreased by 100 msec for the 8,600 s⁻¹ channels, with increased downstream velocities observed by the 240 msec exposure channel.

At this time, the exact cause of the increase in rolling velocity following transient high shear exposure is unknown. One possible explanation is that high shear exposure causes the neutrophil's cytoskeleton to rearrange and stiffen. Previous studies using fixed cells and PSGL-1 coated beads have demonstrated that the elastic nature of microvilli²⁴² and cell deformation^{251,329} are important regulators of neutrophil rolling velocity. As cells lose the ability to deform, the contact area available for selectin binding is reduced, which leads to faster and more unstable rolling velocities. In support of this explanation are reports that adherent leukocytes will retract pseudopods and become stiff upon shear exposure^{63,193}. It is also possible that PSGL-1 redistribution causes the more irregular rolling observed. We believe that cell stiffening is the most likely explanation; however, this explanation is tentative and currently under investigation in our lab.

The importance of our findings is underscored by the fact that leukocyte rolling velocity determines the amount of time that leukocytes are in direct contact with the blood vessel wall to integrate multiple signals (e.g., chemokines, integrin ligands) that direct their infiltration into tissue and innate immune function. For example, using a mouse model of TNF- α -induced inflammation, Ley and coworkers demonstrated that slow leukocyte rolling (i.e., long rolling times) was necessary for efficient leukocyte recruitment^{143,164}. Our observation that transient exposure to high shear causes neutrophils to roll faster is surprising and would

suggest that leukocyte transit time and recruitment would be reduced. Reduced leukocyte recruitment would contribute to a defect in fighting infection and wound healing. At this time, information on the effects of transient exposure to high shear present in both pathological conditions and blood-contacting medical devices is sparse. Thus, assays that can detect instantaneous changes in leukocyte behavior, such as rolling velocity, are important for studying leukocyte biology and improving medical device performance.

Chapter 4: Altered Neutrophil State and Function Following Short Exposures to High Shear

Introduction:

The first process in the neutrophil lifetime is generally the emigration from the bloodstream to the sites of infection and inflammation¹⁷⁷. In chapter 3, we discussed the first step consisting of leukocyte binding to selectins, P- and E-selectin; this interaction allows for the initial capture and slowing of the free flowing cells. In addition, it also primes the neutrophil via inside-out signaling mechanisms. These intracellular signals lead to changes in the conformations of integrins such as LFA-1 and MAC-1 for subsequent slowing and arrest^{167,175,292}. Upon complementary activation from stimuli (e.g., chemokines), the cells can be further activated, resulting in processes including the opening of integrin headpieces to expose the high affinity binding site, the up-regulation of additional integrins (MAC-1) to the cell surface, and L-selectin shedding, among others^{1,37,129,151}. These types of events are critical for proper emigration of the leukocytes into sites of inflammation. They thus also serve as useful markers for neutrophil activation. There have been observations of these processes being affected by shear exposure, or more accurately, that shear exposure can reduce or amplify the neutrophil's response to various stimuli^{214,215}. These receptors play an important role in signaling proper activation of the cell upon stimuli such as chemokines and bacterial peptides, as well as downstream in some processes such as phagocytosis.

At sites of infection, activated neutrophils perform antimicrobial activity and cell-cell signaling for recruitment and activation. A large arsenal of granules imparts neutrophils with this diverse functionality. Neutrophil activation is not an all or nothing process. It is thought to progress in distinct stages marked by the release of different granule subsets and/or changes in cell surface receptors. Contents vary from cell surface receptors, to chemokines, to peroxidases^{42,65}. As such, they are essential in all stages of neutrophil pathogen response. As a result of this extensive specialization, granules also provide valuable markers for the different stages of activation. The most easily released granules, the secretory vesicles, are released rapidly and from low levels of activating agents. This can even include the priming from PSGL-1 interacting with P- or E- selectin. Thus, secretory vesicle release usually occurs at the beginning of the adhesion cascade⁹⁰. The rapid up-regulation of receptors increases the neutrophil's interaction with inflammatory signals on the endothelium. The next two intermediate granules, tertiary and secondary, are released during the later stages of migration. Tertiary granules contain a variety of gelatinases to breakdown the extracellular matrix¹⁵⁴. Secondary granules contain large pools of surface receptors, such as Mac-1 (CD11b/CD18), that are essential for proper migration^{37,65,92}. As discussed in the introduction, Mac-1 is important for the firm adhesion and migration through the endothelial wall, but also for many downstream functions after migration to inflammatory sites. Primary granules are the last to be released and due to their potent and hazardous contents, can cause significant damage. They are thus typically released either into the phagosome,

or at the site of infection. They contain antimicrobial agents such as the peroxidase MPO, and other proteases such as elastase and cathepsin.

To study neutrophil state and downstream function after transient high shear, we utilized microfluidic devices capable of producing very high shear (80,000-100,000 s⁻¹), with exposure times of 16-73 msec. We examined different markers of neutrophil activation, such as L-selectin shedding, conformational state shifts of CD11b, CD11b up-regulation, primary and secondary granule release, and changes in f-actin levels, following exposures to shear. Post-shear analysis uses a simple device with a fast, reliable, common, and easy method (flow cytometry) for the majority of the data collection.

Methods:

Antibodies and reagents:

CD11b FITC antibody clone cbrm1/5 and anti-MPO FITC were purchased from Biolegend. CD11b PE (phycoerythrin) ICRF44 was purchased from Ansell. Anti-oncostatin M (OSM) was purchased from R&D systems. Anti-CD66b APC (allophycocyanin) was purchased from Ebioscience. Phalloidin Oregon Green was purchased from Molecular Probes. Mouse anti-human 488 secondary antibody was purchased from Life Technologies. Paraformaldehyde (PFA) (16% solution) was purchased from Electron Microscopy Sciences. PharmLyse buffer was purchased from BD. The phagocytosis kit (pHrodo Green E. Coli BioParticles) was purchased from Molecular Probes. DAPI (4'6-diamidino-2-phenylindole) containing mounting media (vectashield) was purchased from Vector Labs. Human serum albumin was purchased from Octapharma. PMA, fMLP, and lipopolysaccharide (LPS) were purchased from Sigma Aldrich.

Blood collection:

Human blood was collected via venipuncture into sodium heparin coated vacutainers from healthy volunteers following informed consent, as approved by the IRB. The initial 3 mL of blood was collected into a separate tube and discarded to avoid activation effects from the draw. All whole blood experiments were run within an hour of the blood draw. Isolated neutrophils were run within 4 hours from the time of the draw.

Neutrophil isolation:

Whole blood was layered upon a poly-lympholyte gradient solution and spun for 30 minutes at 600xg. The neutrophil layer was then collected and washed with 0.4% NaCl in ultrapure water, followed by an equal volume of HBSS without Ca/Mg. Cells are then spun at 450xg for 15 minutes. Liquid is removed and the tube is gently tapped to loosen the cell pellet from the wall of the conical tube. Residual red blood cells were hypotonically lysed with salt solutions, which consists of 0.2% NaCl followed by an equal volume of 1.6% NaCl. The cells were then spun again for 10 minutes. The resulting neutrophils were then washed three times with HBSS with 0.5% HSA without calcium and magnesium. The cells were then resuspended in 0.5% HSA in HBSS with Ca/Mg and allowed to sit for 30 minutes before exposure to shear conditions in the channels.

Microfluidic chamber fabrication:

PDMS channels were made as previously described, with a 1:10 ratio of curing to base agent¹⁷⁶. Silicon wafer molds were created through a standard negative photolithography process²⁷⁵. Device preparation was discussed in chapter 2, and a detailed description of the photolithography process can be found in Appendix B. Channels were sealed permanently to glass cover slips (No. 1.5, Fisher) and slides (75x25x1 mm, VWR) via plasma bonding in a PDC-32G plasma cleaner (Harrick), by exposing them to air plasma for 1 minute on the high setting (18 W) and sealing the pieces together immediately. Channels were allowed to sit for several days (>2) before use to allow for hydrophobic recovery and to improve the seal^{35,169}. Epoxy was applied around the connecting piece

junction to support the seal for the channels (in Straight A and Con. D, 16 msec). Higher exposure time channels (Con. E and F, > 58 msec) had the silastic tubing placed directly into the PDMS of the device without the elbow piece and sealed with an additional layer of PDMS around the tubing to fortify the seal. The 58 msec and higher exposure time devices were sealed to glass slides as opposed to cover slips due to the extended length of the constricted region and for extra support from the high pressures exerted. PDMS devices were connected to syringes via a Luer connector.

Microfluidic device perfusion:

Channels were initially charged with 0.5% HSA in HBSS and allowed to incubate with the HSA for at least 30 minutes prior to the addition of whole blood or cells, to block non-specific adhesion from occurring. Blood or isolated neutrophils were perfused through channels at 125-160 $\mu\text{L}/\text{min}$. Channels were run for 200 μL prior to any collection of effluent. 100-200 μL of blood was collected for each condition and experiment.

Surface receptor staining:

For surface receptor staining, a small aliquot of antibody solution was directly added to the whole blood effluent and allowed to incubate for 30 minutes at room temperature, covered from light. BD RBC Lysis buffer was then added, mixed, and allowed to sit for 15 minutes at room temperature, covered from light. Solutions then appear clear but red in color after lysis. Cells were spun down (5 min at 500xg) and then washed with HSA buffer and resuspended for flow

cytometric analysis. Isolated cells collected from the shear devices were first spun down and an antibody mix was added and allowed to stain on ice for 30 minutes. Cells were then washed with HSA buffer and resuspended for flow cytometric analysis. 10,000 events were collected for all flow cytometry experiments. As a positive control, cells were incubated with 0.5 nM fMLP for 15 min at 37°C while channels were prepped and run. Samples were then stained in parallel with the channels. All flow cytometry data presented throughout this chapter are normalized to the unsheared sample for each donor.

Intracellular granule staining:

For the study of intracellular granules, a flow cytometry kit for human MPO was purchased from Biolegend (San Diego, CA). Briefly, neutrophils were collected from the channels and mixed with 1 mL of Fixation buffer for 20 min in the dark at room temperature (RT). Samples were then centrifuged and washed three times in Intracellular Staining Perm Wash Buffer. The fixed and permeabilized neutrophils were then resuspended in 50-100 μ L of residual Staining Buffer. 20 μ L of the FITC-conjugated MPO antibody was added to the cells and incubated for 30 minutes at RT, protected from light. At this step other antibodies were added depending on the granule components analyzed. For OSM and lactoferrin, a primary antibody was added and incubated during this 30 minute step. For cells stained for multiple granules, an antibody mix in staining buffer was added to the cells. After antibody incubation, the neutrophils were washed twice with Staining and Wash buffer. If necessary, a secondary antibody was added and incubated for 30 min and then washed. Cells were finally

resuspended in HSA buffer for flow cytometric analysis. 10,000 events for each condition were collected.

Actin staining:

For intracellular f-actin staining, whole blood effluent was immediately fixed by addition of cold 4% PFA in HBSS (final concentration 1%) for 10 minutes after collection from the devices. Samples were spun and washed twice (5 min at 500xg) with HBSS before proceeding. Whole blood samples were then lysed using the red blood cell lysis buffer for 15 minutes at room temperature, covered from light. Cells were washed with HSA in HBSS and then permeabilized with 0.1% Triton X-100 for 3 minutes on ice. Cold HSA buffer was then added to dilute the Triton X-100, cells were spun and washed a second time. Prior to staining, cells were incubated with 0.5% HSA for 30 minutes to reduce non-specific binding. Phalloidin (binds f-actin) Oregon Green was then added and allowed to sit for 1 hour at RT, 1:50 dilution (6 units/mL). Cells were then washed twice and resuspended for flow cytometric analysis (10,000 events). For the positive control, cells were incubated with fMLP at 37°C for 1 min and immediately fixed with PFA.

Confocal imaging analysis:

A portion of the neutrophils for the actin and granule experiments were plated for confocal imaging following the fixing and staining protocol as described above. After staining, cells were diluted at a high concentration and plated on lysine coated coverslips. Coverslips were incubated with lysine at 37°C for an

hour, and rinsed 3 times with HBSS before cell addition. Cells were incubated on the plates at 37°C for at least an hour before mounting. Cell solution was removed and the coverslips were allowed to sit for 2 min to remove excess liquid. A 1 µL drop of DAPI (stains DNA) containing mounting media was placed on a larger coverslip, and the cell containing coverslip was placed face down. Mounted coverslips were kept at 4°C in the dark until imaging.

Phagocytosis assay:

For the phagocytosis assay whole blood was run through the microfluidic channels. Neutrophils were collected and evaluated for phagocytic function in accordance with the manufacturer's protocol for the pHrodo phagocytosis kit. Briefly, the whole blood effluent was incubated with the bacterial particles for 15 minutes at 37°C. 100 µL of lysis buffer was added to each tube and incubated at RT for 5 min. 1 mL of Buffer B was then added to each tube and incubated for an additional 5 min at RT. Samples were centrifuged and washed in Wash Buffer and resuspended for flow cytometric analysis. The bacterial particles contain a pH sensitive dye that only fluoresces at the low pH present in the phagosome. Therefore, only ingested particles are detected. For the controls, cells incubated with particles on ice for the 15 minute period were used as recommended by the manufacturer. The cold temperature severely impairs phagocytosis.

Statistical analysis:

Statistical analysis for flow cytometric results was assessed using a one way ANOVA with a Dunnet's multiple comparison test, with $P < 0.05$ considered

statistically significant. Comparisons and normalization were done to the unsheared sample. Results are presented as mean fluorescent intensity \pm SEM.

Results and Discussion:

Surface receptors: selectins and integrins

The surface receptors Mac-1 and L-selectin are some of the most commonly used markers for neutrophil activation. Integrins such as Mac-1 can adopt extended and open/active conformations upon stimulation, while L-selectin is rapidly cleaved and shed as a result of both chemical stimulation and mechanical forces during rolling^{88,89,151,174,268,313}. Thus, we investigated whether exposure of neutrophils to high shear caused changes in the surface expression levels of these receptors.

Isolated neutrophils were exposed to conditions of high shear rate (80,000-100,000 s⁻¹) for a range of exposure times (16-73 msec). As a control, neutrophils were also perfused through a straight channel at 2400 s⁻¹. As a positive control of neutrophil activation fMLP was used; both CD11b up-regulation and L-selectin shedding have been shown to be very sensitive to fMLP^{30,313}. With a single exposure to these high shear rates we observed a significant increase in the CD11b activation with the longer exposure times of 58, 67, and 73 msec (Fig. 4.1A). The change in CD11b activation was measured using the antibody clone cbrm1/5, which recognizes the high affinity binding site of CD11b⁷⁴. As expected, the fMLP control sample had over a two-fold increase in the CD11b activated form⁷⁸, with a majority of the L-selectin shed. No L-selectin shedding was observed under any of the shear conditions tested (Fig. 4.1B).

One possibility for the increase in the activated form of CD11b is an increase in the total levels of CD11b on the cell surface, resulting from granule exocytosis and the release of receptors to the membrane. If the approximate percentage of receptors in an activated state remains the same across the cell surface, then an increase in the total CD11b levels would cause an apparent increase in the activated form. Therefore, the use of an antibody directed against total CD11b levels was examined; this antibody recognizes an epitope in the base of the integrin accessible in both the closed and extended forms. The same shear rates were examined as for the activated form of CD11b, and no differences were observed as compared to the unsheared samples (Fig. 4.1C). The fMLP control again resulted in an increase in the CD11b levels as expected³¹³, this time with an almost 3-fold increase in the total CD11b levels. This suggests the increase observed in the activated form for the shear channels are a result of conformational shifts, not an overall increase in total CD11b surface expression.

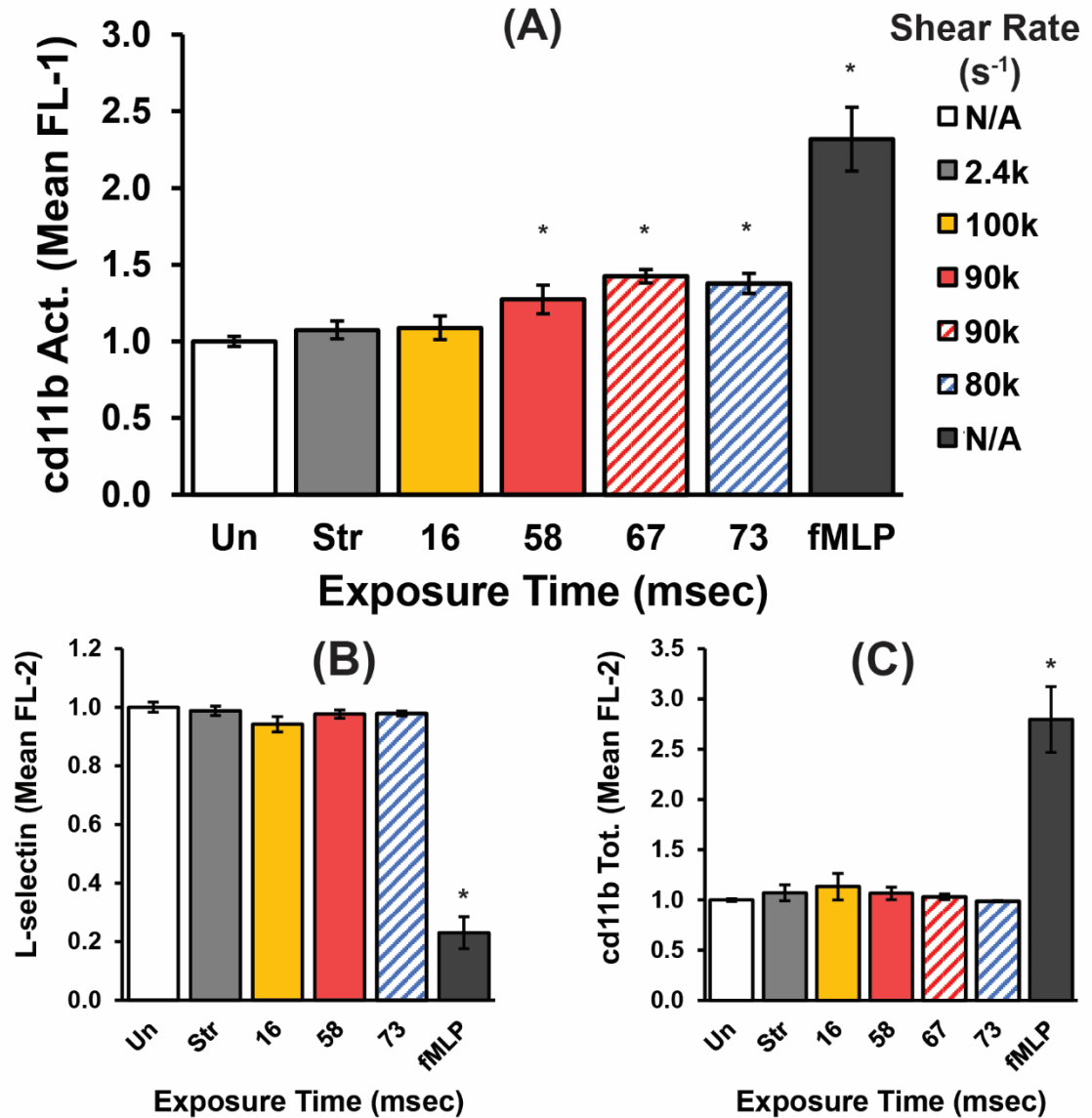


Figure 4.1: CD11b and L-selectin surface expression levels. Panels correspond to the normalized mean fluorescent intensity for (A) CD11b activated form, (B) L-selectin total levels, and (C) CD11b total levels. Colors correspond to the shear rates in the channels with gray for 2,400 s⁻¹, gold for 100,000 s⁻¹, red for 90,000 s⁻¹, and blue for 80,000 s⁻¹. Exposure times are listed for each channel. Channels correspond (from left to right on top figure starting with Str) to Str, A, Con. D, Con. F, and Con. G (stripes). Unsheared and fMLP control samples are shown in white and black respectively. Data shown is mean fluorescent intensity \pm standard error of the mean. Asterisks represent significance of $p < 0.05$ as measured by Dunnet's post hoc ANOVA multiple comparisons test, comparison to the unsheared sample. $N = 3-8$ donors per shear rate condition.

At initial glance the results from the CD11b active form and the L-selectin may appear to be slightly conflicting. From previous literature on chemical activators, we would expect to see changes in both of the receptors and for the L-selectin to be the most sensitive to activation. In both cases the fMLP positive control acted as expected, causing an increase in both the active and overall CD11b levels, as well as a significant amount of L-selectin shedding. However, for the shear samples the CD11b had an increase in the active state conformation, while the overall levels of both molecules remained unchanged. The most likely explanation is that it is not a common “activation” pathway (e.g., GPCR based signaling) that is causing the observed CD11b increase. This result alone indicates more of a priming event, such as that seen with neutrophil rolling on P- or E-selectin, as PSGL-1 engagement can also lead to a shift in conformational states of CD11a and CD11b¹⁶⁷. A potential avenue for this observed conformational shift could be through mechanotransduction, as CD11b/CD18 has been shown previously to respond to shear stress²⁷⁶. It is also possible that another mechanosensor is causing an inside-out signal to drive the conformational shift, such as the formyl peptide receptor (FPR)¹⁹⁴. However, very little is currently known about this aspect of CD11b/CD18 functionality, and the mechanosensing of neutrophil receptors. The lack of both increases in CD11b total surface expression levels and L-selectin shedding are consistent, in that L-selectin shedding generally accompanies secretory vesicle release³⁷. We see no evidence of either at this time.

We next examined the involvement of the shear history of the cells. The idea for this has been demonstrated by other groups using neutrophils with longer exposure times and lower shear rates, as well as for platelets^{215,273,285}. Platelets have been shown to have a shear history, i.e., that cumulative shear rates encountered influence the total activation of the cell²⁷³. This so-called “stress accumulation”, a combination of the exposure times and shear rate magnitudes, could be a potential factor in the state of the cell. However, few studies have combined this approach with the very low exposure times present in VADs and stenosis. For neutrophils, previous shear sensing studies have been limited to much lower shear rate magnitudes, and to investigating how shear affects the later response of the cell to stimuli^{214,215}. Previous work with various chemical activators (e.g., TNF α , LPS, fMLP, GCSF) has shown that neutrophils can adopt a primed state after certain activating events, which will cause a rapid and greater response upon a second stimulation with either higher concentrations or a different stimulus altogether. It is therefore possible that shear stress can act in a similar manner, as a priming or activating event.

We hypothesized that multiple exposures would increase the effect of shear on the neutrophil, even with extremely low exposure times. For the single pass exposures to high shear, we saw an increasing trend with exposure time in the levels of the CD11b activated form. Although not significant, the 16 msec channel did have a small increase in signal, at a value of approximately half that of the 58 msec channel. We thus added an additional channel with two constrictions at the 16 msec, $100,000\text{s}^{-1}$ shear exposure, to investigate the

potential role of cumulative shear exposures, and to see if this small increase would be amplified upon a subsequent exposure. As shown in Figure 4.2, this double exposure proved insufficient to cause any changes in the CD11b levels. However, further examination will be required into the role of repeated exposures. At this time, only a few different exposure time and shear rate combinations have been investigated. Further analysis remains to examine where the threshold lies for various shear rates, as well as the cumulative effect of sequential exposures on this critical exposure time. At this point we do not know if the double 16 msec constriction channel is insufficient in causing activation solely because the total exposure time of 30 msec is too short, or if 16 msec exposures, even in combination, are inadequate to elicit a response. To evaluate the critical exposure time, additional constricted channels will need to be created and examined between the 16 and 58 msec time points utilized here. As was discussed previously in chapter 2, when the channel was introduced, redesigns will be needed to examine some of these conditions, at least for the multi-pass channels. The minimum exposure time to elicit a response in this study was the 58 msec channel, and the total channel length required for a channel such as a double 30 msec was too long for the current investigation. As such, we were unable to include a double 30 msec channel without additional design modifications.

The absence of degranulation following shear exposure, as evident by a lack of change in total receptor levels of CD11b, does not contradict previous literature. In fact, studies with physiological shear rates have observed a

decrease in CD18 levels. Shear was implicated in the results from those previous studies, to cause conformational shifts and subsequent cleavage of Mac-1 by cathepsin B^{4,101,276,339}. However, this appears to be a physiological process designed to reduce unwanted activation, as well as assist with cell migration. This is evident by a recent study that displayed a decreased transmigration following extravasation in the absence of cathepsin B²²². This process can be overridden by other chemical signals, so that CD18 levels are maintained at sites of inflammation¹⁰⁴. With higher shear rate conditions, the lone evidence supporting potential degranulation had a considerably longer exposure time of 10 minutes⁷¹. The absence of L-selectin shedding is somewhat surprising given the CD11b activated form increase, but to the author's knowledge there is currently no evidence of shear based L-selectin shedding, outside of mechanical forces during rolling¹⁷⁴. Although shear may also affect L-selectin distribution¹⁷³. However, the apparent conformational shift in CD11b is a new and intriguing result that will require further analysis.

A previous student in our group examined CD11b following high shear exposures, and saw increases in the activated form of CD11b at 15 msec for 100,000 s⁻¹. He also showed an increase with a few other shear rate magnitudes and exposure times in the 60,000-100,000 s⁻¹ range, using constricted channel D. In the current study, we do not see any evidence of activation at this 16 msec, 100,000 s⁻¹ condition, and only see activation at >58 msec. There are a few potential explanations for the differing results between these two studies. The first, is in the driving force applied to create fluid flow. In the previous study, a

syringe pump was used on the withdraw feature. With the high pressure across the constriction in the device, we were concerned that a lower velocity would occur, leading to a decreased apparent shear rate. Volumes collected from the devices run in this manner were reduced compared to the straight channel controls. Thus, it is likely that the shear rates in the channels were lower than expected in the previous study. Consequently, the exposure times would have been increased as a result of the reduced flow rate. In the current study, we switched to infuse on the syringe pump, to reduce the potential for a decreased flow rate. As described in chapter 2, with long enough constrictions the apparent flow rate does decrease, but we observed no decrease for Con. D. Similarly, the volume output between Con. D and Str. A were identical in the current study. The second factor is the potential for pre-stimulation from LPS. During later rolling experiments an odd behavior was observed: a significant percentage of the cells were adhering rather than rolling on the P-selectin surfaces. The HSA stock being used at the time was discovered to have some LPS (endotoxin) present, which is a potent neutrophil stimulator. However, the exact LPS content in the HSA from the previous study is unknown. The experiments used throughout this thesis utilize a grade of HSA that is endotoxin free. If small contaminating amounts were present in the previous study, the cells may have been primed prior to the shear exposure. The subsequent shear exposure could then potentially increase the activation state of the cell. While stimulation after shear exposure has been examined^{214,215}, the reverse has not. It is currently unknown whether prior

stimulation of neutrophils causes a response from a high shear rate exposure. This would be an interesting avenue for future studies.

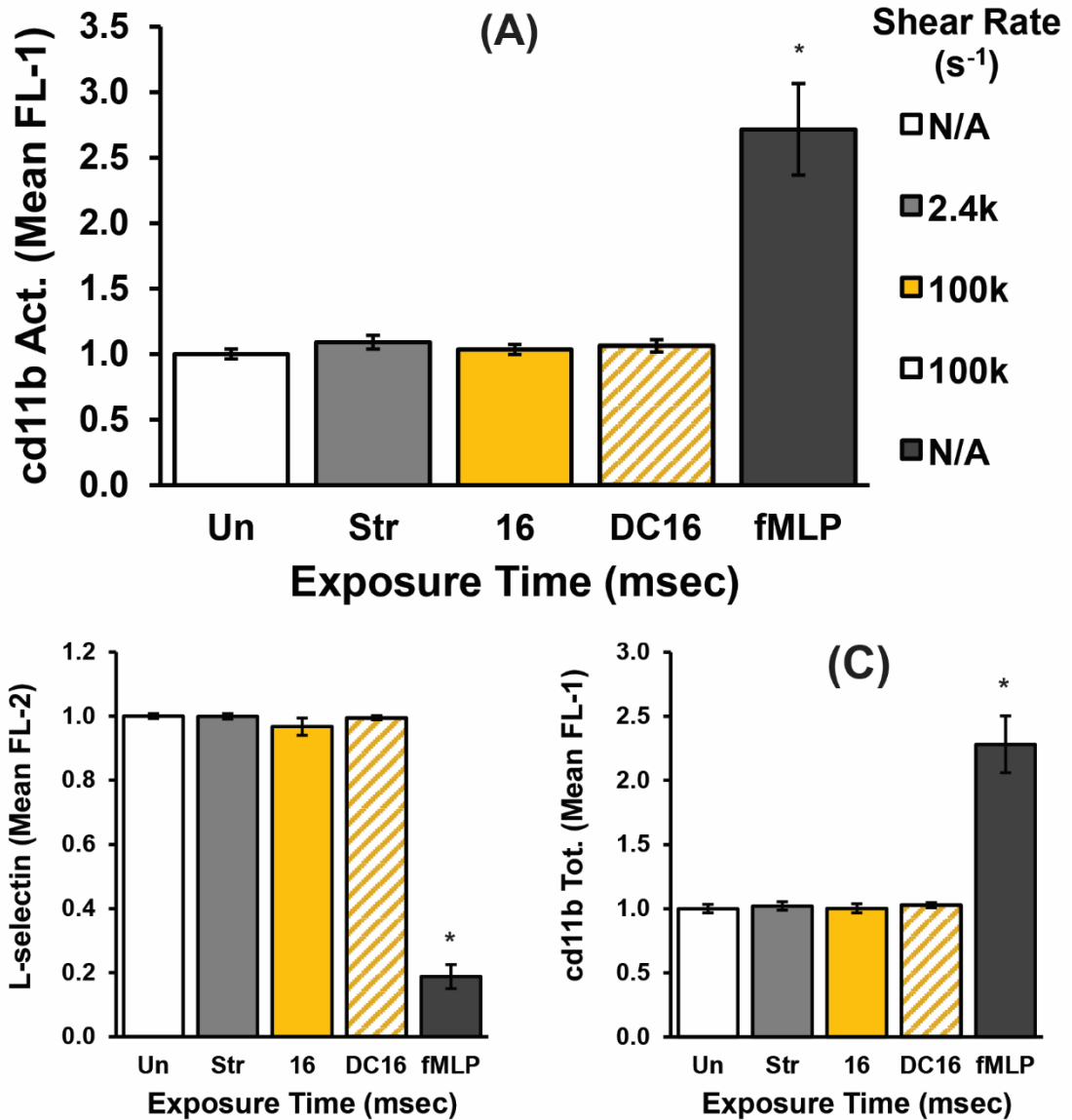


Figure 4.2: Double constriction channel. Surface receptors were investigated with the double constricted channel with (A) CD11b activated form, (B) L-selectin, and (C) CD11b total levels, in isolated cells. Gold bars represent Con. D (single channel) and a double constriction with two constrictions with lengths equal to that of Con. D (stripes, DC16). Data represents normalized MFI \pm SEM for N = 6 donors.

Intracellular granules:

Granules are a highly diverse and essential component of the neutrophil's defense. They are also useful markers for neutrophil activation because they contain specialized, distinct contents and are released at different times and in response to various stimuli. Common ways to measure granule release are with flow cytometry for fusion of granules with the cell membrane (with contents designed to be released to the surface) and ELISA to measure contents released into the extracellular space. Traditional methods to examine intracellular content using ELISA and western blots are very time consuming and often quite costly. We further adapted the more accessible flow cytometry procedure as an alternative, to include the staining for intracellular granule components.

To examine the tertiary and secondary granules, we examined OSM, lactoferrin, and CD66b. OSM and lactoferrin are intracellular granule components found almost exclusively in the tertiary and secondary granules, respectively. As mentioned in the introduction, OSM has recently been investigated as a potential inflammatory marker in VAD patients¹⁸⁴. CD66b was added to complement this portion of the study with a surface receptor. Similar to CD11b, CD66b is released and up-regulated following chemical stimulation and granule exocytosis; it is therefore also used as a sign of neutrophil activation⁷⁹. While CD11b is present throughout several granule subtypes, CD66b is only present in, and can therefore be used as a marker for, the secondary granules⁷⁹. In order to complement the CD11b results in isolated cells, we examined CD66b and OSM in whole blood. Lactoferrin was examined with isolated neutrophils. The combination of these

components allows us to examine both of these granule subtypes to some extent with each of these conditions (whole blood / isolated cells and intracellular / surface receptor). Examining results in this chapter with conditions of both isolated neutrophils and whole blood provides useful and distinct information. An isolated system is important for examining the effects directly on the cells, and avoids interaction and influence from other cell types and blood proteins. However, no common cell isolation procedures today are completely immune to having some effects on neutrophils, which are notoriously sensitive to changes (e.g., temperature) and handling^{84,123}. Examining components in whole blood therefore complements the isolated neutrophil results, while removing potential artifacts from the isolation procedure. In addition, it also demonstrates changes in a more realistic physiological system. However, a whole blood setting has limitations of its own. Platelets and erythrocytes have both been shown previously to be affected by shear^{229,273}. The presence of these other cell types could influence leukocyte behavior. Little is known about these interactions under high shear rates, and could either compound or desensitize the neutrophils' activation in response to shear^{87,157}. Unfortunately, while we keep the velocity and shear rate constant between the isolated and whole blood systems, the shear stress is increased in the latter situation due to the viscosity of the blood.

CD66b and OSM levels in whole blood showed no increase following any of the shear exposures examined (Fig. 4.3 A and B). Similarly, we observed no changes in the intracellular lactoferrin content in isolated neutrophils (Fig. 4.3C). Chemically activated controls using fMLP showed a significant increase in the

signal for CD66b. We observed no significant changes OSM and lactoferrin content in fMLP stimulated cells, a somewhat surprising event given the increase in CD66b on the neutrophils' surface. The two- to three-fold increases in CD11b and CD66b levels suggest degranulation of the later granules with fMLP is occurring, but do not offer much insight into the percentage of exocytosis. However, while fMLP is a potent neutrophil activator, it is expected to cause only modest release of the secondary and tertiary granules^{153,154}. In fact, it seems likely based on the fMLP results that only a small fraction of the granules are released, and this could explain why we do not see a significant change in the intracellular content. While both of these receptors are present on the surface of un-activated neutrophils, these baseline levels constitute only a small percentage of the total receptor quantities that the neutrophils contain. Previous studies suggest that only a small percentage of CD11b is present on un-activated neutrophils, with up to 75% concentrated in the secondary/tertiary granules and 20% in the secretory vesicles²⁷¹. CD66b similarly observes a several (2 to 3) fold increase in surface receptor expression after stimulation with fMLP^{187,266}; this aligns with the results shown in this thesis. CD66b levels can also be increased further (~6-fold from baseline) with pre-stimulation (TNF α) and other activators^{15,267,324}. CD11b was found in one study to increase to even higher surface expression levels, with up to 6-10 fold increases with certain activators, such as higher concentrations of fMLP, and up to 25-fold in response to Ionomycin²⁷¹. These levels of stimulation in comparison to the several-fold increase observed in this thesis, suggest that only modest degranulation is

occurring, even with the fMLP control used. As such, surface receptor flow cytometric analysis appears to be much more sensitive to degranulation. Intracellular levels of CD11b and CD66b were not examined at this time; staining focused solely on surface expression. This could be one aspect for future studies, and could complement the current assay to provide more quantitative information about the percentages of degranulation. It is also possible that the intracellular staining is not as effective as staining for surface receptors, and therefore less sensitive to changes in concentration from release. Another suggestion for future studies would be the inclusion of at least a second, more potent activator such as PMA or ionomycin, which would be expected to induce the release of the majority of the tertiary and secondary granules.

Regardless of these limitations in the current study, we can conclude from the results of this section, along with those of CD11b total surface expression, that we observe no evidence of secondary/tertiary granule exocytosis. This portion of the study also further supports the notion that the increase observed in the activated form of CD11b was from a change in conformation (and a potential mechanosensing event). These results do not demonstrate traditional cell priming, as release of the more mobile granules is commonplace, usually related to the formation of components of the NADPH complex present in these granules^{40,84}.

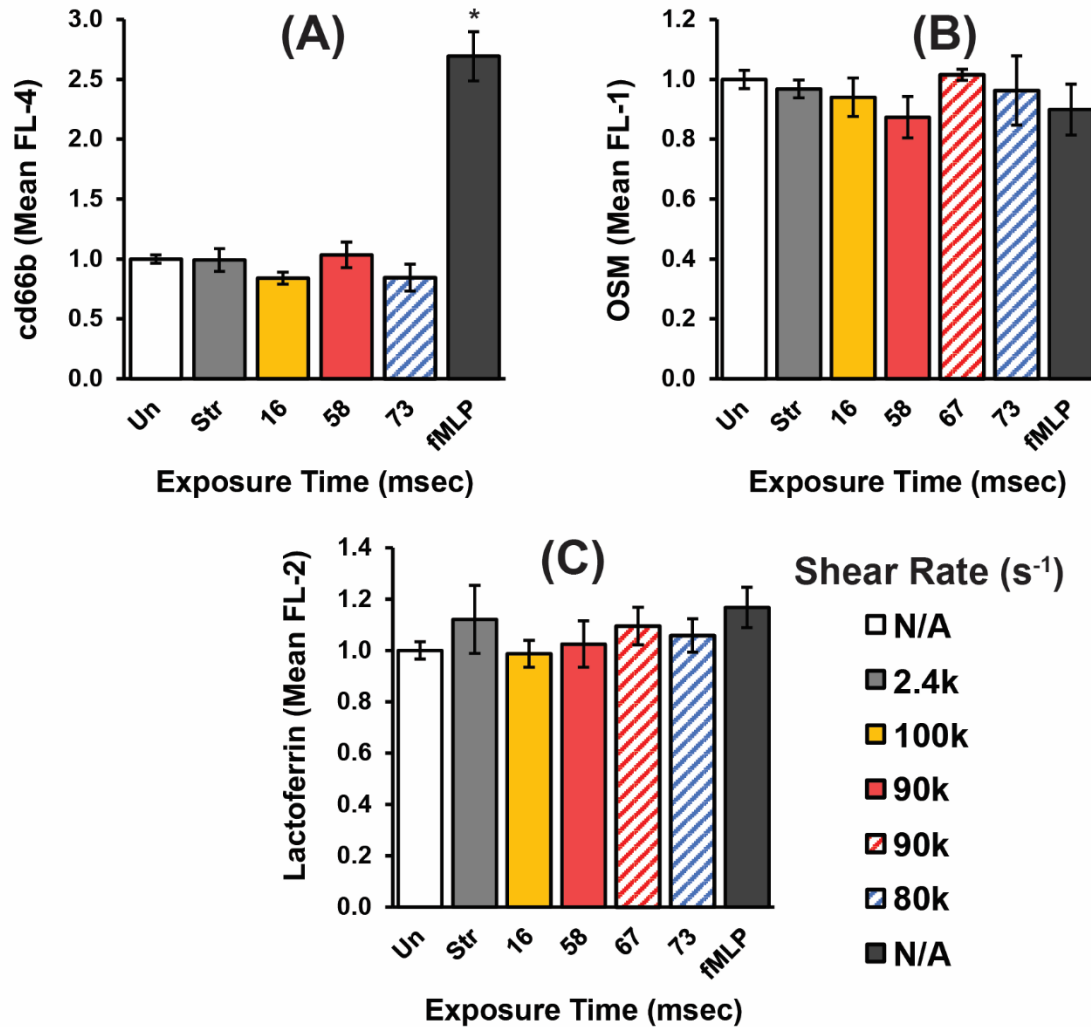


Figure 4.3: Specific and tertiary granule components. (A) CD66b and (B) OSM were measured in whole blood and (C) lactoferrin in isolated cells. Colors represent shear rates as shown by the legend at the bottom right of the figure. Samples/channels from left to right: Unsheared, Straight channel A, Con. D, Con. F, Con. G, Con. G, and fMLP control (no shear). N = 4-5 donors for each condition.

Based on the fact that the secondary and tertiary granules are released during priming events⁸⁴, coupled with the lack of evidence for their degranulation following shear shown here, we would similarly expect no changes in the primary granules. However, as shear does not appear to follow traditional activation

pathways, this is not a foregone conclusion, and we wanted to examine most aspects of neutrophil state with short exposures to high shear. We thus also included a distinct primary granule marker, MPO, in our analysis. We again examine this granule component with both isolated cells and whole blood conditions.

In contrast to the other granule subtypes, the MPO signal in isolated cells showed a significant increase (about 1.2 fold) in all the high shear channels and the fMLP control, but not in the straight, low shear channel control. Additionally, the MPO level was almost identical for all shear conditions tested, as can be seen in Figure 4.4.

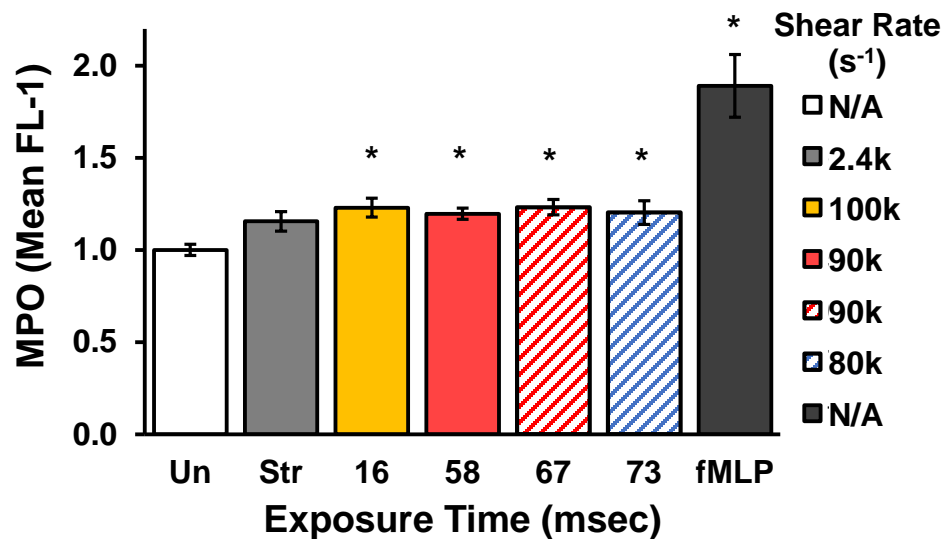


Figure 4.4: Primary granule component MPO in isolated cells. Values represent averages from N=5 donors, normalized to the unsheared sample. All constricted channels and fMLP sample were significant as compared to the unsheared sample ($p < 0.05$).

An increase in the MPO levels was a surprising discovery, as MPO production in the mature neutrophil is not expected, at least not on such a short time scale. Since the assay examines intracellular MPO as opposed to that released from the granules to the extracellular environment, it is possible that the overall levels did not increase, but that the MPO was more accessible to the antibody stain. Possibilities include an aggregation of granules within the cell and/or a localization towards the cell surface. These events would be the beginning stages of release, in which granules fuse together and begin to sequester towards the outer cell membrane, in an actin dependent process^{140,216}. As MPO release is usually one of the latest stages in the activation cycle, it is not surprising to see very little to no release. But these co-localization or aggregation steps could potentially coincide with cell priming, as the cell prepares for later granule release and activation from a subsequent stimulation.

To further study the primary granules we examined the MPO response in whole blood. Interestingly, increases (1.2 and 1.3 fold) were only observed in the 58 and 73 msec channels, with a significant difference in the latter only (Fig. 4.5). The fMLP response again showed a significant increase that was greater than the shear response. The most likely difference between this result in whole blood, and that shown in the isolated cells (significance in the 16 and 58 msec channels also) is potential priming from the cell separation. Cell priming from a first activator causes a pronounced response when exposed to a second stimulus. This phenomenon has been demonstrated previously with chemical activators, where the cell is first primed by a stimulus such as TNF α or LPS, and then

activated by fMLP or GCSF^{84,118}. In this case the isolation procedure could act as the priming event, with shear as the subsequent activating event. In both cases, for the isolated cells and the whole blood samples, the fMLP response was similar at about a two-fold increase. There is another possibility to observing more significant elevation in MPO in the isolated cell case: that other blood cells contribute to a resistance in activation. Erythrocytes have been shown previously to reduce neutrophil activation; one study demonstrated the requirement of a erythrocyte presence to induce pseudopod retraction under shear¹⁵⁷. This seems less likely than priming, as only the 16 msec channel was greatly reduced in the whole blood case. Regardless, due to the potential sensitivity shown in the case of the isolated cells, caution in interpreting this portion of the results will be required until further investigation. Despite this, both cases showed a significant increase in at least one of the longer shear exposures tested, so there appears to be a change in the primary granules occurring from shear exposure. The increase in MPO signal in the isolated neutrophil case suggests that any changes are due to shear sensitivity in the neutrophils, and not from cross-talk or binding with platelets⁸⁷. Further investigation will be required to corroborate these results and probe the potential mechanisms involved.

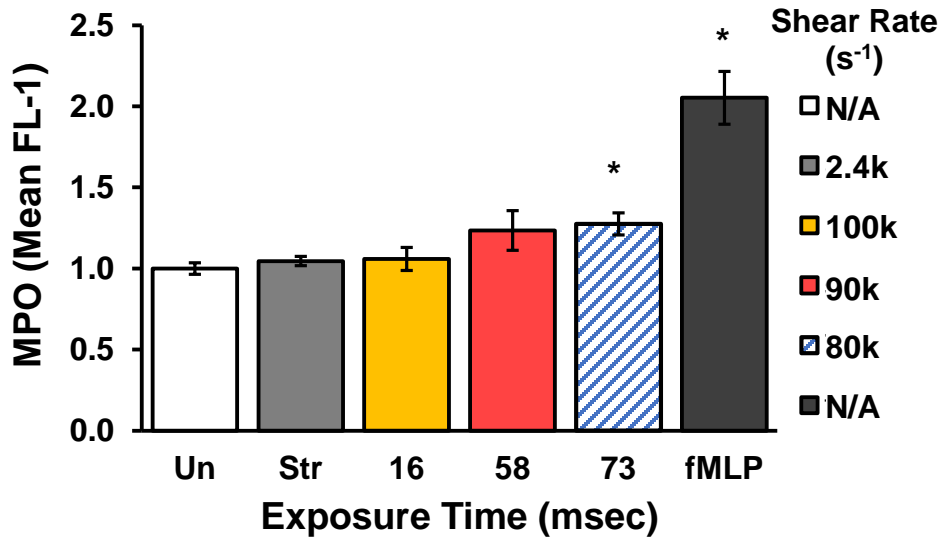


Figure 4.5: MPO in whole blood. Values represent normalized mean fluorescent intensity for N=6 donors. Significance ($p < 0.05$) in the 73 msec and fMLP samples.

Coupled with the other results examining CD11b, CD66b, OSM, and lactoferrin, and the fact that the signal increased rather than decreased for MPO, we observe no evidence for primary granule exocytosis. Therefore, granule translocation is the more likely scenario. Such a short exposure could be causing this priming event (mobilization), and additional time could begin the process of granule exocytosis. While there is very limited data relating shear and granules, a few previous studies observed increased granule movement with high shear rates for long exposure times (>10 min)^{71,217}. One of these studies sheared cells at 20,000-60,000 s⁻¹ and also detected release of beta-glucuronidase, a primary granule constituent⁷¹. While flow cytometry measures the entire cell, it doesn't really allow for differentiation between proteins near/on the surface versus the interior of the cell. We hypothesized that the increased signal observed was a

result of the granules aggregating and moving closer to the cell surface. To probe this possibility, we attempted a second assay to investigate the MPO result, through the use of confocal imaging. This analysis lets us visualize the MPO distribution to investigate its localization within the cell.

Confocal images were examined for the whole blood case. A qualitative analysis was performed to examine the location of MPO signal within the cells. Cells were placed into a few descriptive categories based on whether the signal was distributed evenly throughout the cell or located towards the membrane, whether this membrane based signal was in aggregated pockets of elevated brightness or as a ring around the entire membrane, and if deformation of the cell shape occurred. Representative images for each condition are shown in Figure 4.6. Deformation was included as an expected observation in the fMLP positive control, and is typical for chemically activated cells. To remove potential bias from the researcher, samples were randomly assigned a number as an identification label used until the image analysis was complete. Figure 4.6 also shows a graphical representation of the MPO distribution, as a percentage of the cells in each category, for each shear condition tested. The data in the graph consists of the fraction of cells in each category average for the three days/donors. An analysis using cumulative counts across all three donors resulted in the same trend with similar values.

Unsheared samples were almost entirely filled throughout, with MPO signal randomly distributed. Cells in the straight channel were similar to the unsheared samples. The shear channels were more heterogeneous; some cells

were completely filled, along with filled cells that had bright spots on the cell edges. Approximately 10-20% of the sheared cells displayed bright, aggregated signals in MPO, about twice as much as the unsheared and straight channel. Only a small percentage had a deformed shape. Interestingly, the long exposure, 73 msec sheared samples were the only ones in which a percentage of neutrophils appeared to have the majority of the MPO signal focused as a ring around the cell with little to no inner signal, suggesting localization to, or very near to, the cell membrane. This characterized only a small percentage of the cells at about 15%. The fMLP stimulated cells, similar to the shear channels, had larger, bright spots throughout a subpopulation of the cells. About half of the fMLP stimulated cells had a highly deformed, polarized shape. Only about a third of fMLP stimulated cells had MPO signal throughout the cell interior. The high shear exposures and the fMLP control resulted in an increase in a portion of the cells with aggregated granules concentrated towards the outside of the cell, near the membrane. This subpopulation supports the hypothesized notion of an increase in the mobilization of the granules towards the neutrophil surface. It would be interesting to see if longer exposure times or repeated exposures would increase the percentage of cells in these categories.

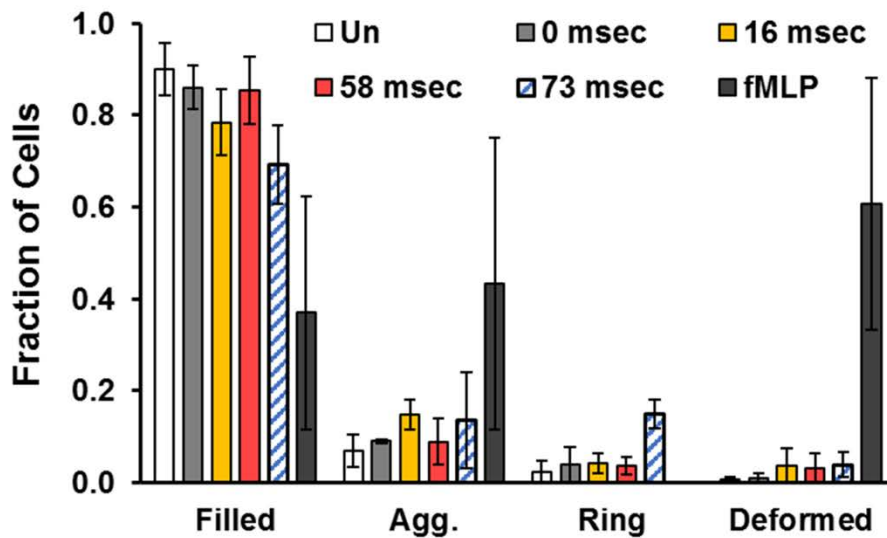
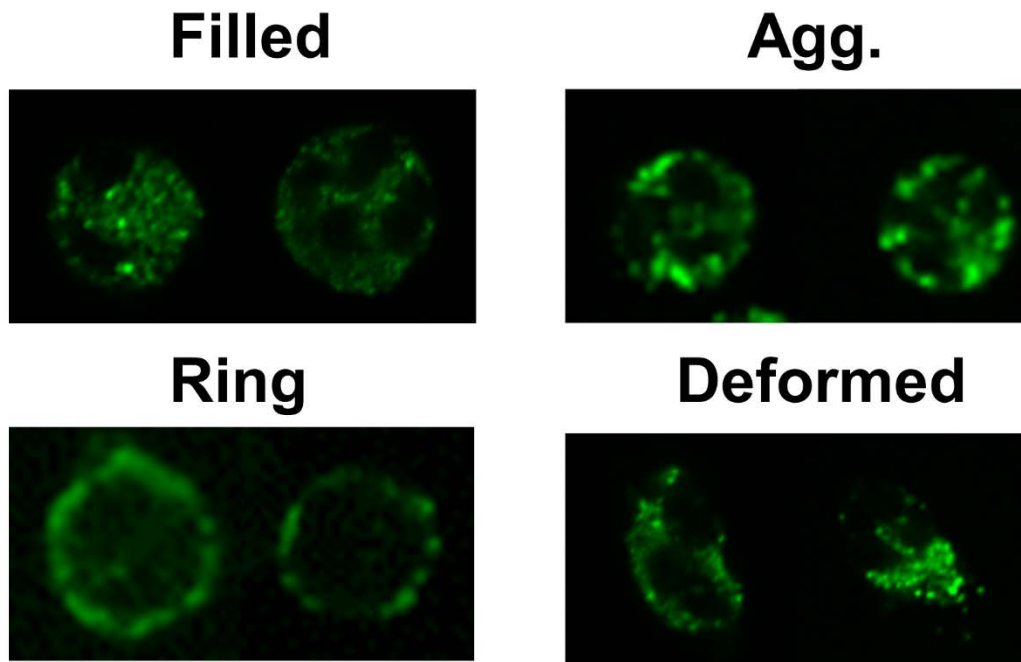


Figure 4.6: Confocal imaging analysis for MPO content in whole blood. Cells were grouped into categories: content distributed throughout the cell (filled), the presence of bright, larger aggregates (Agg.), a prominent ring of MPO signal near the cell membrane (Ring), and a deformed shape (Deformed). Colors represent the exposure time in each channel. Colors correspond to shear rates from previous graphs as well, with No shear; 2400; 100,000; 90,000; 80,000; and no shear fMLP s^{-1} from left to right. Analysis of more than 60 cells for 3 donors.

Phagocytosis:

Up to this point in the chapter we have examined various markers, both on the cell surface and internal granules. While granule release is an important neutrophil function, we wanted to test a functional assay. One of the most important roles of neutrophils as a primary responder in the immune response is the phagocytosis of invading pathogens. As a downstream event it also helps to examine how the altered state of the cell observed in the previous sections affects the cells' functionality. One of the few studies to examine the effects of stenosis level shear rates (Carter et al.) discerned an effect of short exposures to high shear on the phagocytosis ability, but not on physical cell damage. They observed a decrease in phagocytosis using leukocytes in bovine whole blood. The exposure time in this previous study was higher (>100 msec) and the shear rate magnitude lower (< 40,000 s⁻¹) than the current analysis⁴⁶.

A range of shear rate (80,000-100,000 s⁻¹) and exposure time (16-73 msec) conditions was again tested. The assay was done in whole blood, as the uptake of the bacterial particles is greatly increased and reliant upon opsonization by complement proteins present within serum. As a negative control, cells were kept on ice during the particle incubation; these samples had no difference in signal from that of cells without particles added. As can be seen in Figure 4.7, the phagocytosis ability of the cell decreased with the shear exposure. All constricted channel conditions tested showed a significant decrease in the phagocytosis levels as compared to unsheared samples. There was also a decreasing trend with increasing exposure time, as the 58 and 73 msec channels had more than a

20% decrease in phagocytic function, about two-fold more than that of the 16 msec channel. The fMLP induced sample had a similar decrease to the longest time exposure channels. Previous studies with low levels of fMLP demonstrated a similar decrease in phagocytosis, with a very significant increase at higher concentrations, $>10^{-7}$ M^{233,234}. A second activating agent, LPS, was included to demonstrate the functionality of the assay with an activator expected to cause an increase in the phagocytosis ability; in this case a 1.2 fold increase was observed. The straight channel also had a decrease compared to the unsheared sample, but was not statistically significant.

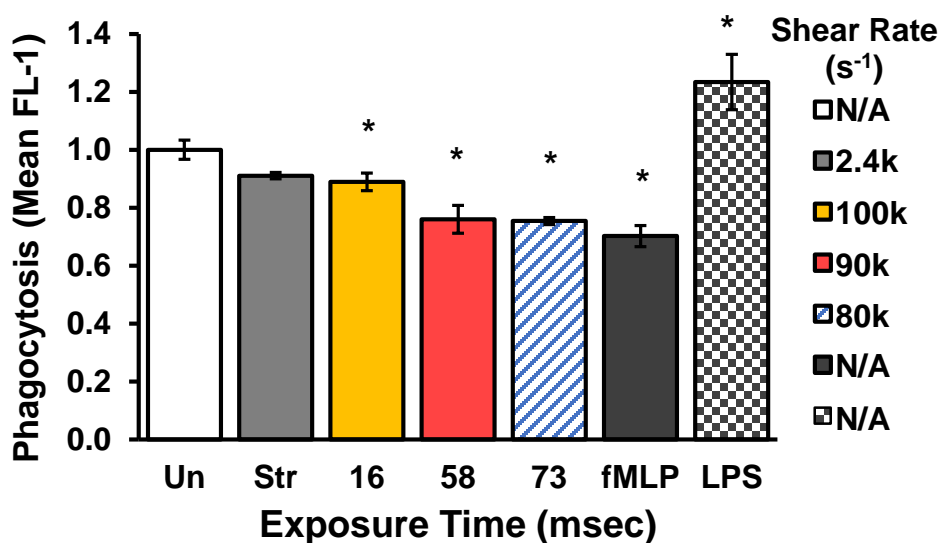


Figure 4.7: Phagocytosis Assay. Whole blood samples were incubated with bacterial particles and then analyzed via flow cytometry. MFI \pm SEM for N = 3-6 donors for each condition.

Actin cytoskeleton:

Actin plays a critical role in almost all neutrophil processes, including those examined within this thesis⁹⁴. In fact, there is even a connection between the

cytoskeleton and the various mechanosensitive receptors¹⁹². Actin content was examined by quantifying the levels of f-actin using flow cytometry. Stained cells were also plated and imaged with a confocal microscope for analysis of actin distribution. The flow cytometry results show an increase in actin content with shear in terms of the mean intensity (Fig. 4.8). However, only the 67 msec channel at 90,000 s⁻¹ shows a significant increase as compared to the unsheared sample in this work. Although not found to be significant, the other shear conditions tested had an increase compared to the unsheared sample, including the straight channel. The constricted channels also show a potential further elevation as compared to the straight channel. The 73 msec at 80,000 s⁻¹ and the 16 msec at 100,000 s⁻¹ are the next highest as expected, as these represent the longest exposure time and the highest shear rate examined.

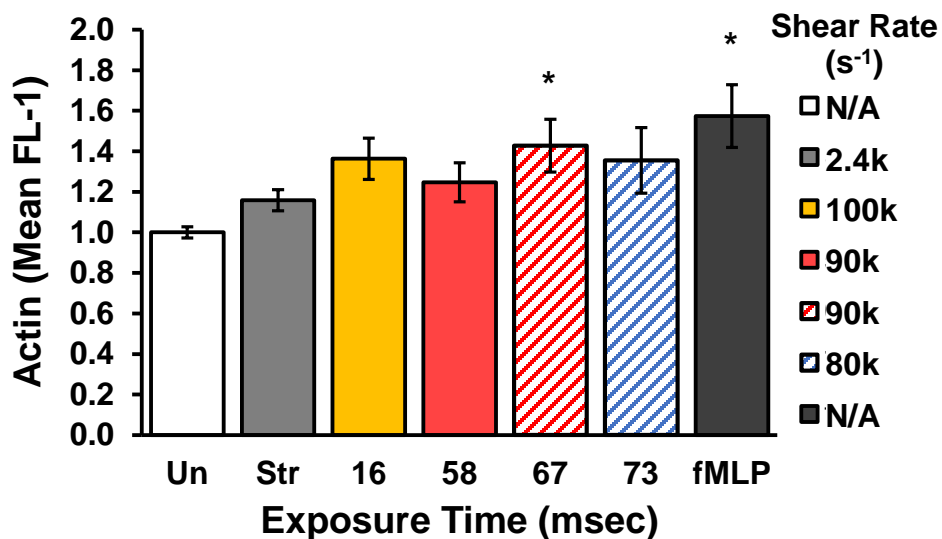


Figure 4.8: Actin content in whole blood. F-actin content was measured using flow cytometry in fixed and permeabilized cells. Significance of $p < 0.05$ in the 67 msec, 90,000 s⁻¹ channel, and fMLP stimulated sample. $N = 4-6$ donors for each condition.

To complement the flow cytometry results we also performed confocal imaging (Appendix D). As was seen with the MPO results, confocal imaging offers an important additional benefit over flow cytometry, as it allows us to examine the distribution of the actin. Actin increases can be localized near the membrane, or with an activator such as fMLP, can also become polarized to the leading edge of the cell. Visually we could not discern a difference in distribution as was done with the MPO. Therefore, we quantitatively examined the actin content near the membrane, in comparison to that distributed throughout the interior of the cell. Cells were thresholded both around the entire cell, as well as excluding the cell membrane. This allowed us to measure the signal in the entire cell, as well as this inner region. We can then compare content between the center of the cell and the outside portion (near the membrane). This method produced no observable differences in the percentage of actin localized in the membrane between the shear channels and the unsheared sample. However, similar to the flow cytometry results we did see an overall increase in signal for the longer exposure time channel, with a 60% increase in signal for the 67 msec, 90,000 s⁻¹ channel.

In order to establish the validity of the actin staining protocol, we tested a single concentration of fMLP for different time intervals. Previous studies have demonstrated rapid, consistent changes in f-actin content with time. Based on the literature a peak was expected around 1 minute. Time points of 1, 5, and 10 minutes were compared to examine actin content over time with chemical activation. As expected, we observed a very fast increase in actin content, which

then quickly began to reduce and level off by 5-10 minutes after the stimulation (Fig. 4.9). We observed a significant increase in all fMLP stimulated samples as compared to the un-activated sample. In addition, the 1 minute time point was significantly higher than the 5 and 10 minute time points. The stimulation was terminated with the addition of paraformaldehyde to initiate cell fixation. Actin dynamics occur on a rapid time scale, and could be some of the first pieces of the cell to be altered with shear. However, such phenomena could also contribute to the high amount of experimental variability, and therefore the reason for the lack of significance in the other shear channels (16, 58, and 73 msec) tested, despite the observed actin signal increase in these channels. Improvements, such as incorporating a fixative simultaneously into the channel output, is a potential design consideration that would be very beneficial for future studies. Further studies into actin dynamics with short exposures to high shear will definitely be useful and required to understand the changes undergoing in the cell, and may potentially link the various results observed in this chapter.

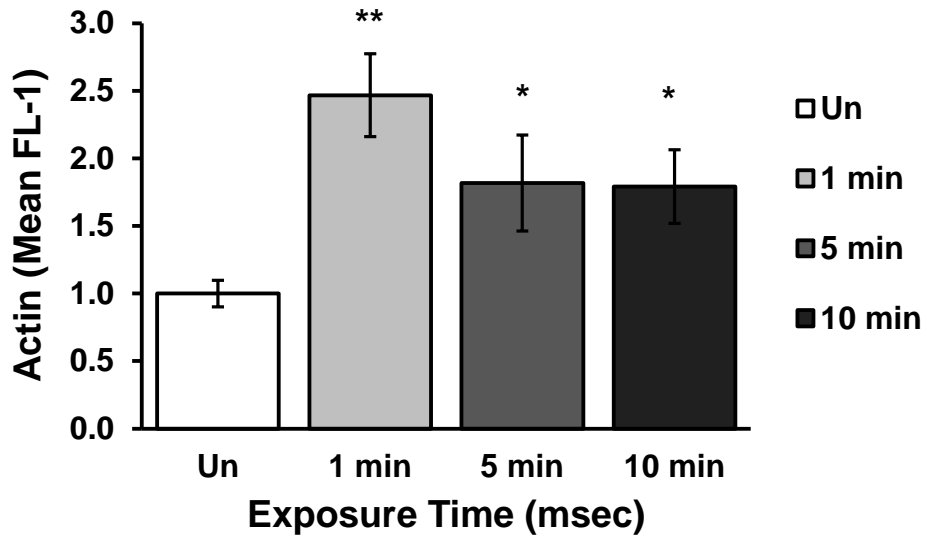


Figure 4.9: Actin content with time of chemical activation. Samples were stimulated with fMLP for 1-10 minutes and f-actin content was examined via flow cytometry. All fMLP stimulated samples were significantly increased ($p < 0.05$) compared to the un-activated control, while the 1 min was also significantly higher than the later time points. Data was normalized to the un-activated sample for each day and for statistical purposes. $N = 4$ different donors.

Conclusions:

In this chapter, we demonstrate that very short exposures (<75 msec) to high shear (80,000-100,000 s⁻¹) are sufficient to cause alterations to the neutrophil state, as well as potential dysfunction. To demonstrate this, we utilized surface receptors sensitive to activation or shear, granule proteins, phagocytosis ability, and f-actin content. We found changes in conformation for one surface receptor: CD11b. No changes were observed in the other surface receptors tested, and no evidence of granule release was observed. Surprisingly, one primary granule component, MPO, actually had an increased internal signal. The phagocytosis ability was shown to decrease for all shear conditions tested, while actin levels increased for the highest shear rate condition.

The results from the cell surface receptors and granule components partially resemble early stages of activation, perhaps what would generally be considered a priming of the cell. The increase in the activated form of CD11b, a conformational shift that occurs after priming events, was observed in the longer exposure time shear conditions. There is often an up-regulation in CD11b levels coinciding with the increase in active conformations. However, there was no observable change in cell surface receptor levels, as measured by L-selectin, CD11b, and CD66b. Further examination of tertiary and secondary granules via OSM and lactoferrin similarly saw no indications of granule exocytosis. Priming, such as during neutrophil rolling/adhesion, generally coincides with release of the early granules^{90,270}. There could, however, be co-localization or mobilization of the primary granules towards the surface, as an increase in MPO levels was

observed. In addition to receptor and granule content changes, actin based, cell-conformational shifts are a rapid, early indicator of neutrophil activation. It is currently the most likely explanation for the observed changes in the neutrophil rolling chapter, as the observed increase in neutrophil rolling could result from a stiffening of the cell from increased actin content that would lead to less surface contact area. Previous studies have indicated the potential for shear based effects on the cytoskeleton, which could also be a result of myosin based tubules and polarization of the cell^{62,63,235}. In this study, actin content was observed to increase only in the highest shear exposure channel. Additional studies will be needed to examine potential alterations to the cytoskeleton. The results throughout this chapter demonstrate an altered neutrophil state, but one that does not appear to conform to traditional priming or activation pathways.

The lack of activation in terms of granule release, follows similar trends to previously reported work utilizing lower, physiological shear levels. These previous studies have generally concluded that shear exposure desensitizes leukocytes, preventing unwanted activation in the bloodstream. The priming style components (CD11b activated form, MPO increase, f-actin increase) provide somewhat contrasting results to previous studies, and as such offer a potentially novel set of events occurring with shear. It is unclear at this time what causes these effects. While signaling pathways were not explored, detection of shear through other potential mechanosensors, such as FPR, could also cause an inside-out signaling style event, which could lead to the observed CD11b conformational shifts¹⁹⁴. A signal from FPR could also account for the actin

increase observed, and possibly the mobilization of the primary granules. Or shear based conformational shifts in CD11b may cause outside-in style signaling^{5,276}. Very few of the previous studies have examined pathological shear rates, and there is thus currently no indication that the same desensitization trend holds under the influence of such regimes. The few studies at elevated shear rates have indicated the potential for granule release and cell destruction / apoptosis with extended, long exposure times^{71,278}. Activation phenotypes linked to shear, such as elevated numbers of neutrophils extending pseudopods in the bloodstream, have been observed in studies of the hypertensive rat¹⁰³. And activation markers such as the high affinity conformation of CD11b have been observed in VAD patients after implantation³²⁶. So our results follow a similar trend to the few previous findings in cases related to pathological shear magnitude. Further analysis into the altered phenotype, as well as the underlying signaling pathways, that occur after short exposures to high shear is required.

Chapter 5: Conclusions and Future Directions:

Conclusions:

This dissertation has described the design, characterization, and implementation of a PDMS based microfluidic device to investigate the effect of short exposures to high shear on neutrophil state and function. These devices allow us to investigate a previously unknown set of shear conditions, with exposure times significantly lower than previous studies. This millisecond time scale with high shear rates are relevant to conditions such as stenosis, and blood-contacting devices such as VADs. We presented throughout this thesis some of the first studies to examine this pathological shear regime on neutrophil state and function.

In chapter 2 we outlined the design aspects for the microfluidic devices used throughout the study. The devices allow for the study of controlled, short exposures to high shear, as well as for the incorporation of low shear regions for cell adhesion. The devices are capable of briefly exposing cells to a wide range of shear rates from 4,700 – 100,000 s⁻¹, with exposure times from 16 – 440 msec. A μ PIV system was used to track beads and create velocity profiles for all conditions tested throughout this thesis and the related publications. We demonstrate that for most channels/conditions the velocity profiles align well with the expected analytical solutions. The velocity profiles were then utilized to calculate the wall shear rates in the channels, and subsequently to estimate the corresponding exposure times. With increasing exposure time and constriction

length, and under high shear rates, we observed a pressure drop across the channel resulting in decreased velocities. Increasing the flow rate led to increases in the velocity profiles in a non-linear fashion. In this chapter, we also introduced a new fabrication method to incorporate glass as support to prevent deformation for the higher shear rate channels used for adhesion studies. This support allows for higher aspect ratio channels to maintain the constant, low shear rate necessary for neutrophil rolling in the wide regions, while maintaining a high shear rate in the constricted region. This technique is very simple to use and allows for the study of higher, pathological shear rates. It can be utilized for other high pressure applications when a PDMS substrate is desired.

These channels were then used to observe changes in neutrophil state and function following short exposures to high shear. We examined both the adhesion cascade through selectin based rolling, as well as downstream functions such as degranulation and phagocytosis. To our knowledge, this is the first examination of neutrophil rolling behavior in combination with pathological shear rates. In chapter 3, an alteration in neutrophil rolling behavior was demonstrated following shear exposures of 4700, 5900, and 8600 s^{-1} for exposure times greater than 340, 310, and 230 msec respectively. The critical exposure time required to observe an increase in the downstream rolling velocity decreased with the increase in shear rate magnitude. An increased rolling velocity could be caused by a few different mechanisms, including receptor re-localization or shedding, as well as reduced deformability of the cell membrane. We suspect the latter to be the cause. To rule out the possibility of receptor

shedding we designed a second set of channels with all dimensions doubled, to increase our flow output and collect a sufficient quantity of cells for flow cytometric analysis. Analyzing PSGL-1 levels in the effluent demonstrates no detectable change in the surface receptor levels. While we cannot rule out the possibility for receptor redistribution at this time, previous studies have demonstrated increases in rolling velocity with reduced deformability³²⁹. Other studies have demonstrated changes in actin content and the stiffness of adhered cells with shear exposure^{63,278}. No such link has been found at this point for PSGL-1.

In chapter 4 of the current study we detected increased f-actin levels with high shear exposures. This finding helps support the hypothesis that shear induced increases in rolling velocity originate from stiffening of the actin cytoskeleton. Along with f-actin, we observed two other markers of neutrophil activation: an increase in the amount of high affinity conformation CD11b receptors on the cell surface and intracellular MPO levels. Confocal imaging suggests that the latter may result from increased aggregation and mobilization of the primary granules towards the cell surface. The combination of these three events suggest a rapid activation or priming of the cell by even millisecond exposures to high shear. The increase of MPO levels without any evidence of degranulation by the more easily mobilized granule types was a surprising finding. The lack of increases in total CD11b surface levels, especially, display a lack of degranulation, as about 20% of the intracellular stores are present in the secretory vesicles²⁷¹. Since secretory vesicles are released early in the activation cycle⁹⁰, the current results suggest more of a priming than an activation. Each of

these events could be explained in such a context. This is further strengthened by the lack of L-selectin shedding, an early and sensitive activation marker.

In contrast to the other results suggesting an increase in the activation state, we observed a decrease in phagocytosis. The mechanism for such an effect remains unknown at this time. However, phagocytosis is highly dependent on the formation of the phagocytic cup by cytoskeletal elements, and a deficiency or stiffening of the cell could cause such an effect. The increased actin content and increased rolling velocities both support the potential notion of increased neutrophil stiffness; lower deformability could lead to less efficient phagocytic uptake. Another intriguing possibility is a deficiency in the formation of the phagosome. The bacterial particles used in this study only fluoresce under the acidic conditions found in the phagosome, so that only ingested particles contribute to the fluorescent signal detected by the flow cytometer. A potential alteration in the movement of the primary granules could reduce maturation of the phagosome, which would lead to the reduced signal detected, even with proper initial ingestion. The changes in MPO levels and the confocal images indeed suggest that the primary granules are affected by shear via a yet unknown pathway.

The results described throughout this thesis outline changes in the neutrophil induced by short transient exposures to high shear, and presents one of the first studies to investigate this important pathological shear regime. This regime is relevant to a variety of conditions present both in naturally occurring conditions such as stenosis, as well as in devices such as VADs and heart valves.

Knowledge of the damage and dysfunction caused by the shear rate conditions allows us to modify designs for future devices to improve upon the quality of life, and ideally reduce the number of infectious events encountered in patients. For devices such as VADs, this remains high. Characterizing the state of the cell with single passes to high shear demonstrates the types of changes that can occur with high shear exposures. Modifying future device designs to avoid the types of shear rate magnitudes (or exposure times) that elicit neutrophil changes can help create safer devices for patients. This will require additional studies with multiple or reoccurring shear exposures. Incorporating shearing devices with animal studies, or an *in vivo* version of these shear regimes (such as an induced, severe stenosis), would provide an interesting investigation into whether the changes observed here in the current study correlate with decreased functionality. Such as, if the increase in rolling velocity directly translates with decreased migration into sites of infection. Or if animals more easily succumb to infections as a result of decreased phagocytosis.

Future Directions:

The body of work examining neutrophil state and function following short exposures to high shear is extremely limited, and the work described here presents indications of neutrophil priming events and dysfunction. There is thus a myriad of potential avenues left to explore, by both expanding upon the areas examined here in this thesis, as well as functions left unexamined at this point.

The first novel result was the increase in neutrophil rolling on P-selectin downstream of a high shear exposure. Expanding upon this work could examine the interaction with other selectin ligands such as L-selectin or E-selectin. Reversing the interaction and patterning PSGL-1 on the surface would allow us to investigate whether the increase in rolling velocity occurs with rolling dominated by other surface receptors; rolling on PSGL-1 is governed through L-selectin on the neutrophil surface. This would carry physiological significance by examining the potential effect of shear on secondary neutrophil capture^{85,163}. Previous studies have shown the susceptibility of this interaction to deformation²⁴³. L-selectin rolling is also an important mechanism for T-cell trafficking in the lymphatic system^{105,319}. In addition, we have only examined one component of the adhesion cascade. Patterning a combination of P- or E- selectin and ICAM-1, would allow for the study of the second portion of leukocyte rolling, slow rolling and arrest. We observed an increase in the high affinity form of CD11b with higher shear rates, but it is currently unknown if LFA-1 is also affected. Both integrins have similar conformational shifts upon activation¹⁹⁰. By utilizing microfluidic techniques, such as the laminar flow patterning recently developed by our lab²⁷⁵, we could study the sequential rolling on pairs of selectins and integrins with well-defined protein regions. If the results observed here are indeed based on cytoskeletal changes, then the integrin rolling interaction would also likely be affected.

Auxiliary studies will be needed to expand the shear rate magnitudes and exposure times from those tested here. Further increasing the shear rate for a

set of channels for the rolling experiments by 1.5- and 2- fold, for example, would allow for examination of the relationship between shear rate magnitude and the critical exposure time. We can also study the effect of multiple exposures by introducing variations of the double constriction channel. For example, at 5900 s^{-1} we observed a significant increase in rolling velocity at 310 msec, but not at 210 msec. Two sequential constrictions with the total combined length of the 310 msec (2x155 msec), two of the 210 msec length (total of 420), and two of the 310 msec (620 msec total) could be a useful starting point to examine the effect of cumulative exposures as compared to a single exposure. The double 310 msec channel corresponds to the current double constriction channel measured in the text.

The double constriction channels are also a logical next step for the work examined in chapter 4. However, these channels will likely need some redesigns for longer exposures. Con. G (46.2 mm constricted region) was the maximum length that we were able to use with the glass slides. The double constriction requires additional space between the two channels, and thus two constrictions with half the length of Con. G were difficult without further modification. Incorporating a circular loop in between constrictions (no curvature to either constricted region) could be a feasible way to create double constricted channels up to the length of Con. G with little redesign, and without significantly altering the shear profile in the constricted regions. Curvature would have to be carefully chosen as to avoid any inertial effects²⁰⁰. Variations such as 2x15 msec (30 total), 4x15 msec (60), and 2x30 msec (60), in combination with single exposure

channels of 15, 30, and 60 msec, could be used to investigate CD11b levels and the critical exposure time for shear based activation. These are just two examples of the potential uses for these multi-shear exposure channels.

A tangential future direction could be the use of microfluidics to replace the traditional cell isolation. Recent techniques have been developed for blood cell isolation utilizing microfluidic devices^{306,328,331}. The channels used for the rolling assays require only small volumes and could thus be sustainable with such an isolation technique. Current isolation techniques have the potential to prime or activate neutrophils and can take several hours to complete^{84,123}, and avoiding this could facilitate more studies with isolated neutrophil systems, especially for sensitive assays such as f-actin analysis. Specifically validating and comparing the activation increases from various isolation techniques, such as with CD35 (specific to secretory vesicles) and CD11b activated form, would be an interesting investigation that has not really been fully detailed in the literature. Or at least not for more recent isolation techniques.

One of the most currently under developed areas of research for neutrophils is the signaling mechanisms that control fluid shear-sensing. Makino et al. have linked shear stress to the action of the Rho GTPases, demonstrating increases in RhoA, and decreases in Rac 1 and 2 (at physiological shear rates)¹⁹³. A recent study then linked a RhoA specific signaling molecule to leukocyte crawling under shear⁹³, which is a function modulated by CD11b. These Rho GTPases control f-actin dynamics, and thus could have far reaching implications on neutrophil behavior^{94,121}. Despite these discoveries, very little

other work relating to GTPases, at least in the context of shear, has occurred. However, these signaling pathways have been investigated in other contexts. Interestingly, Rac2 activity has been selectively linked to the mobilization of the primary granules^{168,216}. Recent evidence also suggests that the mobilization of the different granule types, while all modulated in some extent by intracellular calcium levels, is orchestrated through different series of internal events. For example, secondary degranulation is instead regulated by a different GTPase, Ral⁵³. As was mentioned briefly in the introduction, both types of phagocytosis are also linked to the Rho family¹⁹⁷. Future work should examine the Rho GTPases in the context of high shear rates. Activity levels can be examined, as done at lower levels by Makino et al. Inhibitors for the Rho GTPases could also be used to examine the link between shear stress induced activity, and the downstream responses such as CD11b conformational shifts and primary granule mobilization observed here. Selective inhibitors exist for many of the Rho GTPases¹⁴⁷.

The work from chapter 4 should be supplemented by additional shear rate and exposure time combinations, as mentioned. In addition, the potential priming events warrant an investigation into whether downstream activation events are more potent. For example, studies similar to those presented by Mitchell et al.²¹⁵, but with the elevated shear rates examined here. The reverse could also be investigated, by first activating the cells with a priming agent, and then exposing them to shear, to observe if shear can pose as an activating event. We have so far examined neutrophil state, but have not examined possible cell damage. One

study with adherent neutrophils showed apoptosis after a several hour period²⁷⁸, and work with platelets has shown evidence of apoptosis with pathological shear exposures¹⁷⁸. It is possible that high shear rates could similarly damage neutrophils, and evidence of this could be examined for markers of apoptosis, as well as microparticle formation. The latter has been examined to some extent in VAD patients^{50,75}, and thus warrants a closer look. These studies would be especially relevant to investigation with multiple, repeated exposures. Finally, the work could be supplemented by examining additional neutrophil priming related events. One of the most important that was not touched upon here is the NADPH oxidase complex. The Rac GTPases are an integral part of the complex¹³². In the context of this work it thus provides another important neutrophil function, as well as one that we suspect could be modulated by shear.

Chapter 6: Literature Cited:

1. Abram, C.L., and C.A. Lowell. The ins and outs of leukocyte integrin signaling. *Annu. Rev. Immunol.* NIH Public Access, 27:339–62, 2009.
2. Acharya, D. *et al.* INTERMACS Analysis of Stroke During Support With Continuous-Flow Left Ventricular Assist Devices: Risk Factors and Outcomes. *JACC Hear. Fail.* Elsevier, 5:703–711, 2017.
3. Adrian, R.J. Particle-Imaging Techniques for Experimental Fluid Mechanics. *Annu. Rev. Fluid Mech.* 23:261–304, 1991.
4. Akenhead, M.L., S. Fukuda, G.W. Schmid-Schönbein, and H.Y. Shin. Fluid shear-induced cathepsin B release in the control of Mac1-dependent neutrophil adhesion. *J. Leukoc. Biol.* jlb.3A0716-317RR, 2017.
5. Akenhead, M.L., and H.Y. Shin. The Contribution of Cell Surface Components to the Neutrophil Mechanosensitivity to Shear Stresses. *AIMS Biophys.* 2:318–335, 2015.
6. Akenhead, M.L., X. Zhang, and H.Y. Shin. Characterization of the shear stress regulation of CD18 surface expression by HL60-derived neutrophil-like cells. *Biomech. Model. Mechanobiol.* Springer Berlin Heidelberg, 13:861–870, 2014.
7. Akenhead, M.L., X. Zhang, and H.Y. Shin. Impaired Neutrophil Mechanoregulation by Fluid Flow: A Potential Contributing Factor for Microvascular Dysfunction in Obesity. Springer International Publishing, 2014,

pp. 203–232.

8. Alon, R., S. Chen, R. Fuhlbrigge, K.D. Puri, and T.A. Springer. The kinetics and shear threshold of transient and rolling interactions of L-selectin with its ligand on leukocytes. *Proc. Natl. Acad. Sci. U. S. A.* National Academy of Sciences, 95:11631–11636, 1998.

9. Alon, R., S. Chen, K.D. Puri, E.B. Finger, and T.A. Springer. The Kinetics of L-selectin Tethers and the Mechanics of Selectin-mediated Rolling. *J. Cell Biol.* 138:1169–1180, 1997.

10. Alsmadi, N.Z., S.J. Shapiro, C.S. Lewis, V.M. Sheth, T.A. Snyder, and D.W. Schmidtke. Constricted microfluidic devices to study the effects of transient high shear exposure on platelets. *Biomicrofluidics* 11:64105, 2017.

11. Amulic, B., C. Cazalet, G.L. Hayes, K.D. Metzler, and A. Zychlinsky. Neutrophil Function: From Mechanisms to Disease. *Annu. Rev. Immunol.* 30:459–489, 2012.

12. Anderson, G.H., J.D. Hellums, J.L. Moake, and C.P. Alfrey. Platelet lysis and aggregation in shear fields. *Blood Cells* 4:499–511, 1978.

13. Apel, J., R. Paul, S. Klaus, T. Siess, and H. Reul. Assessment of hemolysis related quantities in a microaxial blood pump by computational fluid dynamics. In: *Artificial Organs* Wiley/Blackwell (10.1111), pp. 341–347, 2001.

14. Arnhold, J., and J. Flemmig. Human myeloperoxidase in innate and acquired immunity. *Arch. Biochem. Biophys.* Academic Press, pp. 92–106,

2010.

15. Aroca, R. *et al.* Immunotherapy reduces allergen-mediated CD66b expression and myeloperoxidase levels on human neutrophils from allergic patients. *PLoS One Public Library of Science*, 9:e94558, 2014.

16. Ashby, M.F. Material profiles. In: *Materials and the Environment* Butterworth-Heinemann, 2013, pp. 459–595.

17. Atherton, A., and G. V Born. Relationship between the velocity of rolling granulocytes and that of the blood flow in venules. *J. Physiol.* 233:157–65, 1973.

18. Bacher, R.P., and M.C. Williams. Hemolysis in capillary flow. *J Lab Clin Med Elsevier*, 76:485–496, 1970.

19. Bainton, D.F., and M.G. Farquhar. Origin of granules in polymorphonuclear leukocytes. Two types derived from opposite faces of the Golgi complex in developing granulocytes. *J. Cell Biol.* 28:277–301, 1966.

20. Bainton, D.F., and M.G. Farquhar. Differences in enzyme content of azurophil and specific granules of polymorphonuclear leukocytes II. Cytochemistry and electron microscop. *J. Cell Biol.* 39:299–317, 1968.

21. Bainton, D.F., and M.G. Farquhar. Differences in enzyme content of azurophil and specific granules of polymorphonuclear leukocytes. I. Histochemical staining of bone marrow smears. *J. Cell Biol.* 39:286–298, 1968.

22. Baldus, S. *et al.* Myeloperoxidase serum levels predict risk in patients with

- acute coronary syndromes. *Circulation* 108:1440–1445, 2003.
23. Baldwin, J.T., S. Deutsch, D.B. Geselowitz, and J.M. Tarbell. LDA measurements of mean velocity and Reynolds stress fields within an artificial heart ventricle. *J. Biomech. Eng.* American Society of Mechanical Engineers, 116:190–200, 1994.
24. Bang, H. *et al.* Active sealing for soft polymer microchips: Method and practical applications. *J. Micromechanics Microengineering* IOP Publishing, 16:708–714, 2006.
25. Bark, D.L., and D.N. Ku. Wall shear over high degree stenoses pertinent to atherothrombosis. *J. Biomech.* Elsevier, 43:2970–2977, 2010.
26. Bark, D.L., A.N. Para, and D.N. Ku. Correlation of thrombosis growth rate to pathological wall shear rate during platelet accumulation. *Biotechnol. Bioeng.* 109:2642–2650, 2012.
27. Bartolo, D., G. Degré, P. Nghe, and V. Studer. Microfluidic stickers. *Lab Chip* 8:274–279, 2008.
28. Beals, C.R., A.C. Edwards, R.J. Gottschalk, T.W. Kuijpers, and D.E. Staunton. CD18 activation epitopes induced by leukocyte activation. *J. Immunol.* 167:6113–6122, 2001.
29. Beebe, D.J., G.A. Mensing, and G.M. Walker. Physics and Applications of Microfluidics in Biology. *Annu. Rev. Biomed. Eng.* 4:261–286, 2002.
30. Berger, M. *et al.* Human neutrophils increase expression of C3bi as well as

C3b receptors upon activation. *J. Clin. Invest.* 74:1566–1571, 1984.

31. Bianchi, E., R. Molteni, R. Pardi, and G. Dubini. Microfluidics for in vitro biomimetic shear stress-dependent leukocyte adhesion assays. *J. Biomech.* 46:276–283, 2013.

32. Björnsdóttir, H. *et al.* Neutrophil NET formation is regulated from the inside by myeloperoxidase-processed reactive oxygen species. *Free Radic. Biol. Med.* Pergamon, 89:1024–1035, 2015.

33. Bluestein, D. Research approaches for studying flow-induced thromboembolic complications in blood recirculating devices. *Expert Rev. Med. Devices* Taylor & Francis, 1:65–80, 2004.

34. Bluestein, D., L. Niu, R.T. Schoephoerster, and M.K. Dewanjeet. Fluid Mechanics of Arterial Stenosis: Relationship to the Development of Mural Thrombus. *Ann. Biomed. Eng.* 25:344–356, 1997.

35. Bodas, D., and C. Khan-Malek. Hydrophilization and hydrophobic recovery of PDMS by oxygen plasma and chemical treatment—An SEM investigation. *Sensors Actuators B Chem.* Elsevier, 123:368–373, 2007.

36. Borregaard, N. *et al.* Stimulus-dependent Secretion of Plasma Proteins from Human Neutrophils. *J. Clin. Invest* 90:86–96, 1992.

37. Borregaard, N. *et al.* Changes in subcellular localization and surface expression of L-selectin, alkaline phosphatase, and Mac-1 in human neutrophils during stimulation with inflammatory mediators. *J. Leukoc. Biol.* Wiley-

Blackwell, 56:80–87, 1994.

38. Borregaard, N. Neutrophils, from Marrow to Microbes. *Immunity* 33:657–670, 2010.

39. Borregaard, N., L. Christensen, O.W. Bjerrum, H.S. Birgens, and I. Clemmensen. Identification of a Highly Mobilizable Subset of Human Neutrophil Intracellular Vesicles That Contains Tetranectin and Latent Alkaline Phosphatase exocytosis * gelatinase* intracellular membranes * subcellular fractionation. *J. Clin. Invest* 85:408–416, 1990.

40. Borregaard, N., J.M. Heiple, E.R. Simons, and R.A. Clark. Subcellular localization of the b-cytochrome component of the human neutrophil microbicidal oxidase: Translocation during activation. *J. Cell Biol.* 97:52–61, 1983.

41. Borregaard, N., L.J. Miller, and T.A. Springer. Chemoattractant-regulated mobilization of a novel intracellular compartment in human neutrophils. *Science* (80-.). 237:1204–1206, 1987.

42. Borregaard, N., O.E. Sørensen, and K. Theilgaard-Mönch. Neutrophil granules: a library of innate immunity proteins. *Trends Immunol.* 28:340–345, 2007.

43. Bruehl, R.E. *et al.* Leukocyte activation induces surface redistribution of P-selectin glycoprotein ligand-1. *J. Leukoc. Biol.* Wiley-Blackwell, 61:489–499, 1997.

44. Campbell, I.D., and M.J. Humphries. Integrin structure, activation, and interactions. *Cold Spring Harb. Perspect. Biol.* pp. 1–14, 2011.
45. Caron, E., and A. Hall. Identification of two distinct mechanisms of phagocytosis controlled by different Rho GTPases. *Science* 282:1717–21, 1998.
46. Carter, J., K. Hristova, H. Harasaki, and W. a Smith. Short exposure time sensitivity of white cells to shear stress. *ASAIO J.* 49:687–691, 2003.
47. Casa, L.D., S.E. Gillespie, and S.L. Meeks. Relative Contributions of von Willebrand Factor and Platelets in High Shear Thrombosis. *J. Hematol. Thromboembolic Dis.* 4, 2016.
48. Casa, L.D.C., and D.N. Ku. High Shear Thrombus Formation under Pulsatile and Steady Flow. *Cardiovasc. Eng. Technol.* 5:154–163, 2014.
49. Cecchi, E. *et al.* Role of hemodynamic shear stress in cardiovascular disease. *Atherosclerosis* 214:249–256, 2010.
50. Chan, C.H. *et al.* The CentriMag Centrifugal Blood Pump as a Benchmark for In Vitro Testing of Hemocompatibility in Implantable Ventricular Assist Devices. *Artif. Organs* 39:93–101, 2015.
51. Chan, C.H.H., A. Hilton, G. Foster, K.M. Hawkins, N. Badiei, and C.A. Thornton. The evaluation of leukocytes in response to the in vitro testing of ventricular assist devices. *Artif. Organs* 37:793–801, 2013.
52. Chen, A.Y., F.A. DeLano, S.R. Valdez, J.N. Ha, H.Y. Shin, and G.W.

Schmid-Schönbein. Receptor cleavage reduces the fluid shear response in neutrophils of the spontaneously hypertensive rat. *Am. J. Physiol. - Cell Physiol.* 299:C1441–C1449, 2010.

53. Chen, C.X.-J., I. Soto, Y.L. Guo, and Y. Liu. Control of secondary granule release in neutrophils by Ral GTPase. *J. Biol. Chem.* American Society for Biochemistry and Molecular Biology, 286:11724–11733, 2011.

54. Chen, H.-Q., W. Tian, Y.-S. Chen, L. Li, J. Raum, and K.-L.P. Sung. Effect of steady and oscillatory shear stress on F-actin content and distribution in neutrophils. *Biorheology* IOS Press, 41:655–664, 2004.

55. Chen, M., and J.G. Geng. P-selectin mediates adhesion of leukocytes, platelets, and cancer cells in inflammation, thrombosis, and cancer growth and metastasis. *Arch. Immunol. Ther. Exp. (Warsz)*. pp. 75–84, 2006.

56. Chen, Q., G. Li, Y. Nie, S. Yao, and J. Zhao. Investigation and improvement of reversible microfluidic devices based on glass-PDMS-glass sandwich configuration. *Microfluid. Nanofluidics* 16:83–90, 2014.

57. Chen, Z., N.K. Mondal, J. Ding, J. Gao, B.P. Griffith, and Z.J. Wu. Shear-induced platelet receptor shedding by non-physiological high shear stress with short exposure time: Glycoprotein Iba and glycoprotein VI. *Thromb. Res.* 135:692–698, 2015.

58. Chung, B.J., A.M. Robertson, and D.G. Peters. The numerical design of a parallel plate flow chamber for investigation of endothelial cell response to shear stress. *Comput. Struct.* 81:535–546, 2003.

59. Coghill, P.A., E.K. Kesselhuth, E.A. Shimp, D.B. Khismatullin, and D.W. Schmidtke. Effects of microfluidic channel geometry on leukocyte rolling assays. *Biomed. Microdevices* Springer US, 15:183–193, 2013.
60. Colace, T. V, and S.L. Diamond. von Willebrand Factor unfolding and elongation on collagen during acute whole blood exposure to pathological flow. *Arter. Thromb Vasc Biol* 1–13, 2013.
61. Corcoran, D., B. Hennigan, and C. Berry. Fractional flow reserve: a clinical perspective. *Int. J. Cardiovasc. Imaging* Springer Netherlands, 33:961–974, 2017.
62. Coughlin, M.F., and G.W. Schmid-Schönbein. Pseudopod projection and cell spreading of passive leukocytes in response to fluid shear stress. *Biophys. J.* 87:2035–42, 2004.
63. Coughlin, M.F., D.D. Sohn, and G.W. Schmid-Schönbein. Recoil and stiffening by adherent leukocytes in response to fluid shear. *Biophys. J.* 94:1046–51, 2008.
64. Cowland, J.B., and N. Borregaard. The individual regulation of granule protein mRNA levels during neutrophil maturation explains the heterogeneity of neutrophil granules. *J. Leukoc. Biol.* 66:989–995, 1999.
65. Cowland, J.B., and N. Borregaard. Granulopoiesis and granules of human neutrophils. *Immunol. Rev.* Wiley/Blackwell (10.1111), 273:11–28, 2016.
66. Cox, D., P. Chang, Q. Zhang, P.G. Reddy, G.M. Bokoch, and S. Greenberg.

- Requirements for Both Rac1 and Cdc42 in Membrane Ruffling and Phagocytosis in Leukocytes. *J. Exp. Med* 186:1487–1494, 1997.
67. Curtas, A.R., H.G. Wood, P.E. Allaire, J.C. McDaniel, S.W. Day, and D.B. Olsen. Computational fluid dynamics modeling of impeller designs for the HeartQuest left ventricular assist device. *Asaio J* 48:552–561, 2002.
68. Davenpeck, K.L., M.E. Brummet, S.A. Hudson, R.J. Mayer, and B.S. Bochner. Activation of Human Leukocytes Reduces Surface P-Selectin Glycoprotein Ligand-1 (PSGL-1, CD162) and Adhesion to P-Selectin In Vitro. *J. Immunol.* 165:2764–2772, 2000.
69. Deng, Z., M.C. Richmond, G.R. Guensch, R.P. Muller, and P.N.N. Laboratory. Study of Fish Response Using Particle Image Velocimetry and High-Speed, High-Resolution Imaging. Richland, WA, , 2004 Oct.
70. Dewitz, T., T.C. Hung, R.R. Martin, and L. V McIntire. Mechanical Trauma in Leukocytes. *J. Lab. Clin. Med.* 90, 1977.
71. Dewitz, T.S., L. V McIntire, R.R. Martin, and H.D. Sybers. Enzyme release and morphological changes in leukocytes induced by mechanical trauma. *Blood Cells* 5:499–512, 1979.
72. Di Carlo, D., D. Irimia, R.G. Tompkins, and M. Toner. Continuous inertial focusing, ordering, and separation of particles in microchannels. *Proc. Natl. Acad. Sci.* National Academy of Sciences, 104:18892–18897, 2007.
73. Diamond, M.S., J. Garcia-Aguilar, J.K. Bickford, A.L. Corbi, and T.A.

- Springer. The I domain is a major recognition site on the leukocyte integrin Mac-1 (CD11b/CD18) for four distinct adhesion ligands. *J. Cell Biol.* 120:1031–1043, 1993.
74. Diamond, M.S., and T.A. Springer. A subpopulation of Mac-1 (CD11b/CD18) molecules mediates neutrophil adhesion to ICAM-1 and fibrinogen. *J. Cell Biol.* 120:545–556, 1993.
75. Diehl, P. *et al.* Enhanced microparticles in ventricular assist device patients predict platelet, leukocyte and endothelial cell activation. *Interact. Cardiovasc. Thorac. Surg.* 11:133–137, 2010.
76. Ding, J. *et al.* Quantification of Shear-Induced Platelet Activation: High Shear Stresses for Short Exposure Time. *Artif. Organs* 39:576–583, 2015.
77. Dolan, J.M., J. Kolega, and H. Meng. High wall shear stress and spatial gradients in vascular pathology: A review. *Ann. Biomed. Eng.* 41:1411–1427, 2013.
78. Domínguez-Jiménez, C. *et al.* Effect of pentoxifylline on polarization and migration of human leukocytes. *J. Leukoc. Biol.* Wiley-Blackwell, 71:588–596, 2002.
79. Ducker, T.P., and K.M. Skubitz. Subcellular localization of CD66, CD67, and NCA in human neutrophils. *J. Leukoc. Biol.* Wiley-Blackwell, 52:11–16, 1992.
80. Duffy, D.C., J.C. McDonald, O.J.A. Schueller, and G.M. Whitesides. Rapid prototyping of microfluidic systems in poly(dimethylsiloxane). *Anal. Chem.*

70:4974–4984, 1998.

81. Dunne, J.L., C.M. Ballantyne, A.L. Beaudet, and K. Ley. Control of leukocyte rolling velocity in TNF- α -induced inflammation by LFA-1 and Mac-1. *Blood* 99:336–341, 2002.

82. Dupuy, A.G., and E. Caron. Integrin-dependent phagocytosis: spreading from microadhesion to new concepts. *J. Cell Sci.* 121:1773–1783, 2008.

83. El-Benna, J., P.M.C. Dang, and M.A. Gougerot-Pocidallo. Priming of the neutrophil NADPH oxidase activation: Role of p47phox phosphorylation and NOX2 mobilization to the plasma membrane. *Semin. Immunopathol.* Springer-Verlag, pp. 279–289, 2008.

84. El-Benna, J., M. Hurtado-Nedelec, V. Marzaioli, J.-C. Marie, M.-A. Gougerot-Pocidallo, and P.M.-C. Dang. Priming of the neutrophil respiratory burst: role in host defense and inflammation. *Immunol. Rev.* Wiley/Blackwell (10.1111), 273:180–193, 2016.

85. Eriksson, E.E., X. Xie, J. Werr, P. Thoren, and L. Lindbom. Importance of Primary Capture and L-Selectin–dependent Secondary Capture in Leukocyte Accumulation in Inflammation and Atherosclerosis In Vivo. *J. Exp. Med* 72051300:205–217, 2001.

86. Etulain, J., K. Martinod, S.L. Wong, S.M. Cifuni, M. Schattner, and D.D. Wagner. P-selectin promotes neutrophil extracellular trap formation in mice. *Blood* 126:242–246, 2015.

87. Evangelista, V., L. Totani, A.A. Manfredi, and N. Maugeri. Platelet–Leukocyte Interactions. In: Platelets in Thrombotic and Non-Thrombotic Disorders Cham: Springer International Publishing, 2017, pp. 407–433.
88. Evans, R. *et al.* Integrins in immunity. *J. Cell Sci.* 122:215–225, 2009.
89. Fan, H., and R. Derynck. Ectodomain shedding of TGF- α and other transmembrane proteins is induced by receptor tyrosine kinase activation and MAP kinase signaling cascades. *EMBO J.* 18:6962–72, 1999.
90. Faurischou, M., and N. Borregaard. Neutrophil granules and secretory vesicles in inflammation. *Microbes Infect.* pp. 1317–1327, 2003.
91. Feng, S., X. Lu, J.C. Resendiz, and M.H. Kroll. Pathological shear stress directly regulates platelet IIb β 3 signaling. *AJP Cell Physiol.* 291:C1346–C1354, 2006.
92. Feuk-Lagerstedt, E., E.T. Jordan, H. Leffler, C. Dahlgren, and A. Karlsson. Identification of CD66a and CD66b as the major galectin-3 receptor candidates in human neutrophils. *J. Immunol.* 163:5592–8, 1999.
93. Fine, N. *et al.* GEF-H1 is necessary for neutrophil shear stress-induced migration during inflammation. *J. Cell Biol.* 215, 2016.
94. Fine, N., S. Khaliq, S. Hassanpour, and M. Glogauer. Role of the Cytoskeleton in Myeloid Cell Function. *Microbiol. Spectr.* 4, 2016.
95. Finger, E.B., K.D. Puri, R. Alon, M.B. Lawrence, U.H. von Andrian, and T. a Springer. Adhesion through L-selectin requires a threshold hydrodynamic

shear. *Nature*. pp. 266–269, 1996.

96. Flannagan, R.S., V. Jaumouillé, and S. Grinstein. The Cell Biology of Phagocytosis. *Annu. Rev. Pathol. Mech. Dis* 7:61–98, 2012.

97. Fraser, K.H., M.E. Taskin, B.P. Griffith, and Z.J. Wu. The use of computational fluid dynamics in the development of ventricular assist devices. *Med. Eng. Phys.* 33:263–80, 2011.

98. Fraser, K.H., T. Zhang, M.E. Taskin, B.P. Griffith, and Z.J. Wu. A Quantitative Comparison of Mechanical Blood Damage Parameters in Rotary Ventricular Assist Devices: Shear Stress, Exposure Time and Hemolysis Index. *J. Biomech. Eng.* 134:81002, 2012.

99. Freeman, S.A., and S. Grinstein. Phagocytosis: receptors, signal integration, and the cytoskeleton. *Immunol. Rev.* 262:193–215, 2014.

100. Fridlender, Z.G., and S.M. Albelda. Tumor-associated neutrophils: friend or foe? *Carcinogenesis* 33:949–55, 2012.

101. Fukuda, S., and G.W. Schmid-Schönbein. Fluid Shear Response in Leukocytes. In: *Molecular Basis for Microcirculatory Disorders* Paris: Springer Paris, 2003, pp. 161–170.

102. Fukuda, S., and G.W. Schmid-Schönbein. Regulation of CD18 expression on neutrophils in response to fluid shear stress. *Proc. Natl. Acad. Sci. U. S. A.* 100:13152–7, 2003.

103. Fukuda, S., T. Yasu, N. Kobayashi, N. Ikeda, and G.W. Schmid-

Schönbein. Contribution of fluid shear response in leukocytes to hemodynamic resistance in the spontaneously hypertensive rat. *Circ. Res.* 95:100–108, 2004.

104. Fukuda, S., T. Yasu, D.N. Predescu, and G.W. Schmid-Schönbein. Mechanisms for Regulation of Fluid Shear Stress Response in Circulating Leukocytes. *Circ. Res.* 86:e13–e18, 2000.

105. Galkina, E. *et al.* L-Selectin Shedding Does Not Regulate Constitutive T Cell Trafficking but Controls the Migration Pathways of Antigen-activated T Lymphocytes. *J. Exp. Med.* 198:1323–1335, 2003.

106. Gardiner, E.E., M. De Luca, T. McNally, A.D. Michelson, R.K. Andrews, and M.C. Berndt. Regulation of P-selectin binding to the neutrophil P-selectin counter-receptor P-selectin glycoprotein ligand-1 by neutrophil elastase and cathepsin G. *Blood* 98:1440–1447, 2001.

107. Gervais, T., J. El-Ali, A. Günther, and K.F. Jensen. Flow-induced deformation of shallow microfluidic channels. *Lab Chip* Royal Society of Chemistry, 6:500, 2006.

108. Giersiepen, M., L.J. Wurzinger, R. Opitz, and H. Reul. Estimation of Shear Stress-Related Blood Trauma in Heart Valve Prostheses in vivo Comparison of 25 Aortic Valves. *Artif. Organs* SAGE PublicationsSage UK: London, England, 12:130–136, 1990.

109. Gifford, J.L., H. Ishida, and H.J. Vogel. Structural insights into calmodulin-regulated I-selectin ectodomain shedding. *J. Biol. Chem.* 287:26513–26527, 2012.

110. Giorgio, T.D., and J.D. Hellums. A cone and plate viscometer for the continuous measurement of blood platelet activation. IOS Press, pp. 605–624, Aug 1, 1988.
111. Goldsmith, H.L., T.A. Quinn, G. Drury, C. Spanos, F. a McIntosh, and S.I. Simon. Dynamics of neutrophil aggregation in couette flow revealed by videomicroscopy: effect of shear rate on two-body collision efficiency and doublet lifetime. *Biophys. J.* 81:2020–2034, 2001.
112. Gordon, R.J. *et al.* Prospective, Multicenter Study of Ventricular Assist Device Infections. *Circulation* 127:691–702, 2013.
113. Gordon, R.J., B. Quagliarello, and F.D. Lowy. Ventricular assist device-related infections. *Lancet Infect. Dis.* 6:426–437, 2006.
114. Grenier, a *et al.* Oncostatin M production and regulation by human polymorphonuclear neutrophils. *Blood* 93:1413–21, 1999.
115. Griffin, J.D. *et al.* Granulocyte-macrophage colony-stimulating factor and other cytokines regulate surface expression of the leukocyte adhesion molecule-1 on human neutrophils, monocytes, and their precursors. *J. Immunol.* 145:576 LP-584, 1990.
116. Griffin, M.T., Y. Zhu, Z. Liu, C.K. Aidun, and D.N. Ku. Inhibition of high shear arterial thrombosis by charged nanoparticles. *Biomicrofluidics* AIP Publishing LLC, 12:42210, 2018.
117. Gupta, S., W.S. Wang, and S.A. Vanapalli. Microfluidic viscometers for

shear rheology of complex fluids and biofluids. *Cit. Biomicrofluidics* 10:43402, 2016.

118. Guthrie, L.A., L.C. McPhail, P.M. Henson, and R.B. Johnston. Priming of neutrophils for enhanced release of oxygen metabolites by bacterial lipopolysaccharide. Evidence for increased activity of the superoxide-producing enzyme. *J. Exp. Med.* 160:1656–71, 1984.

119. Ha, H., and S.-J. Lee. Hemodynamic features and platelet aggregation in a stenosed microchannel. *Microvasc. Res.* 90:96–105, 2013.

120. Hafezi-Moghadam, A., K.L. Thomas, A.J. Prorock, Y. Huo, and K. Ley. L-Selectin Shedding Regulates Leukocyte Recruitment. *J. Exp. Med.* 193:863–872, 2001.

121. Hall, A. Rho GTPases and the actin cytoskeleton. *Science* 279:509–514, 1998.

122. Hardy, B.S., K. Uechi, J. Zhen, and H. Pirouz Kavehpour. The deformation of flexible PDMS microchannels under a pressure driven flow. *Lab Chip* 9:935–938, 2009.

123. Haslett, C., L.A. Guthrie, M.M. Kopaniak, R.B. Johnston, and P.M. Henson. Modulation of multiple neutrophil functions by preparative methods or trace concentrations of bacterial lipopolysaccharide. *Am. J. Pathol.* 119:101–10, 1985.

124. Hathcock, J.J. Flow effects on coagulation and thrombosis. *Arterioscler.*

Thromb. Vasc. Biol. 26:1729–1737, 2006.

125. He, H.-Q., and R. Ye. The Formyl Peptide Receptors: Diversity of Ligands and Mechanism for Recognition. *Molecules* Multidisciplinary Digital Publishing Institute, 22:455, 2017.

126. Heilmann, C. *et al.* Acquired von Willebrand syndrome in patients with ventricular assist device or total artificial heart. *Thromb Haemost* 103:962–967, 2010.

127. Henderson, R.B. *et al.* The Use of Lymphocyte Function–Associated Antigen (Lfa)-1–Deficient Mice to Determine the Role of Lfa-1, Mac-1, and α 4 Integrin in the Inflammatory Response of Neutrophils. *J. Exp. Med.* Rockefeller University Press, 194:219–226, 2001.

128. Hentzen, E.R. *et al.* Sequential binding of CD11a/CD18 and CD11b/CD18 defines neutrophil capture and stable adhesion to intercellular adhesion molecule-1. *Blood* 95:911–920, 2000.

129. Herter, J., and A. Zarbock. Integrin Regulation during Leukocyte Recruitment. *J. Immunol.* 190:4451–4457, 2013.

130. Hidalgo, A., A.J. Peired, M.K. Wild, D. Vestweber, and P.S. Frenette. Complete Identification of E-Selectin Ligands on Neutrophils Reveals Distinct Functions of PSGL-1, ESL-1, and CD44. *Immunity* 26:477–489, 2007.

131. Holden, M.A., S. Kumar, A. Beskok, and P.S. Cremer. Microfluidic diffusion diluter: bulging of PDMS microchannels under pressure-driven flow. *J.*

Micromechanics Microengineering 13:412–418, 2003.

132. Hordijk, P.L. Regulation of NADPH oxidases: the role of Rac proteins. *Circ. Res. American Heart Association, Inc.*, 98:453–62, 2006.

133. Houzelle, A. Decreased Platelet Aggregation Following Single Pass Exposure to Elevated Shear in Microfluidic Devices. University of Oklahoma, , 2014.

134. Hynes, R.O. Integrins: Bidirectional, allosteric signaling machines. *Cell*. pp. 673–687, 2002.

135. Iguchi, T. *et al.* Impact of lesion length on functional significance in intermediate coronary lesions. *Clin. Cardiol.* Wiley Periodicals, Inc., 36:172–177, 2013.

136. Ikeda, Y. *et al.* The role of von Willebrand factor and fibrinogen in platelet aggregation under varying shear stress. *J. Clin. Invest.* 87:1234–1240, 1991.

137. Inglis, D.W. A method for reducing pressure-induced deformation in silicone microfluidics. *Biomicrofluidics* American Institute of Physics, 4, 2010.

138. Itoh, S., C. Susuki, K. Takeshita, K. Nagata, and T. Tsuji. Redistribution of P-selectin glycoprotein ligand-1 (PSGL-1) in chemokine-treated neutrophils: a role of lipid microdomains. *J. Leukoc. Biol.* 81:1414–1421, 2007.

139. Jilma, B., N. Hergovich, M. Homoncik, C. Marsik, C. Kreuzer, and P. Jilma-Stohlawetz. Rapid down modulation of P-selectin glycoprotein ligand-1 (PSGL-1, CD162) by G-CSF in humans. *Transfusion* Blackwell Science Inc, 42:328–

333, 2002.

140. Jog, N.R., M.J. Rane, G. Lominadze, G.C. Luerman, R.A. Ward, and K.R. McLeish. The actin cytoskeleton regulates exocytosis of all neutrophil granule subsets. *AJP Cell Physiol.* 292:C1690–C1700, 2006.

141. Joseph, P., and P. Tabeling. Direct measurement of the apparent slip length. *Phys. Rev. E American Physical Society*, 71:35303, 2005.

142. Judy, J., D. Maynes, and B.W. Webb. Characterization of frictional pressure drop for liquid flows through microchannels. *Int. J. Heat Mass Transf.* 45:3477–3489, 2002.

143. Jung, U., K.E. Norman, K. Scharffetter-Kochanek, A.L. Beaudet, and K. Ley. Transit time of leukocytes rolling through venules controls cytokine-induced inflammatory cell recruitment in vivo. *J. Clin. Invest.* 102:1526–1533, 1998.

144. Jutila, M. a, L. Rott, E.L. Berg, and E.C. Butcher. Function and regulation of the neutrophil MEL-14 antigen in vivo: comparison with LFA-1 and MAC-1. *J. Immunol.* 143:3318–3324, 1989.

145. Kambas, K., I. Mitroulis, and K. Ritis. The emerging role of neutrophils in thrombosis – The journey of TF through NETs. *Front. Immunol.* 3:article 385, 2012.

146. Kastrati, A., S. Elezi, J. Dirschinger, M. Hadamitzky, F.-J. Neumann, and A. Schömig. Influence of lesion length on restenosis after coronary stent

placement. *Am. J. Cardiol. Excerpta Medica*, 83:1617–1622, 1999.

147. Kawaguchi, A., M. Ohmori, K. Harada, S. Tsuruoka, K. Sugimoto, and A. Fujimura. The effect of a Rho kinase inhibitor Y-27632 on superoxide production, aggregation and adhesion in human polymorphonuclear leukocytes. *Eur. J. Pharmacol.* 403:203–208, 2000.

148. Kim, M., Y. Huang, K. Choi, and C.H. Hidrovo. The improved resistance of PDMS to pressure-induced deformation and chemical solvent swelling for microfluidic devices. *Microelectron. Eng.* 124:66–75, 2014.

149. Kim, M.B., and I.H. Sarelius. Role of shear forces and adhesion molecule distribution on P-selectin-mediated leukocyte rolling in postcapillary venules. *Am. J. Physiol. Heart Circ. Physiol.* 287:H2705–H2711, 2004.

150. Kirklin, J.K. *et al.* Interagency Registry for Mechanically Assisted Circulatory Support (INTERMACS) analysis of pump thrombosis in the HeartMate II left ventricular assist device. *J. Hear. Lung Transplant.* 33:12–22, 2015.

151. Kishimoto, T.K., M.A. Jutila, E.L. Berg, and E.C. Butcher. Neutrophil Mac-1 and MEL-14 adhesion proteins inversely regulated by chemotactic factors. *Science (80-)*. Smithsonian Institution Press, 245:1238–1241, 1989.

152. Kishimoto, T.K., M.A. Jutila, and E.C. Butcher. Identification of a human peripheral lymph node homing receptor: a rapidly down-regulated adhesion molecule. *Proc. Natl. Acad. Sci. U. S. A.* 87:2244–2248, 1990.

153. Kjeldsen, L., D.F. Bainton, H. Sengeløv, and N. Borregaard. Structural and functional heterogeneity among peroxidase-negative granules in human neutrophils: identification of a distinct gelatinase-containing granule subset by combined immunocytochemistry and subcellular fractionation. *Blood* 82:3183–91, 1993.
154. Kjeldsen, L., O. Weis Bjerrum, J. Askaat, and N. Borregaard. Subcellular localization and release of human neutrophil gelatinase, confirming the existence of separate gelatinase-containing granules. *Biochem. J* 287:603–610, 1992.
155. Klebanoff, S.J., A.J. Kettle, H. Rosen, C.C. Winterbourn, and W.M. Nauseef. Myeloperoxidase : a front - line defender against phagocytosed microorganisms. *J . Leukoc . Biol* 93:0–0, 2013.
156. Kolaczkowska, E., and P. Kubes. Neutrophil recruitment and function in health and inflammation. *Nat. Rev. Immunol.* 13:159–75, 2013.
157. Komai, Y., and G.W. Schmid-Schönbein. De-activation of neutrophils in suspension by fluid shear stress: A requirement for erythrocytes. *Ann. Biomed. Eng.* 33:1375–1386, 2005.
158. Koo, J., and C. Kleinstreuer. Liquid flow in microchannels: Experimental observations and computational analyses of microfluidics effects. *J. Micromechanics Microengineering* 13:568–579, 2003.
159. Kroll, M.H., J.D. Hellums, L. V McIntire, A.I. Schafer, and J.L. Moake. Platelets and shear stress. *Blood* 88:1525–41, 1996.

160. Kuijper, P.H. *et al.* Neutrophil adhesion to fibrinogen and fibrin under flow conditions is diminished by activation and L-selectin shedding. *Blood* 89:2131–8, 1997.
161. Kuijpers, T.W. *et al.* CD66 nonspecific cross-reacting antigens are involved in neutrophil adherence to cytokine-activated endothelial cells. *J. Cell Biol.* 118:457–465, 1992.
162. Kung, Y.-C., K.-W. Huang, Y.-J. Fan, and P.-Y. Chiou. Fabrication of 3D high aspect ratio PDMS microfluidic networks with a hybrid stamp. *Lab Chip* 15:1861–1868, 2015.
163. Kunkel, E.J., J.E. Chomas, and K. Ley. Role of primary and secondary capture for leukocyte accumulation in vivo. *Circ. Res.* 82:30–38, 1998.
164. Kunkel, E.J., J.L. Dunne, and K. Ley. Leukocyte arrest during cytokine-dependent inflammation in vivo. *J. Immunol.* 164:3301–3308, 2000.
165. Kuo, J.S. *et al.* Microfabricating high-aspect-ratio structures in polyurethane-methacrylate (PUMA) disposable microfluidic devices. *Lab Chip* NIH Public Access, 9:1951–6, 2009.
166. Kutter, D., P. Devaquet, G. Vanderstocken, J.M. Paulus, V. Marchal, and A. Gothot. Consequences of total and subtotal myeloperoxidase deficiency: Risk or benefit? *Acta Haematol.* Karger Publishers, 104:10–15, 2000.
167. Kuwano, Y., O. Spelten, H. Zhang, K. Ley, and A. Zarbock. Rolling on E- or P-selectin induces the extended but not high-affinity conformation of LFA-1 in

neutrophils. *Blood* 116:617–624, 2010.

168. Lacy, P. Mechanisms of Degranulation in Neutrophils. *Allergy, Asthma Clin. Immunol.* BioMed Central, 2:98, 2006.

169. Lam, K.H., A. Fernandez-Perez, D.W. Schmidtke, and N. V. Munshi. Functional cargo delivery into mouse and human fibroblasts using a versatile microfluidic device. *Biomed. Microdevices* Springer US, 20:52, 2018.

170. Lau, D. *et al.* Myeloperoxidase mediates neutrophil activation by association with CD11b/CD18 integrins. *Proc. Natl. Acad. Sci.* National Academy of Sciences, 102:431–436, 2005.

171. Lawrence, M., G. Kansas, E. Kukel, and K. Ley. Threshold levels of fluid shear promote leukocyte adhesion through selectins (CD62L, P, E). *J Cell Biol* 136:717–27, 1997.

172. Le Cabec, V., J.B. Cowland, J. Calafatt, N. Borregaard, and S.J. Klebanoff. Targeting of proteins to granule subsets is determined by timing and not by sorting: the specific granule protein NGAL is localized to azurophil granules when expressed in HL-60 cells. *Cell Biol.* 93:6454–6457, 1996.

173. Lee, D., and M.R. King. Shear-induced capping of L-selectin on the neutrophil surface during centrifugation. *J. Immunol. Methods* 328:97–105, 2007.

174. Lee, D., J.B. Schultz, P.A. Knauf, and M.R. King. Mechanical shedding of L-selectin from the neutrophil surface during rolling on sialyl Lewis x under flow.

J. Biol. Chem. 282:4812–4820, 2007.

175. Lefort, C.T., and K. Ley. Neutrophil arrest by LFA-1 activation. *Front. Immunol. Frontiers*, p. 157, 2012.

176. Lewis, C.S., N.Z. Alsmadi, T.A. Snyder, and D.W. Schmidtke. Effects of Transient Exposure to High Shear on Neutrophil Rolling Behavior. *Cell. Mol. Bioeng.* 11:279–290, 2018.

177. Ley, K., C. Laudanna, M.I. Cybulsky, and S. Nourshargh. Getting to the site of inflammation: The leukocyte adhesion cascade updated. *Nat. Rev. Immunol.* pp. 678–689, 2007.

178. Leytin, V. *et al.* Pathologic high shear stress induces apoptosis events in human platelets. *Biochem. Biophys. Res. Commun.* 320:303–310, 2004.

179. Li, G., L. Zhou, and G. Zhuang. A Facile method for the fabrication of glass-PDMS-glass sandwich microfluidic devices by sacrificial molding. *Sensors actuators B*, 2017.

180. Li, M., N.A. Hotaling, D.N. Ku, and C.R. Forest. Microfluidic Thrombosis under Multiple Shear Rates and Antiplatelet Therapy Doses. *PLoS One*, edited by J.P. Brody. Public Library of Science, 9:e82493, 2014.

181. Li, M.X., J.J. Beech-Brandt, L.R. John, P.R. Hoskins, and W.J. Easson. Numerical analysis of pulsatile blood flow and vessel wall mechanics in different degrees of stenoses. *J. Biomech.* 40:3715–3724, 2007.

182. Li, N., D. Mao, S. Lü, C. Tong, Y. Zhang, and M. Long. Distinct binding

affinities of Mac-1 and LFA-1 in neutrophil activation. *J. Immunol.* American Association of Immunologists, 190:4371–81, 2013.

183. Lindken, R., M. Rossi, S. Grosse, and J. Westerweel. Micro-Particle Image Velocimetry (microPIV): recent developments, applications, and guidelines. *Lab Chip* Royal Society of Chemistry, 9:2551–2567, 2009.

184. Long, J. *et al.* Advancing the science of hemocompatibility: Oncostatin m, a novel biomarker for blood pump induced neutrophil activation. *J. Hear. Lung Transplant.* 36:S370, 2017.

185. Lorant, D.E., R.P. McEver, T.M. McIntyre, K.L. Moore, S.M. Prescott, and G.A. Zimmerman. Activation of polymorphonuclear leukocytes reduces their adhesion to P-selectin and causes redistribution of ligands for P-selectin on their surfaces. *J. Clin. Invest.* The American Society for Clinical Investigation, 96:171–182, 1995.

186. Lu, P.C., H.C. Lai, and J.S. Liu. A reevaluation and discussion on the threshold limit for hemolysis in a turbulent shear flow. *J. Biomech.* Elsevier, 34:1361–1364, 2001.

187. Luerman, G.C. *et al.* Identification of phosphoproteins associated with human neutrophil granules following chemotactic peptide stimulation. *Mol. Cell. Proteomics* American Society for Biochemistry and Molecular Biology, 10:M110.001552, 2011.

188. Lukito, P. *et al.* Mechanical circulatory support is associated with loss of platelet receptors glycoprotein Iba and glycoprotein VI. *J. Thromb. Haemost.*

14:2253–2260, 2016.

189. Lum, A.F.H., C.E. Green, G.R. Lee, D.E. Staunton, and S.I. Simon. Dynamic regulation of LFA-1 activation and neutrophil arrest on intercellular adhesion molecule 1 (ICAM-1) in shear flow. *J. Biol. Chem.* 277:20660–20670, 2002.

190. Luo, B.-H., C. V Carman, and T.A. Springer. Structural basis of integrin regulation and signaling. *Annu. Rev. Immunol.* NIH Public Access, 25:619–47, 2007.

191. Maalej, N., J.E. Holden, and J.D. Folts. Effect of shear stress on acute platelet thrombus formation in canine stenosed carotid arteries: An in vivo quantitative study. *J. Thromb. Thrombolysis* 5:231–238, 1998.

192. Makino, A. *et al.* Mechanotransduction in leukocyte activation: A review. *Biorheology.* IOS Press, pp. 221–249, 2007.

193. Makino, A., M. Glogauer, G.M. Bokoch, S. Chien, and G.W. Schmid-Schönbein. Control of neutrophil pseudopods by fluid shear: role of Rho family GTPases. *Am. J. Physiol. Cell Physiol.* 288:C863-71, 2005.

194. Makino, A., E.R. Prossnitz, M. Bünemann, J.M. Wang, W. Yao, and G.W. Schmid-Schönbein. G protein-coupled receptors serve as mechanosensors for fluid shear stress in neutrophils. *Am. J. Physiol. Cell Physiol.* 290:C1633-9, 2006.

195. Maleszewski, J.J., C.K. Lai, and J.P. Veinot. Anatomic Considerations and

Examination of Cardiovascular Specimens (Excluding Devices). In:
Cardiovascular Pathology: Fourth Edition 2015, pp. 1–56.

196. Mannino, R.G. *et al.* Do-it-yourself in vitro vasculature that recapitulates in vivo geometries for investigating endothelial-blood cell interactions. *Sci. Rep.* Nature Publishing Group, 5:12401, 2015.

197. Mao, Y., and S.C. Finnemann. Regulation of phagocytosis by Rho GTPases. *Small GTPases* 6:1–11, 2015.

198. Mark, D., S. Haeberle, G. Roth, F. von Stetten, and R. Zengerle. Microfluidic lab-on-a-chip platforms: requirements, characteristics and applications. *Chem. Soc. Rev.* Royal Society of Chemistry, 39:1153, 2010.

199. Marsik, C., F. Mayr, F. Cardona, G. Schaller, O.F. Wagner, and B. Jilma. Endotoxin Down-Modulates P-Selectin Glycoprotein Ligand-1 (PSGL-1, CD162) on Neutrophils in Humans. *J. Clin. Immunol.* Kluwer Academic Publishers-Plenum Publishers, 24:62–65, 2004.

200. Martel, J.M., and M. Toner. Particle focusing in curved microfluidic channels. *Sci. Rep.* Nature Publishing Group, 3:3340, 2013.

201. Massai, D., G. Soloperto, D. Gallo, X.Y. Xu, and U. Morbiducci. Shear-induced platelet activation and its relationship with blood flow topology in a numerical model of stenosed carotid bifurcation. *Eur. J. Mech. B/Fluids* 35:92–101, 2012.

202. Massol, P., P. Montcourrier, J.-C. Guillemot, and P. Chavrier. Fc receptor-

mediated phagocytosis requires CDC42 and Rac1. *EMBO J.* 17:6219–6229, 1998.

203. Mayadas, T.N., X. Cullere, and C.A. Lowell. The multifaceted functions of neutrophils. *Annu. Rev. Pathol.* 9:181–218, 2014.

204. Mayadas, T.N., R.C. Johnson, H. Rayburn, R.O. Hynes, and D.D. Wagner. Leukocyte rolling and extravasation are severely compromised in P selectin-deficient mice. *Cell* 74:541–554, 1993.

205. McEver, R.P., and C. Zhu. Rolling Cell Adhesion. *Annu. Rev. Cell Dev. Biol.* Annual Reviews, 26:363–396, 2010.

206. McKennel, R. Cone-Plate Viscometer Comparison with Coaxial Cylinder Viscometer. *Anal. Chem.* UTC, 28:1710–1714, 1956.

207. Mehrabadi, M., L.D.C. Casa, C.K. Aidun, and D.N. Ku. A Predictive Model of High Shear Thrombus Growth. *Ann. Biomed. Eng.* 44:2339–2350, 2016.

208. Mehta, P., R.D. Cummings, and R.P. McEver. Affinity and kinetic analysis of P-selectin binding to P-selectin glycoprotein ligand-1. *J. Biol. Chem.* American Society for Biochemistry and Molecular Biology, 273:32506–13, 1998.

209. Meinhart, C.D., S.T. Wereley, and J.G. Santiago. PIV measurements of a microchannel flow. *Exp. Fluids* Springer-Verlag, 27, 1999.

210. Metzler, K.D., C. Goosmann, A. Lubojemska, A. Zychlinsky, and V. Papayannopoulos. A myeloperoxidase-containing complex regulates neutrophil elastase release and actin dynamics during NETosis. *Cell Rep.* Elsevier, 8:883–

96, 2014.

211. Miner, J.J. *et al.* Separable requirements for cytoplasmic domain of PSGL-1 in leukocyte rolling and signaling under flow. *Blood* 112:2035–2045, 2008.

212. Miralda, I., S.M. Uriarte, and K.R. McLeish. Multiple Phenotypic Changes Define Neutrophil Priming. *Front. Cell. Infect. Microbiol.* Frontiers Media SA, 7:217, 2017.

213. Mishra, H.K., J. Ma, and B. Walcheck. Ectodomain Shedding by ADAM17: Its Role in Neutrophil Recruitment and the Impairment of This Process during Sepsis. *Front. Cell. Infect. Microbiol.* Frontiers Media SA, 7:138, 2017.

214. Mitchell, M.J., and M.R. King. Shear-induced resistance to neutrophil activation via the formyl peptide receptor. *Biophys. J.* 102:1804–14, 2012.

215. Mitchell, M.J., K.S. Lin, and M.R. King. Fluid shear stress increases neutrophil activation via platelet-activating factor. *Biophys. J.* 106:2243–53, 2014.

216. Mitchell, T., A. Lo, M.R. Logan, P. Lacy, and G. Eitzen. Primary granule exocytosis in human neutrophils is regulated by Rac-dependent actin remodeling. *Am. J. Physiol. Cell Physiol.* American Physiological Society, 295:C1354–C1365, 2008.

217. Moazzam, F., F.A. DeLano, B.W. Zweifach, and G.W. Schmid-Schönbein. The leukocyte response to fluid stress. *Proc. Natl. Acad. Sci. U. S. A.* 94:5338–43, 1997.

218. Mócsai, A. Diverse novel functions of neutrophils in immunity, inflammation, and beyond. *J. Exp. Med.* Rockefeller Univ Press, 210:1283–1299, 2013.
219. Mocsai, A., B. Walzog, and C.A. Lowell. Intracellular signaling during neutrophil recruitment. *Cardiovasc Res* 107:373–385, 2015.
220. Moore, K.L. *et al.* P-selectin glycoprotein ligand-1 mediates rolling of human neutrophils on P-selectin. *J. Cell Biol.* 128:661 LP-671, 1995.
221. Murphy, K., Weaver, C. Janeway's Immunobiology. New York: Garland Science,.
222. Nakao, S., S. Zandi, D. Sun, and A. Hafezi-Moghadam. Cathepsin B-mediated CD18 shedding regulates leukocyte recruitment from angiogenic vessels. *FASEB J.* 32:143–154, 2018.
223. Nargang, T.M. *et al.* Liquid polystyrene: a room-temperature photocurable soft lithography compatible pour-and-cure-type polystyrene. *Lab Chip* Royal Society of Chemistry, 14:2698–2708, 2014.
224. Nassif, M.E. *et al.* Relationship between anticoagulation intensity and thrombotic or bleeding outcomes among outpatients with continuous-flow left ventricular assist devices. *Circ. Hear. Fail.* 9, 2016.
225. Nauseef, W.M. Myeloperoxidase in human neutrophil host defence. *Cell. Microbiol.* Wiley/Blackwell (10.1111), pp. 1146–1155, 2014.
226. Nauseef, W.M., and N. Borregaard. Neutrophils at work. *Nat. Immunol.*

15:602–11, 2014.

227. Ndrepepa, G., S. Braun, J. Mehilli, N. Von Beckerath, A. Schömig, and A. Kastrati. Myeloperoxidase level in patients with stable coronary artery disease and acute coronary syndromes. *Eur. J. Clin. Invest.* Wiley/Blackwell (10.1111), 38:90–96, 2008.

228. Neeves, K.B., and S.L. Diamond. A membrane-based microfluidic device for controlling the flux of platelet agonists into flowing blood. *Lab Chip* Royal Society of Chemistry, 8:701, 2008.

229. Nevaril, C.G., E.C. Lynch, C.P. Alfrey, and J.D. Hellums. Erythrocyte damage and destruction induced by shearing stress. *J. Lab. Clin. Med.* Elsevier, 71:784–90, 1968.

230. Nguyen, C.V., A. Fouras, and J. Carberry. Improved accuracy of micro PIV measurement using image overlapping technique. *Exp. Fluids* 49:701–712, 2010.

231. Nguyen, N.T., and S. Wereley. Fundamentals and applications of microfluidics. *Artech House* 111, 2006.

232. Nijhuis, J., S.S. Rensen, Y. Slaats, F.M.H. van Dielen, W.A. Buurman, and J.W.M. Greve. Neutrophil Activation in Morbid Obesity, Chronic Activation of Acute Inflammation. *Obesity* Blackwell Publishing Ltd, 17:2014–2018, 2009.

233. Ogle, J.D., J.G. Noel, R.M. Sramkoski, C.K. Ogle, and J.W. Alexander. Effects of chemotactic peptide f-met-leu-phe (FMLP) on C3b receptor (CR1)

expression and phagocytosis of microspheres by human neutrophils.

Inflammation 14:337–353, 1990.

234. Ogle, J.D., J.G. Noel, R.M. Sramkoski, C.K. Ogle, and J.W. Alexander. Effects of combination of tumor necrosis factor alpha and chemotactic peptide, f-Met-Leu-Phe, on phagocytosis of opsonized microspheres by human neutrophils. *Inflammation* 16:57–68, 1992.

235. Okuyama, M., Y. Ohta, J. Kambayashi, and M. Monden. Fluid shear stress induces actin polymerization in human neutrophils. *J. Cell. Biochem.* 63:432–441, 1996.

236. Olazabal, I.M., E. Caron, R.C. May, K. Schilling, D.A. Knecht, and L.M. Machesky. Rho-kinase and myosin-II control phagocytic cup formation during CR, but not FcγR, phagocytosis. *Curr. Biol.* 12:1413–1418, 2002.

237. Pan, L., and P.E. Arratia. A high-shear, low Reynolds number microfluidic rheometer. *Microfluid. Nanofluidics* 14:885–894, 2013.

238. Papaioannou, T.G., and C. Stefanadis. Vascular wall shear stress: basic principles and methods. *Hell. J. Cardiol.* 46:9–15, 2005.

239. Papautsky, I., B.K. Gale, S.K. Mohanty, T.A. Ameel, and A.B. Frazier. Effects of rectangular microchannel aspect ratio on laminar friction constant. pp. 147–158, 1999.

240. Papayannopoulos, V., K. Metzler, A. Hakkim, and A. Zychlinsky. Neutrophil elastase and myeloperoxidase regulate the formation of neutrophil

extracellular traps. *J. Cell Biol* 191:677–691.

241. Pappano, A.J., and W. Gil Wier. The Microcirculation and Lymphatics. *Cardiovasc. Physiol.* 153–170, 2013.

242. Park, E.Y.H. *et al.* Comparison of PSGL-1 microbead and neutrophil rolling: microvillus elongation stabilizes P-selectin bond clusters. *Biophys. J.* 82:1835–1847, 2002.

243. Paschall, C.D., A.L. Klibanov, and M.B. Lawrence. Regulation of L-selectin-dependent hydrodynamic shear thresholding by leukocyte deformability and shear dependent bond number. *Biorheology* IOS Press, 52:415–432, 2015.

244. Pfund, D., D. Rector, A. Shekarriz, A. Popescu, and J. Welty. Pressure drop measurements in a microchannel. *AIChE J.* 46:1496–1507, 2000.

245. Phillipson, M., B. Heit, P. Colarusso, L. Liu, C.M. Ballantyne, and P. Kubes. Intraluminal crawling of neutrophils to emigration sites: a molecularly distinct process from adhesion in the recruitment cascade. *J. Exp. Med.* 203:2569–2575, 2006.

246. Piccard, H., R.J. Muschel, and G. Opdenakker. On the dual roles and polarized phenotypes of neutrophils in tumor development and progression. *Crit. Rev. Oncol. Hematol.* 82:296–309, 2012.

247. Pickard, J.E., and K. Ley. Micro-PTV measurement of the fluid shear stress acting on adherent leukocytes in vivo. *Biophys. J.* 96:4249–4259, 2009.

248. Pieper, I.L., G. Radley, and C.A. Thornton. Multidimensional Flow

Cytometry for Testing Blood- Handling Medical Devices. In: Multidimensional Flow Cytometry Techniques for Novel Highly Informative Assays 2018, pp. 63–80.

249. Pipe, C.J., and G.H. McKinley. Microfluidic rheometry. *Mech. Res. Commun.* 36:110–120, 2009.

250. Prokopowicz, Z., J. Marcinkiewicz, D.R. Katz, and B.M. Chain. Neutrophil myeloperoxidase: Soldier and statesman. *Arch. Immunol. Ther. Exp. (Warsz)*. SP Birkhäuser Verlag Basel, pp. 43–54, 2012.

251. Ramachandran, V., M. Williams, T. Yago, D.W. Schmidtke, and R.P. McEver. Dynamic alterations of membrane tethers stabilize leukocyte rolling on P-selectin. *Proc. Natl. Acad. Sci. U. S. A.* National Academy of Sciences, 101:13519–13524, 2004.

252. Rice, W., J. Kinkade, and R. Parmeley. High resolution of heterogeneity among human neutrophil granules: physical, biochemical, and ultrastructural properties of isolated fractions. *Blood* 68:541–555, 1986.

253. Rodgers, S.D., R.T. Camphausen, and D.A. Hammer. Sialyl Lewis(x)-mediated, PSGL-1-independent rolling adhesion on P-selectin. *Biophys. J.* 79:694–706, 2000.

254. Roger, V.L. *et al.* Heart disease and stroke statistics-2012 update: A report from the American heart association. *Circulation* 125:e2–e220, 2012.

255. Rorvig, S. *et al.* Ficolin-1 is present in a highly mobilizable subset of

human neutrophil granules and associates with the cell surface after stimulation with fMLP. *J. Leukoc. Biol.* 86:1439–1449, 2009.

256. Rose, E.A. *et al.* Long-Term Use of a Left Ventricular Assist Device for End-Stage Heart Failure. *N. Engl. J. Med.* Massachusetts Medical Society, 345:1435–1443, 2001.

257. Rzeniewicz, K. *et al.* L-selectin shedding is activated specifically within transmigrating pseudopods of monocytes to regulate cell polarity in vitro. *Proc. Natl. Acad. Sci.* 201417100, 2015.

258. Sakariassen, K.S., L. Orning, and V.T. Turitto. The impact of blood shear rate on arterial thrombus formation. *Futur. Sci. OA* 1:15–28, 2015.

259. Samady, H. *et al.* Coronary artery wall shear stress is associated with progression and transformation of atherosclerotic plaque and arterial remodeling in patients with coronary artery disease. *Circulation* 124:779–788, 2011.

260. Sansone, R. *et al.* Macrovascular and microvascular function after implantation of left ventricular assist devices in end-stage heart failure: Role of microparticles. *J. Hear. Lung Transplant.* Elsevier, 34:921–932, 2015.

261. Santiago, J.G., S.T. Wereley, C.D. Meinhart, D.J. Beebe, and R.J. Adrian. A particle image velocimetry system for microfluidics. *Exp. Fluids* Springer-Verlag, 25:316–319, 1998.

262. Sarvepalli, D.P., D.W. Schmidtke, and M.U. Nollert. Design considerations

- for a microfluidic device to quantify the platelet adhesion to collagen at physiological shear rates. *Ann. Biomed. Eng.* Springer US, 37:1331–1341, 2009.
263. Schaff, U.Y., M.M.Q. Xing, K.K. Lin, N. Pan, N.L. Jeon, and S.I. Simon. Vascular mimetics based on microfluidics for imaging the leukocyte-endothelial inflammatory response. *Lab Chip* 7:448, 2007.
264. Schirmer, C.M., and A.M. Malek. Computational fluid dynamic characterization of carotid bifurcation stenosis in patient-based geometries. *Brain Behav.* 2:42–52, 2012.
265. Schmid-Schönbein, H., P. Gaehtgens, and H. Hirsch. On the shear rate dependence of red cell aggregation in vitro. *J. Clin. Invest.* American Society for Clinical Investigation, 47:1447–54, 1968.
266. Schmidt, T. *et al.* CD66b overexpression and homotypic aggregation of human peripheral blood neutrophils after activation by a gram-positive stimulus. *J. Leukoc. Biol.* 91:791–802, 2012.
267. Schmidt, T. *et al.* CD66b overexpression and loss of C5a receptors as surface markers for *Staphylococcus aureus*-induced neutrophil dysfunction. *PLoS One*, edited by T. Akiyama. Public Library of Science, 10:e0132703, 2015.
268. Schü, T., and T.A. Springer. Regulation of integrin affinity on cell surfaces. *EMBO J.* 30333:4712–4727, 2011.

269. Selgrade, B.P., and G.A. Truskey. Computational Fluid Dynamics Analysis to Determine Shear Stresses and Rates in a Centrifugal Left Ventricular Assist Device. *Artif. Organs* 36, 2012.
270. Sengelov, H., P. Follin, L. Kjeldsen, K. Lollike, C. Dahlgren, and N. Borregaard. Mobilization of granules and secretory vesicles during in vivo exudation of human neutrophils. *J Immunol* 154:4157–4165, 1995.
271. Sengeløv, H., L. Kjeldsen, M.S. Diamond, T.A. Springer, and N. Borregaard. Subcellular localization and dynamics of Mac-1 (alpha m beta 2) in human neutrophils. *J. Clin. Invest.* 92:1467–1476, 1993.
272. Shamri, R. *et al.* Lymphocyte arrest requires instantaneous induction of an extended LFA-1 conformation mediated by endothelium-bound chemokines. *Nat. Immunol.* 6:497–506, 2005.
273. Sheriff, J. *et al.* Repetitive Hypershear Activates and Sensitizes Platelets in a Dose-Dependent Manner. *Artif. Organs* 40:586–595, 2016.
274. Shimaoka, M. *et al.* Structures of the α L I Domain and Its Complex with ICAM-1 Reveal a Shape-Shifting Pathway for Integrin Regulation. *Cell Cell Press*, 112:99–111, 2003.
275. Shimp, E.A., N.Z. Alsmadi, T. Cheng, K.H. Lam, C.S. Lewis, and D.W. Schmidtke. Effects of shear on P-selectin deposition in microfluidic channels. *Biomicrofluidics* 10, 2016.
276. Shin, H.Y., S.I. Simon, and G.W. Schmid-Schönbein. Fluid shear-induced

activation and cleavage of CD18 during pseudopod retraction by human neutrophils. *J. Cell. Physiol.* 214:528–36, 2008.

277. Shinohara, K. *et al.* High-speed micro-PIV measurements of transient flow in microfluidic devices. *Meas. Sci. Technol.* IOP Publishing, 15:1965–1970, 2004.

278. Shive, M.S., M.L. Salloum, and J.M. Anderson. Shear stress-induced apoptosis of adherent neutrophils: a mechanism for persistence of cardiovascular device infections. *Proc. Natl. Acad. Sci. U. S. A.* 97:6710–5, 2000.

279. Shoham, S., and L.W. Miller. Cardiac assist device infections. *Curr. Infect. Dis. Rep.* Current Science Inc., pp. 268–273, 2009.

280. Sia, S.K., and G.M. Whitesides. Microfluidic devices fabricated in Poly(dimethylsiloxane) for biological studies. *Electrophoresis* Wiley-Blackwell, 24:3563–3576, 2003.

281. Simon, H.A., L.P. Dasi, H.L. Leo, and A.P. Yoganathan. Spatio-temporal flow analysis in bileaflet heart valve hinge regions: Potential analysis for blood element damage. *Ann. Biomed. Eng.* 35:1333–1346, 2007.

282. Simon, S.I., and H.L. Goldsmith. Leukocyte adhesion dynamics in shear flow. *Ann. Biomed. Eng.* 30:315–332, 2002.

283. Slack, S.M., and V.T. Turitto. Chapter 2 Fluid dynamic and hemorheologic considerations. *Cardiovasc. Pathol.* Elsevier, 2:11–21, 1993.

284. Smith, M.L., T.S. Olson, and K. Ley. CXCR2- and E-Selectin–induced Neutrophil Arrest during Inflammation In Vivo. *J. Exp. Med.* 200:935 LP-939, 2004.
285. Soares, J.S., J. Sheriff, and D. Bluestein. A novel mathematical model of activation and sensitization of platelets subjected to dynamic stress histories. *Biomech. Model. Mechanobiol.* NIH Public Access, 12:1127–1141, 2013.
286. Sollier, E., C. Murray, P. Maoddi, and D. Di Carlo. Rapid prototyping polymers for microfluidic devices and high pressure injections. *Lab Chip.* pp. 3752–3765, 2011.
287. Son, Y. Determination of shear viscosity and shear rate from pressure drop and flow rate relationship in a rectangular channel. *Polymer (Guildf).* 48:632–637, 2007.
288. Song, X. *et al.* Design and Transient Computational Fluid Dynamics Study of a Continuous Axial Flow Ventricular Assist Device. *ASAIO J.* 50:215–224, 2004.
289. Spelman, D., and D. Esmore. Ventricular Assist Device Infections. *Curr. Infect. Dis. Rep.* 14:359–366, 2012.
290. Sperandio, M. *et al.* P-selectin Glycoprotein Ligand-1 Mediates L-Selectin–dependent Leukocyte Rolling in Venules. *J. Exp. Med.* 197:1355–1363, 2003.
291. Spijker, H.T., R. Graaff, P.W. Boonstra, H.J. Busscher, and W. Van Oeveren. On the influence of flow conditions and wettability on blood material

- interactions. *Biomaterials* 24:4717–4727, 2003.
292. Stadtmann, A. *et al.* The PSGL-1-L-selectin signaling complex regulates neutrophil adhesion under flow. *J. Exp. Med.* 210:2171–80, 2013.
293. Steinlechner, B. *et al.* Platelet Dysfunction in Outpatients With Left Ventricular Assist Devices. *Ann. Thorac. Surg.* 87:131–137, 2009.
294. Stocks, S.C., M.A. Kerr, C. Haslett, and I. Dransfield. CD66-dependent neutrophil activation: A possible mechanism for vascular selectin-mediated regulation of neutrophil adhesion. *J. Leukoc. Biol.* Wiley-Blackwell, 58:40–48, 1995.
295. Strony, J., a Beaudoin, D. Brands, and B. Adelman. Analysis of shear stress and hemodynamic factors in a model of coronary artery stenosis and thrombosis. *Am. J. Physiol.* 265:H1787-96, 1993.
296. Su, S.S., and G.W. Schmid-Schönbein. Fluid stresses on the membrane of migrating leukocytes. *Ann. Biomed. Eng.* 36:298–307, 2008.
297. Su, S.S., and G.W. Schmid-Schönbein. Internalization of formyl peptide receptor in leukocytes subject to fluid stresses. *Cell. Mol. Bioeng.* Springer US, 3:20–29, 2010.
298. Swanson, J.A. Shaping cups into phagosomes and macropinosomes. *Nat. Rev. Mol. Cell Biol.* 9:639–49, 2008.
299. Syeda, B., M. Gottsauner-Wolf, S. Denk, P. Pichler, A. Khorsand, and D. Glogar. Arterial compliance: A diagnostic marker for atherosclerotic plaque

burden? *Am. J. Hypertens.* 16:356–362, 2003.

300. Szczur, K., Y. Zheng, and M.D. Filippi. The small Rho GTPase Cdc42 regulates neutrophil polarity via CD11b integrin signaling. *Blood* 114:4527–4537, 2009.

301. Tanaka, M., and A. Miyahima. Onconstatin M, a multifunctional cytokine. In: *Reviews of Physiology, Biochemistry and Pharmacology* pp. 39–52.

302. Tang, J. *et al.* Adam17-dependent shedding limits early neutrophil influx but does not alter early monocyte recruitment to inflammatory sites. *Blood* 118:786–794, 2011.

303. Tedder, T.F., D.A. Steeber, A. Chen, and P. Engel. The selectins: vascular adhesion molecules. *FASEB J. Federation of American Societies for Experimental Biology*, 9:866–873, 1995.

304. Teng, N., G.J. Maghzal, J. Talib, I. Rashid, A.K. Lau, and R. Stocker. The roles of myeloperoxidase in coronary artery disease and its potential implication in plaque rupture. *Redox Rep.* Taylor & Francis, 22:51–73, 2017.

305. Thaysen-Andersen, M. *et al.* Human neutrophils secrete bioactive paucimannosidic proteins from azurophilic granules into pathogen-infected sputum. *J. Biol. Chem.* 290:8789–8802, 2015.

306. Toner, M., and D. Irimia. Blood-on-a-Chip. *Annu. Rev. Biomed. Eng.* Annual Reviews, 7:77–103, 2005.

307. Torsteinsdottir, I., N.-G. Arvidson, R. Hallgren, and L. Hakansson.

Enhanced Expression of Integrins and CD66b on Peripheral Blood Neutrophils and Eosinophils in Patients with Rheumatoid Arthritis, and the Effect of Glucocorticoids. *Scand J Immunol* 50:433–439, 1999.

308. Uriarte, S.M. *et al.* Comparison of Proteins Expressed on Secretory Vesicle Membranes and Plasma Membranes of Human Neutrophils. *J. Immunol.* 180:5575–5581, 2008.

309. Uriel, N. *et al.* Acquired von Willebrand syndrome after continuous-flow mechanical device support contributes to a high prevalence of bleeding during long-term support and at the time of transplantation. *J. Am. Coll. Cardiol.* 56:1207–1213, 2010.

310. van der Veen, B.S., M.P.J. de Winther, and P. Heeringa. Myeloperoxidase: Molecular Mechanisms of Action and Their Relevance to Human Health and Disease. *Antioxid. Redox Signal.* 11:2899–2937, 2009.

311. Vanhamme, L., K. Zouaoui Boudjeltia, P. Van Antwerpen, and C. Delporte. The other myeloperoxidase: Emerging functions. *Arch. Biochem. Biophys.* Academic Press, 649:1–14, 2018.

312. Varnava, A.M., P.G. Mills, and M.J. Davies. Relationship between coronary artery remodeling and plaque vulnerability. *Circulation* 105:939–943, 2002.

313. Videm, V., and E. Strand. Changes in Neutrophil Surface-Receptor Expression after Stimulation with FMLP, Endotoxin, Interleukin-8 and Activated Complement Compared to Degranulation. *Scand. J. Immunol.* Wiley/Blackwell

(10.1111), 59:25–33, 2004.

314. Vincentelli, A. *et al.* Acquired von Willebrand Syndrome in Aortic Stenosis. *N. Engl. J. Med.* Massachusetts Medical Society , 349:343–349, 2003.

315. Voisin, M.-B., and S. Nourshargh. Neutrophil Transmigration: Emergence of an Adhesive Cascade within Venular Walls. *J. Innate Immun.* Karger Publishers, 5:336–347, 2013.

316. Volker Brinkmann, Ulrike Reichard, Christian Goosmann, Beatrix Fauler, Yvonne Uhlemann, David S. Weiss, Yvette Weinrauch, A.Z. Neutrophil Extracellular Traps Kill Bacteria. *Science (80-.).* 303:1532–1535, 2004.

317. von Brühl, M.-L. *et al.* Monocytes, neutrophils, and platelets cooperate to initiate and propagate venous thrombosis in mice in vivo. *J. Exp. Med.* Rockefeller Univ Press, 209:819–35, 2012.

318. Walcheck, B., K.L. Moore, R.P. McEver, and T.K. Kishimoto. Neutrophil-neutrophil interactions under hydrodynamic shear stress involve L-selectin and PSGL-1: A mechanism that amplifies initial leukocyte accumulation on P-selectin in vitro. *J. Clin. Invest.* 98:1081–1087, 1996.

319. Warnock, R.A., S. Askari, E.C. Butcher, and U.H. von Andrian. Molecular mechanisms of lymphocyte homing to peripheral lymph nodes. *J. Exp. Med.* Rockefeller University Press, 187:205–16, 1998.

320. Wayne Smith, C. *et al.* Neutrophil Adhesion and Migration Relative Contribution of LFA-1 and Mac-1 to Relative Contribution of LFA-1 and Mac-1

- to Neutrophil Adhesion and Migration. *J Immunol Ref.* 163:5029–5038, 2018.
321. Wennerberg, K., and C.J. Der. Rho-family GTPases: it's not only Rac and Rho (and I like it). *J. Cell Sci.* 117:1301–1312, 2004.
322. Wereley, S.T., and C.D. Meinhart. Recent Advances in Micro-Particle Image Velocimetry. *Annu. Rev. Fluid Mech.* 42:557–576, 2010.
323. Westein, E., A.D. van der Meer, M.J.E. Kuijpers, J.-P. Frimat, A. van den Berg, and J.W.M. Heemskerk. Atherosclerotic geometries exacerbate pathological thrombus formation poststenosis in a von Willebrand factor-dependent manner. *Proc. Natl. Acad. Sci. U. S. A.* 110:1357–62, 2013.
324. Wittmann, S., G. Rothe, G. Schmitz, and D. Fröhlich. Cytokine Upregulation of Surface Antigens Correlates to the Priming of the Neutrophil Oxidative Burst Response. *Cytom. Part A* 57:53–62, 2004.
325. Wong, K., O. Pertz, K. Hahn, and H. Bourne. Neutrophil polarization: Spatiotemporal dynamics of RhoA activity support a self-organizing mechanism. *Proc. Natl. Acad. Sci.* 103:3639–3644, 2006.
326. Woolley, J.R. *et al.* Temporal leukocyte numbers and granulocyte activation in pulsatile and rotary ventricular assist device patients. *Artif. Organs* 38:447–455, 2014.
327. Wootton, D.M., and D.N. Ku. Fluid Mechanics of Vascular Systems, Diseases, and Thrombosis. *Annu. Rev. Biomed. Eng.* 1:299–329, 1999.
328. Wu, L., G. Guan, H.W. Hou, A.A.S. Bhagat, and J. Han. Separation of

leukocytes from blood using spiral channel with trapezoid cross-section. *Anal. Chem.* American Chemical Society, 84:9324–9331, 2012.

329. Yago, T. *et al.* Distinct molecular and cellular contributions to stabilizing selectin-mediated rolling under flow. *J. Cell Biol.* The Rockefeller University Press, 158:787–799, 2002.

330. Yago, T., J. Wu, C.D. Wey, A.G. Klopocki, C. Zhu, and R.P. McEver. Catch bonds govern adhesion through L-selectin at threshold shear. *J. Cell Biol.* 166:913–923, 2004.

331. Yamada, M., M. Nakashima, and M. Seki. Pinched flow fractionation: Continuous size separation of particles utilizing a laminar flow profile in a pinched microchannel. *Anal. Chem.* American Chemical Society, 76:5465–5471, 2004.

332. Yang, H. *et al.* Interaction between single molecules of Mac-1 and ICAM-1 in living cells: An atomic force microscopy study. *Exp. Cell Res.* Academic Press, 313:3497–3504, 2007.

333. Yin, C., and B. Heit. Armed for destruction: formation, function and trafficking of neutrophil granules. *Cell Tissue Res.* Springer Berlin Heidelberg, pp. 455–471, 2018.

334. Yong, A.S.C. *et al.* Intracoronary shear-related up-regulation of platelet P-selectin and platelet-monocyte aggregation despite the use of aspirin and clopidogrel. *Blood* 117:11–20, 2011.

335. Yoon, J., A. Terada, and H. Kita. CD66b Regulates Adhesion and Activation of Human Eosinophils. *J. Immunol.* American Association of Immunologists, 179:8454–8462, 2007.
336. Zarbock, A. *et al.* Leukocyte ligands for endothelial selectins: specialized glycoconjugates that mediate rolling and signaling under flow. *Blood* American Society of Hematology, 118:181–213, 2011.
337. Zarbock, A., and K. Ley. Mechanisms and consequences of neutrophil interaction with the endothelium. *Am. J. Pathol.* pp. 1–7, 2008.
338. Zarins, C.K. *et al.* Carotid Bifurcation Atherosclerosis: Quantative Correlation of Plaque Localization with Flow Velocity Profiles and Wall Shear Stress. *Circ. Res.* 53:502–514, 1983.
339. Zhang, X., D. Zhan, and H.Y. Shin. Integrin subtype-dependent CD18 cleavage under shear and its influence on leukocyte-platelet binding. *J. Leukoc. Biol.* Wiley-Blackwell, 93:251–258, 2013.

Appendix A: Velocity and Shear Rate Equations:

Starting with the equation of motion:

$$\rho \left(\frac{\partial v_x}{\partial t} + v_x \frac{\partial v_x}{\partial x} + v_y \frac{\partial v_x}{\partial y} + v_z \frac{\partial v_x}{\partial z} \right) = -\frac{dp}{dx} + \mu \left(\frac{\partial^2 v_x}{\partial x^2} + \frac{\partial^2 v_x}{\partial y^2} + \frac{\partial^2 v_x}{\partial z^2} \right) + \rho g_x$$

We then apply a few assumptions to simplify:

- 1) For laminar flow there is no fluid flow in the y and z directions ($v_y, v_z = 0$)
- 2) The fluid is incompressible and there is no change in velocity along the x direction ($\frac{\partial}{\partial x} v_x = 0$)
- 3) The channel is horizontal ($g_x = 0$)
- 4) The flow is at steady state with no time dependence ($\frac{\partial v_x}{\partial t} = 0$)

To arrive at:

$$0 = -\frac{dp}{dx} + \mu \left(\frac{\partial^2 v_x}{\partial y^2} + \frac{\partial^2 v_x}{\partial z^2} \right)$$

Rearranging:

$$\frac{1}{\mu} \frac{dp}{dx} = \left(\frac{\partial^2 v_x}{\partial y^2} + \frac{\partial^2 v_x}{\partial z^2} \right) = \text{constant}$$

The solution to this equation can be solved²³¹, and plugging in a and b as half the height and width provides Equation 3 from Chapter 2:

$$v_x = \frac{16a^2}{\mu\pi^3} \left(-\frac{dp}{dx} \right) \sum_{i=1,3,5,\dots}^{\infty} (-1)^{(i-1)/2} \left[1 - \frac{\cosh(i\pi y_c/2a)}{\cosh(i\pi b/2a)} \right] \frac{\cos(i\pi z_c/2a)}{i^3}$$

Integrating this equation provides Chapter 2 Equation 4:

$$\dot{Q} = \frac{4ba^3}{3\mu} \left(-\frac{dp}{dx} \right) \left[1 - \frac{192a}{\pi^5 b} \sum_{i=1,3,5,\dots}^{\infty} \frac{\tanh(i\pi b/2a)}{i^5} \right]$$

To derive a relationship between the flow rate and the shear rate, Son²⁸⁷ first takes a force balance to relate pressure and shear stress:

$$\Delta P * (WH) = \tau_w * (2WL + 2HL)$$

Rearranging for the shear stress:

$$\tau_w = \left(\frac{\Delta P}{2L} \right) \left(\frac{WH}{H+W} \right) = \left(\frac{\Delta PH}{2L} \right) \left(\frac{1}{H/W + 1} \right)$$

We need to rearrange the equation for the flow rate to solve for the pressure drop per unit length ($-dp/dx = \Delta P/L$), and plugging in $H/2$ and $W/2$ as a and b , respectively:

$$\dot{Q} = \frac{4 \frac{W}{2} \left(\frac{H}{2} \right)^3}{3\mu} \left(\frac{\Delta P}{L} \right) \left[1 - \frac{192 \frac{H}{2}}{\pi^5 \frac{W}{2}} \sum_{i=1,3,5,\dots}^{\infty} \frac{\tanh \left(i\pi \frac{W}{2} / \left(2 \frac{H}{2} \right) \right)}{i^5} \right]$$

Simplifying and including $x=W/H$

$$\dot{Q} = \frac{WH^3}{12\mu} \left(\frac{\Delta P}{L} \right) \left[1 - \frac{192}{\pi^5 x} \sum_{i=1,3,5,\dots}^{\infty} \frac{\tanh \left(\frac{\pi}{2} ix \right)}{i^5} \right]$$

$$\left(\frac{\Delta P}{L} \right) = \mu \frac{12\dot{Q}}{WH^3} \left[1 - \frac{192}{\pi^5 x} \sum_{i=1,3,5,\dots}^{\infty} \frac{\tanh \left(\frac{\pi}{2} ix \right)}{i^5} \right]^{-1}$$

$$\left(\frac{\Delta PH}{2L}\right) = \mu \frac{6\dot{Q}}{WH^2} \left[1 - \frac{192}{\pi^5 x} \sum_{i=1,3,5,\dots}^{\infty} \frac{\tanh\left(\frac{\pi}{2} ix\right)}{i^5} \right]^{-1}$$

Multiply the right side by $(1 + 1/x)^2$

$$\left(\frac{\Delta PH}{2L}\right) = \mu \frac{6\dot{Q}}{WH^2} \left(1 + \frac{1}{x}\right)^2 \left[\left(1 + \frac{1}{x}\right)^2 \left(1 - \frac{192}{\pi^5 x} \sum_{i=1,3,5,\dots}^{\infty} \frac{\tanh\left(\frac{\pi}{2} ix\right)}{i^5} \right) \right]^{-1}$$

$$\left(\frac{\Delta PH}{2L}\right) \left(\frac{1}{1 + \frac{1}{x}}\right) = \mu \frac{6\dot{Q}}{WH^2} \left(1 + \frac{1}{x}\right) \left[\left(1 + \frac{1}{x}\right)^2 \left(1 - \frac{192}{\pi^5 x} \sum_{i=1,3,5,\dots}^{\infty} \frac{\tanh\left(\frac{\pi}{2} ix\right)}{i^5} \right) \right]^{-1}$$

$$\left(\frac{\Delta PH}{2L}\right) \left(\frac{1}{1 + \frac{H}{W}}\right) = \mu \frac{6\dot{Q}}{WH^2} \left(1 + \frac{H}{W}\right) \left[\left(1 + \frac{1}{x}\right)^2 \left(1 - \frac{192}{\pi^5 x} \sum_{i=1,3,5,\dots}^{\infty} \frac{\tanh\left(\frac{\pi}{2} ix\right)}{i^5} \right) \right]^{-1}$$

Therefore:

$$\tau_w = \left(\frac{\Delta PH}{2L}\right) \left(\frac{1}{\frac{H}{W} + 1}\right) = \mu \left(\frac{6Q}{WH^2}\right) \left(1 + \frac{H}{W}\right) f^*\left(\frac{H}{W}\right)$$

Where

$$f^*\left(\frac{H}{W}\right) = \left[\left(1 + \frac{1}{x}\right)^2 \left(1 - \frac{192}{\pi^5 x} \sum_{i=1,3,5,\dots}^{\infty} \frac{\tanh\left(\frac{\pi}{2} ix\right)}{i^5} \right) \right]^{-1}$$

The wall shear rate for a Newtonian fluid can thus be described (as mentioned in Chapter 2, Equation 1) by:

$$\gamma_w = \left(\frac{6Q}{WH^2}\right) \left(1 + \frac{H}{W}\right) f^*\left(\frac{W}{H}\right)$$

Appendix B: Negative Photolithography Protocol

1. Remove an aliquot of the appropriate photoresist from the freezer and let sit until thawed and up to room temperature, at least 30 minutes. This will be assuming KMPR 1050 with a height of 60 μm , spin speeds to be changed for other applications and heights
2. Set up the spin coater with the appropriate program conditions (see below), and cover the surface with foil for easier cleaning
3. Pour a drop of photoresist into the center of the wafer. Allow the photoresist to fall so as to avoid creating bubbles
4. Rotate the wafer by tilting, thus causing the photoresist to move from the center to the outside. Slowly rotate until the photoresist is covering almost the entire wafer, rotating several times as necessary. Shift any edge back towards the center
5. Allow the wafer to sit for 5-10 minutes. This allows the photoresist to spread more evenly across the surface, to minimize height variations across the wafer
6. Spin coat the wafer
500 rpm, 100 rpm/sec, 10 seconds
2800 rpm, 300 rpm/sec, 30 seconds
Using a CEE Spin Coater (Brewer Scientific). Spin speed will need to be adjusted for each spin coater device used
7. Repeat to coat additional wafers as needed, and let sit overnight after spin coating. This helps even out small variations in the photoresist

height after spin coating. Do these initial steps towards the end of the day if possible

8. Pre-bake for 20 minutes at 100 °C. Use one of the Aluminum blocks for even heating. This requires temperatures of the hot plate to be increased to 115 °C to achieve the desired 100 °C. This will also vary with the heating block used.
9. Let wafer cool before exposure
10. Set up mask aligner. Using the Karl Suss Ma6B Contact Printer.
Exposure of 1100 mJ/cm² required, exposure time to be adjusted according to the current bulb power for the I line.
11. Load the wafer and expose. Allow to sit for a minute
12. Post-bake for 4 minutes at 100 °C
13. Let cool, about 5 minutes
14. Develop wafer in SU-8 developer. Shake container slowly (like an orbital shaker). Do not sonicate, as this will remove the small features such as the constrictions. Takes approximately 5 minutes to develop

Appendix C: Neutrophil Isolation Protocol

1-step Lympholyte density separation with RBC salt lysis and buffer washes

Lympholyte (CedarLane CL5071): Sodium diatrizoate and dextran 500 density gradient

All buffers and centrifuge should be at room temperature (centrifuge set at 25 °C)

1. Use a syringe to add 5 mL of lympholyte to a 15 mL conical tube
2. Carefully layer 5 mL of whole blood (sodium heparin anticoagulated) on top

Be careful not to mix the two layers

3. Spin 30 minutes at 600xg until cell bands are visible and distinct
Spin additional 5 minutes if necessary to remove residual RBCs
4. With a pipette carefully remove the second white layer containing the granulocytes

Layers (top/bottom): PRP, lympholyte, mononuclear WBCs,
lympholyte, granulocytes, lympholyte, RBC pellet

5. Add cells to a 50 mL conical. Add up to 10 mL of 0.4% NaCl. Should be 5 mL of cells and 5 mL of salt solution. Invert gently to mix
6. Add 10 mL of HBSS (w/o Ca/Mg) on top. Invert gently to mix
7. Spin 15 min at 450xg
8. Remove liquid and gently tap pellet to remove from wall of centrifuge tube

9. Add 10 mL of 0.2% NaCl and gently invert to mix
10. Add 10 mL of 1.6% NaCl and gently invert to mix
11. Spin 10 min at 450xg
12. Remove liquid, tap to loosen pellet, and resuspend in 5 mL of 0.5% HSA (in HBSS w/o Ca/Mg). Invert gently to mix and transfer to a 15 mL conical. Wash in 7-10 mLs if you have more than two tubes of blood/lymphocyte (in the first step) for the separation
13. Spin 5 min at 450xg
14. Repeat steps 12-13 for two additional washes
15. Resuspend in an appropriate volume of 0.5% HSA (now in HBSS with Ca/Mg)

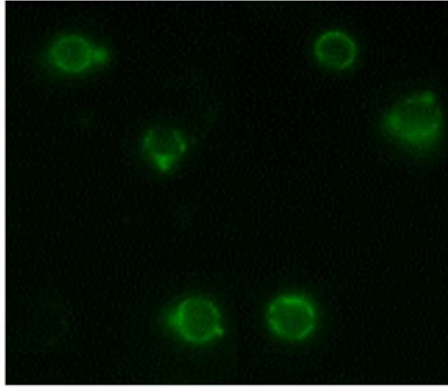
Transfer to new conical tube

Generally about 1-5 million cells per mL

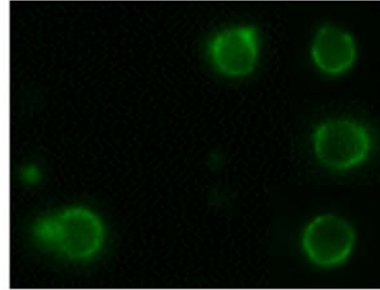
Count and add additional buffer as necessary for assay concentration

Appendix D: Actin Confocal Images

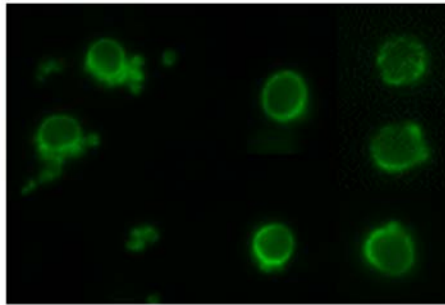
(A) Unsheared



(B) 16 msec



(C) 67 msec



Representative confocal images for f-actin staining in whole blood are shown above for three conditions: unsheared, 16 msec at $100,000 \text{ s}^{-1}$, and 67 msec at $90,000 \text{ s}^{-1}$. The latter sample had an increase in f-actin content as measured by flow cytometry (Figure 4.8). F-actin content as measured throughout the entire cell (with confocal images, using ImageJ) was also significantly higher ($P < 0.05$) for the 67 msec channel as compared to the unsheared sample, and was not for the 16 msec channel. No visual differences were observed at this time between samples.